Structural Integrity Assessment of C-Mn Pipeline Steels Exposed to Sour Environments

Colum Holtam

TWI Ltd
Granta Park
Great Abington
Cambridge
CB21 6AL
UK

Centre for Innovative and Collaborative Engineering (CICE)
Loughborough University
Loughborough
Leicestershire
LE11 3TU
UK

STRUCTURAL INTEGRITY ASSESSMENT OF C-MN PIPELINE STEELS EXPOSED TO SOUR ENVIRONMENTS

By
Colum Holtam

A dissertation thesis submitted in partial fulfilment of the requirements for the award of the degree Doctor of Engineering (EngD), at Loughborough University

[April 2010]

TWI Ltd
Granta Park
Great Abington
Cambridge
CB21 6AL
UK

Centre for Innovative and Collaborative
Engineering (CICE)
Loughborough University
Loughborough
Leicestershire
LE11 3TU
UK

ACKNOWLEDGEMENTS

This EngD research project was funded by the Industrial Members of TWI, as part of the Core Research Programme and the Engineering and Physical Sciences Research Council. The author would like to acknowledge the support of his academic supervisors at Loughborough University, Dr. Ian Ashcroft and Professor Rachel Thomson and in particular the technical guidance from his industrial supervisor and former colleague Dr. David Baxter. Further thanks go to Richard Pargeter, Technology Fellow for Ferritic Steels and Sour Service at TWI, for his continuing interest in this area of research.

ABSTRACT

Oil and gas fields can contain significant amounts of hydrogen sulphide and the behaviour of C-Mn pipeline steels exposed to sour environments (i.e. those containing water and hydrogen sulphide) continues to be one of the most active areas of research in the oil and gas industry. This project is aimed at improving the procedures used to assess the significance of flaws in offshore pipelines and risers operating in such environments.

Experimental work has focused on examining the behaviour of C-Mn pipeline steel in a sour environment with respect to both static and fatigue crack growth behaviour, for which there is a paucity of data. In particular, the critical influence of crack depth on the crack growth rate has been studied, in order to ensure that test methods and assessment procedures used in industry are appropriately conservative.

Under cyclic loading conditions, an environmental crack depth effect has been demonstrated, whereby, shallow flaws appear to grow faster than deeper flaws at the same (low) value of ΔK. The observed behaviour is believed to be dominated by bulk hydrogen charging, i.e. hydrogen charging by absorption from the external surfaces of the specimen rather than at the crack tip, and a lower concentration of hydrogen exists in the centre of the specimen than at the edges.

The novel data generated have been applied to real-life pipeline defect assessments to demonstrate the influence of the observed crack growth rate, with a view to developing an improved assessment method. Example engineering critical assessments have been performed for circumferential surface-breaking girth weld flaws located on the internal surface of a typical steel catenary riser, operating in a sour environment and subject to vortex induced vibration fatigue loads.

Companies operating in the oil and gas sector will derive benefit from this research programme through the application of new validated test methods and the development of improved in-service assessment procedures.

KEY WORDS

Defect assessment, fatigue, pipeline steel, sour service.

PREFACE

The research presented within this thesis was conducted in partial fulfilment of the requirements for the award of an Engineering Doctorate (EngD) degree at the Centre for Innovative and Collaborative Engineering (CICE), Loughborough University. The EngD is in essence a PhD based in industry, designed to produce doctoral graduates that can drive innovation in engineering with the highest level of technical, managerial and business competence. This EngD research project was sponsored by TWI Ltd, and the Engineering and Physical Sciences Research Council (EPSRC).

The EngD is examined on the basis of a thesis containing at least three (but not more than five) research publications and/or technical reports. This discourse is supported by five technical publications, located in Appendices A to E.

SYMBOLS AND DEFINITIONS

Symbol	Definition	Units
a	Flaw depth	mm
a_{cal}	Flaw depth used for calibration of direct current potential drop system	
a_0	Critical crack size (as defined in BS 7910) or average original crack length (as defined in BS 7448-1)	mm
B	Specimen thickness	mm
C	Constant in Paris fatigue crack growth law	
d	Distance between current input and crack plane in direct current potential drop system	mm
D	Diffusivity	cm^2s^{-1}
da/dt	Rate of crack propagation with time	mms^{-1}
da/dN	Rate of crack propagation per cycle	$mmcycle^{-1}$
f	Distance between wire and crack plane in direct current potential drop system	mm
f_{SCC}	Factor of Safety (as defined in BS 7910) with respect to Stress Corrosion Cracking ($f_{SCC} > 1.0$)	
F_Q	Force (as defined in BS 7448-1)	N
J	J-integral; a line or surface integral that encloses the crack front from one crack surface to the other, used to charaterise the local stress-strain field around the crack front (as defined in BS 7910)	Nmm^{-1}
J_{ISCC}	Threshold J-integral for stress corrosion cracking	Nmm^{-1}
k	Calibration coefficient	
K or K_I	(Applied) stress intensity factor	$Nmm^{-3/2}$ $MPam^{0.5}$
K_{IC}	Material fracture toughness or critical stress intensity for failure under mode I static loading conditions	$Nmm^{-3/2}$ $MPam^{0.5}$
K_{ISCC}	Threshold stress intensity factor for stress corrosion cracking	$Nmm^{-3/2}$ $MPam^{0.5}$
K_{max}	Maximum value of stress intensity factor during the fatigue cycle	$Nmm^{-3/2}$ $MPam^{0.5}$
K_{min}	Minimum value of stress intensity factor during the fatigue cycle	$Nmm^{-3/2}$ $MPam^{0.5}$
ΔK	Applied stress intensity factor range	$Nmm^{-3/2}$ $MPam^{0.5}$
ΔK_{TH}	Threshold stress intensity factor range	$Nmm^{-3/2}$ $MPam^{0.5}$
ΔK_{eff}	Effective stress intensity factor range	$Nmm^{-3/2}$ $MPam^{0.5}$
K_r	Fracture ratio of applied elastic K value to material fracture toughness (as defined in BS 7910)	$Nmm^{-3/2}$ $MPam^{0.5}$
K_{IH}	Measure of material fracture toughness for embedded or external flaws in hydrogen charged material	$Nmm^{-3/2}$ $MPam^{0.5}$
K_Q	Provisional value of K_{IC} (as defined in BS 7448-1)	$Nmm^{-3/2}$ $MPam^{0.5}$

L_r	Ratio of applied load to yield load (as defined in BS 7910)	
M_k	Stress concentration factor at weld toe	
m	Exponent in Paris fatigue crack growth law	
N	Fatigue life (i.e. the number of cycles to failure at a certain stress range)	
R	Stress ratio (ratio of minimum to maximum stress in any fatigue cycle)	
S	Span between outer loading points in three point bend tests (as defined in BS 7448-1)	mm
v	Instantaneous voltage	volts
v_{cal}	Voltage used for calibration of direct current potential drop system	volts
W	Specimen width	mm
Y	Geometrical stress intensity factor correction (as defined in BS 7910)	
δ	Crack tip opening displacement or CTOD (as defined in BS 7448-1)	mm
σ	(Applied) stress	Nmm^{-2} MPa
σ_{SCC}	Threshold stress for SCC	Nmm^{-2} MPa
$\Delta\sigma$	(Applied) stress range	Nmm^{-2} MPa
$\Delta\sigma_{TH}$	Threshold stress range	Nmm^{-2} MPa
σ_Y or σ_{YS}	Yield strength (e.g. 0.2% proof strength) at the temperature of the fracture test	Nmm^{-2} MPa
τ	Decay constant	
AUT	Automated Ultrasonic	
CT	Compact Tension	
CTOD	Crack Tip Opening Displacement	
DCB	Double Cantilever Beam	
DCPD	Direct Current Potential Drop	
EAC	Environment Assisted Cracking	
ECA	Engineering Critical Assessment	
EDM	Electrical Discharge Machining	
FAD	Failure Assessment Diagram	
FCGR	Fatigue Crack Growth Rate	
FFS	Fitness-For-Service	
HAZ	Heat Affected Zone	
HIC or HPIC	Hydrogen (Pressure) Induced Cracking	
LEFM	Linear Elastic Fracture Mechanics	
NDT	Non-destructive Testing	
PWHT	Post Weld Heat Treatment	
SCC	Stress Corrosion Cracking	
SCR	Steel Catenary Riser	
SENB	Single Edge Notched Bend	
SENT	Single Edge Notched Tension	

SMYS	Specified Minimum Yield Strength
SOHIC	Stress Oriented Hydrogen Induced Cracking
SSC	Sulphide Stress Cracking
SSR	Slow Strain Rate
TDP	Touchdown Point
UTS	Ultimate Tensile Strength
VIV	Vortex Induced Vibration

TABLE OF CONTENTS

Appendices

LIST OF FIGURES

LIST OF TABLES

LIST OF PAPERS

The following papers, included in the appendices, have been produced in partial fulfilment of the award requirements of the Engineering Doctorate during the course of the research.

Journal papers

Holtam C M, Baxter D P, Ashcroft I A and Thomson R C, 2009: 'The behaviour of shallow cracks in a pipeline steel operating in a sour environment', Journal of Offshore Mechanics and Arctic Engineering (OMAE), August 2009, Vol. 131, 3, 031302, ASME.

Holtam C M, Baxter D P, Ashcroft I A and Thomson R C, 2009: 'Influence of fatigue loading on the engineering critical assessment of steel catenary risers in sour deepwater oil and gas developments', Key Engineering Materials, Vols. 413-414, pp313-325, Trans Tech Publications, Switzerland.

Holtam C M, Baxter D P, Ashcroft I A and Thomson R C, 2010: 'Effect of crack depth on fatigue crack growth rates for a C-Mn pipeline steel in a sour environment', International Journal of Fatigue 32 (2010) pp288-296, Elsevier.

Holtam C M, Baxter D P, Ashcroft I A and Thomson R C, 2010: 'A survey of fitness-for-service trends in industry', Journal of Pressure Vessel Technology (PVT), ASME. *Paper in press.*

Holtam C M, Baxter D P, Ashcroft I A and Thomson R C, 2010: 'An investigation into fatigue crack growth test methods in a sour environment', International Journal of Offshore and Polar Engineering (IJOPE). *Paper in press.*

Refereed conference papers

Holtam C M and Baxter D P, 2007: 'Environment assisted cracking assessment methods: The behaviour of shallow cracks', Ninth International Conference on Engineering Structural Integrity: Research, Development and Application, China Machine Press.

Holtam C M, Baxter D P, Ashcroft I A and Thomson R C, 2008: 'The behaviour of shallow cracks in a pipeline steel operating in a sour environment', OMAE2008-57083, 27th International Conference on Offshore Mechanics and Arctic Engineering, ISBN 0-7918-3827-8, ASME.

Holtam C M, Baxter D P, Ashcroft I A and Thomson R C, 2008: 'A Survey of Fitness-for-Service Trends in Industry', Pressure Vessels and Piping Conference, ISBN 0-7918-3828-5, ASME.

Holtam C M, Baxter D P, Ashcroft I A and Thomson R C, 2009: 'An investigation into fatigue crack growth test methods in a sour environment', Proceedings of the 19th International Offshore and Polar Engineering Conference (ISOPE), ISBN 978-1-880653-53-1 (Set), ISSN 1098-618.

Holtam C M, Baxter D P, Ashcroft I A and Thomson R C, 2009: 'Influence of fatigue loading on the engineering critical assessment of steel catenary risers in sour deepwater oil and gas developments', 8th International Conference on Damage Assessment of Structures (DAMAS 2009), China.

Holtam C M, Baxter D P, Ashcroft I A and Thomson R C, 2010b: 'Fatigue crack growth performance of sour deepwater riser welds', Proceedings of the 2010 Deep Offshore Technology (DOT) International Conference, Houston, USA.

1 INTRODUCTION

This Engineering Doctorate (EngD) research project was sponsored by the Structural Integrity Technology Group (SITG) at TWI Ltd, one of the world's foremost independent research and technology organisations for welding and joining. TWI is a membership-based not-for-profit organisation that provides a technical consultancy service across several industry sectors. This EngD was funded through TWI's Core Research Programme, which is one of the ways that TWI uses the fees paid by its members, and the Engineering and Physical Sciences Research Council (EPSRC).

In 2008, approximately 40% of TWI's income and over 60% of SITG's income came from the oil and gas sector, with projects ranging from short-term single client consultancy work to longer term joint industry and collaborative research programmes. This research project is in line with one of SITG's currently identified 'hot topics' where there is a perceived need to further develop technical expertise in assessing the integrity and behaviour of structures which are prone to environment assisted cracking (EAC), i.e. crack growth caused, or exacerbated, by the presence of aggressive corroding environments. More specifically, this research project is aimed at improving the procedures used to assess the significance of shallow surface flaws in offshore pipelines and risers operating in sour environments (i.e. those containing water and hydrogen sulphide). TWI has a long history of helping industry to develop an understanding of pipeline steels in sour service environments and boasts one of the largest sour service testing facilities in the world. It is envisaged that companies operating in the capital-intensive oil and gas sector will derive benefit from this research programme, through the application of new validated test methods and improved in-service assessment procedures.

1.1 STRUCTURAL INTEGRITY ASSESSMENTS

Fracture mechanics-based structural integrity assessments, most commonly referred to as either engineering critical assessments (ECAs) or Fitness-For-Service (FFS) assessments, are not a new concept, dating back to the 1960s, but they have found more widespread acceptance over the past ten years. The nuclear and offshore oil and gas industries were the main drivers behind the development of formal FFS procedures. In the latter case these were particularly aimed at assessing the structural integrity of welded offshore structures in the hostile North Sea environment. This led to the development of BS PD 6493 (1991), a British Standard Published Document focusing on the assessment of brittle fracture and fatigue in fusion welded structures. Nowadays it is widely accepted that all welded structures contain flaws. As further research was carried out, and as additional damage mechanisms were considered, PD 6493 became British Standard 7910 in 1999. BS 7910 has three levels of assessment for fracture, based around the failure assessment diagram (FAD) concept. More details about fracture mechanics-based assessment methods and the FAD approach are provided within Section 2.1.

Structural integrity assessments can be used at the design stage, to estimate the maximum flaw size that will not grow to an intolerable size during the life of the component, or to assess defects that have grown after time in service. To do this requires information about defect tolerance, which itself relies on the availability of representative and reliable experimental data on which to base any defect assessment calculations. For structures operating in inert environments, the primary material properties that are needed for this type of assessment are

the tensile properties, fracture toughness and fatigue crack growth rate (FCGR), and for common structural steels these data are widely available. However, for structures exposed to corrosive environments, other degradation mechanisms need to be considered, such as the possibility of EAC. Methods for evaluating EAC within current integrity assessment procedures are usually based on avoiding the phenomena by limiting the stress, $\sigma<\sigma_{SCC}$, for crack free components, or limiting the stress intensity factor, $K<K_{ISCC}$, where a flaw already exists. Under fatigue loading, the corresponding characterising parameters are the applied stress range ($\Delta\sigma$) or stress intensity factor range (ΔK).

However, determining conditions for the avoidance of EAC has long been a major challenge due to the number of variables that have a significant effect on material behaviour. It is therefore imperative that service conditions are properly characterised and that the mechanism of environmental damage is fully understood. Only then can a reasoned judgement be made regarding the manner in which the environmental damage influences structural integrity.

One area where there is still significant uncertainty is the behaviour of shallow flaws and how to ensure that the assessment of these flaws remains conservative. There is evidence to suggest that shallow cracks can behave differently to deeper flaws in aggressive corroding environments; crack growth rates may be higher (e.g. Gangloff, 1985) or the true threshold for avoiding crack extension may be lower (e.g. Sponseller, 1992). As behaviour in the shallow crack regime may dominate the overall life of structures containing typical fabrication flaws, it is evident that improved understanding of material behaviour and the development of appropriate assessment procedures are of high importance.

For the purposes of this thesis the terms ‘shallow’ and ‘deep’ shall be used to describe the through thickness crack size. However, it should be noted that in fatigue applications the terms ‘short’ and ‘long’ are also often used to describe the through thickness extent of cracks. This can be confusing since the terms ‘short’ and ‘long’ are often misinterpreted as referring to the lateral extent of a crack, which may not be the case.

1.2 PIPELINE STEELS

C-Mn steel is generally the most economic material for the construction of pipelines. A pipeline is an assembly of shorter lengths of line pipe (say 12-15 m) that are welded together. The most widely used standard for specifying line pipe is the international standard API 5L/ISO 3183 (2007), although the construction code DNV-OS-F101 (2007) is also being increasingly used internationally for subsea pipelines.

API 5L contains two product specification levels; PSL1 and PSL2, the latter having additional mandatory requirements for chemical composition, notch toughness and strength properties, and additional non-destructive testing (NDT). API 5L traditionally identifies different grades of steel via an alphanumeric designation that indicates the specified minimum yield strength (SMYS). For example, API 5L grade X65 has a SMYS of 65 ksi (448 MPa), and a specified minimum ultimate tensile strength (UTS) of 77 ksi (531 MPa). Grade X65 therefore combines medium strength with good ductility and toughness and is commonly used for offshore pipelines and risers. A riser is the connecting piping between a subsea pipeline on the seabed and the installations above water, e.g. Floating Production, Storage and Offloading (FPSO) systems or drilling platforms, as shown in Figure 1.1, of which there are several different types. Steel catenary risers (SCRs) tend to be the most popular for deepwater developments,

i.e. water depths greater than approximately 500 m. Higher strength steels, such as X80 or X100, sacrifice ductility in favour of strength, but the harder microstructures that result are often more susceptible to EAC mechanisms such as hydrogen embrittlement.

Figure 1.1 Floating Production, Storage and Offloading vessel, illustrating subsea pipelines and risers (image courtesy of Maritime Pusnes AS).

Table 1.1 shows the chemical composition for standard PSL2 grade X65 line pipe, along with the more stringent requirements from Annex J (for offshore service) and Annex H (for sour service). DNV-OS-F101 generally conforms with API 5L Annex J. Offshore grades of steel have a lower carbon content (to improve weldability) and line pipe intended for sour service has the lowest sulphur content, as well as being leaner generally, e.g. lower phosphorous (Palmer and King, 2008). Too high a sulphur content is known to have a detrimental effect on the properties of the steel and also increases susceptibility to EAC, for example, by combining to form manganese sulphide which can trap hydrogen and lead to cracking. Typically, the chemical compositions imposed by the contractor or operator specifying pipe for sour service will be even more stringent, as will be seen from the chemical composition of the actual X65 pipes used in this research project. Pipeline steels usually exhibit a ferritic-pearlitic microstructure.

Table 1.1 Chemical composition for (seamless and welded) API 5L grade X65 line pipe steel (ANSI/API, 2007).

Steel Grade	Maximum Composition (wt.%)								
	C	Si	Mn	P	S	Cu	Ni	Cr	Mo
X65 (PSL2, standard)	0.18	0.45	1.7	0.025	0.015	0.5	0.5	0.5	0.5
X65 (PSL2, Annex J, offshore)	0.16	0.45	1.65	0.02	0.01	0.5	0.5	0.5	0.5
X65 (PSL2, Annex H, sour)	0.16	0.45	1.65	0.02	0.003	0.45	0.5	0.45	0.35

1.2.1 PIPE MANUFACTURE

Line pipe is either seamless or welded. Seamless pipe can be manufactured via several processes, all based around piercing a solid billet of steel to form a hollow cylinder, which is then extruded to produce a pipe of the desired diameter and wall thickness. Heat treatments are performed to improve the strength and toughness of the pipe, which, in the oil and gas industry, tends to be delivered in either the normalised or quenched and tempered state. Seamless pipe is routinely manufactured up to 16 inch (406.4 mm) diameter and its principal advantage is the absence of a longitudinal weld.

The two most common forms of longitudinally welded pipe are high-frequency welded (HFW) pipe, also known as electrical resistance welded or ERW pipe, and submerged-arc welded (SAW) pipe. HFW pipe is manufactured from steel plate that is rolled into a tube. As the pre-prepared edges are brought together, high frequency current is introduced, either via sliding contacts or an induction coil around the tube. There is sufficient local heating due to electrical resistance, that when the two edges are pressed together, a weld is formed. HFW pipe can be manufactured more quickly, more cheaply and to tighter tolerances than seamless pipe. There are, however, a number of quality issues such as the avoidance of weld line flaws.

SAW pipe (often termed UOE pipe) is manufactured from plate that is first formed into a U and then into a tube (O). After welding, the pipe is expanded (E) to modify the diameter and ensure circularity. The SAW process involves striking an arc between a continuously fed electrode and the pipe, under a blanket of flux powder to protect the weld zone. SAW is usually a mechanised process and is extremely well suited to the production of longitudinal and circumferential girth welds in larger diameter line pipe. SAW tends to be preferred for critical offshore applications, including sour service, but API 5L does not exclude the use of HFW pipes.

1.2.2 GIRTH WELDS

Circumferential girth welds are a critical location for the structural integrity of pipelines and risers, and are produced using mechanised welding processes. Welding involves the heating of metal to its melting temperature followed by rapid cooling. As the weld metal cools it contracts, and the cooling rate influences the type of microstructure and mechanical properties that result. A root pass, often produced using tungsten inert gas (TIG) welding, also known as gas tungsten arc welding or GTAW, is followed by a hot pass with higher heat input to temper the heat affected zone (HAZ) of the root pass, and reduce the risk of cold (hydrogen) cracking. Pipe ends require (sometimes complex) preparation to ensure full root penetration. Filler and capping runs are less critical than the root and hot passes and are often produced using metal inert gas (MIG) welding (also known as gas metal arc welding, GMAW).

Welding procedures are usually designed such that the weld is overmatched with respect to yield strength and UTS compared to the base metal. However, the harder weld and HAZ microstructures that result can be more sensitive to EAC. Good weldability is essential for offshore pipelines; the quicker welds of sufficient quality can be produced, with the minimum number of repairs, the faster the pipeline can be installed and the lower the costs of installation. Post weld heat treatment (PWHT) tends not to be performed because girth welds are produced on location as part of the pipe-laying process and local PWHT is known to be far less effective than PWHT that is performed in a fabrication shop. Figure 1.2 shows an

image of a girth weld, typical of that produced using mechanised welding processes, taken from a 14 inch (355.6 mm) outside diameter SCR to API 5L grade X65.

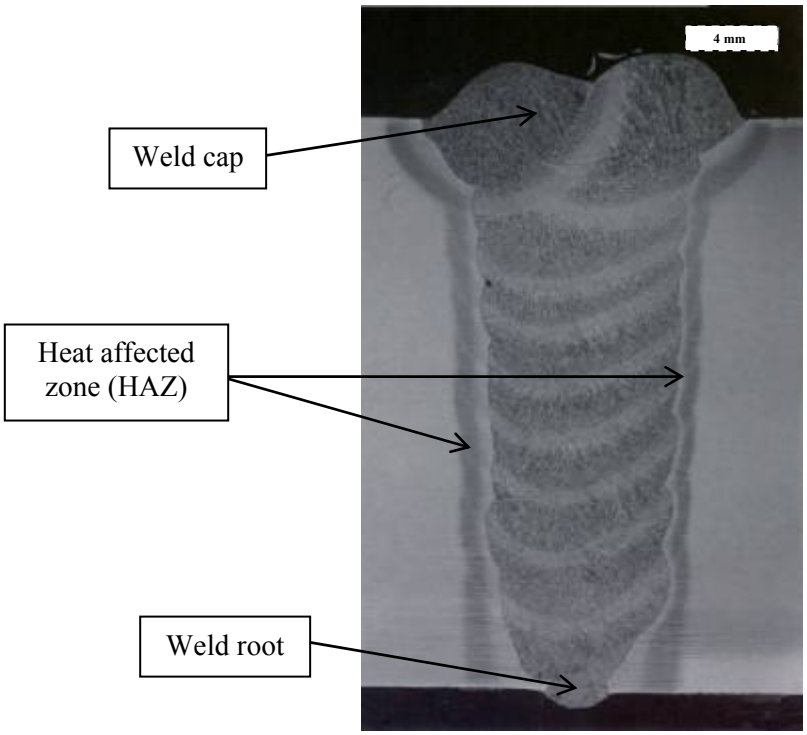

Figure 1.2 Macro image of a steel catenary riser girth weld, typical of that produced using mechanised welding processes, taken from a polished and etched cross-section.

Welding residual stresses can often provide a significant part of the driving force for EAC, and are dependent on the welding process and parameters used, and whether any PWHT was performed. As highlighted above, SCR girth welds tend not to be heat treated and therefore a uniform welding residual stress of yield strength magnitude is often assumed for assessment purposes, in line with the guidance provided in BS 7910 (7.2.4.1, 2005). This stress will relax under the influence of applied load, but if the applied loads are low then this will have a negligible effect. For an internal circumferential surface-breaking flaw at a pipeline girth weld, the residual stress profile perpendicular to the flaw (and in this case the weld) will be limiting. While the assumption of uniform residual stresses of yield strength magnitude is a common approach, it is also recognised as being highly conservative. For relatively thick-walled pipe it has also been shown that residual stresses tend to be lower, or even compressive, on the inner surface of a pipeline girth weld, but it is difficult to provide generic quantitative guidance. A combination of residual stress measurement and modelling (for a specific welding procedure) does, however, provide a possible method for determining an appropriate but less conservative assumption regarding the residual stress-state.

1.3 SOUR SERVICE

A sour environment can be described as one containing water and hydrogen sulphide (H_2S). The severity of such an environment depends on metallurgical characteristics and environmental conditions. Oil and gas fields can contain significant amounts of H_2S and pipeline steels exposed to a sour environment can be susceptible to a number of different cracking mechanisms, for example hydrogen induced cracking (HIC) - sometimes termed

hydrogen pressure induced cracking or HPIC, stress oriented hydrogen induced cracking (SOHIC) and sulphide stress cracking (SSC). Aqueous corrosion in acidic conditions produces hydrogen as a product of the reduction reaction. This would usually combine and evolve as molecular hydrogen gas but in sour conditions the presence of iron sulphide (FeS) scale 'poisons' the combination reaction, thereby, encouraging hydrogen uptake into the steel. The rate of hydrogen production is primarily controlled by pH.

The behaviour of C-Mn pipeline steels in a sour environment continues to be one of the most active areas of research in the oil and gas industry. It is possible to design out many of the problems associated with sour service conditions through the use of corrosion resistant alloys (CRAs) or internally CRA clad materials. However, it is critical to balance the increased costs of using corrosion resistant materials to reduce the risk of in-service cracking, with the increased risk of cracking and therefore higher in-service inspection costs and associated rates of weld repair for C-Mn steels. It simply is not financially viable to construct all pipelines and risers out of the more expensive CRAs or CRA clad materials. A more detailed discussion of the issues surrounding sour service can be found in Section 2.4.

1.4 SHALLOW FLAWS

An area where both experimental data and a validated assessment methodology are lacking is the behaviour of shallow cracks. The phrase 'crack initiation' usually refers to the formation of a 1-10 μm sized flaw from a defect free surface, but the subsequent transition to shallow crack growth is hard to define. The 'shallow crack growth' regime usually refers to defects that are small in relation to the scale of the microstructure or plastic zone size, but can also refer to instances where the defect size has an influence on crack tip chemistry, in which case cracks may be described as 'environmentally' or 'chemically' small (Jones and Simonen, 1994). In corrosive environments, shallow fatigue cracks have been shown to grow faster than deeper flaws subject to the same ΔK (e.g. Gangloff, 1985), and this highlights the need for care, as non-conservative assessments may result from the use of 'deep crack' experimental data to predict the behaviour of shallower flaws.

Unfortunately, experimental data in the shallow crack regime are scarce, and can be challenging to generate. Assessment procedures tend to focus on quantifying the behaviour of relatively deep cracks, and are based on determining a critical value of stress intensity factor for EAC (K_{ISCC}). It can be shown that for pipeline steels in a sour environment the expected regime of shallow crack behaviour is for flaw depths of the order of a few millimetres (Holtam and Baxter, 2007). It should however be noted that in many cases investigations into so called 'short crack behaviour' focus on sub-millimetre sized flaws (e.g. Murtaza and Akid, 1995). Nevertheless, for the specific application of interest (i.e. pipeline steels) modern NDT techniques cannot reliably detect sub-millimetre sized flaws, so defect acceptance limits are usually at least a few millimetres. The current work is restricted to flaws that are greater than 1 mm deep. A more detailed discussion of the approaches to modelling EAC in the shallow crack regime is provided in Section 2.7.

1.5 AIMS AND OBJECTIVES

The aim of this research project was to extend and validate integrity assessment procedures for environmentally damaged structures, such as those found in BS 7910 (2005), API 579-1/ASME FFS-1 (2007), R6 (2001) and FITNET (2008). Within this framework, experimental

work has primarily focused on examining the behaviour of C-Mn pipeline steel in a sour environment, with respect to both static and fatigue crack growth behaviour. These data have been used to develop assessment procedures for pipelines operating in such environments. In particular, the critical influence of crack depth on observed crack growth rates has been studied to ensure that test methods and assessment procedures are appropriately conservative. Although some aspects of the work may be transferable to other material-environment systems, the principal aim of this research has been to provide guidance on the assessment of shallow surface flaws in C-Mn pipeline steels operating in sour environments. Specific objectives of the research are to:

- Review integrity assessment procedures across different industry sectors;
- Determine experimental shallow crack test data to quantify the static (K_{ISCC}) behaviour of a C-Mn pipeline steel exposed to a sour environment;
- Determine experimental shallow crack test data to quantify the FCGR behaviour of a C-Mn pipeline steel exposed to a sour environment;
- Evaluate and develop test methods for generating shallow crack FCGR data in a sour environment to ensure that experimental test data are appropriately conservative;
- Provide guidance on performing ECA calculations for circumferential internal surface-breaking flaws in C-Mn steel pipelines subject to fatigue loading;
- Establish whether the above guidance for parent material is transferable to pipeline girth welds.

1.6 STRUCTURE OF THESIS

This thesis begins by describing the fundamentals of fracture mechanics-based assessment procedures, followed by a critical review of how these are applied to the more complicated case of EAC, with a specific focus towards SSC. A comprehensive review of published sour test data is provided, followed by a detailed discussion of the problems associated with modelling and exploring behaviour in the shallow crack regime. The various experimental techniques available are then reviewed before describing the specific details of the research methodology adopted in the different phases of the research project. Finally, a detailed discussion of the research carried out is provided, highlighting the novelty and industrial significance of the results, along with a number of recommendations for further work.

2 RELATED WORK

2.1 STRUCTURAL INTEGRITY ASSESSMENT PROCEDURES

Structural integrity assessment procedures exist for many different damage mechanisms, and fracture mechanics methods have been used to assess the structural integrity of pressure equipment for many years. Fracture describes a failure mechanism that involves the propagation of a crack. How that crack propagates depends on three variables: flaw size, material properties and the stress-state in the region of the flaw. If one understands the interaction between these three parameters then it is possible to predict how, and even when, failure might occur. In Irwin's stress intensity approach, fracture occurs when the stress intensity factor at the crack tip (or driving force) exceeds the material fracture toughness: i.e. the material's resistance to fracture. Temperature, environment, loading rate, microstructure and geometry (or constraint) can all influence a material's fracture toughness.

The principles of linear elastic fracture mechanics (LEFM) were developed in the 1950s by Irwin (1957), after previous research by Griffith (1920), and introduce the concept of a stress intensity factor (K). The stress intensity factor is a single parameter that represents the crack driving force and characterises the stress field at the crack tip. The generic equation for calculating K (eqn. 1) is based on a geometry dependent term (Y), the applied stress in the region of the flaw (σ) and the size of the flaw (a). There are two commonly used SI units for K; 1 $Nmm^{-3/2} = 0.0316$ $MPam^{0.5}$.

$$K = Y\sigma\sqrt{\pi a} \qquad (1)$$

When the applied K exceeds a critical value (termed the material's fracture toughness, K_{IC}) then fracture will occur. However, LEFM theory is limited by the fact it assumes an infinitely sharp crack and a purely elastic response. If this was the case then one would expect the stress to tend to infinity as the distance from the crack tip tends to zero (Figure 2.1). This, however, cannot be true because metal will deform plastically once the material yield stress has been reached. Therefore LEFM is only valid for brittle materials. For ductile materials the local stress-state close to the crack tip is such that plasticity occurs (Figure 2.1) and when this is significant (i.e. when the extent of plasticity becomes significant with respect to the component or specimen dimensions), then K is no longer an appropriate means of characterising behaviour.

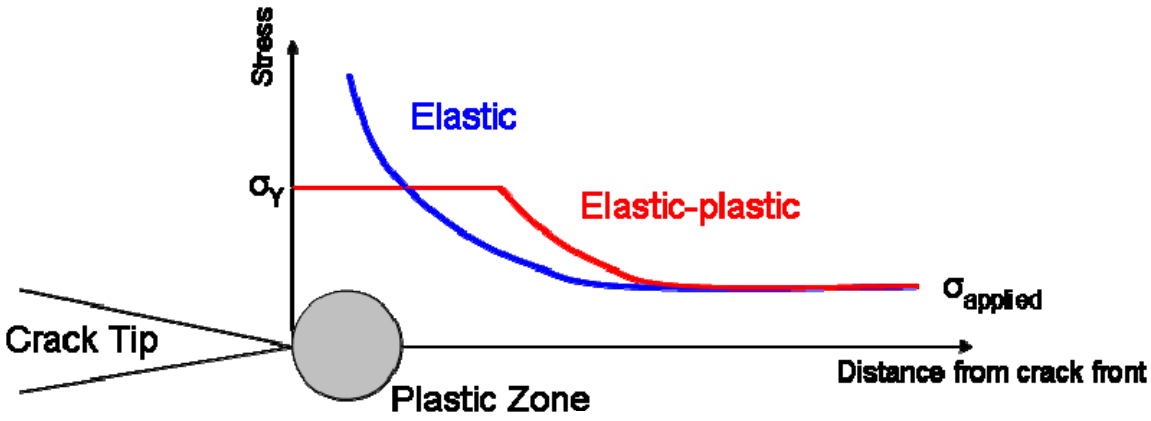

Figure 2.1 The variation of stress with distance from the crack tip for a purely elastic response and after correction for plasticity (after Irwin, 1960).

To account for plasticity at the crack tip, additional parameters are required to characterise fracture toughness such as the crack tip opening displacement (CTOD or δ), which is a strain-based parameter, and the J-integral, which is an energy-based parameter. Converting between the three different parameters is not straightforward but in many cases all three can be derived from one experiment, if specimens are adequately instrumented.

Structural integrity assessment methods can be used at the design stage to estimate the maximum flaw size that will not grow to an intolerable size during the life of the component, or to assess defects that have grown after time in service. It is possible to represent material properties, defect geometry and loading conditions in a mathematical form, and generate what is known as a failure assessment diagram (FAD). In this regard, the FAD approach can be considered as independent of component geometry.

A FAD represents a two-parameter approach, where both the propensity for fracture, either brittle or ductile, and plastic collapse are considered simultaneously. For fracture to occur the K at the crack tip must be greater than the material fracture toughness or critical stress intensity factor (K_{IC}). However, plastic collapse can also occur if the stress is high relative to the material proof stress or UTS, hence the need for a two-parameter approach. The two most widely used assessment procedures in the oil and gas industry, BS 7910 (2005) and API 579-1/ASME FFS-1 (2007) (Holtam et al., 2010c), both use a FAD approach for the assessment of crack-like flaws. A typical FAD is shown in Figure 2.2.

The vertical axis of the FAD represents the criteria for brittle or ductile fracture, often known as the fracture toughness ratio (K_r), which is the ratio of stress intensity factor (K_I) to material fracture toughness (K_{IC}). Both primary and secondary stresses, such as residual stresses, contribute to the applied K. The horizontal axis represents the likelihood of plastic collapse, often known as the load ratio (L_r), which is the ratio of the in-service (or reference) stress to yield strength (or 0.2% proof strength) or flow stress. Secondary stresses, such as residual stresses, do not contribute towards plastic collapse. K_r and L_r are connected via a locus, and the proximity to this locus is an indication of how close a specific material, flaw and stress combination is to failure. On or below the locus represents an acceptable or stable flaw, whereas a point outside the locus represents an unacceptable flaw where the risk of failure cannot be tolerated.

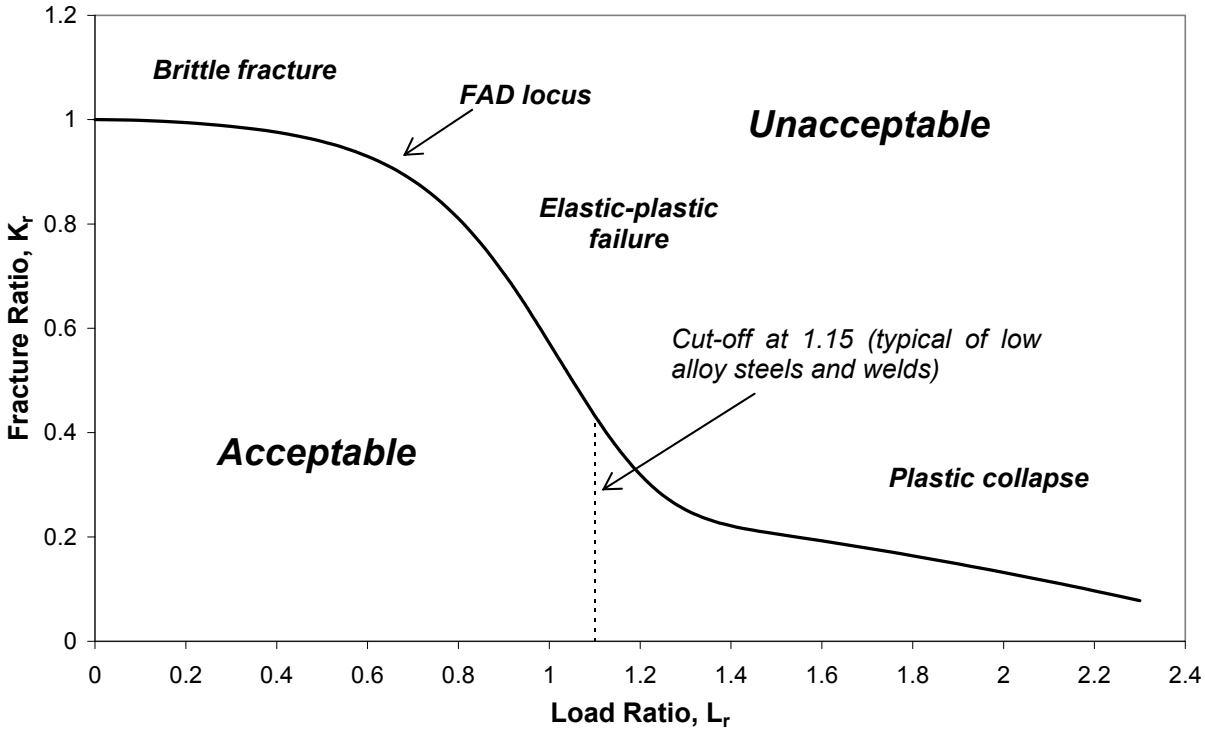

Figure 2.2 Generalised Level 2A failure assessment diagram with typical cut-off for low alloy steels and welds (after BS 7910, 2005).

2.2 FATIGUE

Fatigue has been recognised as a specific failure mechanism since the early nineteenth century, and refers to a process by which failure occurs by the repeated application of a cyclic or fluctuating load. The applied loading is therefore characterised by an applied stress range ($\Delta\sigma$) rather than a single value of stress, and in fracture mechanics terms a given flaw can then be considered to experience a stress intensity factor range (ΔK). The other term often encountered when characterising an applied fatigue cycle is the stress ratio (R) defined as the ratio of the minimum stress to the maximum stress (Figure 2.3).

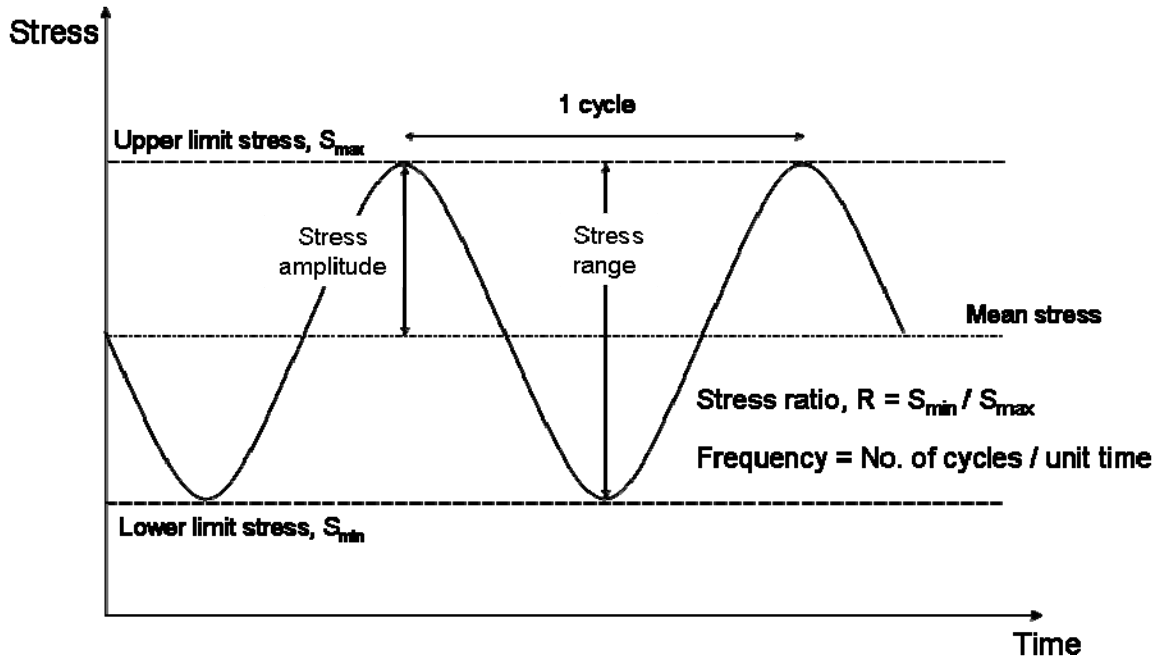

Figure 2.3 Terminology used to describe constant amplitude fluctuating stress fatigue loading.

Although each individual stress cycle is too small to cause failure by itself, the accumulation of damage as a result of the repeated application of these loads can eventually lead to what is known as fatigue failure. For the specific case of offshore pipelines and risers, fatigue stresses can result from numerous sources including the pressure cycles experienced by the riser during operation, wave and tidal motion and vortex induced vibration (VIV). The extent of fatigue damage is dependent on the combination of stress range and the number of cycles, and in many cases this is a significant factor in the overall design of offshore components.

There are two main methods for estimating fatigue life; the stress-life (S-N) approach (which essentially assumes a nominally defect free component) and a fracture mechanics approach, where the rate of growth of a pre-existing flaw is modelled. The current research has focused on the latter, where the rate of crack growth is determined from an empirical 'crack growth law' which is expressed in terms of the applied ΔK.

The assumed fatigue crack growth rate (FCGR) usually takes the form of a Paris law which relates the crack growth per cycle (da/dN) to the range of stress intensity factor (where $\Delta K = K_{max} - K_{min}$) where m and C are constants (eqn. 2) (Paris and Erdogan, 1963).

$$\frac{da}{dN} = C(\Delta K)^m \qquad (2)$$

In a log-log plot of da/dN versus ΔK the Paris law represents a straight line of slope m (Figure 2.4). Below a certain value of ΔK (known as the threshold value, ΔK_{TH}) no fatigue crack growth is expected, and material behaviour in this regime departs from a simple Paris law representation. Similarly, as K_{max} approaches the material's fracture toughness (K_{IC}) the crack growth rate increases rapidly. Published assessment procedures, for example BS 7910 (2005), contain standard crack growth laws for steels in air and in marine (i.e. seawater) environments. However, in other more aggressive environments, FCGRs can be significantly higher.

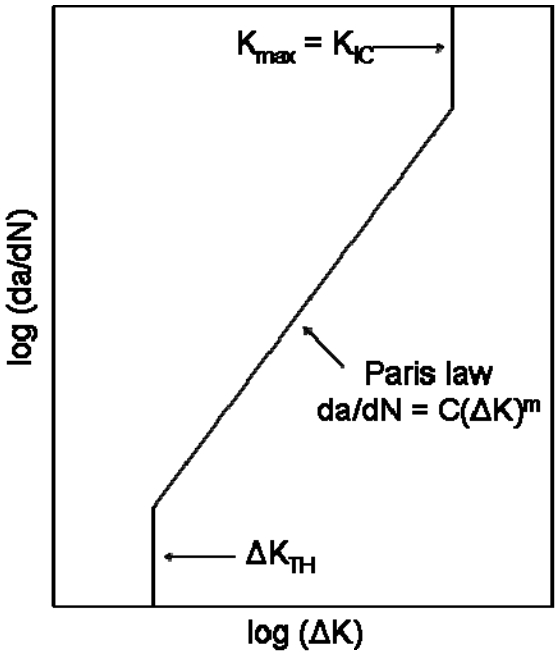

Figure 2.4 Paris crack growth relationship (after Paris and Erdogan, 1963).

As the stress ranges associated with fatigue damage are often low, in comparison with the static stresses associated with fracture, a LEFM characterisation is usually sufficient, and the applied ΔK is the primary parameter used to characterise behaviour. However, other factors can influence a material's response to fatigue loading, and one potentially significant factor is the possible occurrence of what is termed 'crack closure'.

Crack closure results from contact between the crack faces behind an advancing crack tip (Elber, 1970). There are numerous postulated mechanisms for crack closure, for example plasticity, surface roughness and the build up of corrosion or oxidation products (e.g. Suresh and Ritchie, 1982, Ruppen and Salzbrenner, 1983) but all are assumed to result in 'premature' closing of the crack during cyclic loading, thereby reducing the ΔK experienced at the crack tip. The validity of specific models of crack closure remains somewhat controversial (e.g. Vasudevan et al., 1994), but the possibility of crack closure does warrant consideration, particularly where crack closure may occur during laboratory tests (thereby reducing the observed crack growth rate) and such data are then used to derive design curves which are used to predict the behaviour of flaws where crack closure may be less significant. Testing at high R can minimise the influence of crack closure by forcing the crack wider open, although it is not clear whether this is effective when closure is associated with the build up of corrosion products.

2.3 ENVIRONMENT ASSISTED CRACKING

Environment assisted cracking (EAC) is a process whereby cracking is induced or accelerated by the presence of an aggressive environment. It requires the combination of a corrosive environment, a susceptible material and a stress, and includes what may be referred to as stress corrosion cracking (SCC) and corrosion fatigue (Figure 2.5).

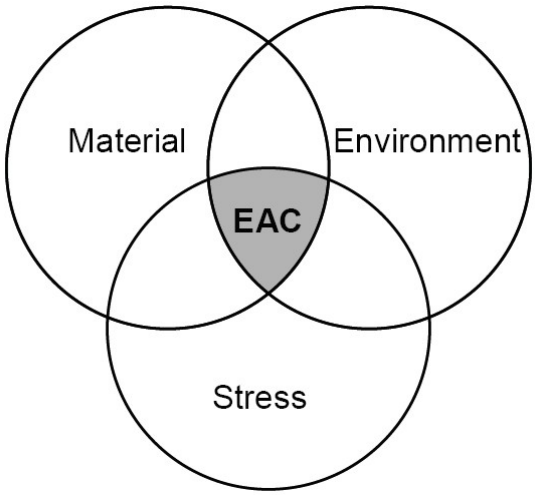

Figure 2.5 Environment assisted cracking refers to the combination of a corrosive environment, a susceptible material and a stress.

SCC is defined as the cracking of metal by the combined action of corrosion and tensile stress (applied or residual), and can cause a massive reduction in a material's strength with minimal material loss (e.g. Humphries et al., 1989). As SCC refers to crack growth under the application of a static rather than cyclic stress, the crack growth rate is specified with respect to time as opposed to cycles. Typical relationships between stress corrosion crack velocity (da/dt) as a function of applied K are shown in Figure 2.6 (McIntyre, 1973, BS 7910, 2005). SCC will not occur unless the applied K is higher than a critical value, termed K_{ISCC}. Above K_{ISCC} stress corrosion cracks tend to grow at a constant rate (assuming no changes to the local stress-state or environmental conditions) until they reach the material's fracture toughness and failure occurs. However, the crack velocity is material-environment specific.

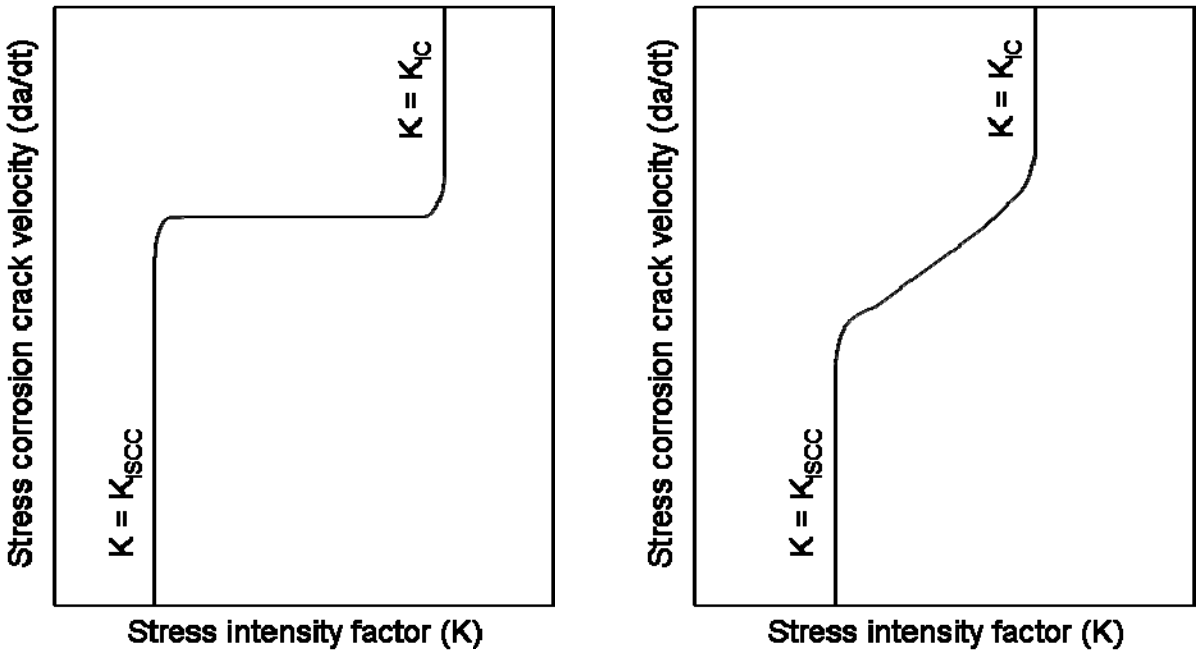

Figure 2.6 Schematic illustration of typical stress corrosion cracking behaviour showing (a) a relatively distinct plateau region of crack growth (after McIntyre, 1973) and (b) a more gradual change in crack growth rate with stress intensity factor (after BS 7910, 2005).

Corrosion fatigue refers to damage or failure of a material as a result of the combined action of cyclic stresses and a corrosive environment. Depending on the particular material-environment combination and the cyclic loading, this can result in higher crack growth rates when compared to standard mechanical fatigue in an inert environment. The role the environment plays in propagating cracks tends to decrease as the loading frequency increases (Atkinson and Lindley, 1977). Because corrosion fatigue is dependent on the specific material, environment and load combination, any quantitative modelling is particularly complex, although various approaches have been proposed (Figure 2.7) e.g. (Gallagher, 1971, Gallagher and Wei, 1971, McEvily and Wei, 1971, Austen and Walker, 1977).

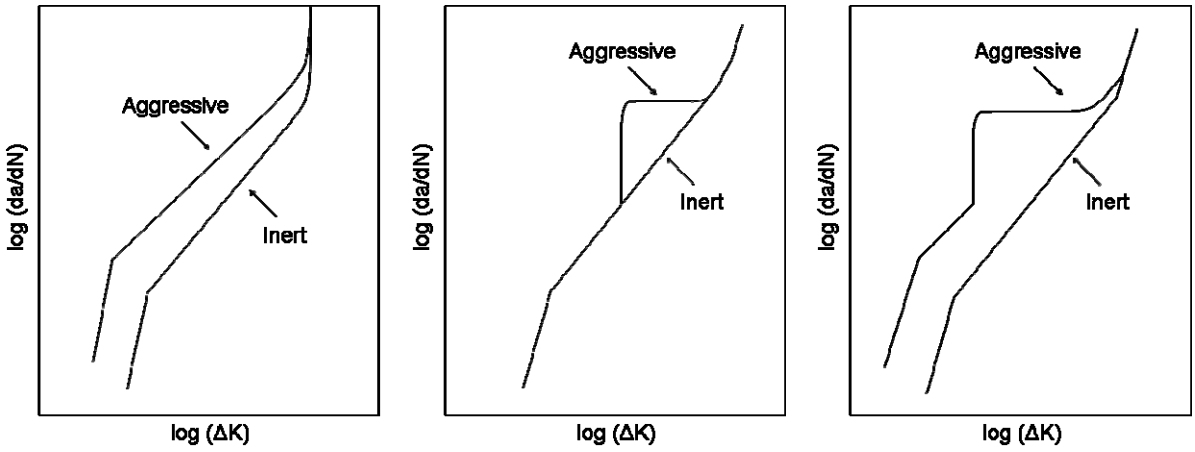

Figure 2.7 Types of corrosion fatigue crack growth (after Austen and Walker, 1977).

The underlying mechanism responsible for EAC will depend on the specific material-environment system under consideration. However, in broad terms, behaviour can be attributable to either localised anodic dissolution or hydrogen embrittlement (Turnbull, 1993).

Many forms of SCC involve anodic dissolution as a key process, and this is usually localised along a susceptible microstructural path such as grain boundaries. Anodic reaction processes are further categorised by Turnbull (1993) as follows:

- Slip-dissolution model.
- Anodic reaction induced cleavage (including film-induced cleavage and dissolution enhanced plastic flow leading to cleavage).
- Surface mobility model.

However, Turnbull also emphasises that there remains much debate over the applicability of such crack growth models due to the complexity of EAC processes. An accurate description of local crack tip reactions and transport phenomenon is acknowledged as being one of the key uncertainties when attempting to model EAC processes (Scully and Gangloff, 2002).

Hydrogen embrittlement involves the absorption of hydrogen atoms onto the surface or into the bulk of a material from the environment. There are many different mechanisms dependent on the material-environment combination of interest. Hydrogen can be absorbed into all metals and the fact that it is a very small atom allows it to diffuse more rapidly than larger atoms. Hydrogen tends to be attracted to regions of high triaxial tensile stress where the metal structure is dilated (e.g. the regions ahead of crack tips or notches that are under stress) and then assists fracture, possibly by making cleavage (brittle transgranular fracture) easier or possibly by assisting in the development of intense local plastic deformation (NPL, 2000). For steels, sensitivity to hydrogen embrittlement tends to increase with increasing alloy strength, although it is not possible to specify a precise strength limit above which problems will occur since many variables play a part, including the composition and microstructure of the steel, the amount of hydrogen in the steel, the applied stress and the severity of the stress concentration. Hydrogen embrittlement is often thought unlikely for modern steels with yield strengths below 600 MPa but likely to become a major problem above 1000 MPa (NPL, 2000). However, previous work at TWI and elsewhere has shown that pipeline steels with much lower yield strengths can be susceptible to some forms of embrittlement. Potential sources of hydrogen include:

- Welding;
- Process fluid/gases;
- Cathodic over-protection (in seawater);
- By-product of corrosion (CO_2, H_2S, crevice corrosion giving low pH).

2.4 SOUR SERVICE

As highlighted previously, a sour environment is defined as one containing water and H_2S. Oil and gas fields can contain significant amounts of H_2S, depending on the geological period from which the fuel is being extracted. The Triassic, Brent and Devonian periods are acknowledged as being periods that are likely to contain H_2S while Tertiary, Upper or Lower Cretaceous and Jurassic are less likely. Wells can also sour over time, often due to the use of enhanced recovery methods such as when water flooding is used to extract oil from the formation. Under static loading conditions, C-Mn pipeline steels exposed to a sour environment can fail via a number of different cracking mechanisms such as hydrogen induced cracking (HIC), stress oriented hydrogen induced cracking (SOHIC) and sulphide stress cracking (SSC).

HIC is a parent material phenomenon whereby the atomic hydrogen, which would normally diffuse into and pass through the steel, becomes trapped and collects at inclusions, bands of segregation and other small defects. The trapped atomic hydrogen recombines to form molecular hydrogen, which is too large to diffuse out of the steel. As more molecular hydrogen accumulates, the pressure builds, leading to localised ruptures and fissures parallel to the plate surface within the steel, or if close to the surface, blistering.

HIC-resistant steels either limit the sulphur content to very low levels (often termed 'clean' steels), to reduce the number of inclusions and potential hydrogen accumulation sites, or control inclusion morphology via additions to hinder crack initiation. HIC takes time to develop whereas SSC, caused by the presence of hydrogen in steel subject to a tensile stress (applied or residual), can occur very rapidly. A higher stress means a higher risk of SSC and, hence, a PWHT can be beneficial. The susceptibility to SSC is known to depend on microstructure, hardness and hydrogen concentration. Weldments, most notably the HAZ, are known to be particularly susceptible to SSC owing to the hardened material (e.g. containing untempered or partially tempered martensite and bainite) in this region (Figure 2.8). SOHIC also requires a tensile stress to develop and describes an array of cracks perpendicular to the applied stress, usually formed by the link-up of small HIC cracks in the steel. SOHIC is most commonly observed in the through thickness direction adjacent to the HAZ of a weld (API/ASME, 2007).

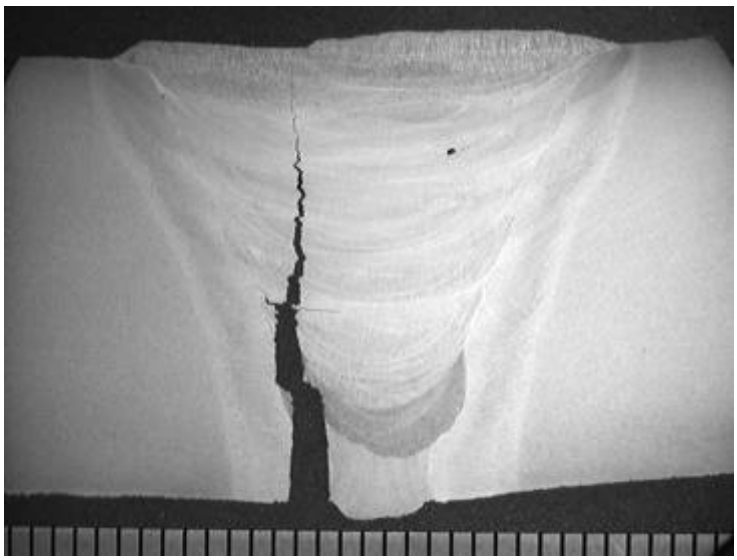

Figure 2.8 Sulphide stress cracking at a weld (mm scale shown).

Susceptibility to SSC is primarily controlled by restricting hardness levels to below a critical level (Pargeter et al., 1990). NACE MR0175/ISO 15156-2 (2003) specifies a 250 HV maximum hardness limit in the root of the weld (base metal, HAZ and weld metal) and 275 HV in the weld cap region (base metal, HAZ and weld metal) for carbon, C-Mn and low alloy steel weldments. This guidance is also referenced in DNV-OS-F101 (2007). Although API 5L (2007) allows grade X70, grade X65 is currently the highest grade of line pipe that is commonly used in offshore sour service applications, as it allows welds to be sufficiently over-matched on UTS while still meeting the 250 HV hardness limit (Noecker et al., 2009). However, many steel and pipe manufacturers are undertaking research with a view to using

higher strength steels in sour service. The precise relationship between hardness and cracking sensitivity depends on both the microstructure of the steel and the severity of the environment (i.e. its propensity to induce hydrogen pick-up) (Gooch, 1982).

The severity of a sour environment with respect to SSC of a carbon or low alloy steel can be evaluated using the domain diagram in NACE MR0175/ISO 15156-2 (2003) and The European Federation of Corrosion (EFC) publication number 16 (2009) (Figure 2.9), which plots solution pH against partial pressure of H_2S. Conditions in Region 1 are not considered to be sour and SSC is not expected to occur. Region 2 is a Transition Region where judgement is required in determining the metallurgical requirements and Region 3 is considered sour service, ie SSC may occur. In many instances Region 2 will also be considered as sour service. The concentration of hydrogen is controlled largely by pH and to a lesser extent by the partial pressure of H_2S. Laboratory testing of metals for resistance to SSC in a sour environment is covered in NACE TM0177 (2005). Corrosion inhibitors can be added to oil wells and/or process streams, via continuous injection or batch treatments, to control SSC by reducing the rate of corrosion and, therefore, the uptake of hydrogen into the steel. Protective coatings that isolate the steel from the sour environment can also be an effective way of preventing SSC.

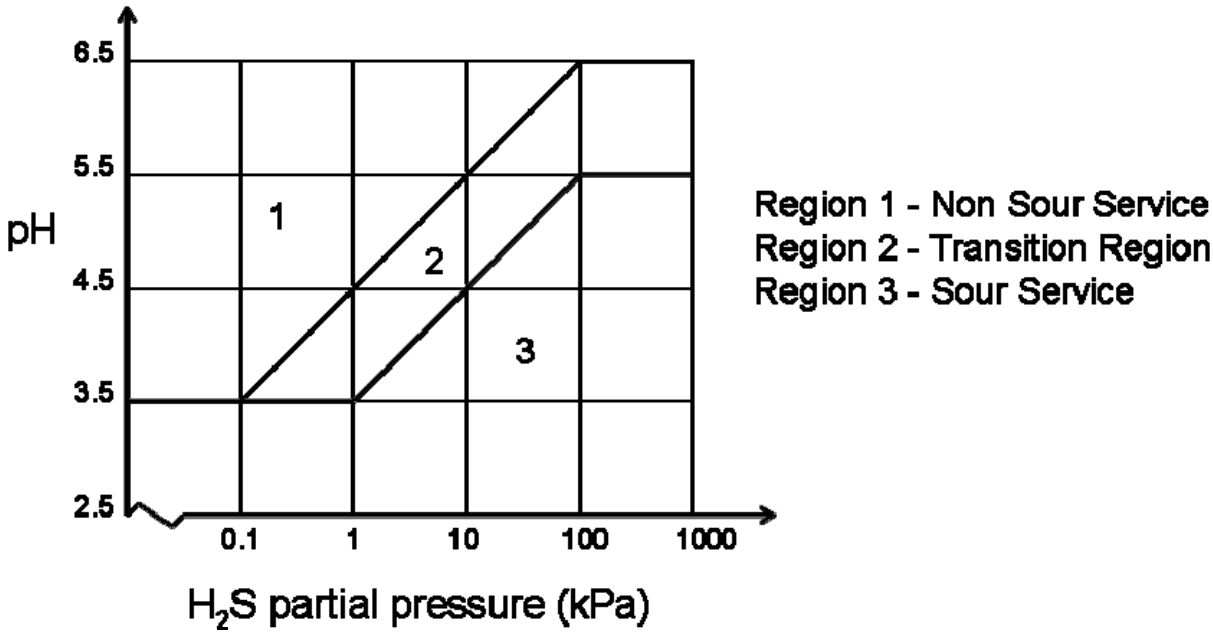

Figure 2.9 Domain diagram for evaluating the severity of a sour environment with respect to sulphide stress cracking of a carbon or low alloy steel (after NACE/ISO, 2003, EFC, 2009).

SSC results from the absorption of atomic hydrogen which subsequently diffuses into the steel. The atomic hydrogen itself is formed as a by-product of the corrosion reaction, as detailed below:

$$Fe + 2H^{+} = Fe^{++} + 2H_{ad} \quad (3)$$

$$2H_{ad} = H_2 \text{ (i.e. hydrogen gas harmlessly evolves).} \quad (4)$$

$$H_{ad} = H_{ab} \text{ (i.e. dissolved hydrogen diffuses into the steel).} \quad (5)$$

This corrosion reaction, which is favoured at acidic pH, involves the anodic dissolution of iron (eqn. 3), and the formation of atomic hydrogen adsorbed onto the steel surface, H_{ad}. This atomic hydrogen can then either recombine to form molecular hydrogen and evolve as gas (eqn. 4), or be absorbed into the steel, H_{ab} (eqn. 5) (Grabke and Riecke, 2000). Importantly, the recombination reaction is poisoned by the presence of an iron sulphide (FeS) scale which forms on the surface of steel in the presence of H_2S, as described by the reaction below:

$$H_2S + Fe = FeS + 2H_{ad} \quad (6)$$

The presence of H_2S therefore encourages the absorption of hydrogen into the steel, a process commonly referred to as hydrogen charging. The presence of absorbed hydrogen in the region of material directly ahead of a crack tip is known to have an adverse effect on the properties of common pipeline steels. A high concentration of hydrogen can cause a significant reduction in fracture toughness (Humphries et al., 1989). It is therefore important to use an appropriate estimate of toughness in fracture mechanics-based structural integrity assessments, although this may not be straightforward as hydrogen embrittlement is itself affected by temperature and strain rate (with the greatest effects observed at ambient temperature and slow strain rate, SSR). The following sections provide a review of published data for pipeline steels exposed to sour environments, firstly under static loading conditions (K_{ISCC} data) and secondly under cyclic loading conditions (corrosion fatigue data).

2.4.1 K_{ISCC} DATA

A review of published K_{ISCC} data (Table 2.1) confirmed that there are relatively few test data for pipeline steels exposed to sour environments. Furthermore, shallow crack data for this material-environment system is particularly sparse.

Table 2.1 Published K_{ISCC} data.

Reference	Material	Hardness	Test Method	Environment	K_I or K_{ISCC} ($Nmm^{-3/2}$ / $MPam^{0.5}$)	σ_Y or σ_{SCC} (MPa)	UTS (MPa)	Notes
Pargeter et al., 1990	Steel (various)	200-250	Notched and un-notched bend specimens	NACE Solution	948-1264 / 30-40	100-120% yield strength		
				Seawater containing 80-100 ppm H_2S	1580-2212 / 50-70			
		250-300		NACE Solution	379-758 / 12-24	20-60% yield strength		
				Seawater containing 80-100 ppm H_2S	1422-1738 / 45-55			
Carneiro et al., 2003	Two steels comparable to API 5L X60 Measured yield strength 460-470 MPa		NACE TM0177-96 Method A using cylindrical tensile specimens and a proof ring	NACE solution		60-70% yield strength (for material in controlled rolled condition)		A refined homogenous quenched and tempered bainite/mertensite microstructure appeared to increase resistance to both HIC and SSC while ferritic-pearlitic microstructures appeared to be more susceptible to SSC
Contreras et al., 2005	Welded API 5L X52		Slow strain rate tensile	Air			391 (25^oC)	All sour tests resulted in failure within the HAZ as expected.
				NACE TM0177-96 solution saturated with H_2S			249 (25^oC) 233 (50^oC)	
	Welded API 5L X70			Air			462 (25^oC)	
				NACE TM0177-96 solution saturated with H_2S			213 (25^oC) 355 (50^oC)	
Tang et al., 2006	Two low alloy steel weldments used for liquefied petroleum gas (LPG) storage tanks		Slow strain rate tensile	Air		328		The higher strength material showed a greater susceptibility to environmental cracking with failure dominated by SSC, as opposed to a combination of HIC and SSC in the lower strength material.
				500 ppm H_2S solution				
				Air		490		
				500 ppm H_2S solution				
Albarran et al., 1999	API 5L X80 plate material		Modified wedge opening loading (M-WOL)	H_2S saturated synthetic seawater	822-1011 / 26-32			Specimens were heat treated to produce a variety of microstructures, and were tested by applying an initial stress intensity factor of 948-1264 $Nmm^{-3/2}$ / 30-40 $MPam^{0.5}$. Initial crack propagation rates were high (approximately $8.8x10^{-9}$ ms^{-1}).
Kumar and Pandey (1985)	Hot rolled microalloyed pipeline steel		Tensile tests using cylindrical specimens and fracture toughness tests using rectangular pre-cracked SENB specimens	Air	3239 / 102.5 (inferred from J)	404	516	J-integral approach used to characterise behaviour due to low strength and high toughness of the steel used. Crack growth rates of $6.3x10^{-3}$ and $3.6x10^{-2}$ $mmhr^{-1}$ recorded for the NaCl and H_2S

				3.5% NaCl (pH5.5)	J_{ISCC} = 40-45 kJm^{-2}			environments respectively indicating that, as expected, the sour environment is far more aggressive than the chloride solution with crack growth rates 5-6 times higher. Results are significantly higher than those determined by Albarran et al., although the steel used did exhibit a lower yield strength.
			Pre-cracked SENB specimens	H_2S saturated acetic acid (pH3.0)	2180-2370 / 69-75 (inferred from J_{ISCC} = 21-25 kJm^{-2})			
Sponseller, 1992	C-90 low alloy steel		NACE TM0177-90 Method D using double cantilever beam (DCB) (This test method utilises a DCB specimen loaded to a fixed displacement, and as the crack grows the applied K decreases until the crack arrests. An estimate for K_{ISCC} can be determined by measuring the final crack depth).	100% H_2S	758-1517 / 24-48			Inter-laboratory comparison. Most of the variation in K_{ISCC} was attributed to differences in the initial applied displacement. Use of a larger initial displacement resulted in higher values of K_{ISCC}. For a larger initial displacement the crack depth associated with a given applied K is higher, and it was argued that for deeper cracks there was reduced access of the environment to the crack tip, and reduced hydrogen charging of the plastic zone, and this led to a higher value of K_{ISCC}.
Yang et al., 2009a	DNV 450 I SUD Measured yield strength 512 MPa		NACE TM0177 Method D (2005) using DCB specimens	NACE Test Solution A (100% H_2S, pH2.7)	948 / 30			
Yang et al., 2009b	ISO 3183-3 L450MCS grade line pipe steel SMYS = 450 MPa		NACE TM0177 Method D (2005) using DCB specimens	NACE Test Solution A (100% H_2S, pH2.7)	1074 / 34			

Assuming a K_{ISCC} value of approximately 30 MPam$^{0.5}$, and a threshold stress σ_{SCC} = 220-440 MPa the transition from K-controlled to stress controlled behaviour should occur at a crack size of approximately 3-6 mm (for Y = 1) (Holtam and Baxter 2007). It is clear that this is a regime of particular interest as flaws of this size are often encountered in pipeline girth welds for instance, and are readily detectable using standard NDT methods. Furthermore, it is the behaviour of flaws of this size that may be dominating the total life of a structure.

2.4.2 FATIGUE CRACK GROWTH RATE DATA

When production fluids are sour, the fatigue resistance of C-Mn steel is significantly degraded in comparison with the performance in air as a result of SSC; the endurance limit is lower (Buitrago and Weir, 2002, McMaster et al., 2007, Buitrago et al., 2008, McMaster et al., 2008) and the FCGR is higher (Baxter et al., 2007, Bristoll and Roeleveld, 1978, Webster et al., 1985, Vosikovsky and Rivard, 1982, Vosikovsky et al., 1983, Watanabe et al., 1998). The

successful design of pipelines or risers is critically dependent on the availability of appropriate experimental data to quantify the extent to which fatigue lives are reduced, and rates of fatigue crack growth are increased, by exposure to sour environments.

Both environmental variables (e.g. pH, temperature, H_2S concentration) and mechanical variables (e.g. ΔK, R, cyclic loading frequency) can influence fatigue performance in sour environments. A recent review of published sour data highlighted the extent to which each of these variables can affect performance (Baxter et al., 2007). Bristoll and Roeleveld (1978) tested non-welded plain C-Mn steel in seawater saturated with H_2S (3000 ppm) at 20^{o}C with $R \geq 0.6$ and a loading frequency of 0.2 Hz. They found that crack growth rates were up to 50 times higher than those observed in air. This contrasts with corresponding tests in seawater (with no H_2S) in which crack growth rates increased by only 2-3 times. The increase in crack growth rate was also seen to be dependent on the ΔK, with a less noticeable increase observed at low values of ΔK. This trend was also reported by Webster et al. (1985) who tested BS 4360 Grade 50D steel in seawater saturated with H_2S at 25^{o}C with stress ratios of 0.05 and 0.07 and a frequency of 0.17 Hz. At intermediate values of ΔK, crack growth rates were approximately 20 times faster than in air whereas at high ΔK the difference was as much as 100 times. The effect of ΔK has also been reported by numerous other researchers carrying out tests in a variety of sour service environments (Vosikovsky and Rivard, 1982, Vosikovsky et al., 1983, Watanabe et al., 1998).

In a more recent study, Eadie and Szklarz (1999a) investigated the influence of several mechanical and environmental parameters on fatigue crack growth. A medium strength low alloy steel was tested in a sour dilute brine at 30^{o}C, and a higher partial pressure of H_2S was found to increase the FCGR. This agreed with earlier work by Vosikovsky (Vosikovsky and Rivard, 1982, Vosikovsky et al., 1983). However, it was noted that the influence of partial pressure was less noticeable at low ΔK and low test frequency (0.1 Hz compared to 1 Hz) (Eadie and Szklarz, 1999a). R did not noticeably influence crack growth rates at medium to high values of ΔK, although a higher R did lower the apparent ΔK threshold (Eadie and Szklarz, 1999b).

A number of researchers have reported a diminished influence of a sour environment at low values of ΔK. In many cases it is behaviour in this low ΔK regime that dominates the prediction of total fatigue life. Experimental crack growth rate data (da/dN-ΔK) are typically determined in simulated operating environments, and upper bound curves can be used in fracture mechanics calculations to calculate critical flaw sizes. Experimental data at low values of ΔK are often determined using a decreasing ΔK type test, where the crack is relatively deep by the end of the test. However, in some instances predicting the behaviour of relatively shallow flaws, using test data derived from specimens containing much deeper flaws, has been shown to be non-conservative.

Several researchers have reported increased crack growth rates in the shallow crack regime and this is often attributed to differences in crack tip chemistry. For example, Gangloff (1985) tested 4130 steel in 3% NaCl solution and observed that shallow cracks (0.1-1.0 mm) grew 6-7 times faster than deep cracks (30-44 mm). Corresponding tests in air gave similar crack growth rates for the two crack sizes, so the effect was above and beyond what might be termed a ‘mechanical crack depth effect’ associated with differences in crack closure. It is, therefore, possible that an ‘environmental crack depth effect’ may occur, even under conditions where the ‘mechanical driving force’ is constant. Gangloff attributed the difference

in crack growth rate to a difference in the crack tip environment, in particular the pH, which led to enhanced hydrogen production and uptake in the case of shallow cracks.

Nakai et al. (1986) examined the behaviour of HY130 steel in 3.5% NaCl under constant ΔK conditions using specimens containing fatigue pre-cracks as shallow as 0.4 mm. Four regimes of behaviour were reported. Regime I was considered to represent the initial growth from the starting crack where the crack growth rate was fairly low. The crack growth rate then increased up to Regime II where a steady-state short crack growth rate was reached. Regime III was a transition between the short crack regime and the long crack regime (IV) and beyond this the crack growth rate again reaches a plateau, lower than in Regime II.

Akid (1994) also provides evidence that shallow cracks behave differently in a corrosive environment compared to air, concluding that the effect of the corrosive environment becomes more significant at low stress levels. In another study, Murtaza and Akid (1995) make the point that only a brief introduction of an aggressive environment can lead to crack propagation and subsequent air fatigue failure. This comment may also be relevant to the use and effectiveness of corrosion inhibitors. For example, a short inhibitor outage may be all that is required for the onset of EAC. Much of Akid's work refers to sub-millimetre sized flaws that are smaller than those investigated in this work.

In other work examining fatigue behaviour in inert environments, it has been suggested that near threshold crack growth rate data can depend on the type of test used, owing to differences in crack closure. Pippan et al. (1994) reviewed three methods for determining the threshold value of ΔK; decreasing ΔK maintaining a constant R, increasing ΔK (on specimens pre-cracked in compression) and decreasing ΔK maintaining constant maximum stress intensity factor (K_{max}). All three methods predicted very similar thresholds at high R. At low R, however, the observed threshold depended on the test method; decreasing ΔK at constant K_{max} gave the lowest threshold value (which would therefore lead to the most conservative assessment) followed by increasing ΔK, with decreasing ΔK at constant R giving the highest threshold values. The authors attributed these differences to crack closure effects.

2.5 FRACTURE MECHANICS-BASED APPROACH FOR ASSESSING ENVIRONMENT ASSISTED CRACKING

As highlighted previously, none of the established FFS standards contain comprehensive assessment procedures for EAC. Methods for evaluating EAC within current integrity assessment procedures are usually based on avoiding the phenomena by limiting the stress (or range of stress for fatigue loading), $\sigma<\sigma_{SCC}$, for crack free components, or limiting the stress intensity factor (or range of stress intensity factor for fatigue loading), $K<K_{ISCC}$, where a crack already exists. In a recent review within the European Fitness-for-Service Thematic Network (FITNET) programme (2008), a number of weaknesses in assessment methods for EAC were highlighted, one of which was material behaviour in the shallow crack regime, where test data are scarce and the assessment method is unclear.

For relatively deep cracks, a threshold stress intensity factor (K_{ISCC}) is an appropriate characterising parameter, as suggested in BS 7910 (2005), and standard test techniques can be used to determine material and environment specific data (e.g. BS 7539 Parts 6 and 9). Similarly, for plain surfaces, where the initiation of cracks is the dominant factor on life, a threshold stress (σ_{SCC}) is appropriate, and again test techniques exist for generating suitable

data (e.g. BS 7539 Parts 2-5 and 7). Shallow cracks fall between these two extremes, and it is currently unclear how behaviour in this regime should be characterised.

2.6 REVIEW OF CURRENT ENVIRONMENT ASSISTED CRACKING ASSESSMENT PROCEDURES

The following section describes the current approach to EAC within the main published FFS assessment procedures.

2.6.1 BS 7910: GUIDE TO METHODS FOR ASSESSING THE ACCEPTABILITY OF FLAWS IN METALLIC STRUCTURES

BS 7910 describes a flaw acceptance criterion as follows:

$$K_I < \frac{K_{ISCC}}{f_{SCC}} \tag{7}$$

where K_I is the applied stress intensity and f_{SCC} is a factor of safety, to be agreed between the parties involved. This results in a modified FAD, similar to that illustrated in Figure 2.10, where for $K_I<K_{ISCC}/f_{SCC}$ the flaw is tolerable, and no crack growth is expected. However, when $K_I>K_{ISCC}/f_{SCC}$ the possibility for stress corrosion crack growth should be recognised. Under these circumstances it is often the case that some remedial action will be taken to prevent further crack extension, such as modification of the environment, elimination of the flaw via component replacement, weld repair, or PWHT. As an alternative it may be possible to assess whether the flaw is likely to grow to an unacceptable size within the design life of the structure or within the appropriate inspection interval. This assessment is based on stress corrosion crack velocity data (da/dt) as a function of K, similar to that depicted in Figure 2.6. It is important to note however that these data are highly specific to the particular material-environment system concerned, and considerable care is required to ensure that the environment chosen for laboratory tests is truly representative of that encountered in service. It is often the case that crack velocity data for the precise application of interest are not available, and in this case no sub-critical crack growth can be tolerated.

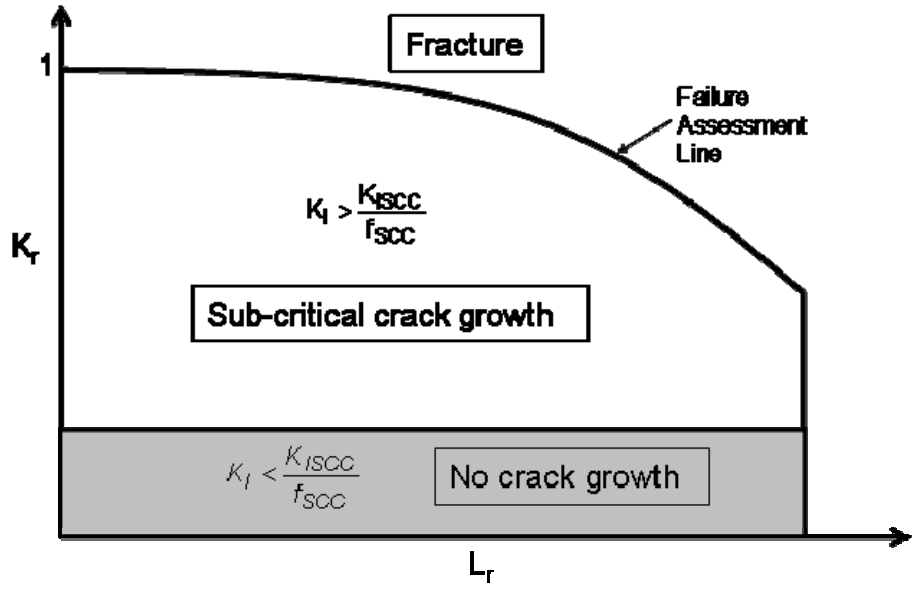

Figure 2.10 Failure assessment diagram incorporating cut-off for stress corrosion cracking (after BS 7910, 2005 and FITNET, 2008, p9-11).

In such cases where crack extension via SCC is not tolerated, an alternative methodology is to define the FAD envelope in terms of 'sour service' properties, for example using K_{ISCC} as the measure of material fracture toughness (Figure 2.11). This differs slightly from the approach defined in documents such as BS 7910 (2005), but is believed to be conservative. This approach is the subject of ongoing research at TWI and elsewhere.

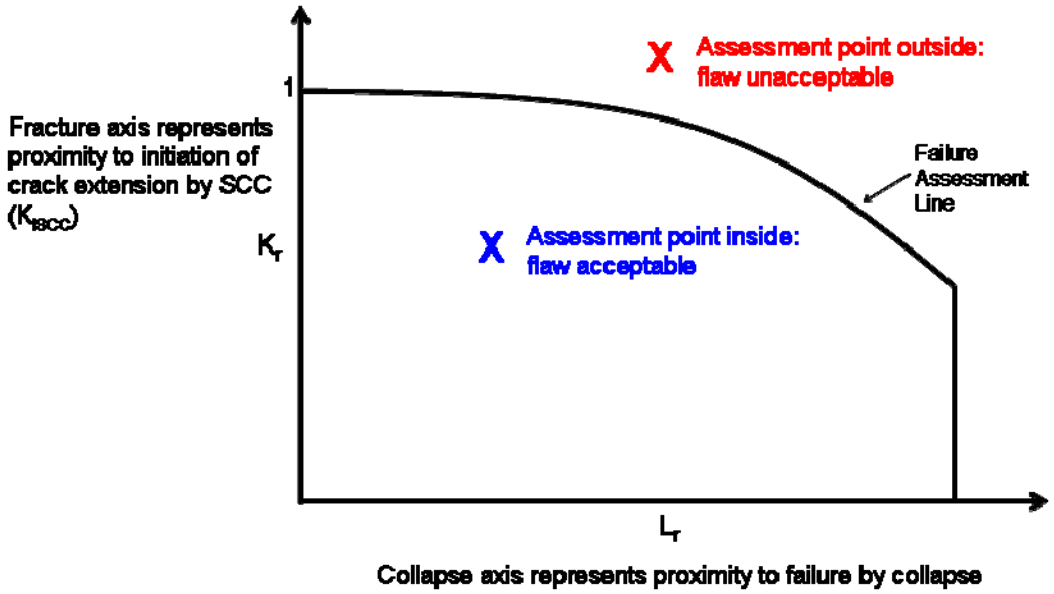

Figure 2.11 Failure assessment diagram envelope defined in terms of 'sour service' properties (e.g. using threshold stress intensity factor for stress corrosion cracking as the measure of material fracture toughness).

2.6.2 API 579-1/ASME FFS-1: FITNESS-FOR-SERVICE

Part 9 of the joint publication API 579-1/ASME FFS-1 adopts a similar approach to BS 7910 (2005) for the assessment of crack-like flaws, and states that the material properties used in an assessment should take account of any change over time as a result of, for example, ageing, service environment or past operation. Fracture toughness can be a key parameter and Annex F in API 579-1/ASME FFS-1 provides guidance on how to derive a lower bound estimate of fracture toughness. In particular it focuses on ferritic steels that may be hydrogen charged as a result of prolonged exposure to the service environment. As material specific data are often not available, a lower bound toughness is defined based on crack arrest data. It is argued that fracture initiation is enhanced by the presence of hydrogen, but that once rapid unstable crack propagation starts, hydrogen can no longer keep pace with the growing crack. The resistance to rapid crack propagation increases with increasing propagation rate, which decreases until an equilibrium subcritical crack growth rate is reached between crack growth and hydrogen delivery rate. It is proposed that crack arrest data can therefore be taken as a conservative estimate of the toughness of a steel containing dissolved hydrogen. However, this approach does not provide a threshold against subcritical crack growth.

API 579-1/ASME FFS-1 Part 7 provides assessment procedures for hydrogen blisters and hydrogen damage associated with HIC and SOHIC. However, the procedures in this new section explicitly exclude SSC, and hydrogen embrittlement of high strength steels (with hardnesses above HRC22 or tensile strength above 793MPa) (API/ASME, 2007).

2.6.3 BRITISH ENERGY R6 PROCEDURE

Similar to BS 7910 (2005) and API 579-1/ASME FFS-1 (2007), the British Energy R6 (2001) assessment procedures use a two-parameter FAD approach to combine ductile and brittle failure mechanisms. Crack growth due to EAC processes is again described in terms of fracture mechanics parameters, such as K_{ISCC}, and avoidance of cracking is ensured by adopting a criterion similar to that in eqn. 7. The R6 document also mentions the need for care when considering fatigue crack growth in an aggressive service environment. It stresses the importance of considering the influence of crack depth on the crack tip environment, and makes the recommendation that test data should be derived from specimens containing cracks of a size comparable to those being assessed.

2.6.4 FITNET: FITNESS-FOR-SERVICE PROCEDURE

The European FITNET document (2008) is structured along similar lines to the other published procedures described above, but also provides a review of assessment methods for EAC. It highlights a number of weaknesses in current materials testing and integrity assessment procedures, in particular, highlighting the importance of only using data relevant to the actual environmental and loading conditions.

2.7 APPROACHES TO MODELLING EAC IN THE SHALLOW CRACK REGIME

EAC generally progresses from initiation to propagation in a number of phases. Jones and Simonen (1994) describe the following sequence of events:

1. Initiation;
2. Short (i.e. shallow) crack growth;
3. Stage I growth;

4. Stage II growth;
5. Crack coalescence;
6. Failure.

For stage I and stage II growth, cracks are usually large enough to be characterised in terms of the applied K. Most experimental data are associated with stage II growth, where a plateau in the crack growth rate is often encountered, as illustrated in Figure 2.6(a). Stage I growth precedes this period and describes a regime where the crack growth rate increases rapidly (as the applied K increases). Experimentally, stage I and stage II data are usually determined from specimens containing cracks that are very much deeper than those typically seen in service. There is a paucity of data in the shallow crack regime.

Assessment procedures therefore focus on quantifying the behaviour of relatively deep cracks (Sections 2.5 and 2.6). However, the analysis implicitly assumes that K is an appropriate characterising parameter, which will not be the case in the shallow crack regime. Conventional test techniques to determine K_{ISCC} (or da/dt) use fracture mechanics specimens containing relatively deep fatigue pre-cracks. For crack sizes greater than some minimum, the data generated may be independent of crack depth. However, it has long been recognised that small cracks may behave differently from deep cracks.

Shallow cracks tend to be categorised as one of the following (Jones and Simonen, 1994, Suresh, 1991):

- Mechanically small (with respect to crack tip plasticity);
- Microstructurally small (relative to grain size);
- Physically small (< ~1 mm);
- Chemically small (environment at the crack tip may be different from the bulk environment).

The first work to highlight the 'shallow crack problem' was based on fatigue test data, which showed that size independence broke down when the crack was small compared with the extent of crack tip plasticity or microstructure. The Kitagawa-Takahashi diagram, first introduced in 1976 (Kitagawa and Takahashi, 1976), describes the relationship between crack size and the observed threshold stress range ($\Delta\sigma_{TH}$). For deep cracks, data lie on a straight line (on a log scale) and this represents a condition of constant threshold stress intensity factor range (ΔK_{TH}). However for shallow cracks, crack growth was observed at applied ΔK values lower than the deep crack threshold (ΔK_{TH}), and tended towards the smooth specimen threshold stress range ($\Delta\sigma_{TH}$). Models for the transitional behaviour were based on determining an 'effective' stress intensity factor range (ΔK_{eff}) that took into account the extent of crack closure, which was significantly less in the shallow crack regime.

The work referenced in Section 2.4.2 clearly shows that shallow fatigue cracks can grow faster than deep fatigue cracks, at the same ΔK, and, therefore, highlights the potential non-conservatism in assessing shallow flaws based purely on deep crack data. Similarly, there is some evidence to suggest that shallow stress corrosion cracks may grow faster than deep cracks under static loading conditions, although in some cases it is found that crack growth rates may in fact be slower (Jones and Simonen, 1994).

The FITNET document highlights the need for caution when assessing shallow cracks using conventional fracture mechanics calculations, and introduces the concept of a two-parameter approach to the assessment of EAC, similar to that shown in Figure 2.12. This diagram describes a transition between K-controlled and stress-controlled behaviour as the crack size is reduced, and emphasises the need for care in the shallow crack regime as the critical stress may be lower than that obtained by extrapolating the deep crack data. As crack size decreases, departure from the K-controlled regime is of course inevitable, and is not necessarily linked with environmental effects associated with differences in crack tip chemistry. The Kitagawa-type graphical representation shown in Figure 2.12 does not of course say anything about the *rate* of crack growth, it simply suggests that in the shallow crack regime the 'threshold stress' is expected to be lower than anticipated by extrapolating the deep crack data. This will of course be true even in the absence of an environmental crack size dependence associated with differences in crack tip chemistry, as the mechanical driving force will no longer be characterised by the parameter K.

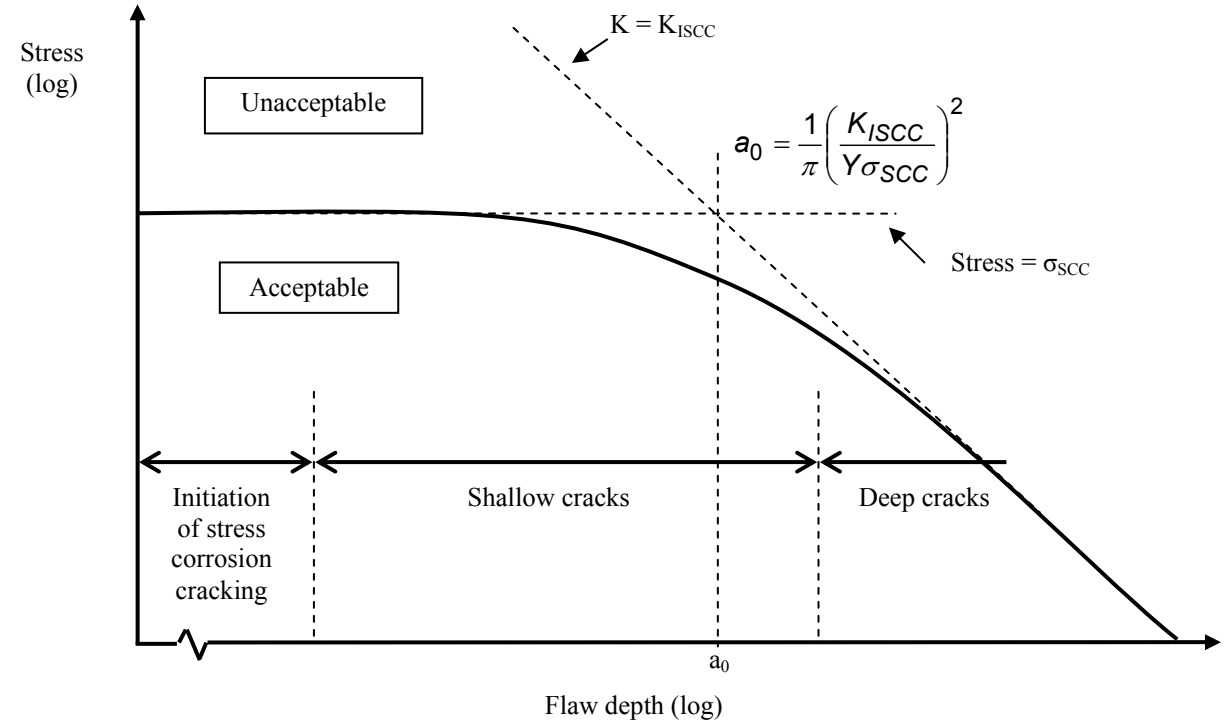

Figure 2.12 Two-parameter approach to stress corrosion cracking (after FITNET, 2008).

A rather different approach to modelling the early stages of EAC has been reported by Turnbull et al. (2006). This work focused on predicting the transition between pitting and cracking in a steam turbine disc steel. The transition between pit and crack was modelled in terms of a process competition between the rate of pit growth and the rate of crack growth, the latter being described by a power law for shallow cracks, and a constant for cracks deeper than a critical value. This was a similar approach to earlier work carried out to model the transition between pitting and fatigue cracking (Kondo, 1989, Chen et al., 1996). By using a Weibull distribution to create an initial set of corrosion pit depths it was possible to predict the evolution of pits into cracks in a way that was consistent with available experimental data. Cracks were assumed to be of equal depth to the pit at the point of transition. However, more

recent work suggests that the Kondo approach is not sufficient to model the complex process of pit to stress corrosion crack transition (Turnbull et al., 2009). It was noticed that after short exposure times, several cracks may initiate from a pit before coalescing into a single crack after longer exposure times.

There are clearly a number of ways that the early stages of EAC may be modelled. The diagram in Figure 2.12 describes one aspect of the shallow crack problem, in that the appropriate characterising parameter changes from K to stress as the crack size decreases. In the transitional regime, models developed to explain the nature of this transition will rely on the availability of suitable shallow crack test data, such as that generated as part of this research project for the specific material-environment system of a C-Mn pipeline steel in a sour environment.

The importance of crack tip chemistry and the potential influence that this has on observed thresholds or crack growth rates should also be noted. Crack size dependency associated with differences in crack tip chemistry may of course occur over a different scale to that described in Figure 2.12, where the shallow crack regime is essentially defined by the relative magnitude of K_{ISCC} and σ_{SCC}. Different types of testing procedure may be applicable in each of these cases.

2.8 SUMMARY OF THE RELATED WORK AND IDENTIFICATION OF NOVELTY IN THE CURRENT WORK

In many practical situations behaviour in the shallow crack regime will dominate the overall life of structures containing typical fabrication flaws, therefore an improved understanding of material behaviour and the development of appropriate assessment procedures are of high importance. There is a lack of shallow crack data in the public domain, particularly for pipeline steels and girth welds exposed to sour environments. Much of the data generated as part of this research project are, therefore, novel. In order to provide such data, novel test methods have been developed and these will lead to ‘best practice’ recommendations for carrying out corrosion fatigue tests in a sour environment, possibly as an extension to existing standards. The test matrix was structured such that the underlying mechanism responsible for the observed behaviour, which is not well understood, could be investigated. The novel data generated have also been applied to real-life pipeline defect assessments, with a view to developing an improved assessment method.

3 RESEARCH METHODOLOGY

This research project is predominantly quantitative and, in addition to a review of the literature, has implemented a worldwide industry survey aimed at gathering valuable market information, and generating extensive unique data through a variety of laboratory-based tests. Laboratory testing has focused on filling identified gaps in existing published data, as identified in Section 2, to improve the understanding of the behaviour of shallow surface flaws in C-Mn pipeline steels exposed to sour environments, under both static and cyclic loading conditions. The test data generated have also been applied to real-life ECAs of direct relevance to the offshore oil and gas industry. The fundamental reason for performing laboratory tests is to reproduce in-service conditions without having to test large and complex structures such as offshore installations for an unfeasibly long time (e.g. 30 years). Often it is possible to predict how a structure will behave based on laboratory test data subject to a certain level of conservatism (commonly referred to as safety factors) to account for uncertainties, estimates and any assumptions made. However, the challenge of exactly reproducing in-service conditions in a laboratory environment should not be underestimated. For example, the stresses generated in the lab may not match the stresses in the field, the material may not be exactly the same grade or the welding procedure may be slightly different.

This section begins by reviewing different methods for performing fracture toughness and FCGR tests, including the different specimen geometries that are available and methods for monitoring crack extension. Considerations specific to testing in a sour environment are then discussed along with methods for introducing and monitoring shallow surface flaws. Finally the defect assessment approach is introduced. In each case the methods most relevant to this research project are identified.

3.1 FRACTURE TOUGHNESS TESTING

Fracture toughness is a critical material input parameter in any structural integrity assessment, and where possible estimates of toughness should be based on laboratory tests using specimens made from materials and welds representative of those in service. When appropriate material is available for testing, the two main standards covering fracture toughness test methods are BS 7448 (in four parts) and ASTM E1820 (2008). While these standards are very similar, only BS 7448 gives specific advice with respect to testing welds (in Part 2, 1997), which is relevant to this research project. A number of specimen geometries may be used; all contain a pre-existing flaw of some type, usually introduced at a notch through fatigue cycling. The most popular geometries are the single edge notched bend (SENB) specimen or the compact tension (CT) specimen (Figures 3.1 and 3.2).

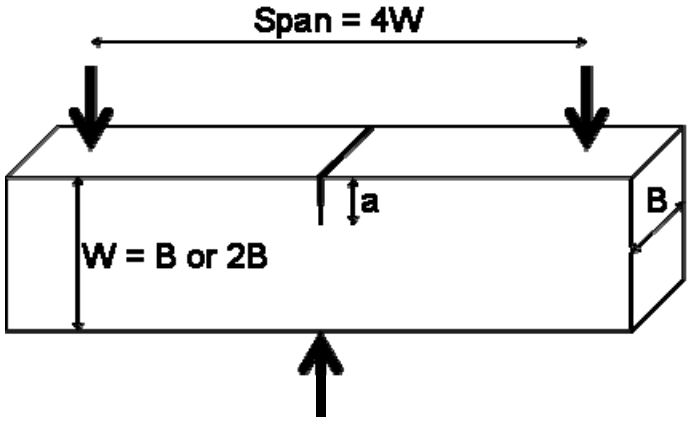

Figure 3.1 Single edge notched bend specimen geometry (loaded in three point bending).

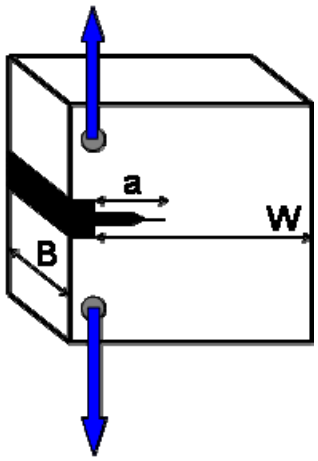

Figure 3.2 Compact tension specimen geometry.

Both of these specimen geometries give a high level of crack tip 'constraint' which helps to ensure that derived values of fracture toughness are conservative and are, therefore, appropriate for subsequent use in predicting the behaviour of material under a wide range of service loading conditions. However, in some circumstances the use of a test specimen exhibiting a lower level of crack tip constraint can be justified, as long as the level of constraint expected in service is lower than that used during testing. An example of this is the single edge notched tension (SENT) specimen (Figure 3.3), which is widely used to quantify the fracture toughness of pipeline girth welds. Data derived from tests on this type of specimen can only be used when the level of constraint associated with service loading conditions can be shown to be lower than those in the SENT specimen. For typical conditions experienced during the installation of pipelines, it is generally accepted that this is likely to be the case (e.g. Chiesa et al., 2001). However, during operation of the pipeline, some loading conditions (such as internal pressure superimposed on global bending) are more complex and it is not straightforward to demonstrate conservatism. For operational loading, it is therefore common practice to use fracture toughness data derived from SENB or CT specimens, and as this research focuses on material behaviour exposed to sour (operating) environments, all tests have been carried out using SENB specimens. A study into the use of SENT specimens for tests in a sour environment has recently been reported elsewhere (Yang et al., 2009a, Yang et al., 2009b).

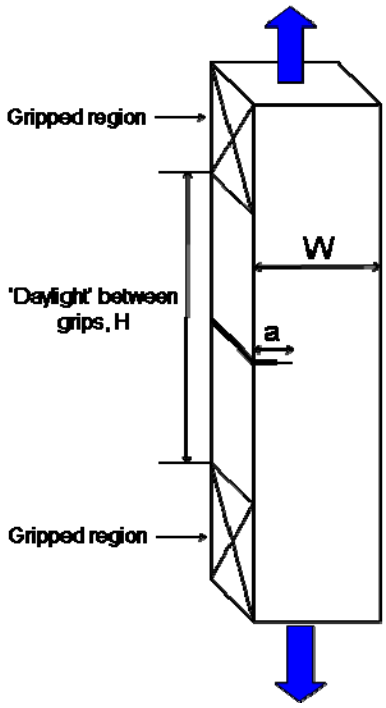

Figure 3.3 Single edge notched tension specimen geometry.

Regardless of the specimen geometry being used, the location and orientation of the notch is important, particularly for welded joints, to ensure crack growth is measured through the desired microstructure. BS 7448-2 (1997) gives detailed guidance on how so-called 'weld-positional' or 'specific microstructure' tests may be carried out. BS 7448 and ASTM E1820 also give detailed 'validity criteria' to ensure that test data are reproducible and appropriately conservative, particularly in terms of the shape, size and position of the flaw. For example, it is necessary to ensure that the crack tip plastic zone, as a result of fatigue pre-cracking, is small compared with the plastic zone produced during subsequent testing. This is achieved by limiting the loads used during fatigue pre-cracking, but can lead to experimental difficulties, for example when trying to introduce shallow pre-cracks.

Having introduced a suitable fatigue pre-crack, fracture toughness tests are then performed by loading the specimen (usually in displacement control) while monitoring the force, displacement, temperature and other relevant environmental parameters. Detailed guidance is provided in BS 7448-1 (1991). The equation used for determining the applied K for a SENB specimen is as follows:

$$K_Q = \frac{F_Q S}{BW^{1.5}} \times f\left(\frac{a_0}{W}\right) \qquad (8)$$

where:

$$f\left(\frac{a_0}{W}\right) = \frac{3\left(\frac{a_0}{W}\right)^{0.5}\left[1.99 - \left(\frac{a_0}{W}\right)\left(1 - \frac{a_0}{W}\right)\left(2.15 - \frac{3.93a_0}{W} + \frac{2.7{a_0}^2}{W^2}\right)\right]}{2\left(1 + \frac{2a_0}{W}\right)\left(1 - \frac{a_0}{W}\right)^{1.5}} \qquad (9)$$

3.2 FATIGUE CRACK GROWTH RATE TESTING

FCGR tests are carried out using similar fracture mechanics test specimens as those used for fracture toughness tests. SENB and CT specimens are again the two most widely used geometries. A cyclic load is applied using a universal servo-hydraulic testing machine with computer control and data logging and the crack depth is recorded as a function of the number of applied loading cycles. The two main standards covering FCGR testing are BS ISO 12108 (2002) and ASTM E647 (2008).

3.2.1 MEASUREMENT AND MONITORING OF CRACK EXTENSION

A variety of methods may be used to monitor the growth of fatigue cracks during testing, the two most common being those based on measuring the change in either specimen compliance or electrical resistance. Details are again provided in BS ISO 12108 (2002) and ASTM E647 (2008).

All FCGR tests conducted in this research project used the direct current potential drop (DCPD) technique, where two wires were resistance welded to the specimen, one either side of the crack. A constant current was then passed through the specimen (i.e. across the crack plane) and the measured potential difference across the crack used to determine the crack depth. According to the latest version of ASTM E647 (Annex A6, 2008), DCPD wires should be attached diagonally at either edge of the specimen, so that the measured electrical resistance provides an estimate of the average crack depth for non-uniform crack fronts. However, TWI's established procedures for conducting such tests in a sour environment involve attaching the wires across the entire width of the specimen. No noticeable difference in the performance of the DCPD system has ever been observed using this approach, and measurements of crack depth at the end of the test are generally in very good agreement with those predicted from the DCPD system.

A current (10-40 amps, depending on specimen size) is passed through the specimen, which is electrically insulated from the load frame, and the potential difference between the two sides of the crack is measured. Rather than leaving the current on throughout the test, the current is switched on and off at regular intervals and readings taken. This prevents the specimen from heating up as the current passes through it, and avoids the possibility of current flow interacting with electrochemical processes occurring at the crack tip. Through appropriate calibration (derived either experimentally, analytically or numerically) the potential drop measured on either side of the crack plane can be related to the crack depth. As crack depth increases, the area of the remaining ligament decreases, resulting in an increase in electrical resistance and an increase in potential difference. At TWI the crack depth is derived from the instantaneous voltage (v) between the two wires using the analytical expression below (Cooke and Robinson, 1973).

$$a = \frac{2W}{\pi}\cos^{-1}\sqrt{\left[\frac{1-B_1^{\,2}}{B_2 - B_1^{\,2}B_3}\right]} \tag{10}$$

where:

$$B_1 = \frac{e^{v/2k}-1}{e^{v/2k}+1} \tag{11}$$

$$B_2 = \sec h^2\,\frac{\pi f}{2W} \tag{12}$$

$$B_3 = \sec h^2\,\frac{\pi d}{2W} \tag{13}$$

and:
W = specimen width;
f = distance between wire and crack plane;
d = distance between current input and crack plane;
k = calibration coefficient.

The calibration coefficient for each specimen is obtained from an observation of crack depth (a_{cal}) at a corresponding voltage (v_{cal}) by using:

$$k = \frac{v_{cal}}{2\log_c\left[\mathrm{mod}\left(\frac{\alpha+\beta}{\alpha-\beta}\right)\right]} \tag{14}$$

where:

$$\alpha = \sqrt{\mathrm{mod}\left[\sec h^2\,\frac{\pi f}{2W}\cos^2\frac{\pi a_{cal}}{2W} - 1\right]} \tag{15}$$

$$\beta = \sqrt{\mathrm{mod}\left[\sec h^2\,\frac{\pi d}{2W}\cos^2\frac{\pi a_{cal}}{2W} - 1\right]} \tag{16}$$

Resolution depends on the material conductivity and precise specimen geometry, but is typically 10-20 μm, depending on the quality of equipment used, and the maximum systematic error in crack depth is estimated to be approximately ±2%. No correction for crack front shape is used but after each test the specimen is broken open after immersion in liquid nitrogen and the fracture surface examined to determine the initial and final crack depths based on a weighted nine point average, as described in BS 7448-4 (1997). Each time a voltage reading is taken, the total number of cycles and loads are also recorded. Crack growth

rates (da/dN) are determined using an incremental secant method (BS ISO 12108, 2002) and a measurement interval of 0.2 mm. The corresponding ΔK is then calculated having determined K_{max} and K_{min} using eqn. 8. Depending on the test duration and the extent of corrosion it is not always possible to determine the initial crack depth for tests performed in a sour environment. Figure 3.4 shows a FCGR specimen mounted in an environmental test rig, instrumented with a DCPD system.

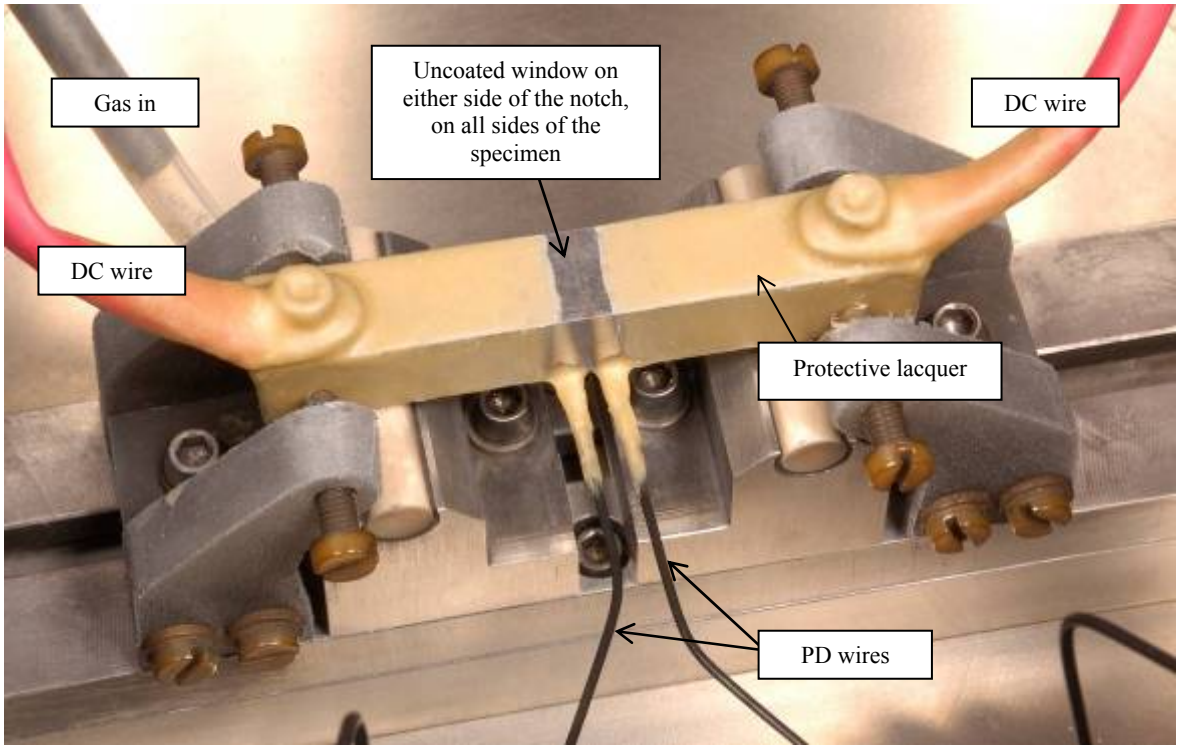

Figure 3.4 Single edge notched bend fatigue crack growth rate specimen mounted in an environmental crack growth rig, instrumented with a direct current potential drop system.

3.2.2 TYPES OF FATIGUE CRACK GROWTH RATE TEST

There are a number of different methods for determining FCGR data as a function of applied ΔK. For moderate or high values of ΔK the simplest way is to conduct the test under conditions of constant applied load range. As the crack extends the applied ΔK will naturally increase and the crack will accelerate. This test method may be referred to as 'increasing ΔK' and is necessarily carried out at a fixed R. For shallow flaws this method is inconvenient as it requires fatigue pre-cracking to be carried out at low ΔK which is time consuming.

An alternative is therefore to conduct the test under conditions of 'decreasing ΔK' by continually shedding the applied load range at a specified rate. A maximum permissible rate is specified in testing standards to ensure that test data are not influenced by prior loading cycles. A 'decreasing ΔK' test may be conducted under conditions of either constant R or constant K_{max}, by controlling the minimum and maximum loads accordingly. The use of load shedding to maintain a constant R is the standard decreasing ΔK test technique as described in ASTM E647 (2008) and BS ISO 12108 (2002), but testing under conditions of constant K_{max} is potentially useful for minimising the extent of crack closure at low ΔK. Environmentally-induced crack closure might be expected to be most pronounced under decreasing ΔK conditions because the rate of crack extension is lowest at the end of the test when ΔK is also lowest and corrosion product build-up is expected to be highest.

A further option is to conduct tests under conditions of 'constant ΔK' by continually shedding the applied load as above, but in such a way that the decrease in load range counteracts the increase in crack depth. This provides a means of exploring the influence of other testing parameters, as observed variations in crack growth rate can then be attributed to factors other than the applied ΔK. Although care is needed when interpreting this type of test data, this approach can be used to examine the influence of parameters such as microstructure (different areas of a weld or HAZ for example), cyclic loading frequency and crack depth.

3.3 TESTING IN SOUR ENVIRONMENTS

3.3.1 TYPES OF TEST

For pipelines carrying sour production fluids the appropriate measure of toughness for assessing internal surface-breaking flaws in ECA calculations is K_{ISCC}. A variety of test techniques are available to quantify the performance of material in simulated sour service environments, for example constant load tests using SENB specimens, constant displacement tests using DCB specimens and SSR tests.

Fracture mechanics tests use a fatigue pre-cracked specimen loaded and immersed in an appropriate sour environment, which has direct access to the crack tip, as in the case of an actual internal surface-breaking flaw. The two specimen geometries that are most popular for this type of test are the SENB (Figure 3.1) and the DCB (Figure 3.5).

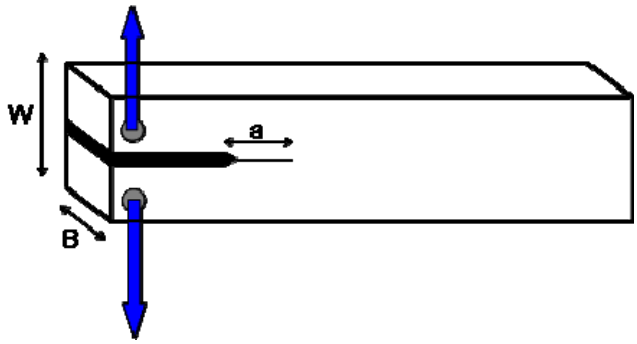

Figure 3.5 Double cantilever beam specimen geometry.

DCB specimens are tested under conditions of constant displacement, and K decreases as crack growth occurs. Threshold data are therefore associated with deep cracks, so this specimen geometry is clearly not appropriate for examining the behaviour of shallow flaws. When using SENB specimens, test duration is typically 720 hours (30 days) to allow sufficient time for the environment to interact with the material. By testing multiple specimens containing the same crack size at different loads, K_{ISCC} can be determined. Reproducibility of crack depths can be problematic, hence the need to repeat tests on nominally identical specimens at the same load.

In practice a programme of K_{ISCC} testing can be both time consuming and expensive, since each test will only provide one data point. It is possible to use step load tests initially to give a broad estimate of K_{ISCC}, whereby the load is increased each week (based on an initial conservative estimate of K) until the specimen fails. A series of constant load tests (720 hours duration) can then be targeted close to the threshold to back up the results of the step load

tests. Figure 3.6 shows a SENB specimen loaded in a K_{ISCC} test rig; the environmental test chamber has been removed to allow the specimen to be viewed.

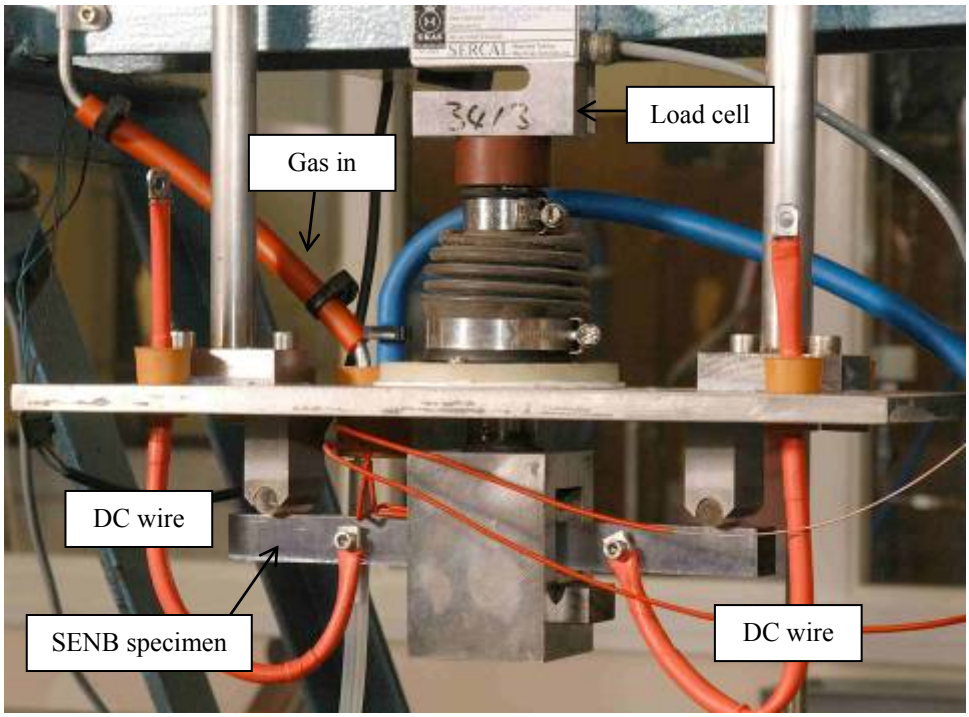

Figure 3.6 Single edge notched bend specimen mounted in constant load test rig; sour test chamber has been removed.

SSR tensile tests are often used to determine overall 'susceptibility' to EAC in a given environment but this approach can be overly aggressive, particularly if the 'ductility ratio' is used as an indicator. This is due to the material being dynamically strained in the corrosive environment, which is unlikely to occur in service. Also, post yield, the ductility is more likely to drop than the strength which again is not wholly relevant to in-service conditions. For fracture mechanics tests, a significant advantage of testing under SSR conditions is that they can provide a result in a reasonably short timeframe, say 3-5 days. However, the concern then is that the tests may be non-conservative as they may not allow sufficient time for the environmental effect to be maximised. However, one could also argue that dynamic loads occur in real-life structures and that a totally static load is unrealistic. BS 7539 (Part 9, Figure 13, 2003) refers specifically to SSR fracture mechanics tests and provides a typical plot of K_{ISCC} versus displacement rate, which decreases and then reaches a plateau. The key is demonstrating that the plateau has genuinely been reached.

Similar considerations are required when conducting FCGR tests in a sour environment which, in some instances, can be long (e.g. >1 month) in duration. A number of additional complications also arise. Recalling Figure 3.4, a protective coating is applied to the specimen to protect the bulk of the specimen and instrumentation (e.g. DC and PD wires) from the corrosive environment and to minimise the extent of solution contamination. Typically a 10 mm window is left uncoated on each side of the notch on all sides of the specimen to allow interaction between the environment, the local surface and the crack tip.

SENB specimens are appropriate for examining the behaviour of shallow flaws and were selected for both constant load and FCGR tests in a sour environment in this research project.

3.3.2 ENVIRONMENTAL CONTROL

There are a number of environmental variables to consider when testing in a sour environment. For surface-breaking flaws, temperature, solution pH and the partial pressures of H_2S and/or CO_2 are all important parameters that can influence material behaviour. In some cases it may be possible to consider a 'worst case' environment but it is not always clear what, or even where, this might be. Moreover the use of such an environment in laboratory testing may lead to highly conservative results. Therefore, TWI usually recommends carrying out tests in an environment which mimics (as closely as possible) the conditions expected to occur within the real pipeline or riser. Testing at ambient temperature, low pH and with a high partial pressure of H_2S tends to maximise the environmental effect associated with hydrogen embrittlement/SSC.

All tests were carried out at 25°C (±3°C). For the static testing programme specimens were immersed in standard NACE Test Solution A (NACE, 2005). The specimen was immersed in an aqueous solution of 5% sodium chloride acidified to a pH of approximately 2.5-3.0 using acetic acid. This solution was purged with nitrogen to remove oxygen to less than 20 ppb (measured using an Orbisphere) and a test gas of 100% H_2S was then introduced at 0.1 MPa. This combination of pH and partial pressure of H_2S falls in Region 3 of the domain diagram (Figure 2.9).

For the FCGR testing programme, specimens were immersed in an aqueous solution of 5% sodium chloride and 0.4% sodium acetate, acidified to a pH of approximately 3.5 using acetic acid. This solution was also purged with nitrogen to remove oxygen to less than 20 ppb. A test gas of 7% H_2S in N_2 was then introduced at 0.1 MPa. This combination of pH and partial pressure of H_2S also falls in Region 3 of the domain diagram (Figure 2.9). Following an initial fast purge (typically overnight but in all cases at least 7 hours) the gas flow was reduced, but was continuously passed through the test solution to maintain saturation. Ordinarily, cycling commenced immediately after the gas flow had been reduced but the influence of pre-soaking was also explored. Solution pH and H_2S content were monitored at intervals during the test.

3.3.3 HYDROGEN ANALYSIS

As described in Section 2.4, the presence of H_2S in a sour service environment leads to the absorption of hydrogen into the steel, which can lead to the onset of SSC or enhanced rates of fatigue crack growth. Material behaviour may be expected to depend on the concentration of hydrogen within the steel, and there are a number of techniques to determine this experimentally.

Unfortunately there are no simple methods for directly measuring the local concentration of hydrogen as a function of spatial position (for instance ahead of a crack tip). However, the average concentration within a sample can be determined by thermal extraction. The amount of diffusible hydrogen in a steel sample can be determined using gas chromatography, after heating at approximately 150°C for six hours. At room temperature it may take several days for hydrogen to diffuse out of a sample completely but at 150°C total evolution is expected within 6 hours. Diffusible hydrogen is not necessarily the total amount of hydrogen present in the steel. Higher temperature techniques can be used to analyse the total amount of hydrogen in a sample, for instance when investigating the amount of hydrogen in welds made using different consumables. Hydrogen can become 'trapped' at sites such as inclusions and a far higher temperature (e.g. 650°C for ferritic steels) is required to remove all the hydrogen trapped in the steel.

One experimental difficulty when measuring diffusible hydrogen content is the high mobility of hydrogen in steel, even at room temperature, which results in gradual diffusion losses out of the sample. Maintaining a sample at low temperature prior to analysis resolves this issue, although it is recognised that some hydrogen losses will inevitably occur (Jenkins, 1990). The reproducibility of results also remains a challenge. It is necessary to specify rigorous procedures for taking a representative sample, storing the sample and preparing the sample for analysis. A reasonable surface finish is desirable to allow the hydrogen to diffuse out of the steel however it is important not to allow the specimen to heat up significantly during surface preparation. Temperature is often controlled by intermittent immersion in liquid nitrogen.

A possible alternative technique is secondary ion mass spectrometry (SIMS), which can provide a spatial resolution of the order of 1 μm and has previously been used to profile crack tip hydrogen in pre-charged steels. However, there are experimental difficulties associated with using SIMS to evaluate the hydrogen concentration at different regions on a fracture face. The technique relies on a flush surface finish between the sample and the holder as the sample-to-extraction optics require a particular distance so that the electrical field strength is fixed. This was deemed unfeasible to achieve due to surface roughness after testing in a corrosive environment. Measurement of hydrogen concentration as a function of depth would also be extremely difficult.

For the purposes of this research project, gas chromatography, after heating at approximately 150^{o}C for six hours, was selected as being the most appropriate technique for analysing the concentration of diffusible hydrogen in test specimens. This decision was based predominantly on this technique having previously been successfully adopted for similar applications, and the availability of equipment.

3.4 METHODS FOR INTRODUCING AND MONITORING SHALLOW CRACKS

There are several methods available for generating shallow cracks. The most widely used methods involve promoting the initiation of naturally small surface or corner cracks. Rectangular surface crack specimens can be tested in either tension or bending. Three point bending provides a convenient way of localising the crack initiation site (e.g. at a notch). Cylindrical surface crack or rectangular corner crack specimens may also be used, the latter having the advantage that two measurements of crack length or depth can be taken using visual methods.

Electrical discharge machining (EDM) or low stress grinding are the preferred machining methods for introducing small artificial flaws, since they result in lower residual stresses than other operations. However, some pre-cracking is usually required to take the crack tip out of the distressed zone before test data are acquired, so the resulting flaw is inevitably substantially larger than the ‘naturally small’ surface cracks described above. One practical difficulty can then be in generating a uniform pre-crack of the desired shape (i.e. uniform across the entire specimen thickness, or of the desired aspect ratio). Testing straight from an EDM notch eliminates this difficulty, but the flaw is then less representative of those likely in service. An alternative technique is to grow a conventional deep crack (by notching and fatigue pre-cracking) and then machine away some of the specimen material to leave the required physically shallow crack.

A novel solution to the problem is to use accelerated focused ion beam (FIB) milling techniques that can create 'flaws' in almost any material with a precision of a few tens of nanometres (Romano-Rodriguez and Hernandez-Ramirez, 2007). Such a technique could be used in this application to accurately machine extremely sharp notches that would perhaps remove the need for fatigue pre-cracking (Tsui and Joo, 2001). However, generating a FIB notch across the entire width of even a relatively small fracture mechanics test specimen would take an unfeasibly long time to machine and therefore has very high associated costs. FIB technology is a precision tool and there would inevitably be a pay-off between the amount of material removed and the quality and sharpness of the notch being generated.

Another alternative approach for introducing very shallow flaws is to use a nano-scratch technique, which involves moving a sample while being in contact with a diamond tip and can be used to introduce a scratch of the order of 5-10 μm deep. This could be used either as a shallower alternative to EDM notching (i.e. followed by fatigue pre-cracking in air prior to testing) or to initiate a crack directly from the nano-scratch in the sour environment during testing.

A summary of the techniques discussed above is provided in Table 3.1. The range of interest for typical weld flaws is 1-2 mm upwards and a conventional EDM notch followed by fatigue pre-cracking was deemed the most appropriate method for flaw depths greater than 1 mm. The method of machining away an over-sized specimen containing a conventional deep crack (to leave a shallow flaw) was also used. For shallower flaws (i.e. <1 mm) other methods would need to be explored. Short practical trials were performed to assess the merits of both FIB and nano-scratch techniques but as yet technical challenges remain for the current desired application. For such shallow flaws the DCPD method of measuring crack depth is also brought into question. In an inert environment it is possible to periodically interrupt a test and take measurements during a test but in a sour environment this is not considered to be feasible.

Table 3.1 Summary of techniques for generating shallow cracks.

Technique	Resolution	Advantages	Disadvantages
EDM Notch	0.3-0.5 mm	Reproducible	Less representative of in-service cracks
Fatigue pre-crack	>1 mm	Representative of in-service cracks	Tricky to obtain uniform crack
Machine away part of conventional deep crack	-	Representative of in-service cracks	Time consuming. Wasted material.
Natural fatigue crack	<0.3 mm	Representative of in-service cracks Appropriate for SSR or constant load SSC tests	Labour intensive.
FIB machining	>10 nm	Novel, precision milling technique	Highly specialised equipment Specimen dimensions limited to 150mm (diameter) x 20mm Time/cost constraints for notching SENB specimens
Nano-scratch	5-10 μm	Novel, precision technique.	Limits on maximum specimen dimensions. Time/cost constraints for scratching SENB specimens.

A variety of methods have been developed to measure the growth rate of small fatigue cracks. Many of these techniques are discussed in ASTM Special Technical Publication STP 1149 (ASTM, 1992). In addition to the DCPD technique described previously, replication is perhaps the most precise method of measuring surface crack length, where small pieces of thin cellulose acetate sheet are softened with acetone and applied to the specimen surface. Subsequent examination, using either an optical or scanning electron microscope, enables surface crack length to be measured to within 0.1-1.0 μm. Periodic replication can be used to monitor crack growth and although this is clearly a more labour intensive procedure it would provide a way of introducing very small flaws that could then be used in subsequent constant load or FCGR tests. The main disadvantage of replication to monitor crack extension during a test is that it requires interruption of the test, making it unfeasible to apply in a sour environment, for example.

Direct observation of surface cracks (during testing) using either optical or scanning electron microscopy does provide a way of monitoring fatigue crack growth without interrupting the test. However this requires the use of highly specialised equipment, such as a loading stage located within the SEM chamber, and neither technique is particularly suitable for monitoring crack advance associated with SSC.

A summary of the methods for monitoring crack growth described above is shown in Table 3.2. The DCPD method was selected for monitoring crack growth in the current work, primarily because its use had been trialled in a sour environment, but also because many specimen geometries are amenable to the technique.

Table 3.2 Summary of methods for monitoring crack growth.

Technique	Resolution	Advantages	Disadvantages
DCPD	10-20 μm	No interruption of test Equipment readily available Adequate resolution for SCC	-
Replication	0.1-1.0 μm	Good resolution	Interruption of test
Direct Observation	-	No interruption of test	Highly specialised equipment Not appropriate for SCC

3.5 DEFECT ASSESSMENTS

As highlighted previously, a fracture mechanics-based approach can be used to provide maximum allowable flaw sizes at the manufacture and installation stage to ensure that, for example, pipeline girth weld flaws do not reach a critical size during the projected life of the component. The benefit of an ECA approach is that, often, a larger acceptable flaw size can be demonstrated than relying solely on the workmanship requirements in offshore codes and standards (eg DNV, 2007).

In the current research, defect assessments have been performed within the framework of BS 7910 (2005), using TWI's software, CRACKWISE 4. BS 7910 is the most widely used procedure in the oil and gas transportation (i.e. pipeline) industry for the assessment of crack-like flaws (Section 4.2) (Holtam et al., 2010c) and is widely regarded as the benchmark for assessing weld defects, with many of the procedures having been developed by TWI.

TWI's commercial software package CRACKWISE 4 automates the fracture and fatigue assessment procedures in BS 7910, to assist engineers in performing ECA calculations (Figure 3.7). Critical flaw sizes can be calculated for a wide range of flaw geometries based on a number of input parameters such as applied and residual stresses, material properties, fracture toughness and weld misalignment. An additional benefit of the software is the ability to perform sensitivity analyses for the critical input parameters.

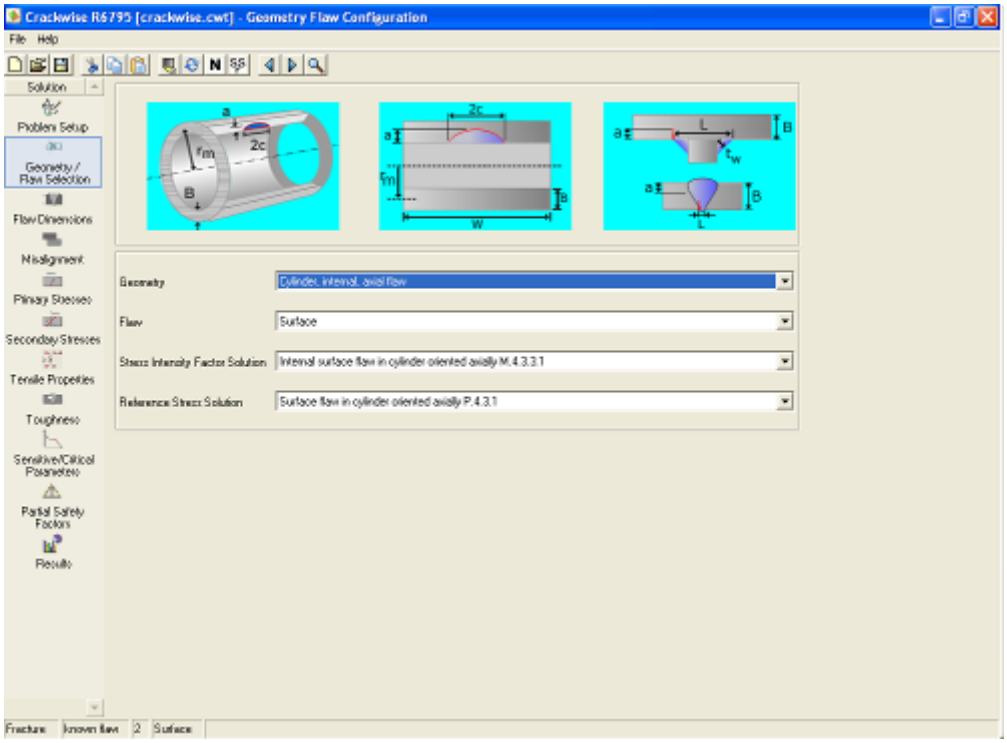

Figure 3.7 Screenshot from TWI's CRACKWISE 4 software.

3.6 SUMMARY

This section has reviewed the experimental procedures pertaining to fracture toughness and FCGR testing in a sour environment. The different specimen geometries and methods for monitoring crack extension that are available have been reviewed, along with methods for introducing and monitoring shallow surface flaws. Finally the defect assessment approach was introduced. In each case the methods most relevant to this research project were identified, taking specific consideration of the need to perform tests in a sour environment. Section 4 presents the results of the research undertaken using the methodologies identified above. An overview of the research carried out is presented in Figure 3.8.

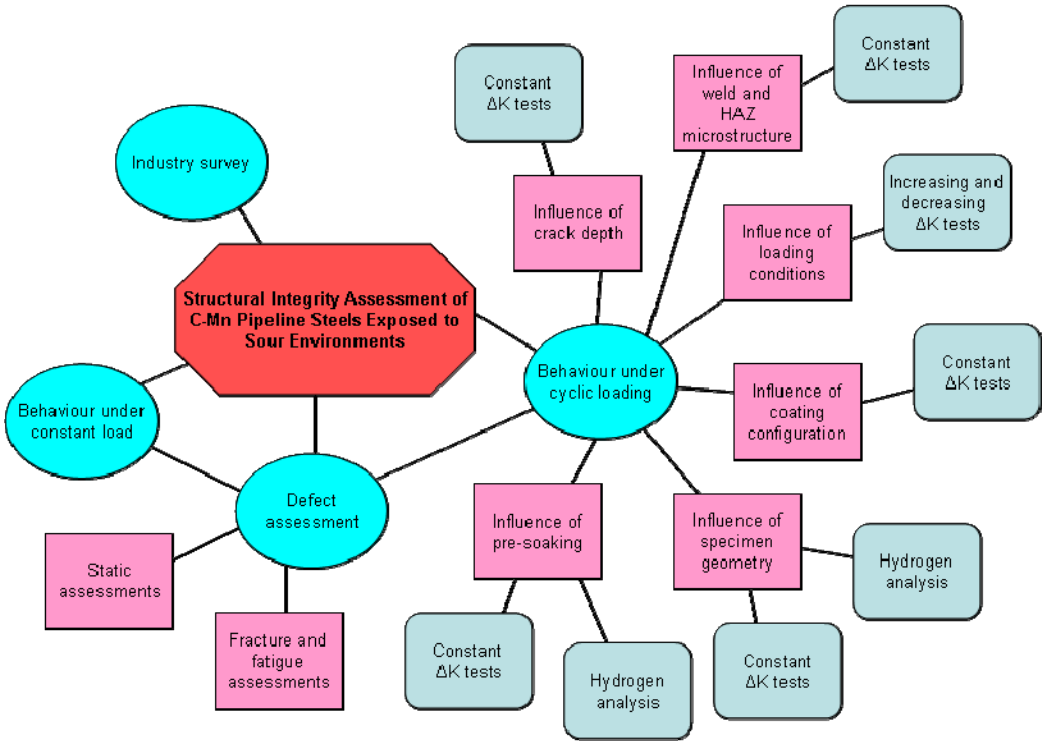

Figure 3.8 Overview of the research carried out.

4 ENGD RESEARCH

4.1 RESEARCH DEVELOPMENT PROCESS

As highlighted in Section 1, the need to further develop technical expertise in assessing the integrity and behaviour of structures which are prone to EAC is an identified 'hot topic' for TWI's Structural Integrity Technology Group. Such research needs are developed based on discussions with, and feedback from, TWI's external Research Board, a committee of representatives from TWI Industrial Member companies whose main function is to determine the content, and guide the progress of TWI's Core Research Programme. At the beginning of this research project, a brainstorming meeting was held with a selection of senior TWI technical personnel from the Structural Integrity, Materials and Corrosion, and NDT Technology Groups. The purpose of this meeting was to gain a wider understanding of the issues surrounding EAC and to try to gauge the key issues industry was facing. A summary of possible research areas that resulted from this brainstorming meeting is provided in Table 4.1.

Table 4.1 Key issues surrounding environment assisted cracking.

Issue/Research Area	Target Sector
Chloride induced SCC in austenitic and/or duplex stainless steels: to build on previous TWI research projects in this area with a particular focus towards assessment procedures.	Oil and Gas
Pitting vs. cracking: when is a pit smooth enough to avoid using fracture mechanics and what implications does this have on the inherent conservatisms in current assessment procedures such as API 579, BS 7910, FITNET, B31.G? Under what conditions do pits transform into cracks? How best to detect and monitor pitting, including pitting under insulation? Possible comparison with crevice corrosion? (This work would most likely be looking at carbon steels for offshore pipelines and onshore pressure vessels but several environments could be investigated such as H_2S, CO_2 etc.).	Oil and Gas/Power
Do hydrogen blisters actually propagate into cracks long-term, and if so how is this related to their internal pressure?	Oil and Gas
How do aggressive environments affect weldments? Topics might include, for example, preferential weld corrosion, HAZ cracking, dissimilar metal joint cracking.	Oil and Gas
An investigation into the suitability of weld repair procedures for components used in corrosive environments.	Oil and Gas/Power
An investigation into the assessment of CO_2 corrosion, for which numerous assessment models exist. How does one account for differing morphologies?	Oil and Gas
Assessing colonies of environmental cracks (e.g. SCC, SSC, HIC, SOHIC): is it possible to halt SCC and analyse statically? Why do we model damaged regions as a semi-ellipse/ellipse/cone?	Oil and Gas/Power
An investigation into the effect of stress raisers and discontinuities on volumetric flaws: under what circumstances do they become crack-like?	Oil and Gas
Practical guidelines on how to report flaws detected by NDT (embedded and/or surface-breaking) for subsequent use in recognised assessment procedures? What makes a defect reportable?	Oil and Gas
SCC in stainless steels with a particular focus towards assessment procedures.	Power
An investigation into the occurrence of corrosion fatigue in steam plant.	Power
Development of risk-based best practice guidelines for assessing steam lines in both conventional and supercritical power plants.	Power
An investigation into steam oxidation resistance of 9-12%Cr boiler tubes.	Power
An investigation into the occurrence of vibration fatigue in steam turbine plant.	Power

Subsequent to this meeting, it was agreed that this research project should focus on improving the procedures used to assess the significance of shallow surface flaws in offshore pipelines and risers operating in sour environments. Figure 4.1 provides an overview of the research

development process. Initially literature reviews were instigated to examine the current best practice methods for the assessment of EAC and to establish the extent of published data for pipeline steels in a sour environment, under both static and cyclic loading conditions. One of the key findings was that shallow crack test data is particularly sparse in aggressive corroding environments such as wet H_2S, perhaps due to the small number of dedicated sour testing facilities in the world. Consequently, there is a lack of guidance on the methods for generating shallow crack data in existing test standards (e.g. BS 7539-9, 2003) and the assessment of EAC in general (Section 2). Therefore, any data generated in a sour environment is somewhat novel.

In parallel with the literature reviews, an industry survey was also developed and distributed. This was aimed at gaining an insight into how structural integrity assessment procedures are viewed and used throughout industry. One of the key findings of this survey (Section 4.2), with respect to the current research, was confirmation that assessment procedures for EAC require further development. Figure 4.1 also illustrates that research carried out as part of the TWI's Core Research Programme is reviewed internally and presented annually to the Research Board, to demonstrate progress and to ensure research quality and alignment with current industry needs.

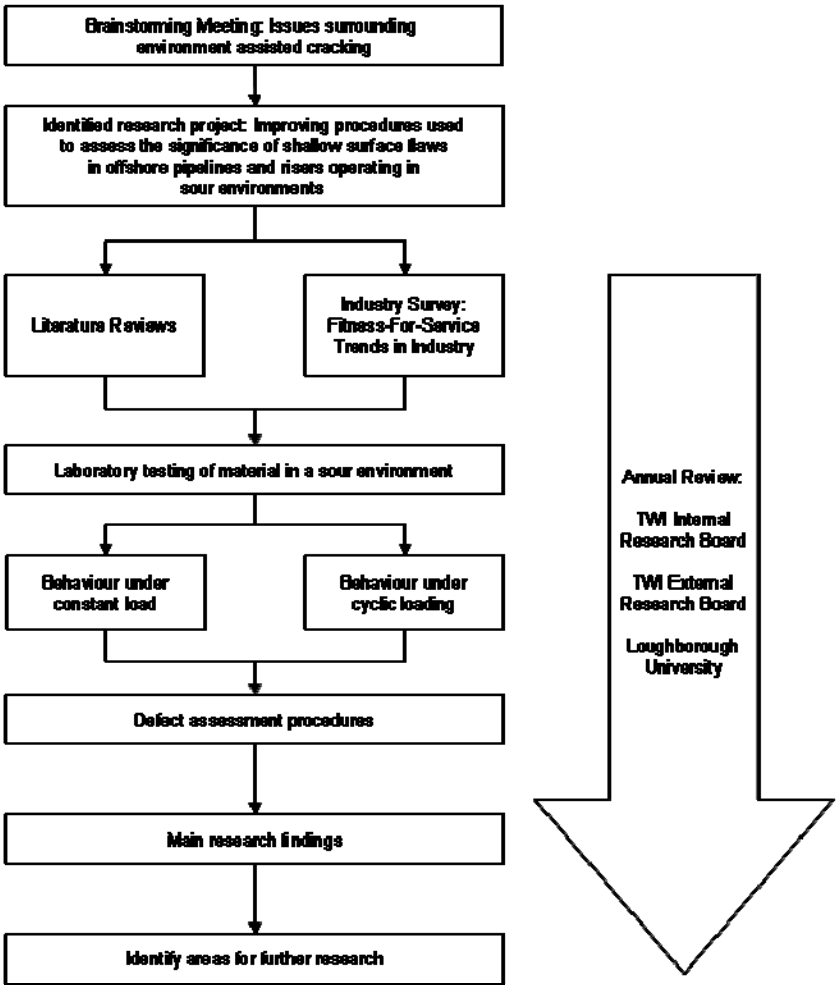

Figure 4.1 Overview of research development process during this EngD research project.

Two testing programmes were developed initially, to address the identified gaps in the published data by investigating the influence of crack depth on the behaviour of C-Mn pipeline steels exposed to sour environments under both static and cyclic loading. Both test programmes were initially with respect to parent material, however, pipeline girth welds were later also tested under cyclic loading conditions. A key aspect of any EngD is demonstrating the application of new knowledge in an industrial situation. The new knowledge generated via the fatigue testing programme (and to a certain extent the static testing programme) was therefore applied to a real-life ECA of a circumferential surface-breaking flaw on the internal surface of a steel catenary riser (SCR), located at a girth weld and subject to vortex induced vibration (VIV) fatigue loads. A novel assessment approach using a four stage FCGR law was developed to demonstrate the possible implications/benefits of incorporating reliable sour test data generated at low ΔK into ECAs.

A detailed description of the research undertaken is provided below. Reference is made to each of the papers published during this research project. Five published papers are reproduced in full in **Appendix A to E**. Additional publications that resulted from this EngD research project are also referenced.

4.2 INDUSTRY SURVEY

At the start of this research project a survey aimed at evaluating the latest FFS trends in industry was developed. The results of the survey were presented at the *2008 ASME Pressure Vessels and Piping Division Conference* and subsequently accepted for publication in the *ASME Journal of Pressure Vessel Technology*, and are reproduced in full in **Appendix A** (Holtam et al., 2010c). The survey was not specific to EAC in the oil and gas industry but aimed to gain an insight into current FFS trends across several industry sectors and how these may change in the future. Information was gathered as to how different companies handle their FFS activities, both in terms of the types of flaw they assess and the complexity of the assessments they undertake. The survey also investigated how safety regulating authorities view FFS activities and whether or not they accept the results as the basis for plant integrity management decisions.

The survey proved to be very successful compared to previous surveys (Iravani and Speck, 2002, Filiou et al., 2003) with 197 completed surveys being received, demonstrating that FFS assessment techniques are now widely used throughout industry. Approximately three quarters of respondents came from the oil and gas industry and approximately one third considered their organisations to have a worldwide operating presence. API 579-1/ASME FFS-1 was found to be the most widely used published assessment procedure within the oil and gas and petrochemical industry sectors, considering all damage mechanisms. However, among those companies who assess fracture most frequently, BS 7910 was confirmed as the most widely used. The survey suggested that structural integrity assessments are now accepted by 80% of safety regulating authorities around the world as the basis for assessing the condition of plant for continued operation, which is a significant increase compared to five years previously (Iravani and Speck, 2002). This is indicative of how much more widespread and better understood the quality and potential benefits of FFS techniques are and emphasises the industrial relevance and importance of the current research project.

The survey confirmed that EAC is one of the most common problems faced throughout the oil and gas industry (Figure 4.2) (Holtam et al., 2010c). This is interesting because, although industry's knowledge and experience of EAC has improved markedly over recent years, it is

still not well covered in the main published assessment standards. Most published procedures simply point out that EAC is complicated, highlight the importance of only using data relevant to the actual environment and loading conditions and suggest that expert assistance be sought. This is perhaps one of the reasons why in-house assessment procedures still feature widely throughout the oil and gas sector (Figure 4.3) (Holtam et al., 2010c). Complex assessment cases, such as EAC, require a degree of pragmatism and, therefore, a codified approach is not always possible or indeed appropriate.

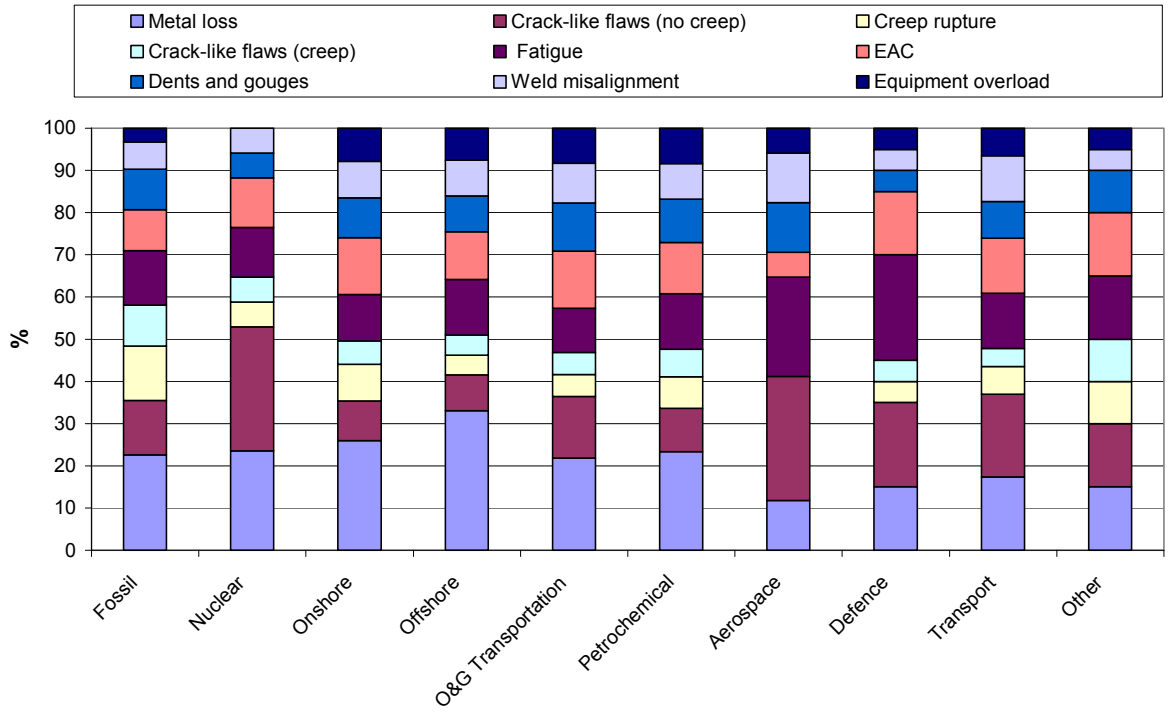

Figure 4.2 Frequency of use of Fitness-For-Service assessment procedures by survey respondents' companies.

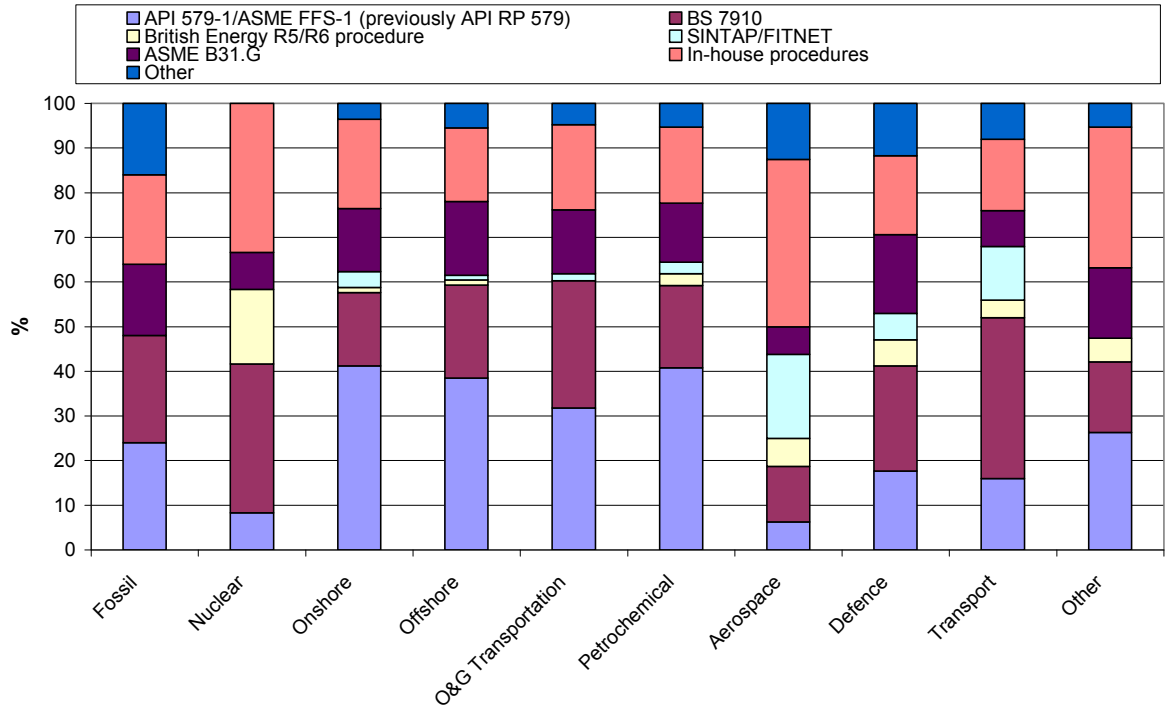

Figure 4.3 Frequency of use of published Fitness-For-Service assessment procedures by survey respondents' companies.

4.3 LABORATORY TESTING OF MATERIAL IN A SOUR ENVIRONMENT

4.3.1 BEHAVIOUR UNDER CONSTANT LOAD

The key results from the investigation into material behaviour under constant load are described in a paper published in the *Journal of Offshore Mechanics and Arctic Engineering (OMAE)* (Holtam et al., 2009a), reproduced in full in **Appendix B**. The material used in this testing programme was seamless C-Mn line pipe parent material to API 5L grade X65. The supplied pipe had an outer diameter of 355.6 mm (14 inch) and a wall thickness of 20.6 mm. Tests were carried out to confirm the properties of the material. The chemical composition of the steel, determined using optical emission spectrometry (OES), is summarised in Table 4.2. Hardness and tensile property data are shown in Table 4.3.

Table 4.2 Chemical composition of the API 5L X65 C-Mn steel used for the tests on parent material (wt.%), balance Fe.

C	Si	Mn	P	S	Cr	Mo
0.11	0.28	1.12	0.010	0.003	0.082	0.11
Ni	B	Cu	Nb	Ti	V	
0.099	0.0003	0.14	0.018	0.002	0.058	

Table 4.3 Hardness and tensile property data for the API 5L X65 C-Mn steel used.

Hardness, HV10	196
UTS, MPa	576
0.2% proof stress, MPa	478

Square section SENB specimens were extracted from the pipe material. Specimen geometry was B = W = 16 mm, and testing was in three point bending using a span (S) of 200 mm. Specimens were notched using EDM to introduce a starter notch approximately 0.5 mm deep. This notch was oriented circumferentially with respect to the pipe in order to simulate crack growth in the through thickness direction, from the internal surface of the pipe (Figure 4.4). This starter notch was then subjected to fatigue loading (R = 0.1, cyclic loading frequency up to 100 Hz) to provide several different flaw sizes, ranging from a total fatigue pre-crack depth of 1.6 mm (a/W ~ 0.1) to 8.0 mm (a/W ~ 0.5), based on surface measurements either side of the specimen.

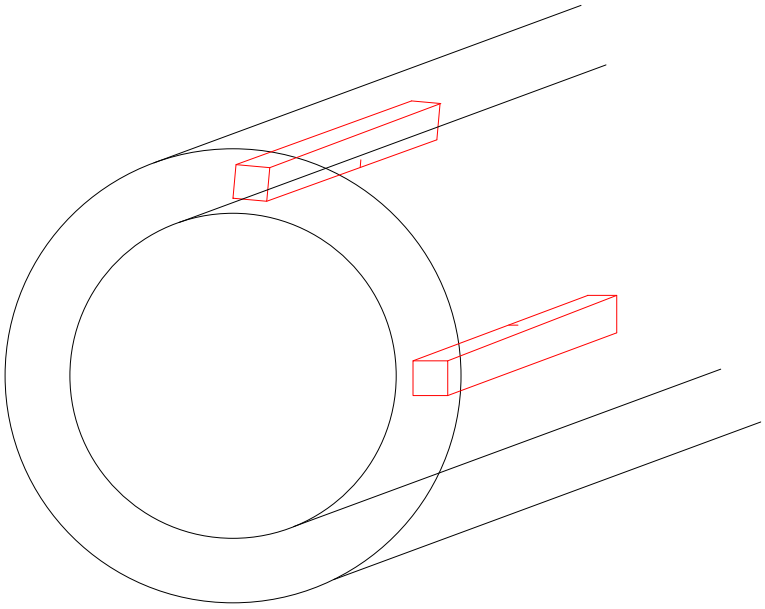

Figure 4.4 Orientation of specimen notch relative to pipe.

Specimens were tested under conditions of constant load. A summary of the crack depths tested, based on a weighted nine point average BS 7448-4 (1997) measured after breaking each specimen open, can be found in Table 4.4. This table shows the specimen identification number, the initial crack depth, the load applied during the test, a calculated K (BS 7448-1, 1991) and an indication of whether the specimen failed or not. Prior to the testing in a sour environment two calibration tests were carried out in air; one deep crack (specimen pre-cracked to a/W ~ 0.5) and one shallow crack (specimen pre-cracked to a/W ~ 0.1). Tests were carried out in a standard servo-hydraulic testing machine with computer control and data logging, and were instrumented with a clip gauge to provide a load-displacement plot and allow determination of J or CTOD.

Table 4.4 Constant load test results - pre-cracked specimens (after Holtam et al., 2009a).

Specimen ID		Actual Flaw Size, a (mm)	Test Parameters		Result
Thesis	Published Paper		Load (kN)	K ($Nmm^{-3/2}$ / $MPam^{0.5}$)	
CL1	M02-07	8.24	1.51 1.90	813 / 26 1023 / 32	Step load test (1-week at each applied load until specimen failed)
CL2	M02-08	8.33	1.51	828 / 26	Constant load test Specimen still intact after 720 hrs
CL3	M02-09	7.92	1.70	859 / 27	Constant load test Specimen still intact after 720 hrs but crack extension visible
CL4	M02-10	8.47	1.80	1016 / 32	Constant load test Specimen failed after ~180hrs
CL5	M02-21	8.36	1.60	883 / 28	Constant load test Specimen failed after ~40hrs
CL6	M02-13	2.10	4.90 6.10	906 / 29 1128 / 36	Step load test (1-week at each applied load until specimen failed)
CL7	M02-16	2.18	4.90	922 / 29	Constant load test Specimen still intact after 720 hrs
CL8	M02-17	1.60	5.60	918 / 29	Constant load test Specimen failed after ~200 hrs
CL9	M02-26	1.55	5.30	857 / 27	Constant load test Specimen failed after ~365 hrs
CL10	M02-19	3.69	3.60 4.60	887 / 28 1133 / 36	Step load test (1-week at each applied load until specimen failed)
CL11	M02-20	5.34	2.60 3.30 4.00	834 / 26 1058 / 33 1283 / 41	Step load test (1-week at each applied load until specimen failed)
CL13-OS	M07-01	1.11	8.1	1157	Constant load test. Applied load 8.1 kN Specimen still in tact after 720 hrs
CL14-OS	M07-02	0.91	9.0	1168	Constant load test. Applied load 9.0 kN Specimen failed after ~120 hrs
CL15-OS	M07-03	1.11	8.5	1276	Constant load test. Applied load 8.5 kN Specimen still in tact after 720 hrs

The first two tests in a sour environment were step load tests; one at a flaw depth of a/W ~ 0.5 and one at a flaw depth of a/W ~ 0.1. The load was increased each week, based on an initial conservative estimate of K, until the specimen failed. A series of constant load tests (720 hours duration) were then targeted close to the threshold at both a/W ~ 0.5 (deep flaw) and a/W ~ 0.1 (shallow flaw) to back up the results of the step load tests. At the end of the test programme two additional step load tests were carried out at intermediate crack depths, a ~ 3 mm and a ~ 5 mm. An un-notched specimen was also step loaded to failure (Table 4.5).

Table 4.5 Constant load test result - un-notched specimen (Holtam et al., 2009a).

Specimen ID		Actual Flaw Size, a (mm)	Test Parameters		Result
Thesis	Published Paper		Load (kN)	Stress (MPa)	
CL12-UN	M02-23	Un-notched	6.0 7.0 8.0 9.0 10.0 11.0	439 513 586 659 732 806	Step load test (1-week at each applied load until specimen failed) Failed when test was increased to 11.0 kN

In all cases the loads applied in the sour tests were below the elastic limit determined from the two calibration tests, therefore all subsequent analyses considered only the elastic component. The results of the constant load test programme are reproduced in Figure 4.5 with K plotted against a. Step loaded tests are indicated by dashed arrows.

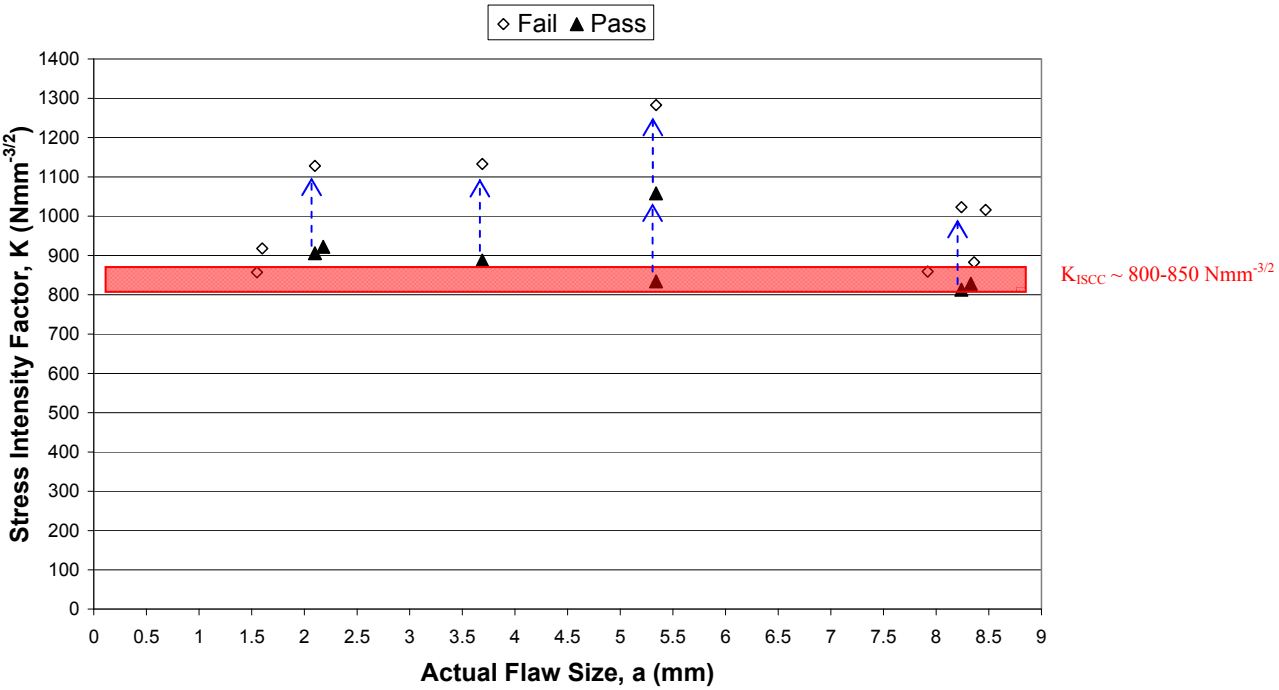

Figure 4.5 Results of constant load tests in a sour environment; arrow indicates a step load test (after Holtam et al., 2009a).

Figure 4.5 shows K_{ISCC} to be approximately 800-850 $Nmm^{-3/2}$ (25-27 $MPam^{0.5}$). This is broadly comparable with that observed elsewhere, for steels of a comparable hardness (Section 2.4.1) (Pargeter et al., 1990, Albarran et al., 1999, Sponseller, 1992, Yang et al., 2009a, Yang et al., 2009b). SENB specimens containing shallow cracks tend to exhibit higher toughness than deep cracked specimens due to a lower level of crack tip constraint (e.g. Chiesa et al., 2001). However, in the current work there was no apparent influence of crack depth, ie no increase in resistance to SSC for shallow flaws (Figure 4.5). Figure 4.5 also illustrates the problems with relying solely on step loaded tests as these tend to over-estimate K_{ISCC}, hence the need to back up these tests with constant load tests. The data in Figure 4.5 can be re-plotted as a Kitagawa-type diagram (Figure 4.6) by determining the outer surface stress associated with the applied load.

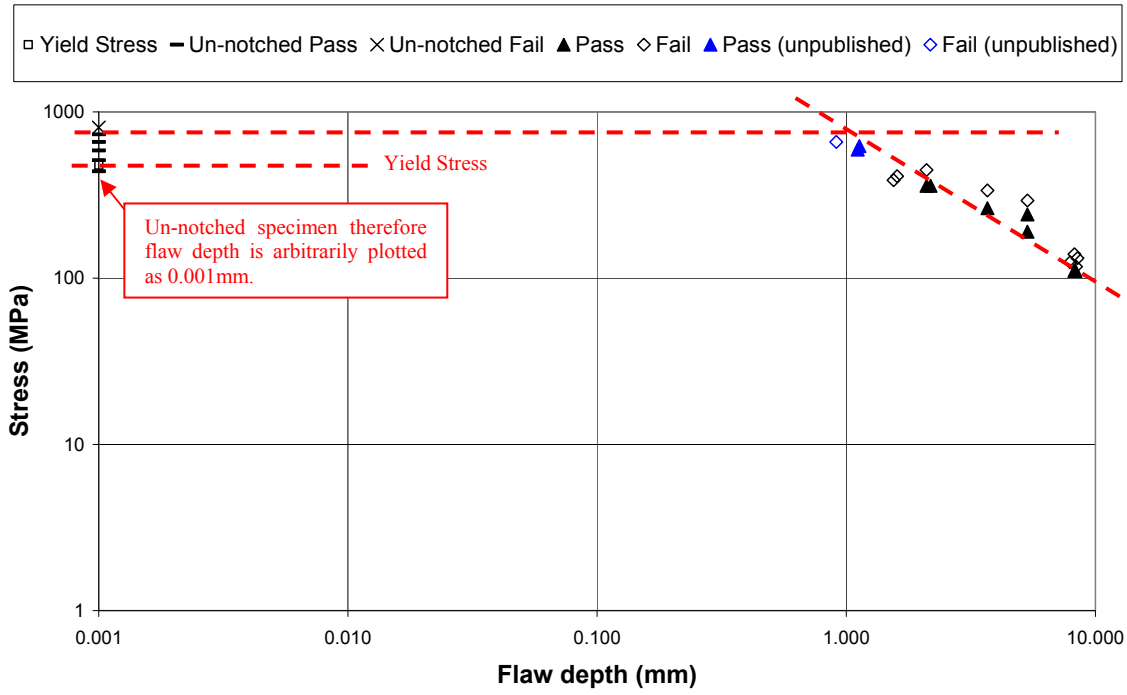

Figure 4.6 Log-log plot of stress versus flaw size - Kitagawa-type diagram (after Holtam et al., 2009a).

Figure 4.6 shows a log-log plot of stress versus flaw size. The points plotted on the left of the diagram are the results of the step loaded un-notched specimen (i.e. flaw size is effectively zero but arbitrarily plotted as 0.001 mm). A horizontal line has been added to the diagram to represent stress-controlled behaviour at a stress value of 732 MPa, the stress at which the un-notched specimen survived for one week before failing. On the right hand side of the diagram are the results of the constant load tests in a sour environment, again plotted in terms of stress. The three shallowest flaws (unpublished data) were achieved by machining away over-sized specimens containing a conventional deep crack to leave a shallow pre-crack of approximately 0.5 mm visible on each side of the specimen. Post test measurements confirmed that this technique was successful in producing flaw depths of approximately 1 mm, once bowing of the crack front had been allowed for (Figure 4.7).

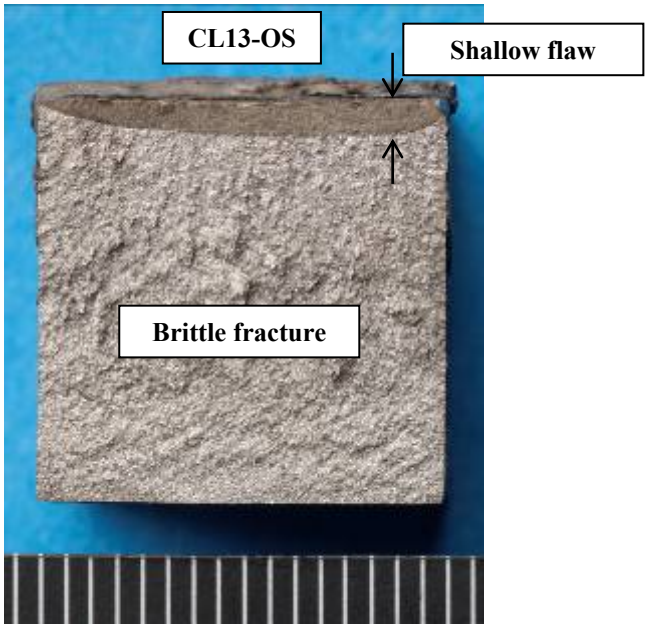

Figure 4.7 Fracture face from specimen CL13-OS; an over-sized specimen containing a conventional deep crack machined away to leave a shallow flaw (mm scale shown).

An approximate line of best fit has been added to Figure 4.6 for the passed tests. The two lines intersect at a flaw size of approximately 1 mm suggesting that there may be a transition from K-controlled to stress-controlled behaviour in this regime. This is comparable to that predicted in earlier work based on a review of published data (Section 2.4.1) (Holtam and Baxter, 2007).

An alternative way of presenting these data is to construct a FAD based on sour service material properties, i.e. using K_{ISCC} as a measure of the material's 'toughness' (Section 2.6.1). A generalised Level 2A FAD has been plotted in Figure 4.8 using the equations in BS 7910 (2005). At Level 2 the less conservative load ratio (the ratio of reference stress to yield stress) is used on the horizontal axis. The vertical line represents the cut-off for this material, termed the maximum load ratio, calculated using the tensile properties of the material. The un-notched specimen test results are also plotted to show that the assessment line falls roughly where the un-notched specimen failed. A material fracture toughness of 828 $Nmm^{-3/2}$ (26 $MPam^{0.5}$) was chosen when constructing the Level 2A FAD. This estimate is based on the deep crack test data only, and is a conservative estimate because it is the value of the lowest definite pass after a 720 hour duration test.

The FAD indicates that for the range of flaw depths tested, all assessment points lie in a similar region of the FAD, towards the K-controlled region (Figure 4.8). It should be noted, however, that all of the points relating to specimen failure are above the assessment line, which indicates that the use of a deep crack K_{ISCC} value remains conservative for the range of flaw sizes examined in this work.

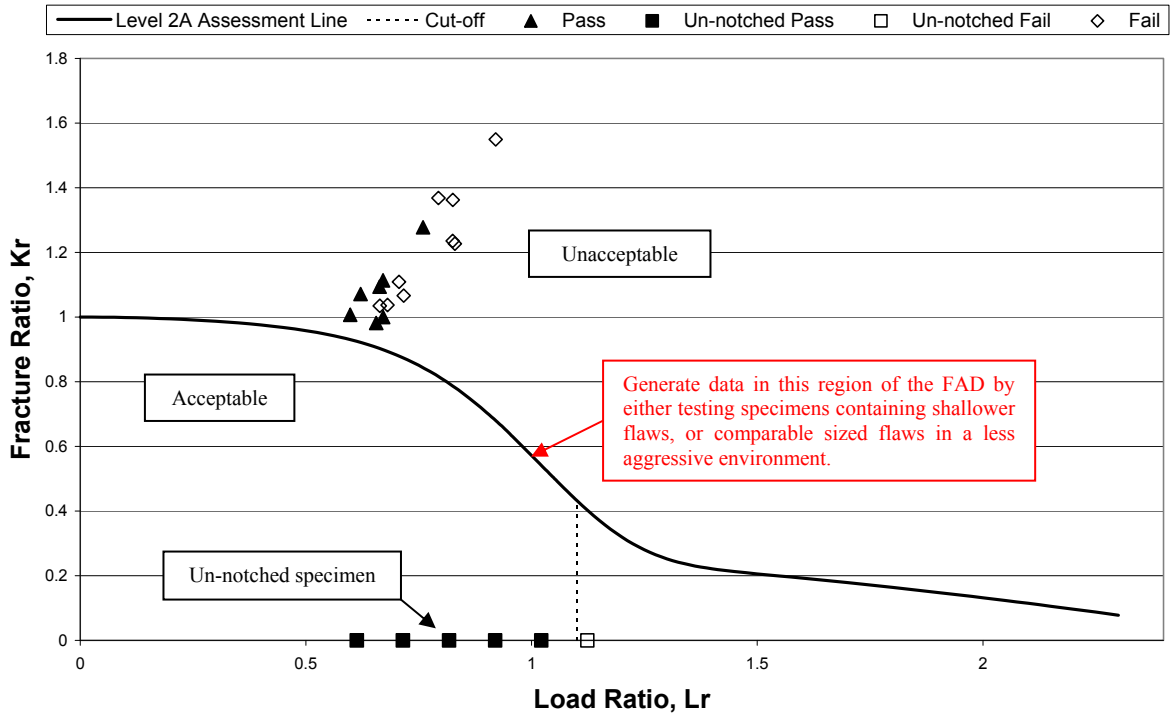

Figure 4.8 Failure assessment diagram using K_{ISCC} as a measure of material's 'toughness' (after Holtam et al., 2009a).

4.3.2 BEHAVIOUR UNDER CYCLIC LOADING

The preliminary results from the investigation into material behaviour under cyclic loading are also featured in the paper published in the *Journal of Offshore Mechanics and Arctic Engineering (OMAE)* (Holtam et al., 2009a), reproduced in **Appendix B**. A more detailed discussion exploring the mechanism responsible for the observed environmental crack depth effect is provided in a paper published in the *International Journal of Fatigue* (Holtam et al., 2010a), reproduced in full in **Appendix C**. Additional work examining the influence of a number of key variables has been accepted for publication in the *International Journal of Offshore and Polar Engineering* (Holtam et al., 2010d), reproduced in full in **Appendix D**. The testing programme investigated the influence of the following variables on the FCGR behaviour of X65 pipeline steel in a sour environment:

- Crack depth;
- Loading conditions;
- Specimen geometry;
- Pre-soaking;
- Coating configuration;

For convenience, a summary of all FCGR tests carried out as part of this research project is provided in Table 4.6. In some instances multiple specimen IDs have been used for the same specimen, to aid comprehension in individual publications, as highlighted in Table 4.6.

Table 4.6 Main testing parameters for fatigue crack growth rate tests.

Specimen ID		**Specimen geometry** (mm)	**Coating configuration**	**Environment**	**One week pre-soak?** (Y/N)	**Loading conditions** (ΔK, $Nmm^{-3/2}$ / $MPam^{0.5}$)	**Stress ratio**	**Test frequency,** Hz
Thesis	**Published Paper**							
S1	M02-11 (Paper 2) M02-05 (Paper 3) S1 (Paper 4)	B = 16 W = 16	n/a	Air	n/a	Constant ΔK (300 / 9)	0.5	5-10
S2	M02-04 (Paper 1) M02-06 (Paper 3) S2 (Paper 4)	B = 16 W = 16	Standard	Sour	N	Constant ΔK (300 / 9)	0.5	0.1
S3	M02-14 (Paper 2) M02-07 (Paper 3) S3 (Paper 4)	B = 16 W = 16	Standard	Sour	N	Constant ΔK (300 / 9)	0.5	0.1
S4	M02-15 (Paper 2) M02-01 (Paper 3)	B = 16 W = 16	n/a	Air	n/a	Increasing ΔK (316-916 / 10-29)	0.5	5-10
S5	M02-12 (Paper 2) M02-02 (Paper 3) S4 (Paper 4)	B = 16 W = 16	Standard	Sour	N	Increasing ΔK (253-664 / 8-21)	0.5	0.1
S6	M02-25 (Paper 2) M02-03 (Paper 3)	B = 16 W = 16	Standard	Sour	N	Decreasing ΔK (379-790 / 12-25)	0.5	0.1
S7	M02-27 (Paper 2) M02-04 (Paper 3) S5 (Paper 4)	B = 16 W = 16	Standard	Sour	N	Decreasing ΔK (316-664 / 10-21)	0.5	0.1
T1	T1	B = 6 W = 16	Standard	Sour	N	Constant ΔK (300 / 9)	0.5	0.1
W1	W1	B = 32 W = 16	Standard	Sour	N	Constant ΔK (300 / 9)	0.5	0.1
S6-P	S6-P	B = 16 W = 16	Standard	Sour	Y	Constant ΔK (300 / 9)	0.5	0.1
S7-P-S	S7-P-S	B = 16 W = 16	Single-sided exposure	Sour	Y	Constant ΔK (300 / 9)	0.5	0.1

W1-HAZ (weld, notched in HAZ)	W1-HAZ (weld, notched in HAZ)	B = 12.5 W = 25	n/a	Air	n/a	Constant ΔK (300 / 9)	0.5	5-10
W2-WELD (weld, notched in weld)	W2-WELD (weld, notched in weld)	B = 12.5 W = 25	n/a	Air	n/a	Constant ΔK (300 / 9)	0.5	5-10
W3-P-S-HAZ (weld, notched in HAZ)	W3-P-S-HAZ (weld, notched in HAZ)	B = 12.5 W = 25	Single-sided exposure	Sour	Y	Constant ΔK (300 / 9)	0.5	0.1
W4-P-S-WELD (weld, notched in weld)	W4-P-S-WELD (weld, notched in weld)	B = 12.5 W = 25	Single-sided exposure	Sour	Y	Constant ΔK (300 / 9)	0.5	0.1
HAZ1 (simulated HAZ)	HAZ1 (simulated HAZ)	B = 16 W = 16	n/a	Air	n/a	Constant ΔK (300 / 9)	0.5	5-10
HAZ2-P-S (simulated HAZ)	HAZ2-P-S (simulated HAZ)	B = 16 W= 16	Single-sided exposure	Sour	Y	Constant ΔK (300 / 9)	0.5	0.1
S8	M02-39	B = 16 W = 16	n/a	Air	n/a	Increasing ΔK (178 - 434 / 6-14)	0.75	5-10
S9	M02-40	B = 16 W = 16	Single-sided exposure	Sour	N	Increasing ΔK (166-457 / 5-14)	0.75	0.1
S10	M02-41	B = 16 W = 16	n/a	Air	n/a	Increasing ΔK (109-213 / 3-7)	0.9	5-10
S11	M02-43	B = 16 W = 16	Single-sided exposure	Sour	N	Increasing ΔK (100-192 / 3-6)	0.9	0.1

Test specimens were extracted from the same seamless X65 pipe that was used in the constant load testing programme. The standard specimen geometry was also a square section SENB with B = W = 16 mm, but a standard S of 64 mm (i.e. 4W) was used. Specimens were again EDM notched and fatigue pre-cracked, in each case to provide a total fatigue pre-crack depth of approximately 1.6 mm (based on surface measurements either side of the specimen).

All tests were carried out using R = 0.5. For those tests carried out in air, the loading frequency was 5-10 Hz, as one would not expect frequency to strongly influence FCGRs for steels in an inert environment (Frost et al., 1974). For those tests carried out in a sour environment the loading frequency was reduced to 0.1 Hz to allow time for the environment to interact with the specimen. During each test, the applied load range was continuously monitored and adjusted to generate test data under the desired loading conditions.

4.3.2.1 Influence of crack depth

The objective of the reported work was to assess the influence of crack depth on the FCGR for a pipeline steel exposed to a sour environment, therefore many of the tests have been carried out under conditions of constant ΔK, to ensure that the influence of crack depth can be directly observed. While the applied ΔK will have an effect on the FCGR, it was not the aim of this work to develop a full crack growth rate law for all possible conditions. Test data from the constant ΔK tests are illustrated in Figure 4.9.

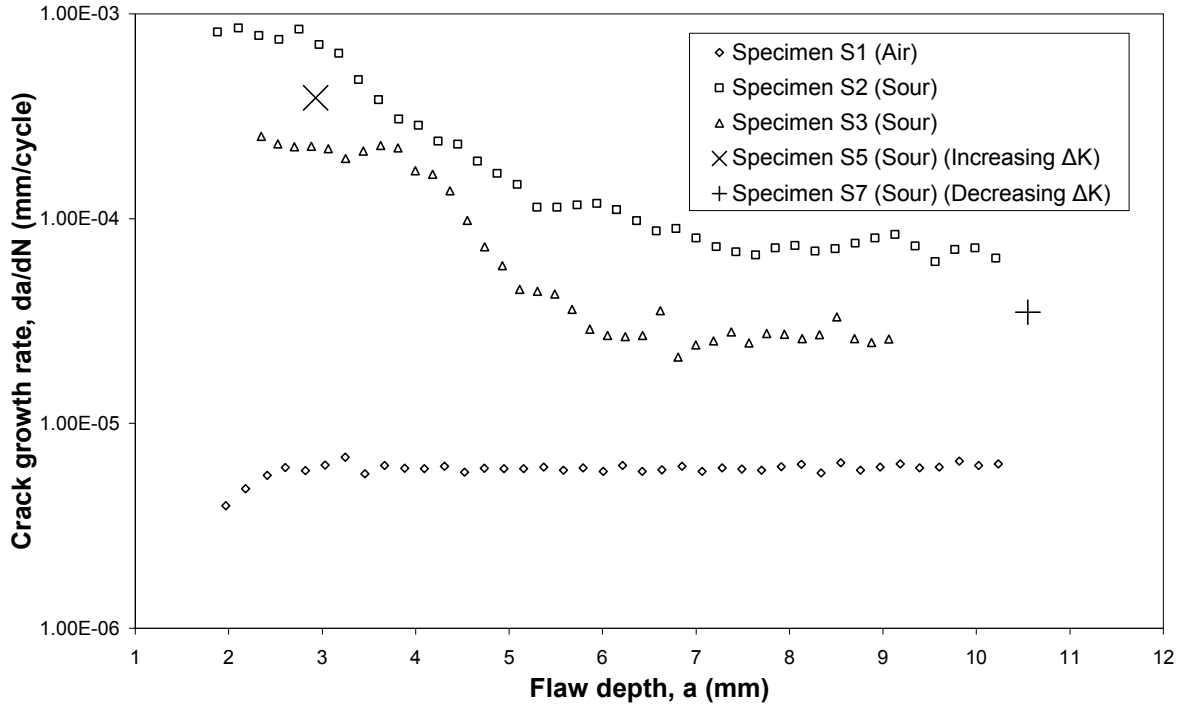

Figure 4.9 Results of constant ΔK (~300 $Nmm^{-3/2}$ / ~9 $MPam^{0.5}$) tests in a sour environment and in air. Also plotted for comparison are the crack growth rates from the beginning and end of an increasing ΔK and a decreasing ΔK test respectively (after Holtam et al., 2010a).

All constant ΔK tests were carried out at low ΔK and a crack depth effect is observed. In the test carried out at constant ΔK in air, the observed crack growth rate remained approximately constant at 6 x 10^{-6} $mmcycle^{-1}$ (at least beyond ~2.5 mm). This is higher than that seen at the beginning of the increasing ΔK test (ΔK ~316 $Nmm^{-3/2}$ / ~10 $MPam^{0.5}$) carried out in air (Section 4.3.2.2), but very close to that expected from the mean curve for steels in air taken from BS 7910.

In the tests carried out at constant ΔK in a sour environment, the FCGR was initially (a ~ 2-4 mm) a factor of between 30 and 130 times higher than in air, which is similar to that observed in the corresponding part of an increasing ΔK test (a ~ 3 mm) (Section 4.3.2.2), as shown in Figure 4.9. By the end of the tests, FCGRs fell to a factor of between 5 and 12 times higher than in air (a ~ 6-10 mm), which is similar to that in the corresponding part of the decreasing ΔK test (a ~ 10 mm) (Section 4.3.2.2), also shown in Figure 4.9. Therefore in the low ΔK regime there appears to be an influence of crack depth on the observed FCGR.

The constant ΔK data (Figure 4.9) exhibit three distinct regions of behaviour as crack depth increases. For relatively shallow flaws (up to 3-4 mm) FCGRs were approximately constant -

although there was roughly a factor of three variation between the two tests. As crack depth increased to approximately 6 mm the FCGR decreased, by approximately an order of magnitude. For crack depths of greater than 6-7 mm, the FCGR remained constant for the rest of the test. This is similar to a trend reported by Nakai et al. (1986), described in Section 2.4.2. The results presented in this paper appear to correspond to Regimes II to IV. The absence of Regime I is most probably because the shallowest flaw tested was around 2 mm. Nakai et al. (1986) tested specimens containing fatigue pre-cracks as shallow as 0.4 mm, therefore the results presented here possibly start towards the end of Regime II.

Examination of the specimen fracture surfaces suggested higher FCGRs at the specimen edges than at the specimen centre (Figure 4.10) (Holtam et al., 2010a). Together with the observation that FCGRs were also higher when the entire crack front was close to the top face of the specimen, this may suggest that bulk hydrogen charging effects are dominating, i.e. hydrogen charging by absorption from the external surfaces of the specimen rather than at the crack tip, and a lower concentration of hydrogen exists in the centre of the specimen than at the edges. However, neither crack closure effects nor differences in crack tip chemistry can be ruled out entirely.

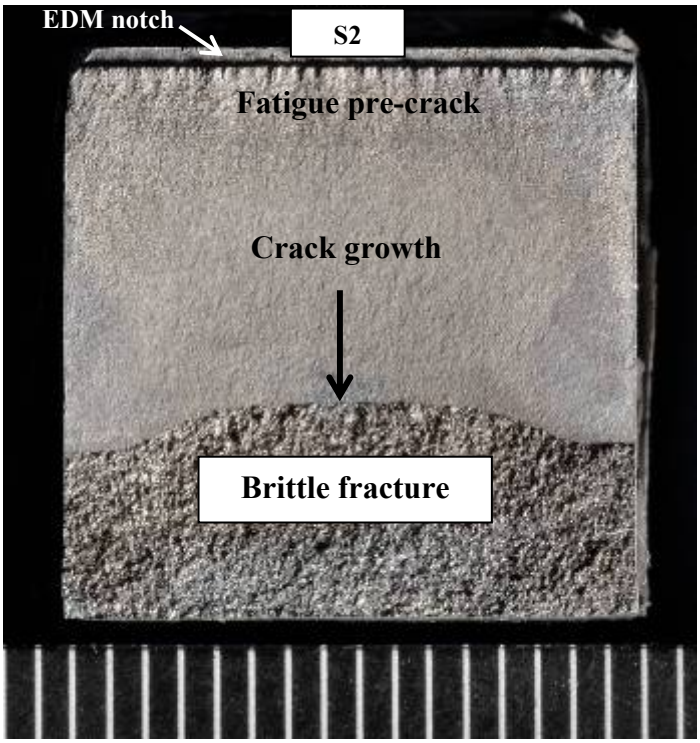

Figure 4.10 Fracture face from a fatigue crack growth rate test carried out in a sour environment under constant ΔK conditions (mm scale shown) (after Holtam et al., 2010a). Time spent in the sour environment: 216 hours.

4.3.2.2 Influence of loading conditions

Conventionally, tests are carried out under conditions of either increasing or decreasing ΔK to generate ΔK data over the ΔK range of interest. In particular, low ΔK data are often generated under conditions of decreasing ΔK (for experimental convenience). For those tests carried out under conditions of increasing or decreasing ΔK, the range of ΔK that can be derived for a single test is predominantly a function of specimen size, and for the pipe material of interest (wall thickness 20.6 mm), and the specimen geometry used (SENB), the ΔK increases by

approximately a factor of two. The range examined (284-600 $Nmm^{-3/2}$ / 9-19 $MPam^{0.5}$) is typical of that experienced by hypothetical flaws under consideration within an assessment of wave or VIV loading of a SCR. Test data from the increasing ΔK and decreasing ΔK tests are illustrated in Figure 4.11.

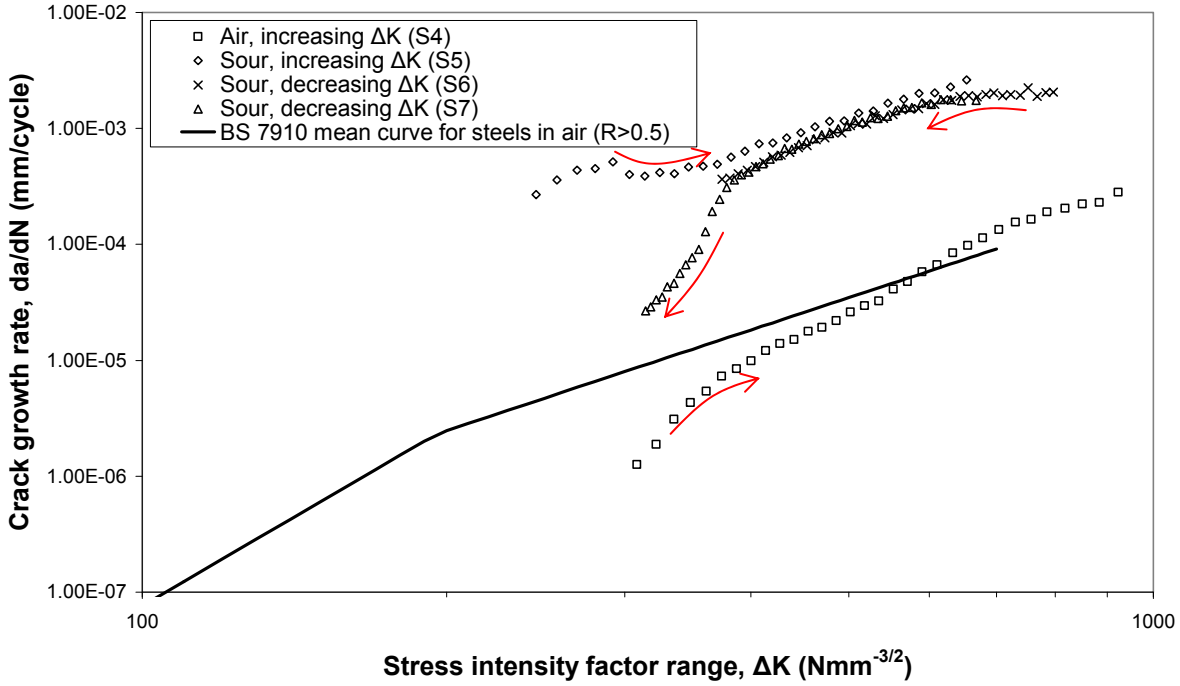

Figure 4.11 Results of increasing and decreasing ΔK tests in a sour environment and in air. Arrows indicate increasing crack depth in each test (after Holtam et al., 2010a).

For the increasing ΔK test carried out in air, the observed FCGRs were similar to those in the mean curve for steels in air (R ≥ 0.5) given in BS 7910 (2005). For the comparable test (increasing ΔK) carried out in a sour environment, FCGRs were typically a factor of 30 higher than in air at high ΔK (> 411 $Nmm^{-3/2}$ / 13 $MPam^{0.5}$), but this increased at lower ΔK (284-411 $Nmm^{-3/2}$ / 9-13 $MPam^{0.5}$).

For the decreasing ΔK tests (carried out in a sour environment), data from the two test specimens were very close where ΔK values overlapped. FCGRs at high ΔK (i.e. the beginning of the test) were similar to those seen in the increasing ΔK sour test, for a given ΔK. However, at lower ΔK (284-379 $Nmm^{-3/2}$ / 9-12 $MPam^{0.5}$) the FCGR seen in specimen S7, when the crack depth was between 8.4 mm and 11.1 mm, was significantly lower than that seen under conditions of increasing ΔK (specimen S5) when the crack depth was between 2.7 mm and 4.1 mm. During this region of the test, the FCGR decreased rapidly - more than an order of magnitude.

Test data from the decreasing ΔK tests are in broad agreement with other published data (Bristoll and Roeleveld, 1978, Webster et al., 1985). FCGRs at high ΔK are typically 30 times higher than in air. At lower ΔK (< 379 $Nmm^{-3/2}$ / 13 $MPam^{0.5}$) the influence of the sour environment appeared to lessen and the FCGR approached that described by the mean curve for steels in air given in BS 7910 (2005). Under conditions of increasing ΔK the FCGR at high ΔK (> 411 $Nmm^{-3/2}$ / 13 $MPam^{0.5}$) was similar to that seen under conditions of decreasing ΔK (for a given ΔK). However, at lower ΔK the FCGR data determined under conditions of increasing ΔK were noticeably higher than those determined under conditions of

decreasing ΔK. At high ΔK there appears to be no influence of crack depth and FCGRs are the same in each type of test. However at low ΔK, shallow cracks (increasing ΔK test) are seen to grow substantially faster than deeper flaws (decreasing ΔK test).

The constant ΔK tests reported above suggest that the observed environmental crack depth effect is due to the influence of bulk hydrogen charging. However, it is also possible that the observed influence of crack depth is as a result of differences in the extent of crack closure. At low ΔK, crack closure may be more significant at the end of the decreasing ΔK test than at the beginning of the increasing ΔK test. This in itself may be attributable directly to the difference in crack depth or to the progressive build up of corrosion products during the test. Irrespective of the mechanism involved, this highlights a potential non-conservatism associated with generating FCGR data under conditions of decreasing ΔK.

Although a number of authors have indicated a more noticeable influence of sour environments at high ΔK, precise test conditions are not always reported and therefore it is not possible to say whether this is genuinely the case or whether this is an artefact of testing under conditions of decreasing ΔK. To investigate this area further, increasing ΔK tests using specimens containing shallow flaws starting at low ΔK were performed to provide a more conservative means of establishing upper bound FCGRs. This investigation is ongoing but four FCGR tests have been completed (two in air and two in a sour environment) using the same specimen geometry as the previous increasing and decreasing ΔK tests and containing a total fatigue pre-crack depth of approximately 1.6 mm, based on surface measurements either side of the specimen (Table 4.6). Environmental conditions were also the same as in the previous increasing and decreasing ΔK tests, except that those specimens tested in a sour environment had single-sided exposure (see Section 4.3.2.5). Tests were performed at higher R to facilitate generating data at lower ΔK, to try to establish the threshold value of ΔK when using the current method of EDM notching followed by fatigue pre-cracking to introduce shallow flaws. Test data from the tests at low ΔK are plotted in Figure 4.12, alongside the previous experimental data from Figure 4.11 and the mean curve for steels in air ($R \geq 0.5$) taken from BS 7910 (2005). So far, the results suggest that any reduced influence of a sour environment at low ΔK is an artefact of how the data is generated (i.e. testing under decreasing ΔK conditions) and not a true effect.

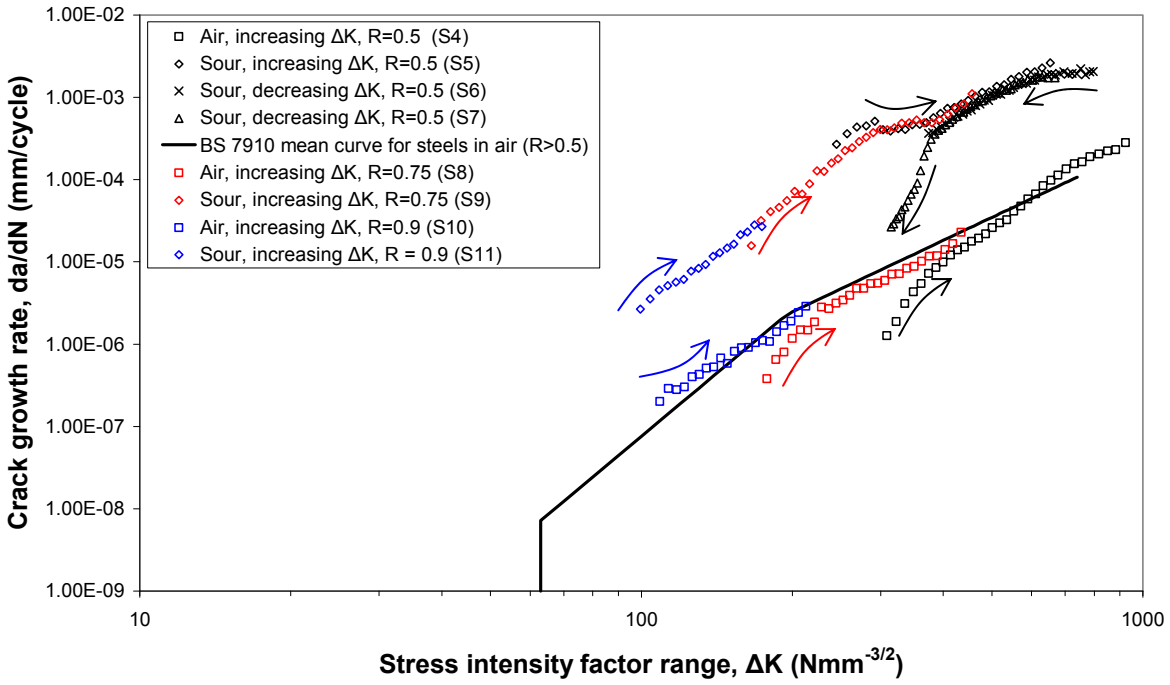

Figure 4.12 Results of increasing ΔK tests at high stress ratio and starting at low ΔK in a sour environment and in air, plotted alongside previous data from Figure 4.11. Arrows indicate increasing crack depth in each test.

4.3.2.3 Influence of specimen geometry

In order to investigate the effects of bulk hydrogen charging further, two non-standard specimen geometries were used, one with B = 6 mm (thin) and one with B = 32 mm (wide). In each case a standard S of 64 mm (i.e. 4W) continued to be used. The shape of the crack front in the thin specimen (T1) was essentially straight, although, the crack depth at the specimen edges was slightly deeper than at the centre of the specimen (Figure 4.13). The wide specimen (W1) however exhibits a similar shape crack front to that in Figure 4.10, indicating that at the end of the test the crack depth was greater at the specimen edges than in the specimen centre (Figure 4.14).

Figure 4.13 Fracture face from thin specimen T1 tested under constant ΔK conditions (~300 $Nmm^{-3/2}$ / ~9 $MPam^{0.5}$) (mm scale shown) (Holtam et al., 2010d).

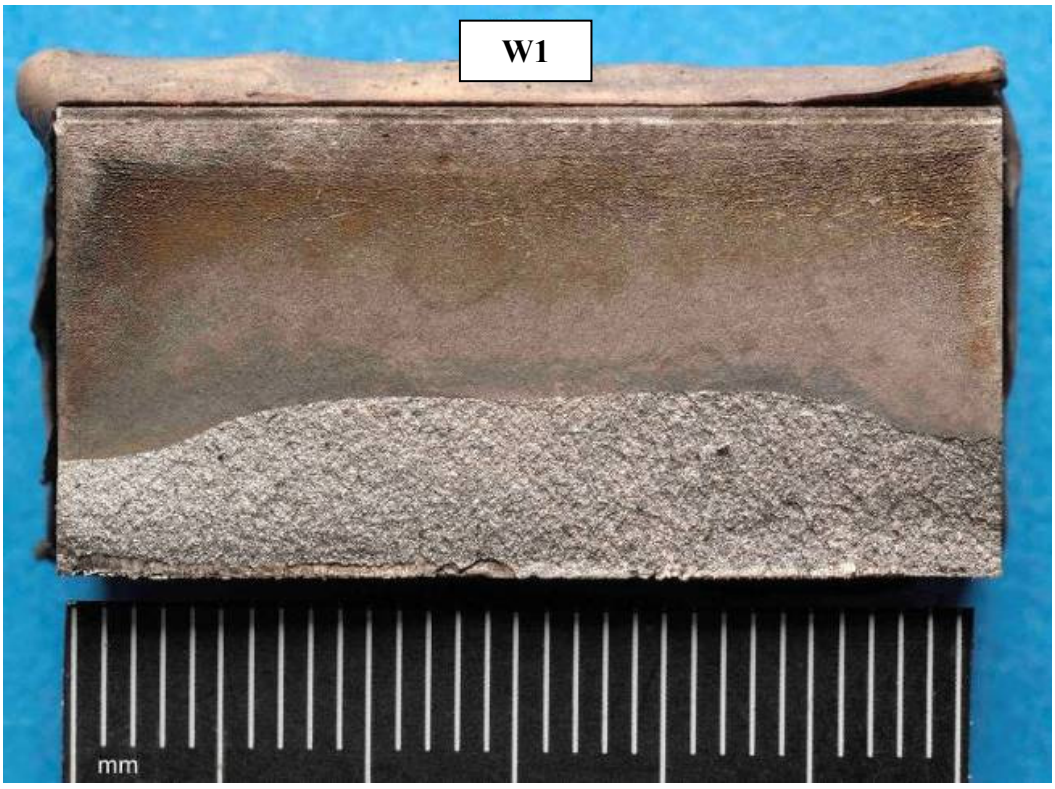

Figure 4.14 Fracture face from wide specimen W1 tested under constant ΔK conditions (~300 $Nmm^{-3/2}$ / ~9 $MPam^{0.5}$) (Holtam et al., 2010d).

The results of the constant ΔK tests in a sour environment using the thin and wide specimen geometries are reproduced in Figure 4.15, alongside comparable results from the square section specimens reported in Figure 4.9. In both cases there still appeared to be three distinct regimes of behaviour, whereby, shallower flaws are growing faster than deeper flaws. However, the thin specimen did not exhibit as marked a drop-off in FCGR for deeper flaws.

The shape of the crack fronts and the test data from the thin and wide specimens further supports the idea that bulk hydrogen charging from exposed surfaces is dominating. In addition to shallow flaws growing faster than deeper flaws, FCGRs in material close to an exposed surface are faster than in material far away from an exposed surface.

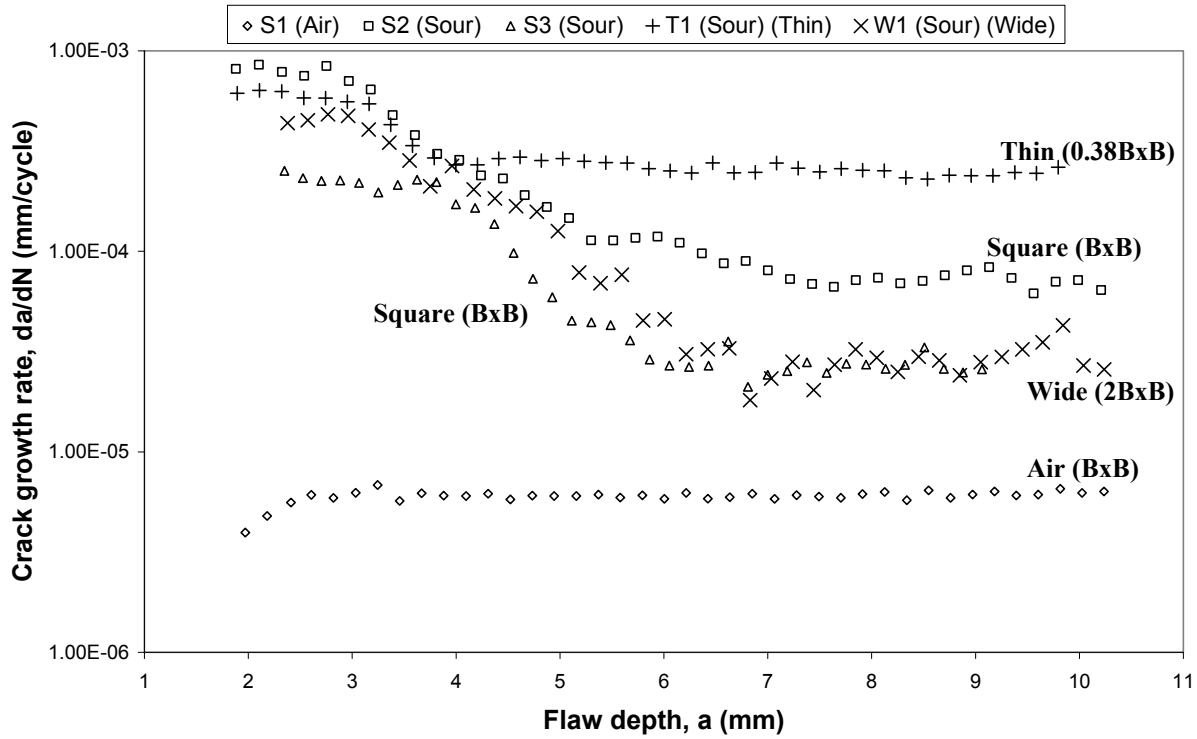

Figure 4.15 Results of constant ΔK (~300 $Nmm^{-3/2}$ / ~9 $MPam^{0.5}$) tests on thin and wide specimens in a sour environment, plotted alongside previous constant ΔK data in Figure 4.9 (Holtam et al., 2010d).

4.3.2.4 Influence of pre-soaking

Under conditions where bulk hydrogen charging is dominant it becomes necessary to consider the rate at which hydrogen diffuses into the bulk material, with respect to both test specimens and real pipelines, to ensure that test conditions and associated data are appropriately conservative. A 'pre-soak' period (i.e. immersing the specimen in the corrosive environment for a period of time prior to cycling commencing) can be used to allow hydrogen to diffuse into the bulk of the material and therefore maximise the environmental effect. For example Griffiths et al. (1993) pre-charged a specimen for 147 days prior to testing and observed a significant increase in FCGR.

In the FCGR tests carried out thus far, cycling commenced immediately after the gas flow had been reduced. To investigate the effect of pre-soak, a simple hydrogen analysis was performed to estimate the required pre-soak period, as described in **Appendix D** (Holtam et al., 2010d). For an infinite plate exposed on both sides, the same dimensions as the standard

SENB specimen geometry being used, a lower bound estimate for the time taken for the specimen to become saturated with hydrogen is approximately 3-4 hours, while the corresponding upper bound estimate is approximately 100-200 hours. This is primarily due to uncertainties in the estimated value of diffusivity (D) for ferritic materials at ambient temperature. A pre-soak period of one week (168 hours) was subsequently selected.

The result of the constant ΔK test in a sour environment on a standard specimen geometry but with an additional one week pre-soak in the sour environment (S6-P) is plotted in Figure 4.16, alongside the previous test data generated using standard specimen geometries. There was no noticeable effect of pre-soak on the observed crack growth rates. There still appeared to be three distinct regimes of behaviour with deeper flaws growing slower than shallower flaws at the same value of ΔK.

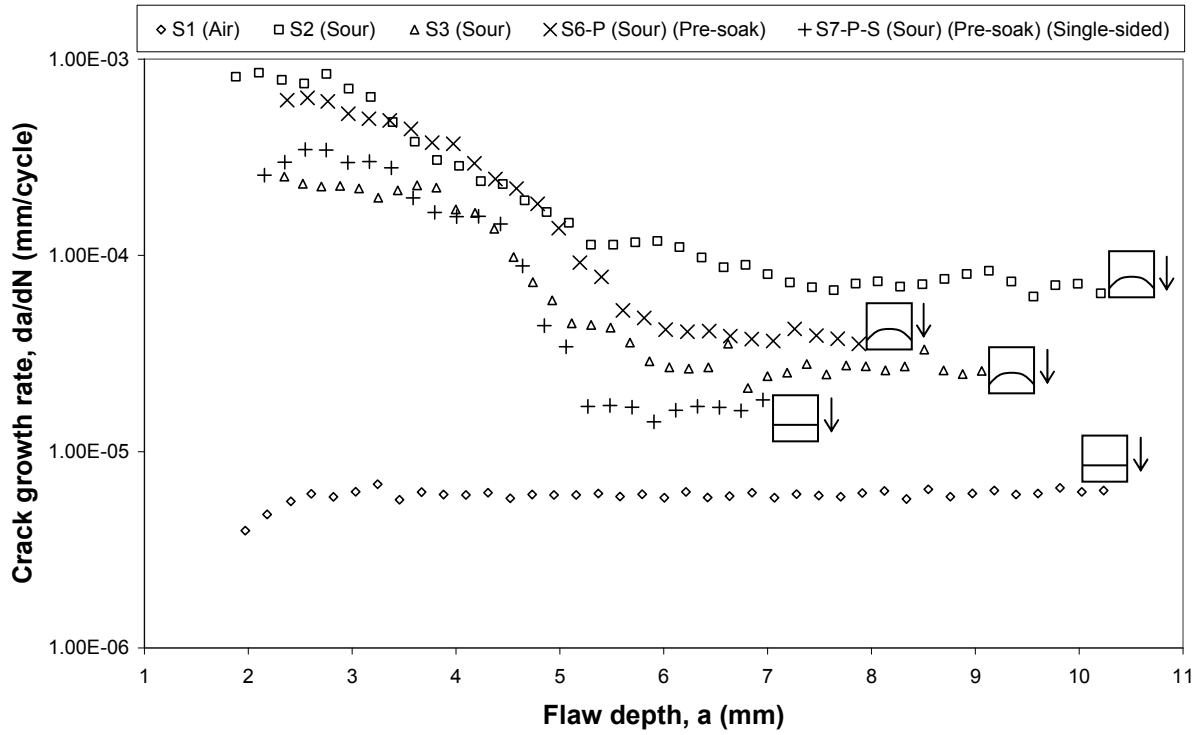

Figure 4.16 Results of constant ΔK (~300 $Nmm^{-3/2}$ / ~9 $MPam^{0.5}$) tests in a sour environment with additional pre-soak and different coating configurations plotted alongside previous constant ΔK data in Figure 4.9. The direction of crack growth and the shape of the crack front at the end of each test are also indicated (Holtam et al., 2010d).

Examination of the fracture face of specimen S6-P also indicated that at the end of the test the crack depth was still greater at the specimen edges than at the specimen centre. If local hydrogen concentration is the dominant factor controlling the observed crack growth rate then this would suggest that a uniform distribution of hydrogen is not developed within the test period. If this is the case then perhaps the pre-soak period should be increased. However, according to the hydrogen analysis calculations (Holtam et al., 2010d), hydrogen should have diffused into the centre of the specimen (i.e. 8 mm) during the test period, even with a lower bound estimate of diffusivity. Moreover, in the case of a pipeline steel in a sour environment a longer pre-soak period will not necessarily correspond to a higher concentration of hydrogen in the bulk material due to the build-up of the iron sulphide scale on the surface of the steel as a by-product of the corrosion process (Section 2.4).

4.3.2.5 Influence of coating configuration

'Stopping off' lacquer was applied to all FCGR specimens tested in a sour environment, to protect the bulk of the specimen and instrumentation from the corrosive environment, and to minimise the extent of solution contamination. For the standard specimen, a 10 mm window was left uncoated on each side of the notch on all sides of the specimen (Figure 3.4). However, a final test (S7-P-S) was carried out with the specimen completely coated on all sides, except for the notched surface (Figure 4.17), from now on referred to as single-sided exposure.

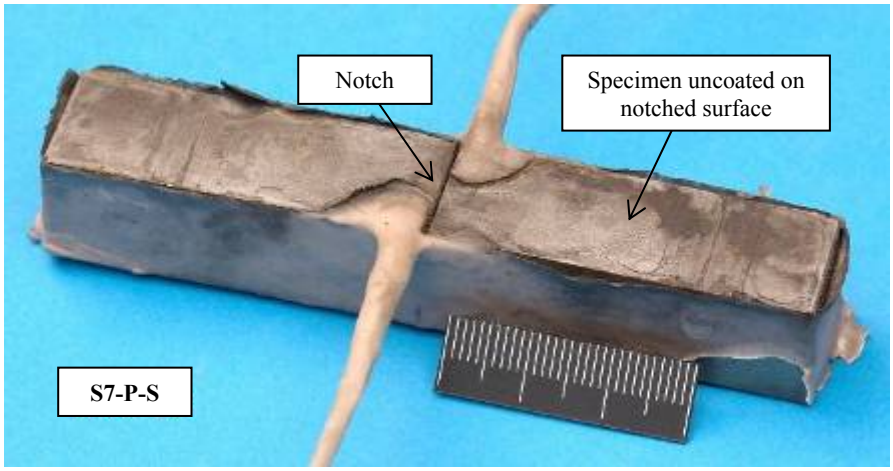

Figure 4.17 Single-sided exposure coating configuration (S7-P-S) (mm scale shown). Photo taken upon completion of the test (Holtam et al., 2010d).

The result of the constant ΔK test in a sour environment on a standard specimen geometry with an additional one week pre-soak period in the sour environment and single-sided exposure (S7-P-S) is plotted in Figure 4.16. Also indicated in Figure 4.16 is the shape of the crack front at the end of each test. While there still appeared to be three distinct regimes of behaviour as reported above, Specimen S7-P-S exhibited the lowest crack growth rates observed in any of the sour FCGR tests. In contrast to all the previous fracture faces, specimen S7-P-S exhibited a straight crack front (Figure 4.18); in fact the crack depth was slightly shallower at the specimen edges, as was the case for the specimens tested in air.

Figure 4.18 Fracture face from specimen S7-P-S tested under constant ΔK conditions (~300 $Nmm^{-3/2}$ / ~9 $MPam^{0.5}$) after a one week pre-soak in the sour environment and with single-sided exposure (mm scale shown) (Holtam et al., 2010d).

Measurements of diffusible hydrogen concentration were carried out using two coupons with single-sided exposure immersed in a sour environment. Both coupons were exposed to the sour environment for significantly longer than the one-week pre-soak period. Upon completion of each test, the coupon was removed from the environmental test chamber and transferred into storage in liquid nitrogen. The amount of diffusible hydrogen was determined using gas chromatography after heating at approximately 150^{o}C for six hours (Section 3.3.3). Each coupon was cut into four sections, so that the hydrogen concentration could be determined at different through thickness locations relative to the exposed surface (e.g. Figure 4.19). Care was taken to ensure that specimen heating was minimised during the cutting procedure, by intermittent immersion in liquid nitrogen.

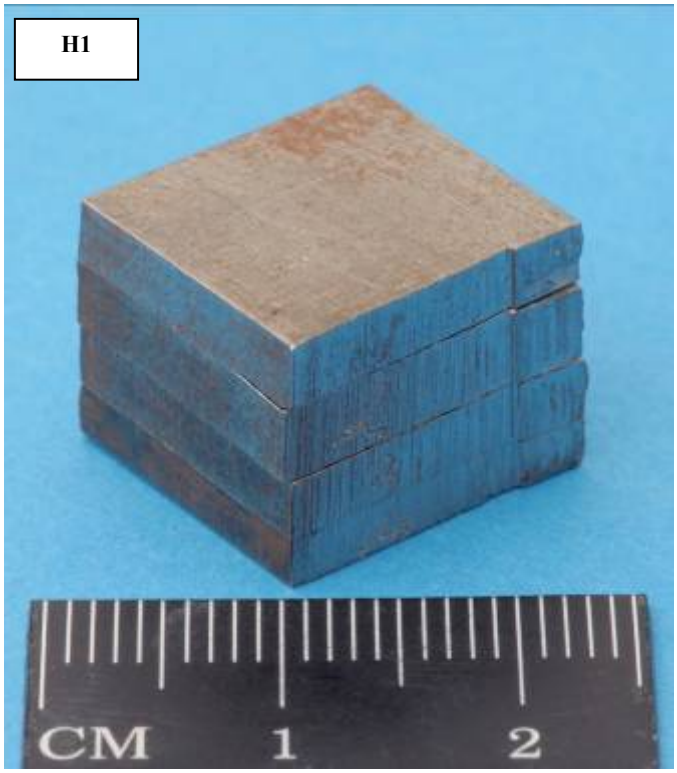

Figure 4.19 Hydrogen analysis coupon H1 cut into four sections, to allow hydrogen concentration to be determined at different through thickness locations relative to the exposed surface.

The results of the two separate hydrogen analyses (H1 and H2) are plotted in Figure 4.20. Also stated in Figure 4.20 is the test duration in each case, defined as the time from when the sour environment was introduced to when the test vessel was purged with nitrogen prior to the sample being removed. A through thickness variation in diffusible hydrogen content was observed in both specimens, with the highest concentration occurring closest to the exposed surface.

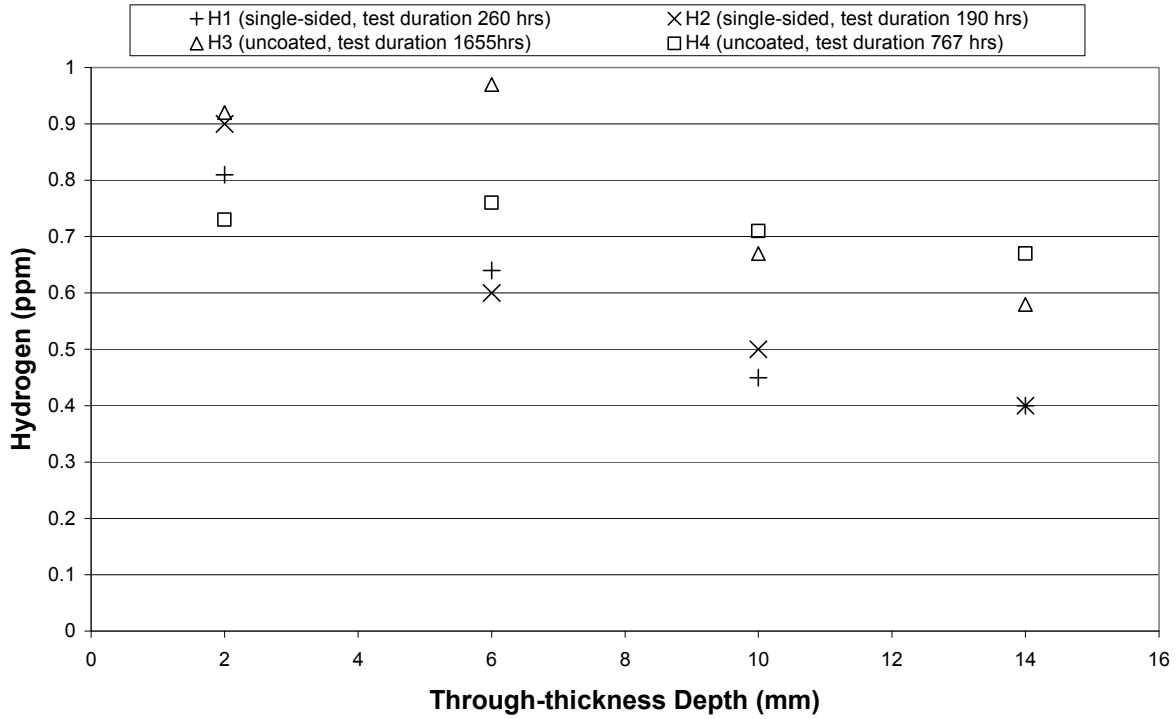

Figure 4.20 Average hydrogen concentration versus through thickness depth (specimens with single-sided exposure only) as measured on four fatigue crack growth rate specimens (two with single-sided exposure and two uncoated) after time in a sour environment (after Holtam et al., 2010d).

Having successfully confirmed a higher concentration of hydrogen close to an exposed surface, further supporting the idea that bulk hydrogen effects are dominating, two additional uncoated coupons of material (H3 and H4) were also analysed for diffusible hydrogen content after immersion in the sour environment for 1655 and 767 hours respectively, significantly longer than the exposure times for the coupons with single-sided exposure (Figure 4.20). Both specimens exhibited a higher average concentration of hydrogen than the coupons with single-sided exposure (Table 4.7). In the case of coupon H4, a uniform concentration of hydrogen appears to have developed. This is not the case for coupon H3, however, which was immersed in the environment for the longest period of time. A more detailed discussion regarding hydrogen diffusion into the bulk material is provided in Section 5.2.

Table 4.7 Average concentration of diffusible hydrogen in hydrogen analysis coupons.

Sample ID	**Coating configuration**	**Time spent in sour environment** (hours)	**Average concentration of H_2S** (ppm)
H1	Single-sided	260	0.58
H2	Single-sided	190	0.60
H3	Uncoated	1655	0.79
H4	Uncoated	767	0.72

4.3.2.6 Influence of weld and heat affected zone microstructure

The results of the fatigue tests described above are material-environment specific. In higher hardness materials (e.g. welds) one might expect a higher sensitivity to EAC processes such as SSC, which might result in failure via a different mechanism to that observed in parent

material, and possibly higher FCGRs (Hammond and Baxter, 2008). Therefore it is not clear whether the trends seen in tests on parent material will be directly transferable to harder HAZ microstructures and weld metal. An investigation into sour fatigue crack growth performance of pipeline girth welds was therefore instigated. The results were published at the *2010 Deep Offshore Technology (DOT) International Conference* (Holtam et al., 2010b). A summary of the key findings is provided below.

Six FCGR tests (three in air and three in a sour environment) were carried out under conditions of constant ΔK on girth welds (notched in the weld and in the HAZ) and simulated HAZ microstructures (Table 4.6). Girth weld specimens were machined from a different pipe from that used in the previous tests, although still manufactured to API 5L X65 sour service specification, with nominal dimensions 16 inch (406.4 mm) outside diameter and 25.4 mm wall thickness. The chemical composition of the steel, determined using optical emission spectrometry (OES), is summarised in Table 4.8. Hardness and tensile property data are shown in Table 4.9. A simulated HAZ microstructure was generated by heat treating the X65 pipe used for the previous parent material tests, using a typical HAZ thermal cycle. Details of the heat treatment trials are provided elsewhere (Holtam et al., 2010b). While it is acknowledged that the microstructure will vary widely throughout the HAZ of a girth weld, the aim was to generate FCGR data through a broadly representative microstructure.

Table 4.8 Chemical composition of the API 5L X65 C-Mn steel used for the tests on pipeline girth welds (wt.%), balance Fe.

C	Si	Mn	P	S	Cr	Mo
0.12	0.27	1.24	0.01	0.002	0.069	0.15
Ni	B	Cu	Nb	Ti	V	
0.3	<0.0003	0.13	0.015	0.004	0.057	

Table 4.9 Hardness and tensile property data for the API 5L X65 C-Mn steel used for the tests on actual pipeline girth welds.

Hardness, HV10	See Table 4.10
UTS, MPa	587
0.5% proof stress, MPa	502

The girth weld was manufactured using a STT (surface tension transfer) process for the root pass, and GMAW (gas metal arc welding) for the fill and capping runs (Figure 1.2). Subsequent dilatometry on the X65 pipe parent material suggested a cooling rate in the weld root region of the HAZ of approximately $25^{o}Cs^{-1}$ (Holtam et al., 2010b). The weld had not been subject to any form of PWHT. Hardness data taken across the weld confirmed its suitability for sour service (Table 4.10) (NACE/ISO, 2003).

Table 4.10 Hardness data for the API 5L X65 C-Mn steel pipeline girth weld.

Hardness 1.5 mm from external surface (HV10)	1	Parent material	213	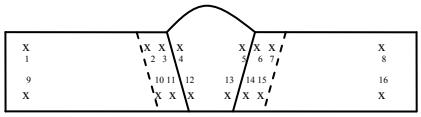
	2	HAZ	207	
	3	HAZ	233	
	4	Weld metal	212	
	5	Weld metal	209	
	6	HAZ	219	
	7	HAZ	199	
	8	Parent material	202	
Hardness 1.5 mm from internal surface (HV10)	9	Parent material	210	
	10	HAZ	221	
	11	HAZ	240	
	12	Weld metal	201	
	13	Weld metal	203	
	14	HAZ	227	
	15	HAZ	199	
	16	Parent material	181	

Two different SENB specimens were used, each tested in three point bending. Weld specimens were as close to full thickness as possible with the weld cap and weld root ground flush. Specimen geometry was B x 2B with B = 12.5 mm. Square section specimens were machined from the simulated HAZ material with B = W = 16 mm, an identical geometry to that used in the previous tests. In both cases a standard span (S) of 4W was used, i.e. 100 mm for the weld specimens and 64 mm for the simulated HAZ specimens. Specimens were again EDM notched and fatigue pre-cracked to provide a total fatigue pre-crack depth of approximately 1.6 mm (i.e. a/W ~ 0.06 for the weld specimens and a/W ~ 0.1 for the simulated HAZ specimens) based on surface measurements either side of the specimen.

All tests were carried out using R = 0.5, a loading frequency of 5-10 Hz for tests in air and 0.1 Hz for tests in a sour environment, and under conditions of constant (low) ΔK. The sour environment was identical to that used in the previous fatigue tests and each specimen had single-sided exposure and a one-week pre-soak to maximise the environmental effect.

The results of the constant ΔK tests in air on pipeline girth weld specimens notched in the HAZ and in the weld are plotted in Figure 4.21, alongside comparable data from Figure 4.9 for a square section parent material specimen (S1). In all three cases the FCGRs remained approximately constant at 6 x 10^{-6} mmcycle^{-1}. This is very close to that expected from the mean curve for steels in air (R ≥ 0.5) taken from BS 7910 (2005).

The results of the constant ΔK tests on pipeline girth weld specimens in a sour environment are also plotted in Figure 4.21, alongside the comparable data from Figure 4.16 for a square section parent material specimen with single-sided exposure and a one week pre-soak (specimen S7-P-S). The test data from specimen W4-P-S-WELD (notched in the weld) shows reasonable correlation with the previous data from specimen S7-P-S. In both cases there were three distinct regimes of behaviour, with shallower flaws growing faster than deeper flaws, as described in Section 4.3.2.1. The crack growth rate data from specimen W3-P-S-HAZ (notched in the HAZ) also correlate well with the other data. The drop-off in crack growth rate occurred over a similar range to specimen S7-P-S. Unusually, specimen W3-P-S-HAZ exhibited a brief increase in crack growth rate (a ~4.2-5.6 mm) between the crack growth rate starting to drop-off (a ~3.5 mm) and reaching a constant rate (a ~6 mm). Examination of the fracture face did not reveal any significant weld defects that might have contributed to the observed increase in FCGR, nor did micro-hardness readings taken along the crack path indicate any significant increase in hardness in this region.

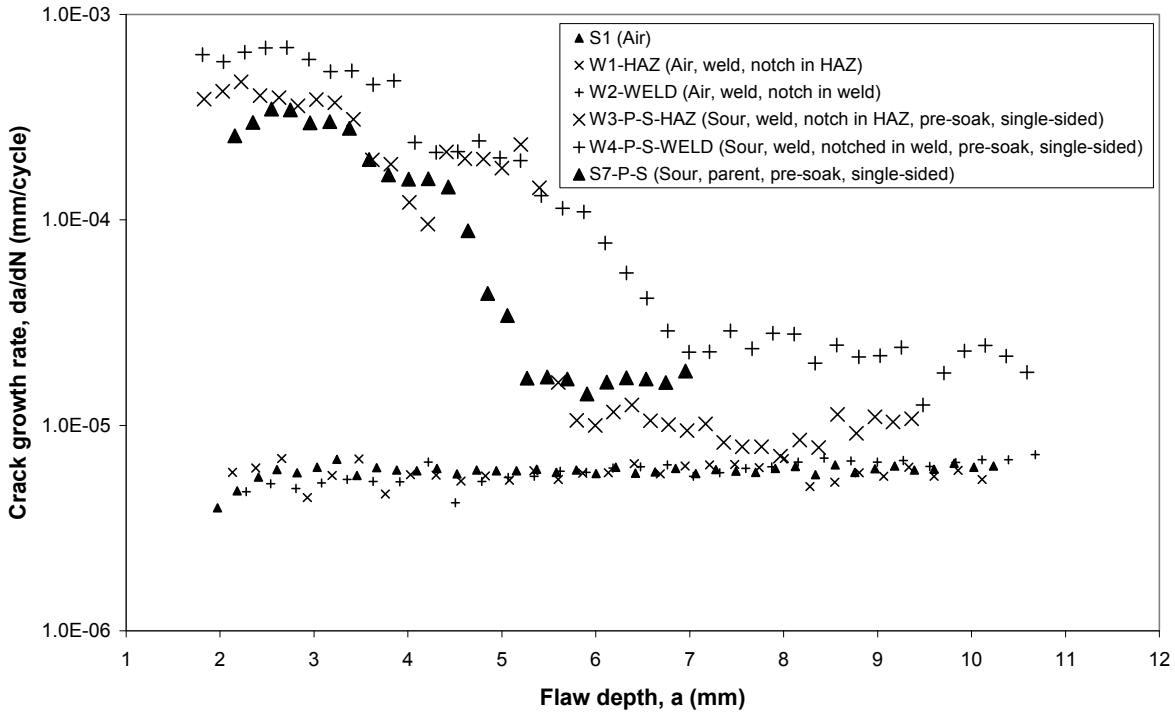

Figure 4.21 Results of constant ΔK (~300Nmm$^{-3/2}$ / ~9MPam$^{0.5}$) tests on girth weld specimens in a sour environment and in air plotted alongside previous comparable constant ΔK data from Figures 4.9 and 4.16.

In Figure 4.22 crack growth rate data for square section simulated HAZ specimens tested in air and in a sour environment have been added to the data plotted in Figure 4.21. The test in air (specimen HAZ1) resulted in crack growth rates around half as fast as had been seen in the previous tests in air, remaining approximately constant at 3 x 10^{-6} mmcycle^{-1} for the duration of the test. Test data from specimen HAZ2-P-S, tested in a sour environment, closely matches that from previous tests in a sour environment, particularly girth weld specimen W3-P-S-HAZ, ignoring the brief increase in crack growth rate highlighted above.

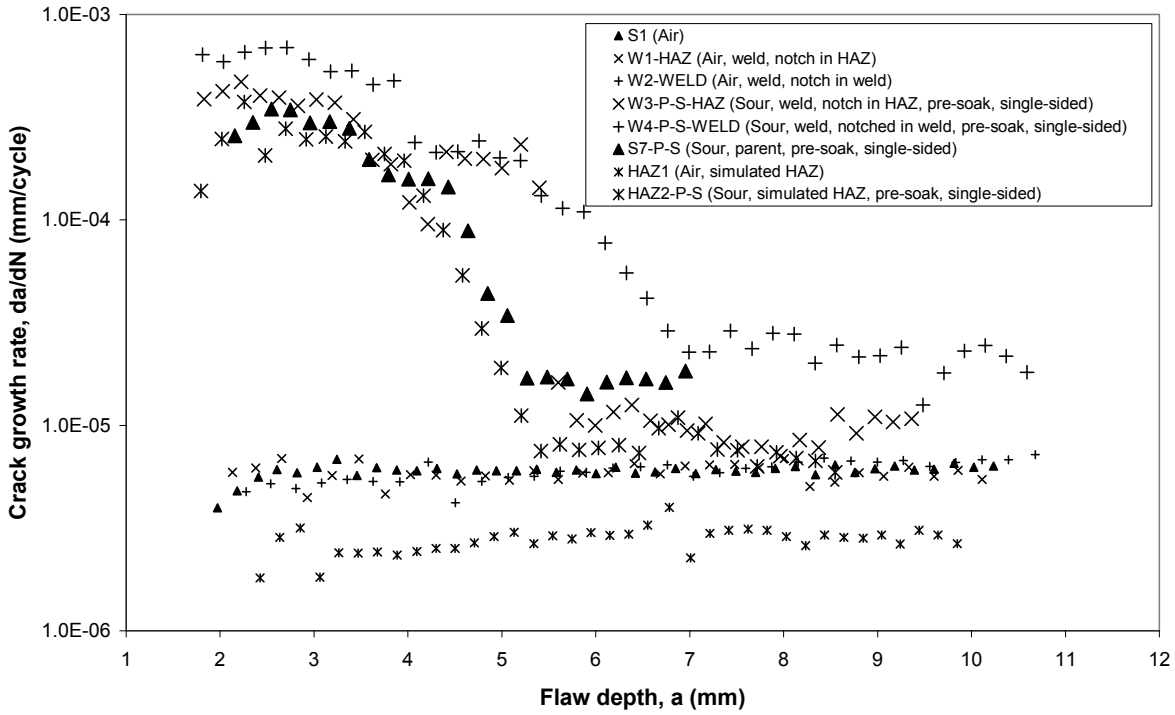

Figure 4.22 Results of constant ΔK (~300 $Nmm^{-3/2}$ / ~9 $MPam^{0.5}$) tests on simulated HAZ specimens in a sour environment plotted alongside tests on girth weld specimens and previous comparable constant ΔK data from Figure 4.21.

Metallographic sections confirmed that for both weld specimens notched in the HAZ (specimen W1-HAZ tested in air and specimen W3-P-S-HAZ), the fatigue crack was successfully grown through the HAZ microstructure from a shallow fatigue pre-crack (e.g. Figure 4.23).

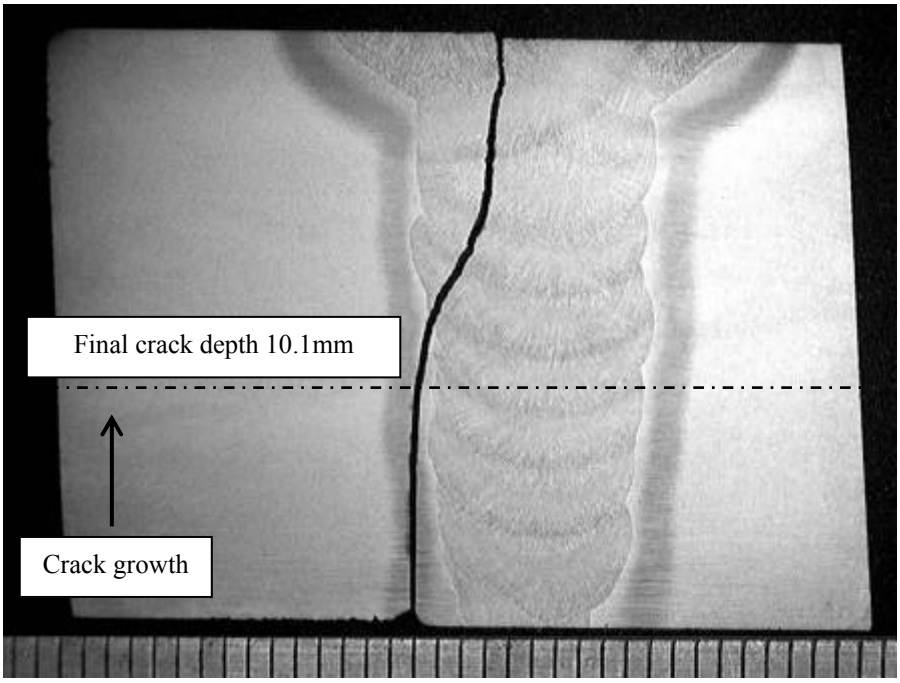

Figure 4.23 Metallographic section from specimen W1-HAZ (mm scale shown). Test was terminated when crack depth reached 10.1mm, measured from the inside surface of the specimen as indicated.

Overall, there was good agreement between the results from the tests on pipeline girth welds and HAZ microstructures and previous FCGR tests on the C-Mn steel parent material. In all tests carried out in a sour environment there were three distinct regimes of behaviour, with shallow flaws growing faster than deeper flaws at the same (low) value of ΔK. It was pleasing to note that the test data from HAZ2-P-S (simulated HAZ) most closely matched that from girth weld specimen W3-P-S-HAZ, which was notched in the actual HAZ. With respect to weldments, the observed environmental crack depth effect is still believed to be influenced by bulk hydrogen charging from exposed surfaces. Therefore the guidance resulting from the previous tests on parent material is believed to be transferable to pipeline girth welds.

It is, however, important to also consider the possible influence of secondary residual stresses. Experience suggests that one would not expect significant residual stresses to be present in seamless line pipe parent material as a result of the manufacturing process. However, when using FCGR data to assess girth weld defects within an ECA it is necessary to allow for welding residual stresses, which themselves are dependent on the welding process used and whether any PWHT was performed. SCR girth welds produced offshore during installation tend not to be heat treated, which was the case for the girth welds tested in the current work. In such cases, the recommendation in BS 7910 (2005) is to assume a uniform welding residual stress of yield strength magnitude in the calculations. This assumption is implicit in the current work as all tests were carried out at a relatively high stress ratio (R = 0.5). Testing at R = 0.5 also minimises any possible crack closure effects (Pippan et al., 1994), unless the environment causes a significant increase in crack opening force.

For an internal circumferential surface-breaking flaw at a pipeline girth weld, the residual stress profile perpendicular to the flaw (and in this case the weld) will be limiting. While the assumption of uniform residual stresses of yield strength magnitude is a common approach, it is also recognised as being conservative, even if the residual stresses are allowed to relax under applied load. For relatively thick-walled pipe it has also been shown that residual

stresses tend to be lower on the inner surface of a multi-pass pipeline girth weld, due to the stress relieving effect of each new weld pass. However, it is difficult to provide generic quantitative guidance and a combination of measurement and modelling is recommended to justify any less conservative assumption.

Comparing the FCGR data from the air tests on parent material and the welded specimens (notched in the weld and in the HAZ) there is no apparent influence of welding residual stresses in the current case (Figure 4.21). This is perhaps not unexpected since there will undoubtedly have been some stress relief in machining the specimens from the pipe. There is no reason why residual stresses would have an influence in a sour environment but not in air.

4.4 DEFECT ASSESSMENT PROCEDURES

The defect assessment work performed as part of this research project was published in *Key Engineering Materials*, and is reproduced in full in **Appendix E** (Holtam et al., 2009b). The case considered assumes a circumferential surface-breaking girth weld flaw on the internal surface of a typical SCR (Figure 4.24), operating in a sour environment and subject to vortex induced vibration (VIV) fatigue loads.

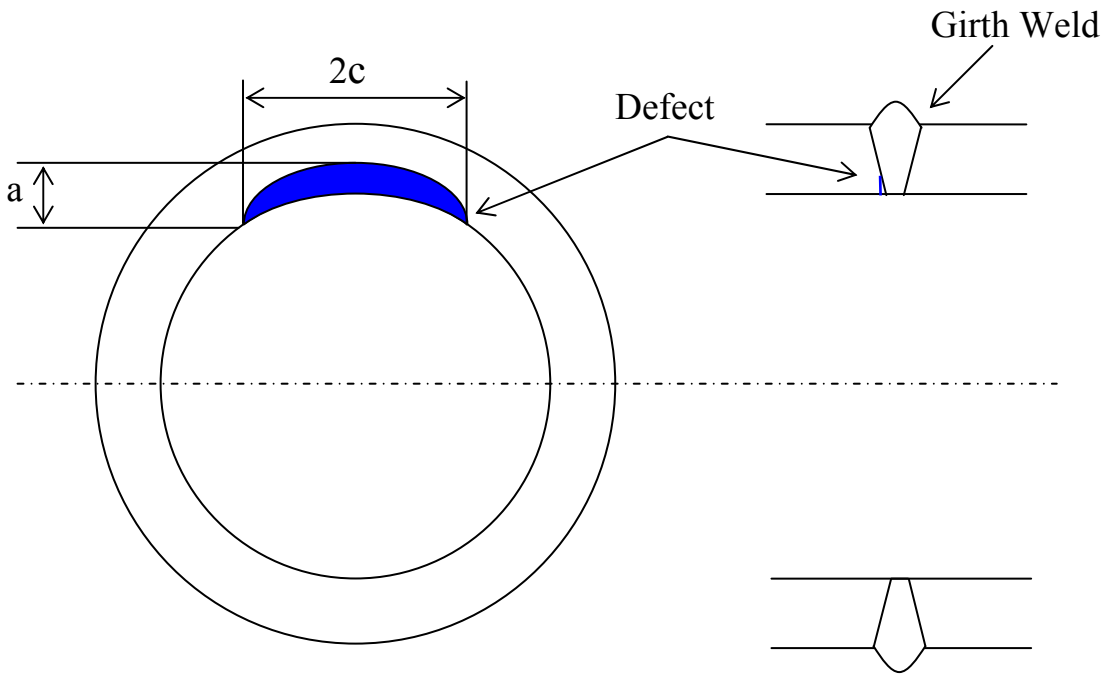

Figure 4.24 Defect orientation relative to steel catenary riser; circumferential internal surface-breaking flaw located at a girth weld (Holtam et al., 2009b).

Example ECA calculations were based on the FAD approach (Section 2.1) within the framework of BS 7910 (2005), using TWI's commercial software CRACKWISE 4. The influence of certain key (mechanical) input variables are demonstrated, including the FCGR, determined from the test results generated as part of the fatigue testing programme. For assessment purposes, surface-breaking flaws are idealised as being semi-elliptical. Standard practice is to calculate K at the base of the flaw (i.e. the deepest point) and at the surface of the flaw. For fatigue assessments, the corresponding increments of crack growth at both

locations are calculated, while for static failure assessments the maximum (or worst case) is used.

The SCR is assumed to be constructed from seamless C-Mn line pipe parent material to API 5L grade X65, with dimensions as indicated in Table 4.11, so as to match as closely as possible the experimental work.

Table 4.11 Assumed geometry of steel catenary riser (Holtam et al., 2009b).

Outside Diameter	355.6 mm (14 ”)
Wall thickness	20.6 mm
Mean radius	167.5 mm
Weld cap width	12 mm
Weld root width	4 mm
Weld Misalignment	1 mm

An aspect ratio of 10 (flaw length to flaw height) was chosen for the initial flaw size. The weld was assumed to be a full-penetration girth weld produced using mechanised processes (e.g. Figure 1.2). The internal surface-breaking flaw is therefore assumed to be located at a girth weld, close to the weld root toe.

4.4.1 INPUT PARAMETERS

The local stress concentration at the weld toe is characterised using the parameter M_k and is dependent on what is termed the attachment length, which in the case of an internal surface-breaking flaw in a full penetration pipeline girth weld is the width of the weld root protrusion. For the purposes of this assessment, a weld root width of 4 mm was adopted (Table 4.11). M_k is maximum near the surface of the pipeline and its influence decreases as flaw depth increases. Axial misalignment can be defined as the offset between the centrelines of the pipe wall across the girth weld. Axial weld misalignment generates a bending stress at the location of the flaw. In the current work a maximum level of misalignment of 1 mm was assumed (Table 4.11). A weld cap width of 12 mm was assumed (Table 4.11). The tensile properties used in the ECA calculations are based on tests carried out at TWI on the X65 parent material used to generate the K_{ISCC} and FCGR test data. Uniform welding residual stresses of tensile yield strength magnitude were assumed, although these were allowed to relax under the influence of applied load, along with a maximum axial static stress of 150 MPa, representing a typical maximum operating stress for a SCR.

Fatigue stresses can result from numerous sources. Experience from the offshore industry suggests that the majority of fatigue damage that occurs in SCRs is due to relatively low stress range cycles (i.e. due to the high number of cycles at these low stresses and the relatively few cycles at higher stresses). In this regard stresses due to VIV often tend to dominate for the specific case of SCRs. Shutdown-restart sequences, which can dominate the fatigue assessment of high pressure, high temperature flowlines subject to lateral buckling, tend not to be significant in the case of SCRs. In the current work, the life of the SCR is also not affected by the position of the flaw around the circumference of the pipe as is the case with the assessment of flaws in reeled pipelines, for example.

For stresses arising from VIV, a safety factor of 20 is often applied to the design life, owing to the high degree of uncertainty in the loading spectrum, to provide a conservative prediction of

fatigue life. The first weld at the top of the SCR and the touchdown point (TDP), where the nominally vertical riser meets the pipeline or flowline on the seabed, are the most stressed locations and are, therefore, critical in terms of fatigue loading (Baxter et al., 2007, Petruska et al., 2006). The critical location for VIV is often the top of the riser since this is subject to higher stress ranges than the TDP, if only for a small number of cycles.

The fatigue spectrum used in the current work is based on a design life of 30 years for the SCR. A typical VIV fatigue spectrum for the TDP and top weld of a SCR was scaled such that a simple S-N analysis, using a class E design curve, as defined in BS 7608 (1993) or DNV-RP-C203 (2005), and a knock-down factor of 30 for the sour environment, gave a design life of 600 years (i.e. 30 years with a safety factor of 20). For stress ranges below the constant amplitude fatigue limit a reduced fatigue slope was used in this S-N analysis, as recommended in BS 7608 (Section 4.4, 1993). The final annual fatigue spectrum for both the TDP and the top weld is shown in Figure 4.25. It can be seen that the TDP is subject to a greater number of low stress cycles whereas the top weld has a greater number of higher stress cycles but fewer low stress cycles.

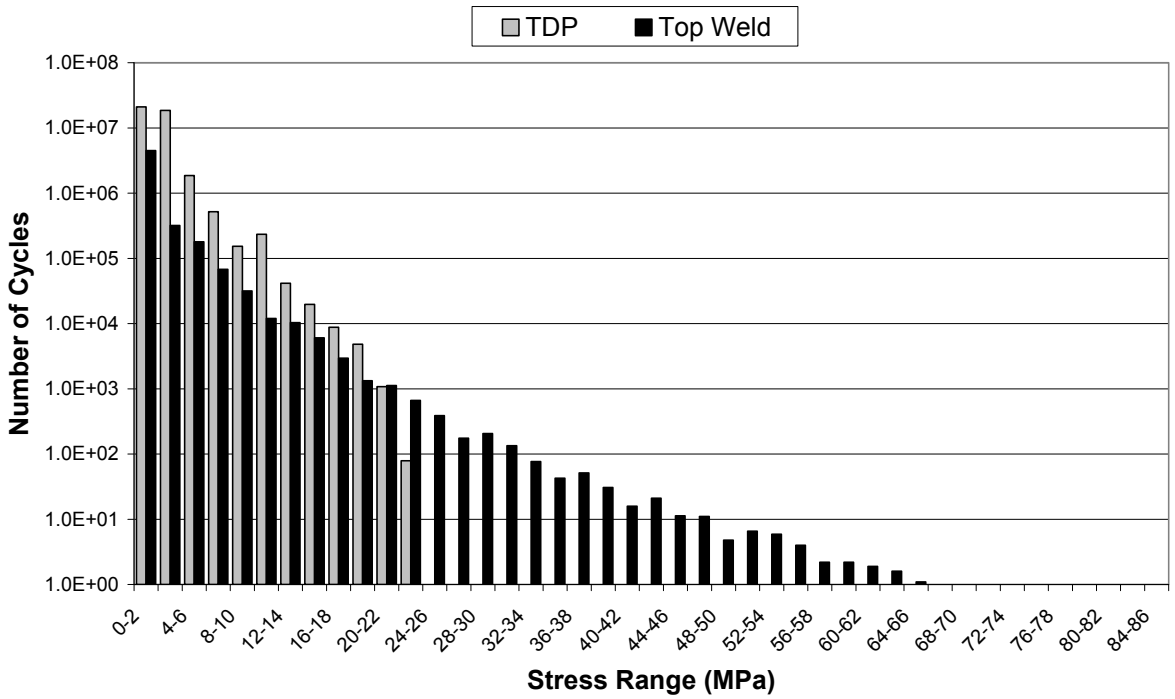

Figure 4.25 Simplified representation of the assumed annual fatigue spectrum due to vortex induced vibration at the touchdown point and top weld (Holtam et al., 2009b).

As noted above, a safety factor of 20 has been assumed in the S-N analysis, and this has been used to scale the fatigue loading spectrum accordingly. It is however standard practice to apply a smaller safety factor on fatigue life when performing ECA calculations. For example a safety factor of 10 would mean a target life of 300 years, a safety factor of 5 would mean a target life of 150 years and no safety factor at all would reduce the target life to 30 years.

Data generated from a decreasing ΔK FCGR test in a sour environment (specimen S7) are shown in Figure 4.26. Also plotted is the mean curve for steels in air ($R \geq 0.5$) taken from BS

7910 (2005), and the design curve for steels in air (i.e. mean plus two standard deviations of log da/dN).

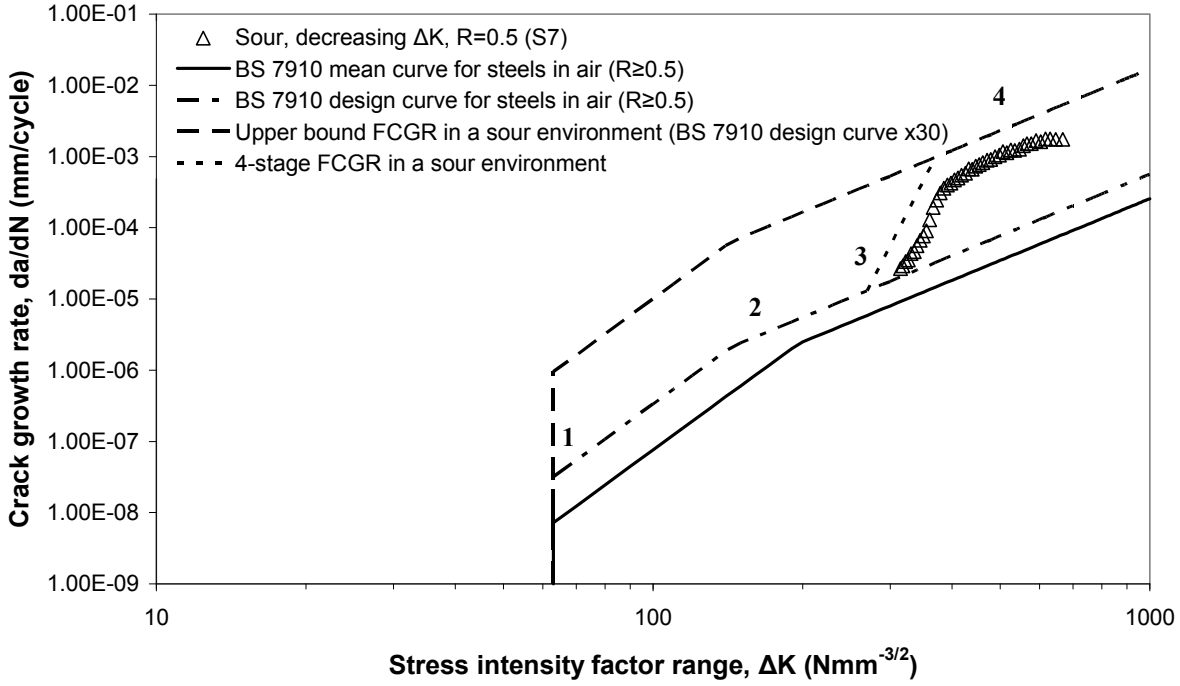

Figure 4.26 Fatigue crack growth rate data used in the engineering critical assessment calculations (Holtam et al., 2009b).

At high ΔK, the FCGR is approximately 30 times higher than the mean curve for steels in air. An appropriate crack growth law for a sour environment can, therefore, be determined by offsetting the design curve for steels in air by a similar amount (Figure 4.26). This provides a relatively simple means of determining an appropriate upper bound to ensure a conservative assessment, but does not take advantage of the fact that the influence of the sour environment appears to be less significant at lower ΔK.

As highlighted in Section 4.3.2.2, at lower ΔK (300-400 $Nmm^{-3/2}$ / 9-13 $MPam^{0.5}$), the FCGR decreased rapidly (more than an order of magnitude) and approached the design curve for steels in air. It is likely that adopting a crack growth law which provides a better fit to the experimental data at low ΔK will have a significant influence on any associated ECA calculations. A four stage law (Figure 4.26) has therefore also been used in the current work to assess the extent to which this affects the determined fatigue lives.

Values of K_{ISCC} are known to depend on environmental parameters such as pH, partial pressure of H_2S and temperature. At ambient temperature and low pH (around 3.5), hydrogen embrittlement effects are expected dominate and K_{ISCC} may be in the range 800-1600 $Nmm^{-3/2}$ (25-50 $MPam^{0.5}$) (Section 2.4.1) (Pargeter et al., 1990, Albarran et al., 1999, Sponseller, 1992, Yang et al., 2009a, Yang et al., 2009b). However, less aggressive environments are often encountered in service (e.g. pH5 and elevated service temperature), corrosion effects become more significant and values of K_{ISCC} may be substantially higher. A K_{ISCC} value of 3160 $Nmm^{-3/2}$ (100 $MPam^{0.5}$) was therefore assumed in the current work, based on TWI's project experience.

4.4.2 STATIC ASSESSMENTS

The first assessment carried out was a static fracture assessment to demonstrate the influence of flaw height (maintaining a constant aspect ratio of 10) for an assumed value of fracture toughness (or K_{ISCC}) of 3160 $Nmm^{-3/2}$ (100 $MPam^{0.5}$), and yield strength magnitude residual stress. Figure 4.27 shows the results of the sensitivity analysis plotted on a FAD for an initial flaw size 3 mm x 30 mm and a final flaw size of 5 mm x 50 mm. Also indicated on Figure 4.27 is the magnitude of K_I for the initial and final flaw sizes. It should be noted, however, that the overall value of K_r also includes a plasticity correction factor to allow for interaction of the primary and secondary stress contributions.

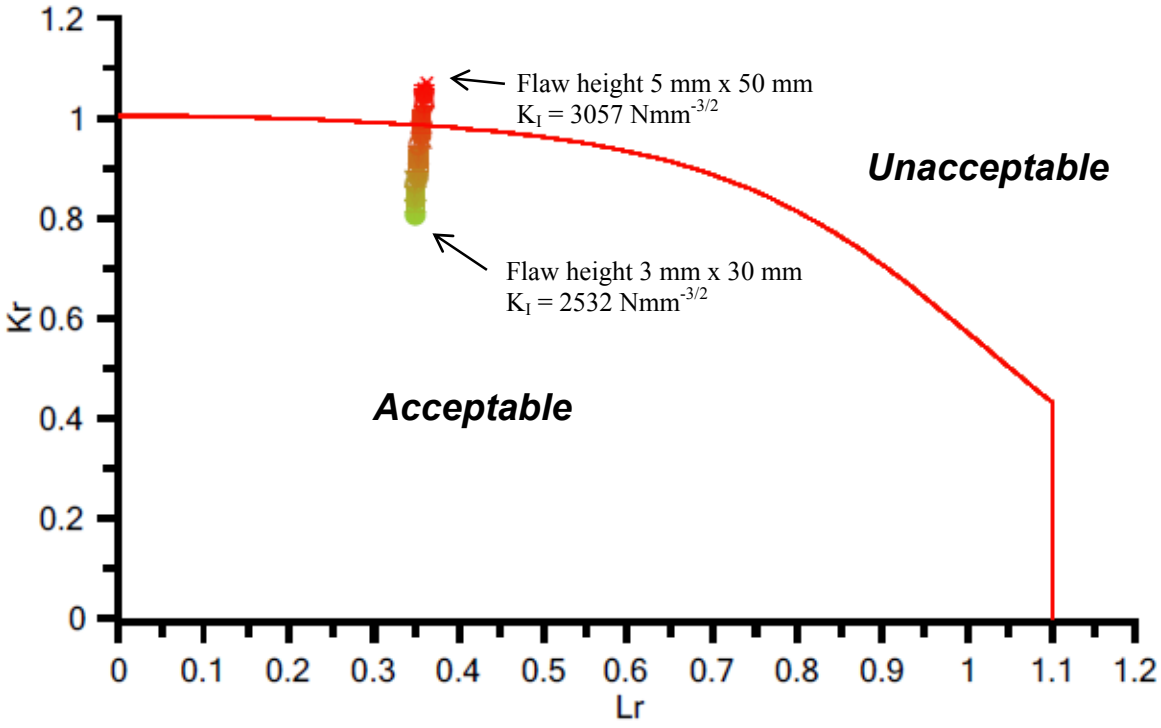

Figure 4.27 Sensitivity analysis for flaw heights (constant aspect ratio of flaw length to flaw height of 10) from 3 mm x 30 mm to 5 mm x 50 mm for assumed value of K_{ISCC} of 3160 $Nmm^{-3/2}$ (100 $MPam^{0.5}$), and yield strength magnitude residual stress.

A second static fracture assessment was then carried out to demonstrate the effect of fracture toughness (or K_{ISCC}) on sour (i.e. low toughness) defect assessments under static loading conditions. A sensitivity analysis was performed whereby critical flaw height (maintaining a constant aspect ratio of 10) was determined as a function of fracture toughness, for yield strength magnitude residual stress. Figure 4.28 shows the resulting plot of critical flaw height against fracture toughness and Figure 4.29 plots the same results on a FAD. Figure 4.28 shows that for an assumed value of K_{ISCC} of 3160 $Nmm^{-3/2}$ (100 $MPam^{0.5}$), and yield strength magnitude residual stress, a maximum tolerable flaw size of 4.5 mm x 45 mm might be tolerated, whereas if the assumed value of K_{ISCC} is 2500 $Nmm^{-3/2}$ (80 $MPam^{0.5}$) a flaw of the order of 3 mm x 30 mm could be tolerated. A 3 mm x 30 mm flaw is of the order of magnitude that could be reliably detected via automated ultrasonic (AUT) inspection while at the same time not triggering an unfeasibly large number of repairs. Figure 4.29 indicates that the critical flaw heights all lie in a similar region of the FAD, towards the K-controlled region.

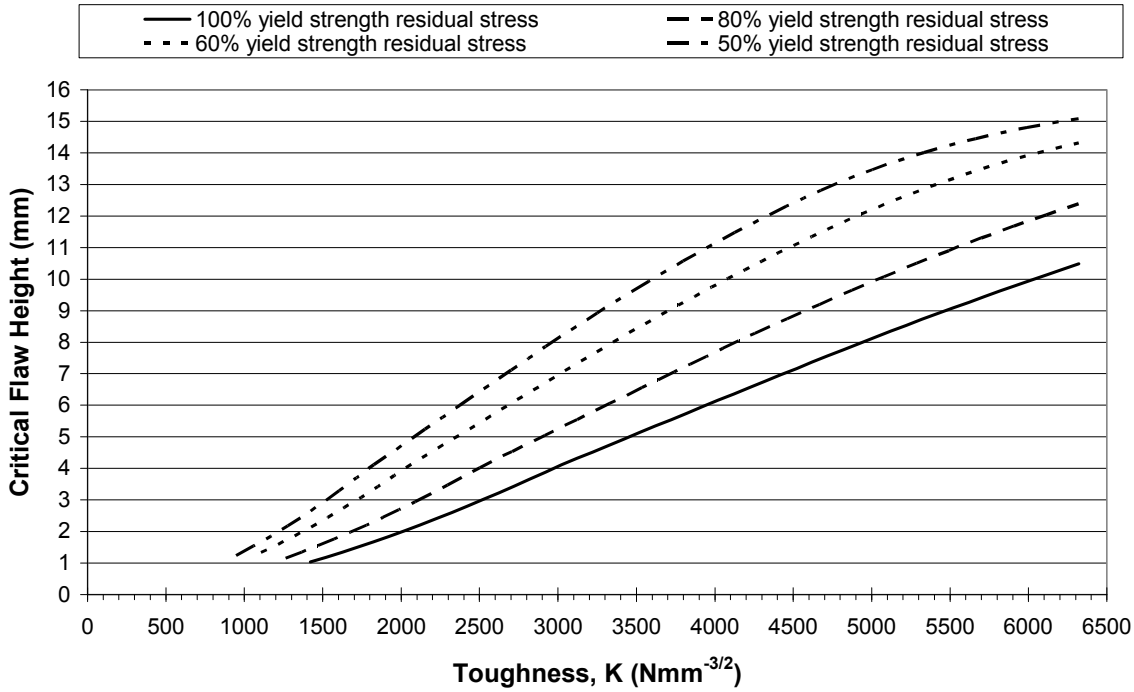

Figure 4.28 Critical flaw height (constant aspect ratio of flaw length to flaw height of 10) as a function of fracture toughness, for different magnitudes of residual stress (Holtam et al., 2009b).

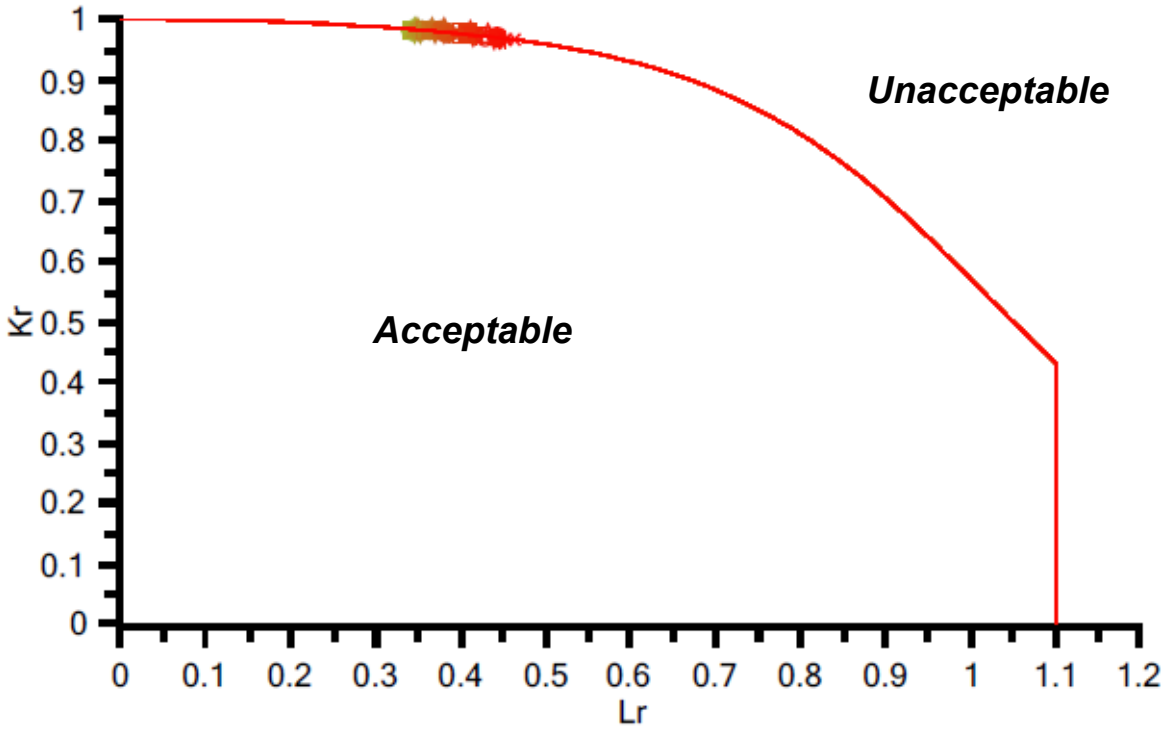

Figure 4.29 Failure assessment diagram showing results of sensitivity analysis whereby critical flaw height (maintaining a constant aspect ratio of flaw length to flaw height of 10) was determined as a function of fracture toughness, for yield strength magnitude residual stress.

Figure 4.28 also demonstrates the effect of welding residual stress. Based on an assumed value of K_{ISCC} of 3160 $Nmm^{-3/2}$ (100 $MPam^{0.5}$), if welding residual stress could be reliably shown to be of only half yield strength magnitude, then the critical flaw size would increase from approximately 4.5 mm x 45 mm to approximately 8.6 mm x 86 mm. Similarly, if this could be shown to be the case then the minimum value of K_{ISCC} for a 3 mm x 30 mm flaw to be tolerable would decrease to approximately 1600 $Nmm^{-3/2}$ (50 $MPam^{0.5}$).

4.4.3 FRACTURE AND FATIGUE ASSESSMENTS

Combined fracture and fatigue assessments were performed using an assumed initial flaw size (for example 3 mm x 30 mm), a K_{ISCC} value of 3160 $Nmm^{-3/2}$ (100 $MPam^{0.5}$) and yield strength magnitude welding residual stresses that were allowed to relax under applied load. Two different fatigue spectrums were used, representing VIV loading at the TDP and top weld (Figure 4.25). At both the TDP and the top weld, three assessments were performed using the following fatigue crack growth laws:

1. In air conditions, based on the two stage design curve for steels in air from BS 7910 (2005).
2. A two stage upper bound sour environment curve, a factor of 30 higher than the two stage design curve for steels in air from BS 7910 (2005) but with the same threshold ΔK_{TH}.
3. A four stage sour environment curve; the first two stages correspond to the design curve for steels in air and the final stage the upper bound sour environment curve (Figure 4.26).

The results of the above assessments are summarised in Table 4.12. For the TDP there is no difference between using the design curve for steels in air and the four stage law for a sour environment, with both achieving the desired fatigue life of 600 years (Figure 4.30). This is because the stresses are so low that they never result in a value of ΔK in either stage 3 or 4 of the four stage fatigue crack growth curve. The transition from stage 2 to stage 3 of the four stage fatigue crack growth curve occurs at a value of ΔK of 270 $Nmm^{-3/2}$ (9 $MPam^{0.5}$). For a 3 mm x 30 mm flaw, a stress range of 24 MPa (the maximum in the annual fatigue spectrum for the TDP) results in a value of ΔK of approximately 92 $Nmm^{-3/2}$ (3 $MPam^{0.5}$). The above assessments only consider fracture and fatigue. For such long lives (>600 years) other damage mechanisms such as corrosion may intervene.

The upper bound curve on the other hand results in a fatigue life of only 22 years (Figure 4.31). A similar result is obtained for the top weld although now there is an observed difference between the in-air curve and the four stage sour curve. This is due to there being higher stress ranges at the top weld (Figure 4.25). For a 3 mm x 30 mm flaw a stress range of 86 MPa (the maximum in the annual fatigue spectrum for the top weld) results in a value of ΔK of approximately 330 $Nmm^{-3/2}$ (10 $MPam^{0.5}$).

Table 4.12 Results of fracture and fatigue engineering critical assessment calculations at the touchdown point and top weld positions for in-air conditions, an upper bound sour environment curve and a four stage sour environment curve (Holtam et al., 2009b).

		Air	Sour - Four Stage	Sour - Upper Bound
TDP	Life (based on initial flaw size of 3 mm x 30 mm)	686 years	686 years	22.2 years
	Final Flaw Size (based on initial flaw size of 3 mm x 30 mm)	4.8 mm x 31.1 mm	4.8 mm x 31.1 mm	4.7 mm x 31.0 mm
	Critical Flaw Size for 30 Years Life (i.e. no safety factor on fatigue life in ECA)	4.2 mm x 42 mm	4.2 mm x 42 mm	2.4 mm x 24 mm
	Critical Flaw Size for 150 Years Life (i.e. safety factor of 5 on fatigue life in ECA)	3.8 mm x 38 mm	3.8 mm x 38 mm	2.0 mm x 20 mm
	Critical Flaw Size for 300 Years Life (i.e. safety factor of 10 on fatigue life in ECA)	3.4 mm x 34 mm	3.4 mm x 34 mm	1.8 mm x 18 mm
Top Weld	Life (based on initial flaw size of 3 mm x 30 mm)	537 years	435 years	17 years
	Final Flaw Size (based on initial flaw size 3 mm x 30 mm)	4.8 mm x 31.7 mm	4.8 mm x 31.5 mm	4.6 mm x 31.6 mm
	Critical Flaw Size for 30 Years Life (i.e. no safety factor on fatigue life in ECA)	4.2 mm x 42 mm	4.1 mm x 41 mm	2.5 mm x 25 mm
	Critical Flaw Size for 150 Years Life (i.e. safety factor of 5 on fatigue life in ECA)	3.8 mm x 38 mm	3.6 mm x 36 mm	1.3 mm x 13 mm
	Critical Flaw Size for 300 Years Life (i.e. safety factor of 10 on fatigue life in ECA)	3.4 mm x 34 mm	3.2 mm x 32 mm	0.9 mm x 9.0 mm

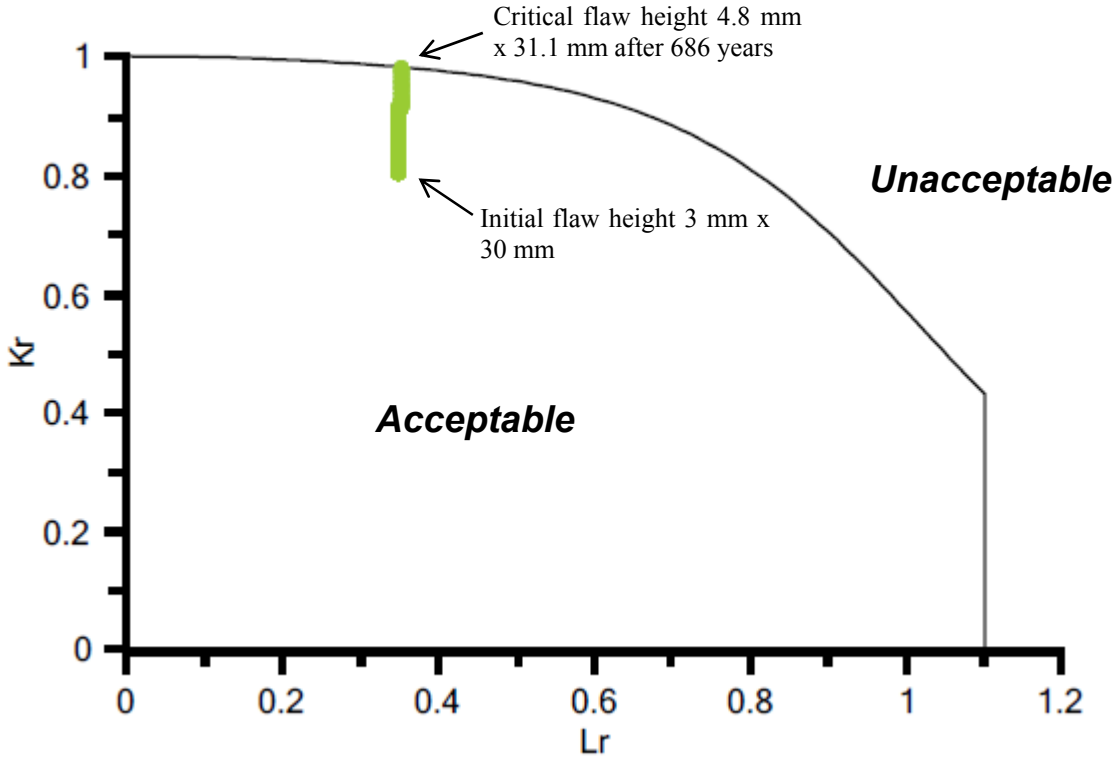

Figure 4.30 Failure assessment diagram showing results of fracture and fatigue assessment at the touchdown point using the four stage law for a sour environment for an assumed K_{ISCC} value of 3160 $Nmm^{-3/2}$ (100 $MPam^{0.5}$) and yield strength magnitude welding residual stresses. The same result was obtained for the design curve for steels in air.

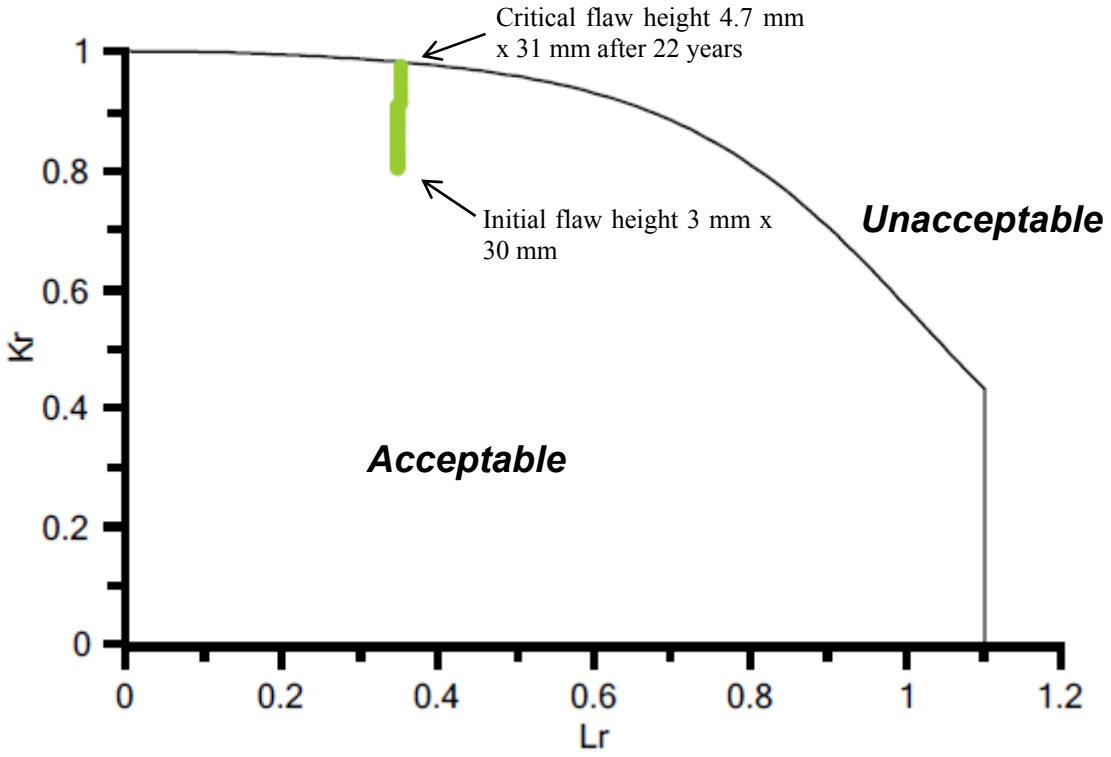

Figure 4.31 Failure assessment diagram showing results of fracture and fatigue assessment at the touchdown point using the upper bound sour environment curve for an assumed K_{ISCC} value of 3160 $Nmm^{-3/2}$ (100 $MPam^{0.5}$) and yield strength magnitude welding residual stresses.

For both the TDP and top weld, critical flaw sizes have also been calculated based on no safety factor on fatigue life in the ECA (target fatigue life 30 years), a safety factor of 5 (target fatigue life 150 years) and a safety factor of 10 (corresponding to a target fatigue life of 300 years) (Table 4.12). Despite the upper bound curve producing short estimates of life for an initial flaw of 3 mm x 30 mm, the TDP could tolerate an initial flaw of 2 mm x 20 mm with a safety factor of 5, which is still close to a typical AUT inspection limit. At the top weld however a safety factor of 5 on fatigue life results in a critical flaw size of approximately 1.3 mm x 13 mm.

4.5 SUMMARY

The aim of this chapter was to describe the key results of the research undertaken. An environmental crack depth effect has been observed whereby shallow flaws appear to grow faster than deeper flaws in a sour environment at the same (low) value of ΔK. The observed behaviour is believed to be dominated by bulk hydrogen charging, i.e. hydrogen charging by absorption from the external surfaces of the specimen rather than at the crack tip, and a lower concentration of hydrogen exists in the centre of the specimen than at the edges. The influence that such an environmental crack depth effect might have on real-life ECA calculations was also demonstrated. The main conclusions and industrial relevance of this research project are summarised in Section 5.

5 FINDINGS & IMPLICATIONS

5.1 INFLUENCING FACTORS ON MATERIAL BEHAVIOUR IN A SOUR ENVIRONMENT

5.1.1 BEHAVIOUR UNDER STATIC LOADING

For X65 pipeline steel tested under static loading conditions in a sour environment, K_{ISCC} does not appear to be crack depth dependent, for flaw depths between approximately 1-8 mm (Figure 4.5). Over this range, deep crack K_{ISCC} data appear to provide a conservative estimate of resistance to crack extension in a sour environment. Possible differences in crack tip chemistry or bulk hydrogen charging do not appear to be affecting material behaviour in this instance. It is therefore possible that these effects only become apparent under conditions of dynamic equilibrium associated with fatigue loading and progressive crack extension. However it is also worth reiterating that the constant load tests were carried out in a much more severely hydrogen charging environment than the FCGR tests, which may mask any crack tip chemistry effects.

Over the range of flaw sizes examined, deep crack K_{ISCC} data appear to provide a conservative estimate of resistance to crack extension in a sour environment. However, for flaws of a depth less than 1 mm, a transition from K-controlled to stress-controlled behaviour is expected. For material behaviour in this regime, a two-parameter assessment methodology is required, and this may take the form of either a Kitagawa-type diagram or a FAD based on sour service properties. The latter provides a convenient means of assessing defect tolerance under these conditions, but it remains to be seen whether standard FAD assessment lines are appropriate for this failure mechanism.

To investigate the transition from K-controlled to stress-controlled behaviour it would be necessary to either test specimens containing shallower flaws (say 0.1 - 1.0 mm) or comparable sized flaws in a less aggressive environment (Figure 4.8). Machining down over-sized specimens containing conventional deep flaws was successful in generating flaw depths of approximately 1 mm, but this is not shallow enough to investigate the transition from K-controlled to stress-controlled behaviour, and it is unlikely that this technique could be used to generate shallower flaws that span the entire specimen. As highlighted previously (Section 3.4), certain novel techniques are available for generating shallower flaws (for example initiating a fatigue crack from a focused ion beam (FIB) notch, which has a far sharper root radius than an EDM notch), but practical trials found these to be unsuitable for the current application. An alternative approach would be to generate semi-elliptical ('thumbnail') cracks (Soboyejo and Knott, 1990). However, it would be very difficult to know the flaw dimensions until the test had been completed and the specimen had been broken open. It is recommended, therefore, that future work to validate the FAD approach for sour ECAs and investigate the transition from K-controlled to stress-controlled behaviour be based around testing in a less aggressive environment whereby $K_{ISCC} > 850$ Nmm$^{-3/2}$ (27 MPam$^{0.5}$).

5.1.2 BEHAVIOUR UNDER CYCLIC LOADING

The aim of the fatigue testing programme was to provide guidance for generating experimental FCGR data in a sour environment, to ensure that experimental test data are appropriately, but not overly, conservative. FCGR data have been generated in air and in a sour environment for four different microstructures (X65 pipeline steel parent material, girth

welds notched in the weld metal and in the HAZ, and simulated HAZ material) and the influence of key variables such as loading conditions, crack depth, specimen geometry, pre-soaking and coating configuration has been investigated.

Regardless of any of the variables investigated, there were increased FCGRs for shallow flaws (at low ΔK) compared to deeper flaws in the same sour environment. This highlights the potential non-conservatism associated with using deep crack data to predict the behaviour of shallow flaws. It is likely that in this instance the observed behaviour is associated with bulk hydrogen charging, i.e. hydrogen charging by absorption from the external surfaces of the specimen rather than at the crack tip, and a lower concentration of hydrogen exists in the centre of the specimen than at the edges.

5.2 UNDERSTANDING OF UNDERLYING MECHANISMS

If bulk hydrogen charging effects are dominating the observed behaviour, one would expect a higher crack growth rate for a shallow flaw (at the start of a test) compared to a deeper flaw, where crack growth will be occurring through material containing less absorbed hydrogen, due to an increased average distance from the nearest exposed surface. Measurements of diffusible hydrogen concentration have confirmed that the concentration of hydrogen is highest close to an exposed surface (Section 4.3.2.5). One would also expect a higher crack growth rate at the edge of the specimen than along the specimen centreline, as was the case for those specimens tested with the standard coating configuration (e.g. Figure 4.10). It would be interesting to analyse the local concentration of hydrogen at different points on a specimen fracture face. Unfortunately there is not currently a suitable method for measuring local hydrogen concentration as a function of spatial position (Section 3.3.3), although the use of SIMS perhaps warrants further investigation.

Crack closure effects could also result in an apparent dependence on crack depth, due to a reduced level of closure for a shallow flaw, or due to the progressive build up of corrosion products within the crack during a test. Crack closure will, of course, not be a contributing factor in the static K_{ISCC} tests, so this may also explain the difference in behaviour observed in the static and cyclic tests. It has not been possible to obtain a direct measurement of the closure load because of the practical difficulties associated with instrumenting the test specimen whilst immersed in a sour environment. However, it is thought to be unlikely that crack closure is the dominant mechanism. Recalling the work by Pippan et al. (1994) highlighted earlier, one would not expect closure effects to influence FCGRs at $R \geq 0.5$, regardless of the test method used, unless the environment causes a significant increase in crack opening force. All tests in the current programme were carried out at $R \geq 0.5$ to minimise any possible crack closure effects, and this is not believed to be the primary influence on material behaviour.

Changes in crack tip chemistry could also, possibly, lead to a crack depth dependence owing to the enhanced production and absorption of hydrogen for a shallow crack arising from a difference in crack tip pH. However, if hydrogen absorption was dominated by crack tip charging, one would expect to see the same crack growth rate at the centre of the specimen as at the specimen edges, and therefore a straight crack front at the end of the test, which was not the case for specimens tested in a sour environment with the standard coating configuration.

The relative importance of crack tip charging and bulk charging has been investigated by Turnbull and Saenz de Santa Maria (1990). These authors examined the corrosion fatigue

cracking of structural steel in cathodically protected seawater where the applied potential, loading frequency and bulk environment can all influence material behaviour, and the relative importance of crack tip versus bulk charging. Their work concluded that bulk charging was the main source of hydrogen for cathodically protected steel in a salt water environment, at a potential more negative than about 900 mV SCE and a loading frequency of 0.1 Hz. However, in a separate study Gangloff and Turnbull (1986) reported no preferential crack growth near the external surfaces of the specimens when they tested 4130 steel in 3% NaCl, and in this case crack tip hydrogen production was believed to be the dominant source of hydrogen atoms.

Both of these studies focussed predominantly on steel in marine environments, however, the relative importance of bulk versus crack tip hydrogen charging has also been examined for wet H_2S containing environments. Kobayashi and Takeshi (1985) examined the influence of specimen thickness and test duration on the observed value of K_{ISCC} for a steel (measured yield strength ~745 MPa, UTS ~824 MPa) exposed to a sour NACE solution, and concluded that hydrogen absorption inside the crack was negligible compared with that from external surfaces. Kobayashi and Takeshi (1985) observed a similar crack front shape to that in Figure 4.10, with higher crack growth rates close to an exposed surface, and similar observations have also been reported by Barsom (1971), this time in relation to steel in a salt water environment.

FCGR tests carried out on non-standard specimen geometries (Section 4.3.2.3) further support the idea that bulk hydrogen charging from exposed surfaces is dominating (e.g. the thin specimen appeared to develop a more uniform hydrogen distribution in the bulk material). Testing thin specimens in different environments may provide a means of controlling the concentration of hydrogen and provide further insight into whether bulk hydrogen concentration really is the governing factor. However, one could argue that testing specimens with single-sided exposure is more representative of real service conditions, where a through wall variation in hydrogen concentration will develop. It is important to ensure that the hydrogen distribution in the test specimen conservatively reflects that in the real pipe.

Under conditions where bulk hydrogen charging is dominant, it becomes necessary to consider the rate at which hydrogen diffuses into the bulk material (with respect to both test specimens and real pipelines) to ensure that test conditions and associated data are appropriately conservative. A pre-soak period of one week was found to have very little influence on the observed FCGR. However, in the case of a pipeline steel in a sour environment a longer pre-soak period will not necessarily correspond to a higher concentration of hydrogen in the bulk material due to the build-up of the iron sulphide scale on the surface of the steel as a by-product of the corrosion process (Section 2.4). The simple analysis performed to estimate the pre-soak period (Holtam et al., 2010d) did not account for this build-up of scale. It also assumed a constant surface concentration of hydrogen and that all of the hydrogen available at the surface of the steel was absorbed, whereas some will evolve as molecular hydrogen (Section 2.4). However, when corrosion rates may be initially high, but then fall due to the formation of surface scale, the surface concentration may itself decay with time. Mishael et al. (2004) presented the results of similar calculations where a decay constant (τ) was used to represent this behaviour, and hydrogen concentrations at the centre of a plate were then predicted to initially rise, but then reach a peak and fall with increasing time. This is a further factor which may have to be taken into account when considering the influence of crack depth on the observed crack growth rate; it may not be

possible to reach an equilibrium condition where the hydrogen concentration is both uniform and constant throughout the test.

During this research project a number of preliminary tests were performed to investigate FCGRs in hydrogen charged material. This is of interest for the assessment of embedded (or external) flaws propagating in pipelines and risers carrying sour production fluids (i.e. flaws in hydrogen charged material but whose crack tip is not exposed to the sour environment). One can postulate that embedded flaws might exhibit increasing FCGRs as they propagate towards the surface exposed to the sour environment. In order to investigate this, specimens were coated in such a way that only the back face (i.e. that opposite to the notched and pre-cracked face) was exposed to the sour environment and the crack was grown as close as possible to the exposed surface (Figure 5.1).

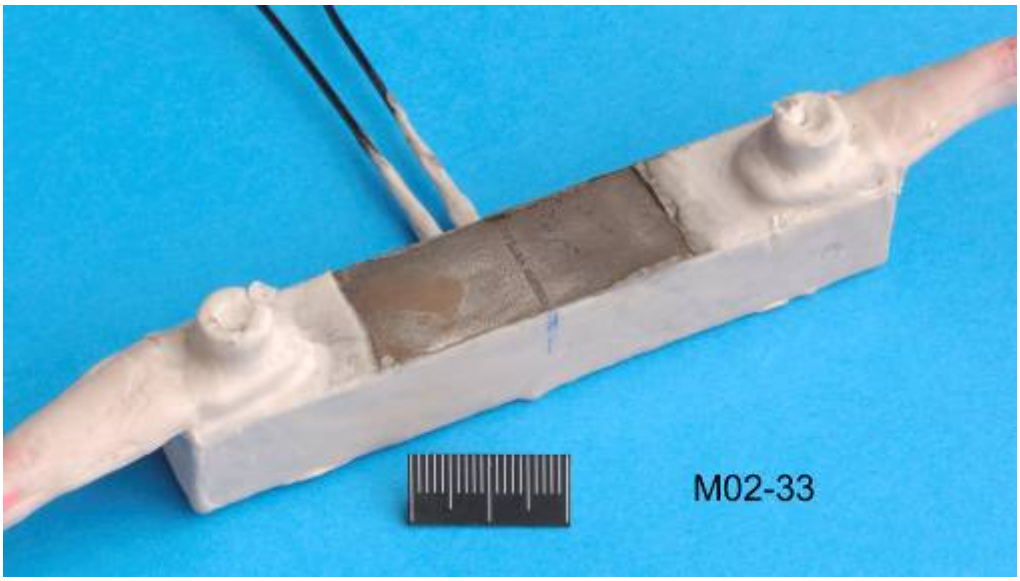

Figure 5.1 Specimen coated such that only the back face (i.e. opposite to that notched and pre-cracked) is exposed to the sour environment (mm scale shown).

Significantly higher FCGRs were observed for embedded flaws in a sour environment compared to in air, and these were largely insensitive to crack depth. However, a number of experimental challenges remain. For example, the protective coating currently used to protect the instrumentation and the bulk of the specimen from the sour environment and minimise the extent of solution contamination successfully prevents the aqueous environment from entering the crack tip. However, examination of the specimen fracture faces after breaking open revealed them to be visibly black, but not corroded (Figure 5.2). This is believed to be due to the diffusion of H_2S through the protective coating (i.e. the coating is not impervious to hydrogen) and the subsequent formation of a thin iron sulphide scale (confirmed via EDX analysis). The presence of H_2S at the crack tip may have accelerated the FCGR and, therefore, the tests were not truly representative of an embedded flaw; they were more representative of FCGRs in dry H_2S.

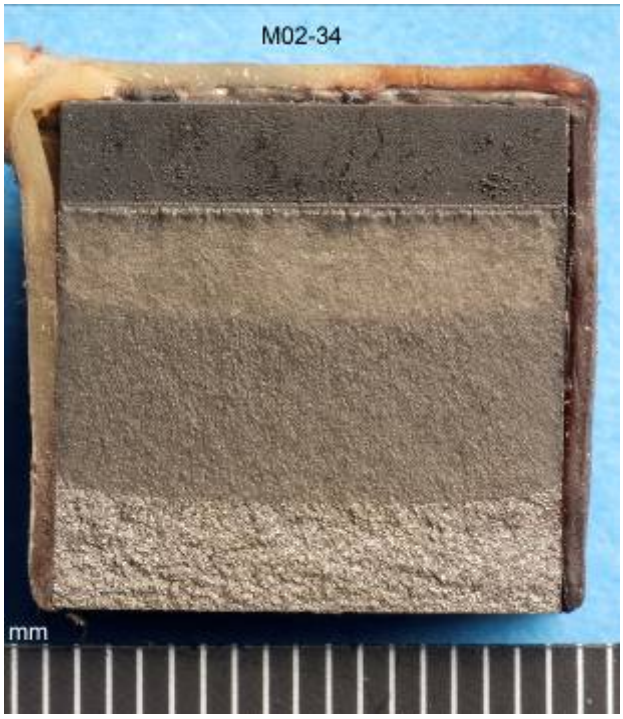

Figure 5.2 Discoloured fracture face from specimen coated such that only the back face was exposed to the sour environment.

These data are unpublished and investigations into FCGRs in hydrogen charged material are ongoing at TWI. The above work will provide valuable insight into the role of crack closure on the observed fatigue crack behaviour. For tests carried out on surface-breaking flaws, corrosion products will build up within the crack over time and may lead to premature crack closure, which will be most noticeable at low ΔK (or more specifically at low K_{min}). This will not be the case for embedded flaws

An alternative approach might be to hydrogen charge specimens in a simulated sour environment but then test them in air. This approach is used to generate toughness (i.e. K_{IH}) data for embedded flaws. In this case specimens are tested in air at slow strain rate (SSR) and measurements of diffusible hydrogen concentration are taken before (on a sample of material exposed to the sour environment for the same length of time as the specimen) and after (on the sample itself) the test. SSR tests are typically complete within a few hours, so hydrogen has sufficient time to diffuse to the crack tip but not enough time to diffuse out of the sample completely. However FCGR tests often take longer than this and by the end of the test most, if not all, of the hydrogen may have diffused out of the sample. Further modelling of the diffusion and transport of hydrogen in pipeline steel specimens would also be of benefit.

5.3 BEST PRACTICE FOR LABORATORY TESTING

Irrespective of the mechanism involved, the possible influence of crack depth on material behaviour should be considered when conducting tests to determine FCGRs for use in fracture mechanics design calculations. The use of a test specimen where the hydrogen concentration varies spatially makes it difficult to generate da/dN–ΔK data in the conventional manner, as the inferred influence of ΔK may be confused with simultaneous variation in local hydrogen concentration. In particular, the use of decreasing ΔK tests may provide a non-conservative estimate of the crack growth rate at low ΔK, as low ΔK data will be generated when the flaw is relatively deep and the hydrogen concentration may be low. In reality a flaw is likely to

grow under conditions of increasing ΔK, and at the beginning of life (when ΔK is low) the flaw will be shallow and the concentration of hydrogen may be high. Therefore, although it is easier to generate low ΔK data under decreasing ΔK conditions, increasing ΔK tests using specimens containing shallow flaws provide a more conservative means of establishing upper bound FCGRs and are recommended whenever possible, to avoid possible crack depth effects at low values of ΔK resulting from testing under decreasing ΔK conditions. While it is acknowledged that the determination of very low ΔK data may then be difficult, the current work has shown that it is possible to generate such data. The use of thin specimens, exposed on all sides, may provide an alternative method for determining conservative data in this regime.

In other work, researchers have successfully fatigue pre-cracked specimens in compression so as to avoid crack retardation associated with prior crack tip plasticity (Hubbard, 1969, Pippan et al., 1994, McKeighan et al., 2008, Newman and Yamada, 2010). Compression-compression pre-cracking results in a short crack that has virtually no load history effect, in theory making it possible to initiate cracks at very low values of ΔK. There is currently no standard method for pre-cracking in compression, although one is currently being developed for CT specimens for future inclusion in ASTM E647 (2008). There is no reason why a similar pre-cracking procedure could not be developed for SENB specimens for inclusion in BS ISO 12108 (2002). The possible benefits of developing a validated procedure for pre-cracking SENB specimens in compression to facilitate generating near threshold FCGR data for C-Mn steel in a sour environment should also be evaluated. For deeper flaws, load history tends to be less of an issue because there is more time to shed the load during pre-cracking once the crack has initiated but before it reaches its target depth.

Single-sided exposure is recommended for specimens tested in a sour environment as this is believed to be more representative of in-service conditions, where a through wall variation in hydrogen concentration will develop. However, it is important to ensure that the hydrogen distribution in the test specimen conservatively reflects that in the real pipe. Specimens with single-sided exposure resulted in almost straight crack fronts, similar to those observed in the tests performed in air. A straight crack front is likely to lead to a slightly more accurate estimate of crack depth via a DCPD system. Pre-soaking a specimen in the sour environment prior to cycling commencing is also recommended, despite not being observed to have a significant effect on the FCGR, to allow hydrogen to diffuse into the bulk of the material and therefore maximise the environmental effect.

5.4 IMPLICATIONS FOR DEFECT ASSESSMENT

To demonstrate the application of new knowledge in an industrial situation, example ECA calculations were performed for internal, surface-breaking, circumferential girth weld flaws, based on the failure assessment diagram (FAD) approach within the framework of BS 7910 (2005). The effect of three critical parameters when performing sour ECAs was demonstrated; the value of K_{ISCC}, the welding residual stress and the assumed FCGR law determined from the test results generated as part of the fatigue testing programme. These were considered in relation to a typical SCR operating under VIV fatigue loading. As highlighted previously, TWI defines the FAD in terms of sour service properties, using K_{ISCC} as the measure of material fracture toughness, which differs slightly from the approach defined in BS 7910, but is believed to be conservative. Deep crack K_{ISCC} data appear to provide a conservative estimate of resistance to crack extension in a sour environment.

Toughness was shown to be a critical parameter in performing sour ECAs under static loading conditions. An accurate estimate of K_{ISCC} is essential as conservative assumptions, in the absence of actual experimental data, could easily lead to failed assessments. Even when experimental data are available, there can be considerable scatter between nominally identical tests. It should also be noted that K_{ISCC} may be strongly influenced by temperature so, for example, K_{ISCC} may be lower during shutdown (at ambient temperature) than during operation (at elevated temperature).

Although K_{ISCC} was shown to be a critical input parameter under static loading conditions, it is interesting to note that this did not appear to be the case within a fracture and fatigue assessment. Examining the upper bound case at the TDP for a fatigue life of 150 years, the critical flaw size is 2.0 mm x 20 mm (Table 4.12) for a value of K_{ISCC} of 3160 $Nmm^{-3/2}$ (100 $MPam^{0.5}$). If K_{ISCC} is increased to approximately 4700 $Nmm^{-3/2}$ (150 $MPam^{0.5}$) the critical flaw size remains at 2.0 mm x 20 mm to achieve a design life of 150 years. If the value of K_{ISCC} is reduced to approximately 2200 $Nmm^{-3/2}$ (70 $MPam^{0.5}$) the critical flaw size is 1.9 mm x 19 mm. In this regard, the value of K_{ISCC} has little effect on the critical flaw size and the assessment is dominated by fatigue. This is also the case for the top weld.

It is therefore apparent that for SCRs subject to VIV, the assumption made regarding fatigue crack growth law may be more significant than the assumption made regarding either K_{ISCC} or welding residual stress. Indeed the assumed fatigue crack growth law, particularly at low ΔK, is likely to be a factor which influences whether a C-Mn material can be used, as opposed to a corrosion resistant alloy or a clad material, particularly at critical locations such as the TDP and top weld.

The test data generated under decreasing ΔK conditions (e.g. Figure 4.26) suggest that the influence of environment at low ΔK is far less severe than at high ΔK, as has also been reported in other work (Bristoll and Roeleveld, 1978, Webster et al., 1985, Vosikovsky and Rivard, 1982, Vosikovsky et al., 1983, Watanabe et al., 1998, Eadie and Szklarz, 1999a, Eadie and Szklarz, 1999b). However, test data generated at low ΔK under increasing ΔK conditions casts doubt on whether FCGRs in a sour environment genuinely approach those seen in air at low ΔK (Figure 4.12) or if this is an artefact of testing under decreasing ΔK conditions. The use of a four stage fatigue crack growth curve (Section 4.4.3), to take advantage of the apparent diminished influence of a sour environment at low ΔK, is therefore believed to be an extremely non-conservative (potentially dangerous) approach to adopt. The most appropriate advice remains therefore, to use an upper bound curve based on experimental crack growth rate data (da/dN- ΔK) generated under increasing ΔK conditions.

The selection of the assumed fatigue crack growth law is, hence, critical when conducting ECA calculations for SCRs subject to VIV. It is recognised that BS 7910 (2005) currently contains only limited guidance on the assessment of flaws in sour service conditions. Methods for the determination of K_{ISCC} and the assessment approach when using this type of laboratory data are still the subject of ongoing research. Guidance pertaining to defect assessment is a key part of this research project, applying the novel sour test data that has been generated to a real-life scenario, and demonstrating the potential impact on current industry practice. Reviewer comments received during publication stated that this work made significant contributions to the advancement of the subject. Although the assessments are based on tests on parent material, the latest work on girth welds has confirmed that the conclusions are transferable.

In the future, as more test data become available, the ECA calculations can be expanded to cover a wider range of flaw types and loading scenarios. For example, the case of an embedded or external flaw has not been considered in the current work due to a lack of relevant FCGR data (Section 5.2). There is already an industry desire to develop models to evaluate flaws that account for a seawater environment on the external surface of a pipeline or riser and a sweet or sour environment on the internal surface. The ability to perform a fracture mechanics test with a specimen exposed to a seawater environment on one surface (perhaps with CP) and a sour environment on the opposite surface is at present unfeasible, but with the increasing investment of time and resources into this research area, will one day likely be possible.

When performing defect assessments, the standard practice is to calculate K at the base of the flaw (i.e. the deepest point) and at the surface of the flaw. For fatigue assessments, the corresponding increments of crack growth at both locations are calculated, whilst for static failure assessments, the maximum (or worst case) is used. However, the same crack growth law is used for through thickness and lateral crack extension. The conservative option is to use a worst case crack growth rate, which for the current research relates to data generated for shallow flaws. However, one could argue that this crack growth rate should only used for assessing lateral crack growth. The through thickness crack growth rate will initially be high (for a shallow flaw) but should then fall (for a given ΔK).

5.5 WIDER IMPLICATIONS AND RECOMMENDATIONS FOR FURTHER WORK

Looking forward, it seems likely that there will be an increased reliance on fracture mechanics-based assessment methods in aggressive corroding environments. There is already the necessity to develop oil and gas reserves in more challenging locations, for example in deepwater or arctic conditions. Many deepwater developments are either sour or expected to become sour through life. The more technically challenging and higher risk the fossil fuel is to extract, the larger the investments required and the higher the breakeven price becomes. In such instances the use of CRAs may not be economically viable. C-Mn steel such as X65 is generally the most economic material for the construction of offshore pipelines and risers but there is an industry need to better understand and quantify its fatigue crack growth behaviour in sour service environments. The oil and gas industry is already considering the use of higher strength carbon steels such as X80 and X100 to meet some of these new technical challenges, despite these being more susceptible to environmental damage such as hydrogen embrittlement. Expectations in terms of safety and pollution control also need to be managed.

There is currently only limited guidance on the assessment of EAC in the main published assessment procedures, such as BS 7910 (2005) and API 579-1/ASME FFS-1 (2007). At the very least it would seem sensible that these documents highlight possible crack depth effects and advise on suitable test methods for generating appropriate data for use in defect assessments. In the case of pipeline steels exposed to sour environments, this lack of guidance is a direct result of the lack of knowledge regarding the limits of use of carbon and low alloy steels. Furthermore, the better industry's understanding of material behaviour in sour environments becomes, the less need there will be for operating companies to undertake project-specific testing to qualify their selected material for their particular service environment.

This research project focused on a single material-environment system; C-Mn steel in a sour environment. The environments that were used for both the static and fatigue testing programmes were quite severe (i.e. high H_2S, low pH and ambient temperature), based on the standard NACE test environments (2005). Complimentary data generated in environments representative of actual service conditions in current offshore developments would certainly be of interest. Furthermore, the service environment will often contain corrosion inhibitor, which could reduce the uptake of hydrogen into the steel. Again, repeating some of this work in an inhibited environment would be of interest to industry. From a testing point of view, one can imagine that the influence of pre-soaking may be different in an inhibited environment. It is important to take measures to ensure that laboratory tests (that are completed in a matter of weeks or months) are representative of actual material conditions, which may have developed after exposure to a corrosive environment over many years. A more fundamental understanding of hydrogen diffusion in and out of steels exposed to sour environments would also be of benefit. The testing of specimens with only the back face exposed to the sour environment (i.e. to represent an external or embedded flaw) would also provide valuable data in this area.

As well as changing the environmental conditions, there are also many other material-environment systems that warrant investigation. For example, duplex stainless steels in a sour environment. In this case there is a noticeable effect on crack growth rate, but the rate of hydrogen diffusion into the bulk of the material is much slower. This would make an interesting comparison with the current work.

The results of tests at low ΔK may provide a means of better understanding fatigue endurance behaviour in a sour environment using strip specimens, and the interaction between initiation and propagation life. Moreover full scale fatigue testing of a pipe in a sour environment would allow the direct qualification of a pipeline girth weld.

5.6 SUMMARY

This research project has investigated the structural integrity assessment of pipeline steels exposed to sour environments. Tests have been performed under constant and cyclic loading. An environmental crack depth effect has been demonstrated under cyclic loading whereby shallow flaws grow faster than deeper flaws at the same (low) value of ΔK. The observed effect is believed to be dominated by bulk hydrogen charging, i.e. hydrogen charging by absorption from the external surfaces of the specimen rather than at the crack tip, and a lower concentration of hydrogen exists in the centre of the specimen than at the edges. The potential influence that such a crack depth effect could have on real-life defect assessments has been demonstrated and recommendations made for how assessments might be improved to account for such crack depth effects.

6 REFERENCES

Akid R, 1994: ‘Modelling environment-assisted short fatigue crack growth’, Advances in Fracture Resistance and Structural Integrity, pp261-269, Pergamon Press.

Albarran J L, Martinez L, Lopez H F, 1999: 'Effect of heat treatment on the stress corrosion resistance of a microalloyed pipeline steel', Corrosion Science 41, pp1037-1049.

ANSI/API, 2007: ANSI/API Specification 5L, ‘Specification for line pipe’, 44th Edition, (Effective date October 1, 2008), The American Petroleum Institute, Washington.

API 579-1/ASME FFS-1, 2007: ‘Fitness-for-service’, The American Petroleum Institute and The American Society of Mechanical Engineers, Washington, 1st Edition.

ASTM STP 1149, 1992: ‘Small crack test methods’, Larsen J M and Allison J E, ASTM, Philadelphia, PA.

ASTM E1820, 2008: ‘Standard test method for measurement of fracture toughness’ American Society for Testing of Materials (ASTM) International, USA.

ASTM E647, 2008: ‘Standard test method for measurement of fatigue crack growth rates’, American Society for Testing of Materials (ASTM) International, USA.

Atkinson J D and Lindley T C, 1977: ‘The effect of frequency and temperature on environmentally assisted fatigue crack growth below K_{ISCC} in steels’, The Influence of Environment on Fatigue, IMechE Conference Proceedings 1977-4, London, pp65-74.

Austen I M and Walker E F, 1977: ‘Quantitative understanding of the effects of mechanical and environmental variables on corrosion fatigue behaviour’, The Influence of Environment on Fatigue, IMechE Conference Proceedings 1977-4, London, pp1-10.

Barsom J M, 1971: ‘Mechanisms of corrosion fatigue below K_{ISCC}’, International Journal of Fracture Mechanics, 7, pp163-182.

Baxter D P, Maddox S J, Pargeter R J, 2007: ‘Corrosion fatigue behaviour of welded risers and pipelines’, OMAE2007-29360 Proceedings of OMAE 2007 26th International Conference on Offshore Mechanics and Arctic Engineering, San Diego, California, USA.

Bristoll P and Roeleveld J, 1978: ‘Fatigue of offshore structures: effect of seawater on crack propagation in structural steel’, Conference Proceedings, European Offshore Steels Research Seminar, ECSC, UK Dept. Energy, Cambridge, Paper 18, The Welding Institute, Cambridge, UK.

British Standards Institution (BSI), 1991: BS PD 6493 ‘Guidance on methods for assessing the acceptability of flaws in fusion welded structures’, British Standards Institution, London.

British Standards Institution (BSI), 1991: BS 7448-1 ‘Fracture mechanics toughness tests, Part 1: Method for determination of K_{IC}. Critical CTOD and critical J values of metallic materials’, British Standards Institution, London.

British Standards Institution (BSI), 1993: BS 7608, 'Code of practice for fatigue design and assessment of steel structures', British Standards Institution, London.

British Standards Institution (BSI), 1995: BS 7539-2, 'Corrosion of metals and alloys - Stress corrosion testing, Part 2: Preparation and use of bent-beam specimens', British Standards Institution, London.

British Standards Institution (BSI), 1995: BS 7539-3, 'Corrosion of metals and alloys - Stress corrosion testing, Part 3: Preparation and use of U-bend specimens', British Standards Institution, London.

British Standards Institution (BSI), 1995: BS 7539-4, 'Corrosion of metals and alloys - Stress corrosion testing, Part 4: Method for the preparation and use of uniaxially loaded tension specimens', British Standards Institution, London.

British Standards Institution (BSI), 1995: BS 7539-5, 'Corrosion of metals and alloys - Stress corrosion testing, Part 5: Preparation and use of C-ring', British Standards Institution, London.

British Standards Institution, 1997: BS 7448-2 'Fracture mechanics toughness tests, Part 2: Method for determination of K_{IC}. Critical CTOD and critical J values of welds in metallic materials, British Standards Institution, London.

British Standards Institution, 1997: BS 7448-4 'Fracture mechanics toughness tests, Part 4: Method for determination of fracture resistance curves and initiation values for stable crack extension in metallic materials, British Standards Institution, London.

British Standards Institution (BSI), 2002: BS ISO 12108, 'Metallic materials - Fatigue testing - Fatigue crack growth method', British Standards Institution, London.

British Standards Institution (BSI), 2003: BS 7539-6, 'Corrosion of metals and alloys - Stress corrosion testing, Part 6: Preparation and use of pre-cracked specimens', British Standards Institution, London.

British Standards Institution (BSI), 2003: BS 7539-9, 'Corrosion of metals and alloys - Stress corrosion testing, Part 9: Preparation and use of pre-cracked specimens for tests under rising load or rising displacement', British Standards Institution, London.

British Standards Institution (BSI), 2005: BS 7539-7, 'Corrosion of metals and alloys - Stress corrosion testing, Part 7: Method for slow strain rate testing', British Standards Institution, London.

British Standards Institution (BSI), 2005: BS 7910, 'Guide to methods for assessing the acceptability of flaws in metallic structures', Amendment 1, British Standards Institution, London.

Buitrago J and Weir M S, 2002: 'Experimental fatigue evaluation of deepwater risers in mild sour service', Deep Offshore Technology Conference, New Orleans, USA.

Buitrago J, Baxter D and Hudak S, 2008: 'High-cycle and low-cycle fatigue resistance of girth welds in sour service', OMAE2008-57545, Proceedings of 27th International Conference on Offshore Mechanics and Arctic Engineering, Estoril, Portugal.

Carneiro R A, Ratnapuli R C and de Freitas Cunha Lins V, 2003: 'The influence of chemical composition and microstructure of API linepipe steels on hydrogen induced cracking and sulphide stress corrosion cracking', Materials Science and Engineering A357, pp104-110.

Chen G S, Wan K -C, Gao M, Wei R P and Flournoy T H, 1996: 'Transition from pitting to fatigue crack growth - Modelling of corrosion fatigue crack nucleation in a 2024-T3 aluminium alloy'. Materials Science and Engineering A219, pp126-132, 1996.

Chiesa M, Nyhus B, Skallerud B, Thaulow C, 2001: 'Efficient fracture assessment of pipelines. A constraint-corrected SENT specimen approach', Engineering Fracture Mechanics, 68, pp527-547, Pergamon Press.

Cooke R J and Robinson J L, 1973: 'Some further considerations of the potential drop method for measuring crack length', Department of Physical Metallurgy and Science of Materials, Research Report, University of Birmingham.

Contreras A, Albiter A, Salazar M and Perez R, 2005: 'Slow strain rate corrosion and fracture characteristics of X-52 and X-70 pipeline steels', Materials Science and Engineering A 407, pp45-52.

DNV-RP-C203, 2005: 'Fatigue design of offshore steel structures', Det Norske Veritas.

DNV-OS-F101, 2007: 'Submarine pipeline systems', Det Norske Veritas, Norway.

Eadie R C and Szklarz K E, 1999a: 'Fatigue crack propagation and fracture in sour dilute brine', Paper No. 611, Proceedings, Corrosion 99, NACE International, Houston, TX.

Eadie R C and Szklarz K E, 1999b: 'Fatigue initiation and crack closure of low alloy steels in sour brine environments', Paper No. 610, Proceedings, Corrosion 99, NACE International, Houston, TX.

Elber W, 1970: 'Fatigue crack closure under cyclic tension', Engineering Fracture Mechanics 2, pp37-45.

European Federation of Corrosion (EFC), 2009: 'Guidelines on materials requirements for carbon and low alloy steels for H2S-containing environments in oil and gas production', Publication Number 16, 3rd edition.

Filiou C, Taylor N, Lejuste P and Houghton R, 2003: 'Survey of current application and future requirements for European fitness-for-service technology', Technical Report No. FITNET/TR2/03, European Fitness-for-Service Thematic Network (FITNET).

FITNET, 2008: 'Fitness-for-Service', Revision MK8, ISBN 978-3-940923-00-4, prepared by the European Fitness-for-Service Thematic Network (FITNET).

Frost N E, Marsh K J and Pook L P, 1974: 'Metal fatigue', Oxford University Press.

Gallagher J P, 1971: 'Corrosion fatigue crack growth rate behaviour above and below K_{ISCC}', Journal of Materials, 6, p941.

Gallagher J P and Wei R P, 1971: 'Corrosion fatigue crack propagation in steels', Proceedings, International Conference on Corrosion Fatigue - Chemistry, Mechanics and Microstructure, Storrs, Connecticut, NACE.

Gangloff R P, 1985: 'Crack size effects on the chemical driving force for aqueous corrosion fatigue', Metallurgical Transactions A, 16A, pp953-969.

Gangloff R P and Turnbull A, 1986: 'Crack electrochemistry modelling and fracture mechanics measurement of the hydrogen embrittlement threshold in steel', Metallurgical Soc AIME Circ, pp55-81.

Gooch T G, 1982: 'Hardness and stress corrosion cracking of ferritic steel', TWI Research Bulletin, 1982, 23(8), pp241-246.

Grabke H J and Riecke E, 2000: 'Absorption and diffusion of hydrogen in steels', Materiali in Tehnologije 34(6), p331.

Griffith A A, 1920: 'Phenomena of rupture and flow in solids', Philosophical Transactions of the Royal Society of London. Series A, 221, pp163-198.

Griffiths A J, Hutchings R B and Turnbull A, 1993: 'Validation of the role of bulk charging of hydrogen in the corrosion fatigue cracking of a low alloy steel', Scripta Metallurgica et Materialia, 29, pp.623-626, Pergamon Press Ltd, USA.

Hammond R I and Baxter D P, 2008: 'Corrosion Fatigue of Simulated C-Mn Steel HAZs in Sour Produced Fluids', OMAE2008-57149, Proceedings of the ASME 27th International Conference on Offshore Mechanics and Arctic Engineering (OMAE), Portugal.

Holtam C M and Baxter D P, 2007: 'Environment assisted cracking assessment methods: The behaviour of shallow cracks', 9th International Conference on Engineering Structural Integrity: Research, Development and Application, China Machine Press.

Holtam C M, Baxter D P, Ashcroft I A and Thomson R C, 2009a: 'The behaviour of shallow cracks in a pipeline steel operating in a sour environment', Journal of Offshore Mechanics and Arctic Engineering (OMAE), August 2009, 131(3), 031302, ASME.

Holtam C M, Baxter D P, Ashcroft I A and Thomson R C, 2009b: 'Influence of fatigue loading on the engineering critical assessment of steel catenary risers in sour deepwater oil and gas developments', Key Engineering Materials, 413-414, pp313-325, Trans Tech Publications, Switzerland.

Holtam C M, Baxter D P, Ashcroft I A and Thomson R C, 2010a: 'Effect of crack depth on fatigue crack growth rates for a C-Mn pipeline steel in a sour environment', International Journal of Fatigue 32, pp288-296, 2010, Elsevier.

Holtam C M, Baxter D P, Ashcroft I A and Thomson R C, 2010b: ‘Fatigue crack growth performance of sour deepwater riser welds’, Proceedings of the 2010 Deep Offshore Technology (DOT) International Conference, Houston, USA.

Holtam C M, Baxter D P, Ashcroft I A and Thomson R C, 2010c: ‘A survey of fitness-for-service trends in industry’, Journal of Pressure Vessel Technology (PVT), ASME. *Paper in press.*

Holtam C M, Baxter D P, Ashcroft I A and Thomson R C, 2010d: ‘An investigation into fatigue crack growth test methods in a sour environment’, International Journal of Offshore and Polar Engineering. *Paper in press.*

Hubbard R P, 1969: ‘Crack Growth under Cyclic Compression’, Journal of Basic Engineering, 91, pp625-631.

Humphries M J, McLaughlin R A and Pargeter R J: 'Toughness characteristics of hydrogen charged pressure vessel steels', Proceedings, International Conference on Interaction of Steels with Hydrogen in Petroleum Industry Pressure Vessel Service, Paris, France, 28-30 March, 1989.

Iravani H and Speck J, 2002: ‘Industry survey of risk based life management practices and their relationship to fitness-for-service assessment’, TWI Report No. 13032/5/02.

Irwin G R, 1957: ‘Analysis of stresses and strains near the end of a crack traversing a plate’, Journal of Applied Mechanics, 24, pp361-364.

Irwin G R, 1960: ‘Plastic zone near a crack and fracture toughness’, Proceedings of the 7th Sagamore Ordnance Materials Research Conference, Paper IV-63.

ISO, 2007: ISO 3183, ‘Petroleum and natural gas industries - Steel pipe for pipeline transportation systems’, 2nd Edition, International Organization for Standardizations (ISO), Switzerland.

Jenkins N, 1990: ‘Progress on hydrogen analysis standardisation’, TWI Bulletin.

Jones R H and Simonen E P, 1994: 'Early stages in the development of stress corrosion cracks', Materials Science and Engineering, A176, pp211-218, 1994.

Kitagawa H and Takahasi S, 1976: 'Applicability of fracture mechanics to very small cracks of the cracks in the early stage’, Proceedings of the Second International Conference on Mechanical Behaviour of Materials, pp627-631.

Kobayashi J I and Takeshi Y, 1985: ‘Evaluation of resistance of steel plate to sulphide stress cracking in sour wet service’, Proceedings of Conference on Predictive capabilities in environmentally assisted cracking (Edited by R. Rungta), ASME, New York, pp223-234.

Kondo Y, 1989: ‘Prediction of fatigue crack initiation life based on pit growth,’ Corrosion, 45(1), pp7-11.

Kumar A N and Panday R K, 1985: 'Process and mechanism of fracture in a pipeline material in chloride and sulphide environments', Engineering Fracture Mechanics 22(4), pp625-633.

McEvily A J and Wei R P, 1971: 'Fracture mechanics and corrosion fatigue', Proceedings, International Conference on Corrosion Fatigue - Chemistry, Mechanics and Microstructure, Storrs, Connecticut, NACE.

McIntyre P, 1973: 'The relationships between stress corrosion cracking and sub-critical flaw growth in hydrogen and hydrogen sulphide gases', Proceedings, International Conference on Stress Corrosion Cracking and Hydrogen Embrittlement of Iron Base Alloys, Unieux Firminy, France.

McKeighan P C, Feiger J H and McKnight D H, 2008: 'The fatigue crack growth rate behaviour of forged A182 steel in lab air, cathodically protected seawater brine and sour brine', Southwest Research Institute (SwRI), Project no. 18.13349.01.001 revised final report (prepared for Mohr Engineering Division, Stress Engineering Services Inc.), San Antonio, Texas, USA.

McMaster F, Thompson H, Zhang M, Walters D and Bowman J, 2007: 'Sour service corrosion fatigue testing of flowline welds', OMAE2007-29060, Proceedings of OMAE2007 26th International Conference on Offshore Mechanics and Arctic Engineering, San Diego, California, USA.

McMaster F, Bowman J, Thompson H, Zhang M and Kinyon S, 2008: 'Sour service corrosion fatigue testing of flowline and riser welds', OMAE 2008-57059, Proceedings of 27th International Conference on Offshore Mechanics and Arctic Engineering, Estoril, Portugal.

Mishael S J, Dean F W H, and Fowler C, 2004: 'Practical applications of hydrogen permeation monitoring', Corrosion 2004, Paper No. 04476, NACE International.

Murtaza G, Akid R, 1995: 'Modelling short fatigue crack growth in a heat-treated low-alloy steel', International Journal of Fatigue, 17(3), pp207-214.

NACE MR0175/ISO 15156-2, 2003: 'Petroleum and natural gas industries - Materials for use in H_2S containing environments in oil and gas production - Part 2: Cracking-resistant carbon and low alloy steels, and the use of cast irons', NACE International, USA.

NACE TM0177, 2005: 'Laboratory Testing of Metals for Resistance to Sulfide Stress Cracking and Stress Corrosion Cracking in H_2S Environments', Item No. 21212, NACE International, USA.

Nakai Y, Tanaka K, Wei R P, 1986: 'Short-crack growth in corrosion fatigue for a high strength steel', Engineering Fracture Mechanics, 24(3), pp433-444.

Newman J C and Yamada Y, 2010: 'Compression precracking methods to generate near-threshold fatigue-crack-growth-rate data', International Journal of Fatigue 32, pp879-885, Elsevier.

Noecker II F F, Pickens G, Wilken G, Dunn G, Lillig D, Jin H and Ayer R, 2009: 'Test method to evaluate the effect of reeling on sour service performance of C-Mn steel linepipe and girth welds', Proceedings of the 19th International Offshore and Polar Engineering Conference, Osaka, Japan, 2009 ISBN 978-1-880653-53-1, ISSN 1098-618.

National Physical Laboratory (NPL), 2000: 'Stress corrosion cracking', Guides to Good Practice in Corrosion Control, update of DTI publication first published in 1982.

Palmer A C and King R A, 2008: 'Subsea Pipeline Engineering', 2nd Edition, Pennwell Corporation, USA.

Pargeter R J, Gooch T G and Bailey N, 1990: 'The effect of environment on threshold hardness for hydrogen induced stress corrosion cracking of C-Mn steel welds', Conference Proceedings Advanced Technology in Welding, Materials, Processing and Evaluation, Japan Welding Society, Tokyo, April 1990.

Paris P C and Erdogan F, 1963: 'A critical analysis of crack propagation laws', Journal of Basic Engineering (Trans. ASME), 85D(4), pp528-534.

Petruska D, Ku A, Masson C, Cook H, McDonald W and Spong R, 2006: 'Calculation of reliability-based safety factors for establishing defect acceptance criteria for deepwater riser welds', Deep Offshore Technology Conference (DOT).

Pippan R, Stuwe H P and Golos K, 1994: 'A comparison of different methods to determine the threshold of fatigue crack propagation', Fatigue, 16, Butterworth-Heinemann Ltd.

Romano-Rodriguez A and Hernandez-Ramirez F, 2007: 'Dual-beam focused ion beam (FIB): A prototyping tool for micro and nanofabrication,' Microelectronic Engineering, 84, pp789-792.

Ruppen J A and Salzbrenner R, 1983: 'The effect of environment on crack closure and fatigue threshold', Fatigue of Engineering Materials and Structures, 6(4), pp307-314, Pergamon Press Ltd.

R6 Revision 4, 2001: 'Assessment of the integrity of structures containing defects', Amendment 7 (April 2009), British Energy Generation Ltd.

Scully J R, Gangloff R P, 2002: 'Environment-assisted cracking: unresolved issues', Corrosion Science: A Retrospective and Current Status, (Organiser) The Electrochemical Society Centennial Meeting, Philadelphia, PA.

Soboyejo W O and Knott J F, 1990: 'An investigation of environmental effects on fatigue crack growth in Q1N (HY80) steel', Metallurgical Transactions A, 21A, November 1990, pp2977-2983.

Sponseller D L, 1992: 'Interlaboratory testing of seven alloys for SSC resistance by the double cantilever beam method', Corrosion, 48 (2), pp159-171.

Suresh S and Ritchie R O, 1982: ‘A geometric model for fatigue crack closure induced by fracture surface morphology’, Metallurgical Transactions 14A, pp1627-1631.

Suresh S, 1991: Fatigue of Materials, Cambridge University Press.

Tang J-Q, Gong J-M, Zhang X-C and Tu S-T, 2006: ‘Comparison on the cracking susceptibility of different low alloy steel weldments exposed to the environment containing wet H_2S’, Engineering Failure Analysis, 13, pp1057-1064.

Tsui T Y and Joo Y-C, 2001: ‘A new technique to measure through film thickness fracture toughness,’ Thin Solid Films 401, pp203-210.

Turnbull A and Saenz de Santa Maria M, 1990: ‘The relative importance of crack-tip charging and bulk charging in hydrogen-assisted cracking in aqueous solutions’, Environment Assisted Fatigue, EGF7 (edited by P. Scott), Mechanical Engineering Publications, London, pp145-153.

Turnbull A, 1993: 'Modelling of environment assisted cracking', Corrosion Science, 34(6), pp921-960.

Turnbull A, McCartney L N and Zhou S, 2006: ‘Modelling of the evolution of stress corrosion cracks from pits,’ Scripta Materialia, 54, pp575-578.

Turnbull A, Horner D A, Connolly B J, 2009: ‘Challenges in modeling the evolution of stress corrosion cracks from pits’, Engineering Fracture Mechanics, 76, pp633-640.

Vasudevan A K, Sadananda K and Louat N, 1994: ‘A review of crack closure, fatigue crack threshold and related phenomena’, Materials Science and Engineering A188, pp1-22, 1994.

Vosikovsky O and Rivard A, 1982: ‘The effect of hydrogen sulphide in crude oil on fatigue crack growth in a pipeline steel’, Corrosion 1982, 38(1), pp19-22.

Vosikovsky O, Macecek M and Ross D J, 1983: ‘Allowable defect sizes in a sour crude oil pipeline for corrosion fatigue conditions’, International Journal of Pressure Vessels and Piping, 13, pp197-226.

Watanabe E, Yajima H, Ebara R, Matsumoto S, Nakano Y and Sugie E, 1998: ‘Corrosion fatigue strength of ship structural steel plates and their welded joints in sour crude oil’, Offshore Mechanics and Arctic Engineering Conference (OMAE 1994), ASME, Vol.III, pp 151-158.

Webster S E, Austen I M and Rudd W, 1985: ‘Fatigue, corrosion fatigue and stress corrosion of steels for offshore structures’, ECSC Report No. EUR 9460, ECSC Steel Publications, European Commission, Brussels.

Yang Z, Da Qin X and Tronskat J P, 2009a: ‘Fracture toughness testing using SENT specimens in a sour environment’, Proceedings of OMAE 2009 28th International Conference on Offshore Mechanics and Arctic Engineering, Honolulu, Hawaii, USA.

Yang Z, Kumar S B and Tronskar J P, 2009b: ‘ECA of pipeline girth weld in sour services’, Proceedings of the 19th International Offshore and Polar Engineering Conference, Osaka, Japan (2009), ISBN 978-1-880653-53-1, ISSN 1098-618.

APPENDIX A

Holtam C M, Baxter D P, Ashcroft I A and Thomson R C, 2010: 'A survey of fitness-for-service trends in industry', Journal of Pressure Vessel Technology (PVT), ASME. *Paper in press.*

A Survey of Fitness-for-Service Trends in Industry

C. M. Holtam
D. P. Baxter
Structural Integrity Technology Group
TWI Ltd
Cambridge
CB21 6AL
UK

I. A. Ashcroft
Wolfson School of Mechanical and Manufacturing Engineering
Loughborough University
Leicestershire
LE11 3TU
UK

R. C. Thomson
Department of Materials
Loughborough University
Leicestershire
LE11 3TU
UK

ABSTRACT

In 2002 TWI Ltd carried out a questionnaire-based survey of 'user experience of plant life management practices', to gain a better understanding of the reality of plant life management and the needs of plant operators [1]. In 2003 the European Fitness-for-Service Network (FITNET) reported the results of their survey on 'current application and future requirements for European Fitness-for-Service (FFS) technology' [2].

In 2006 the management of ageing plant became a regulatory hot topic in the UK with a Health and Safety Executive document on the subject being released [3]. Considering also the recent release of the new API/ASME joint FFS standard [4], TWI Ltd decided 2007 was the ideal time to carry out an updated industry survey, to assess how developments such as these might affect plant life management practices in different industry sectors across the world.

The aims of this survey were to gain an insight into current FFS trends across several industry sectors and how these may change in the future. Information was gathered as to how different companies handle their FFS activities, both in terms of the types of flaw they assess and the complexity of the assessments they carry out. The survey also investigated how Safety Regulating Authorities (SRAs) view FFS activities and whether or not they accept the results as the basis for plant integrity management decisions. Closely related to this is whether there is a need for better regulation of FFS activities, FFS training or indeed whether FFS qualifications should be introduced.

This paper presents the results of the online industry survey and draws pragmatic conclusions that will be of interest to all those involved with FFS activities, from inspectors to researchers and from engineers to insurers.

1 INTRODUCTION

FFS is not a new concept, dating back to the 1960s, but has found more widespread acceptance over the past ten years. Many definitions exist but API 579-1/ASME FFS-1 [4] describes a FFS assessment as 'a quantitative engineering evaluation performed to demonstrate the structural integrity of an in-service component that may contain a flaw or damage'. It is now widely accepted that all welded structures contain flaws of some kind therefore FFS assessments can be used to assess manufacturing flaws prior to a component entering service, or indeed damage that has developed after time in service. To carry out such a task clearly requires a multi-disciplinary approach with input from, for example, metallurgists, corrosion engineers, mechanical engineers, process engineers, fracture mechanics engineers, and inspection personnel.

Numerous papers have been published detailing the historical development of engineering FFS procedures and standards, for example [5-6]. The offshore oil and gas industry was the main driver behind the development of formal FFS procedures, which were particularly aimed at assessing the structural integrity of welded offshore structures in the hostile North Sea environment. The nuclear industry was also involved in the early stages of developing FFS procedures as it was essential to demonstrate the structural integrity and damage tolerance of nuclear reactor vessels, leading to the first revision of the R6 procedure in 1976 [7]. Procedures aimed at the downstream oil and gas industry are a more recent development and represent a shift in FFS approach. It is now clear that there are huge potential economic benefits to be gained by using the results of structural integrity assessments to justify, for example, extending the period between shutdowns or extending the life of ageing components. Nowadays FFS is well established and relied upon across many industrial sectors.

In 2002, as part of a Joint Industry Project (JIP) TWI carried out a questionnaire-based survey aimed at gaining a better understanding of the reality of plant life management and the needs of plant operators [1]. The survey was sent to both sponsors and non-sponsors of the JIP. A total of 91 completed questionnaires were returned to TWI. A survey was also carried out in 2002 (reported in 2003) by the FITNET Thematic Network [2]. The FITNET Thematic Network was launched in 2002 with the aim of developing a European FFS Procedure [8]. The FITNET survey was aimed at providing a picture of the current status of FFS technology and evaluating the priorities for the development of a European FFS code. A total of 68 completed questionnaires were returned to the European Commission.

The release of a joint API/ASME FFS standard [4] potentially represents a significant change in the downstream oil and gas industry since the difference between an API Recommended Practice and an ASME code/standard can be quite significant. Potentially, it will no longer be at the operator's discretion which published FFS standard to use to assess the integrity of their assets; if they are built to ASME codes then it may well become a regulatory requirement to use the ASME FFS standard. With this in mind, it now seems an ideal time to review FFS practices.

2 SURVEY DISTRIBUTION

The survey was distributed via e-mail, containing a brief explanation and a link to the online survey. TWI Ltd is a membership-based research and technology organisation and the survey was sent to TWI's membership database in the oil and gas, power, aerospace, defence and

transport industry sectors. Additionally TWI software licensees or anyone who had downloaded a demo for TWI software in the last 12-months received the survey. TWI also has access to Standard Industrial Classification (SIC) codes and these were targeted based on the industry sectors above. Everyone who had previously attended a TWI training course also received the survey, and finally the survey was made available via TWI's corporate website under 'Latest News'. This section of the website is accessible to non-members.

Clearly the survey did not focus on one industry sector or one region of the world. However, one could argue that the distribution list was not a completely random sample, nor was it a completely 'cold' list; the vast majority of recipients should have at least recognised the name TWI. The total number of completed surveys received was 197, which compares extremely favourably with other similar surveys [1-2]. A survey was considered to have been completed if it was submitted with responses to more than 50% of the questions.

All respondents to the survey were asked to indicate their personal level of FFS experience and the type of assessments they conduct (Figure 1).

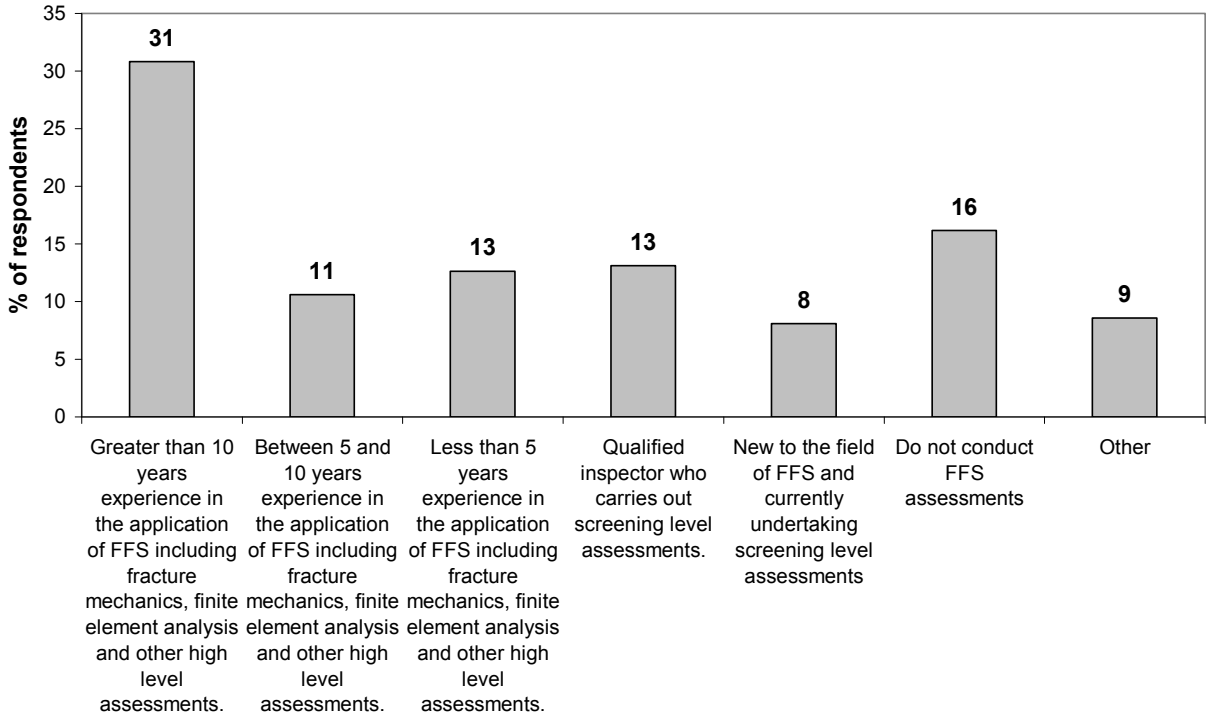

Figure 1 Fitness-for-Service experience of survey respondents.

It is pleasing to note that the survey has canvassed opinions from professionals with a wide range of experience, from those who have never carried out a FFS assessment, to those who have spent more than 10 years applying FFS techniques. The fact that nearly 200 people replied to the survey, almost one third of whom have more than 10 years direct FFS experience provides not only a degree of confidence in the results, but also indicates an increasing use of FFS assessment tools and consequent reliance thereon.

3 SURVEY ANALYSIS

Survey design and analysis techniques have themselves been the subject of much research. Suffice to say data analysis is much more than simply number crunching; it needs to be systematic and consistent. An opinion survey is, after all, a quantitative research method the same as laboratory experiments and numerical methods. A survey should be easily understood and easy to respond to and one should question the reliability of both the data and the analysis used. TWI's 2007 survey contained two types of questions:

1. Constrained (i.e. the respondent must choose the answer that best fits his/her situation from a list of possible answers);
2. Free (i.e. the respondent is free to write whatever they choose).

Constrained questions are useful as the responses are easier to analyse in a quantitative fashion. Free questions often provide useful information but are much more difficult and time consuming to analyse collectively, and indeed accurately. Free questions were therefore kept to a minimum. However, with a view to tempting respondents to provide fuller explanations of their replies a 'free text' box was provided at the end of most constrained questions in which the respondent could make any additional comments. The survey was trialled to last no more than 20 minutes and could be saved at any time to be completed at a later date.

The authors have tried to present as much raw data as possible in this paper. The conclusions that have been drawn are the opinions of the authors and not TWI; they are by no means the only conclusions that could be drawn. It is not possible to present all the survey results in this paper. The authors are not aware of any other formal survey specific to FFS being carried out since 2002. Comparisons will be drawn with both of the surveys discussed previously [1-2], as appropriate, throughout this paper.

The survey included several questions which asked respondents to rank a list of statements or categories, for example in terms of importance. The data obtained from such questions can and has been analysed in a variety of different ways in order to better understand the results. It is always useful to construct a frequency table to indicate the number of rankings for each category. However, when there are numerous categories to choose from such tables are often hard to interpret. Therefore an additional analysis step involved allocating points to each ranking level. For example a ranking of 1 (the most important) would score 7 points (if there were 7 categories to choose from), a ranking of 2 would score 6 and so on down to a score of one point. Zero points were allocated to blank categories indicating zero importance, as stipulated in each question. This points allocation can then be combined with the frequency table to provide an overall score for each category. For example if 20 people ranked a category as being most important and 10 ranked it as being the second most important this would score 200 points (i.e. $20\times7 + 10\times6$). The overall score is then averaged by the total number of responses to provide an indicative average score. While the actual value of the average is of limited use, such a technique can be used to rank the different categories, with the highest average number indicating the most important category. An average calculated in this way does not necessarily tell the complete picture however. For example, lots of high rankings and lots of low rankings would potentially provide a similar average to lots of medium rankings, but this is not obvious from looking at an average alone. Hence the importance of being able to analyse the results in a variety of ways.

The survey results have been filtered by region of the world, industry sector and type of company etc. as appropriate. For the purposes of this paper the results of ranking questions

will be reported in terms of the number of respondents who ranked a particular category as being the most important (i.e. the category that was ranked as '1' most frequently will be reported as being the most important) as this has been found to be indicative of the results in the vast majority of cases. For each ranking question respondents were also given the opportunity to specify additional categories to rank.

4 ANALYSIS AND DISCUSSION OF RESULTS

4.1 GENERAL INFORMATION

Section 1 of the survey focussed on gathering general information about the respondents. For example, respondents were asked to list the region of the world in which their company primarily operated, as shown in Figure 2.

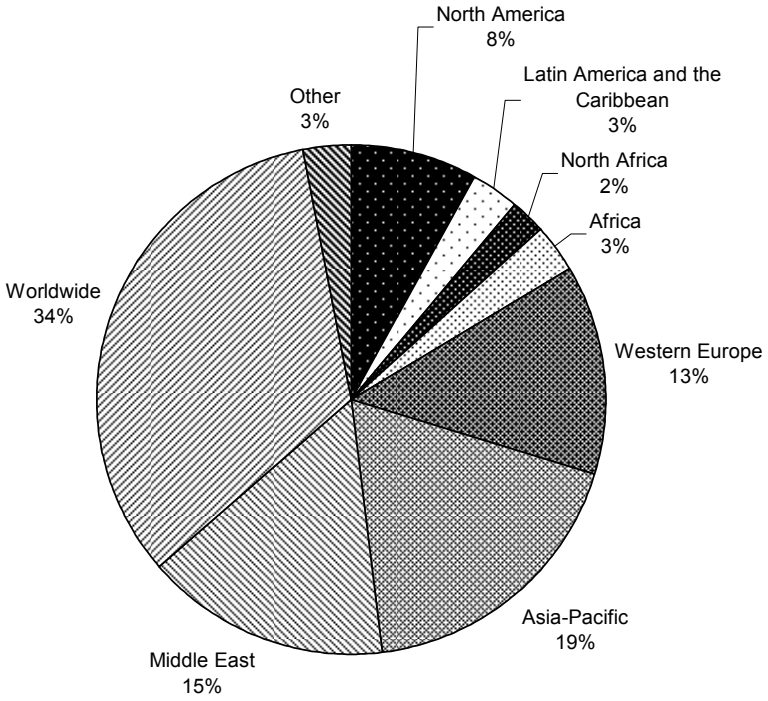

Figure 2 Primary operating regions.

A pleasing spread of responses from around the world was received with approximately one third of respondents considering their companies to have a worldwide operating presence, and the same proportion coming from either the Middle East or Asia-Pacific regions. Those 'other' regions listed tended to be companies that operated in two regions (e.g. Middle East and Africa) as only one selection was permitted.

Respondents were also asked to specify which industry sector their company primarily operated in, as shown in Figure 3. Multiple selections were permitted meaning that the total percentage came out greater than 100%. The results have therefore been normalised by the total number of responses to provide the percentages in Figure 3.

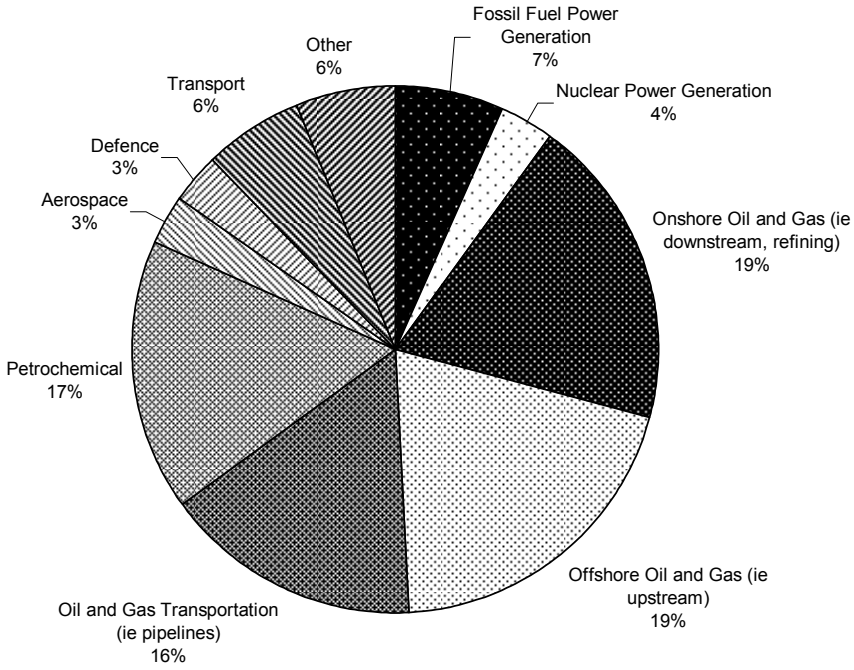

Figure 3 Primary operating sectors.

While all of the industry sectors targeted in the survey responded to some extent, over 70% of the respondents considered themselves to be part of the oil and gas or petrochemical industry sectors. The highest proportion of respondents came from the upstream oil and gas sector, which is perhaps indicative of TWI's membership demographic. Although only 7% of respondents came from the fossil fuel and 4% from the nuclear power generation sectors this represents 26 and 14 responses respectively. The above results may also be indicative of the extent to which FFS tools are used within these sectors. 'Other' sectors listed included, for example, renewables, manufacturing, construction and spacecraft!

Respondents were asked to describe the type of company they worked for (Figure 4). While the vast majority of respondents were either Producers/Operators or Engineering Consultancies/Services Contractor there is good representation from both Equipment Manufacturers/Suppliers and Research and Development Organisations. It is also very pleasing to see that Safety Regulating Authorities (SRAs), Engineering Insurers, Standards Bodies and Universities are each represented.

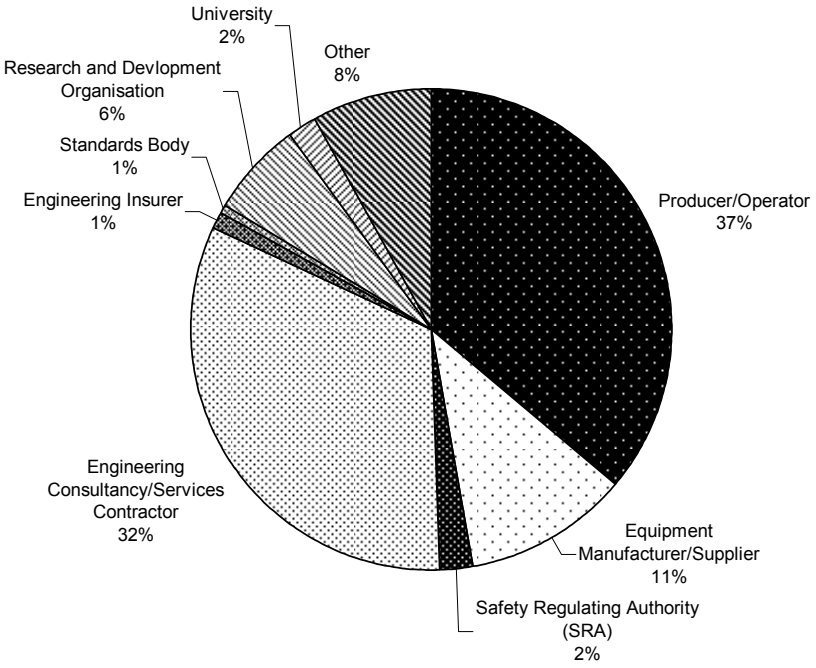

Figure 4 Type of organisation.

4.2 FITNESS-FOR-SERVICE (FFS) METHODS

Section 2 of the survey investigated which FFS methods companies are using. Respondents were asked to describe their companies and/or their local plant's approach to FFS (Figure 5).

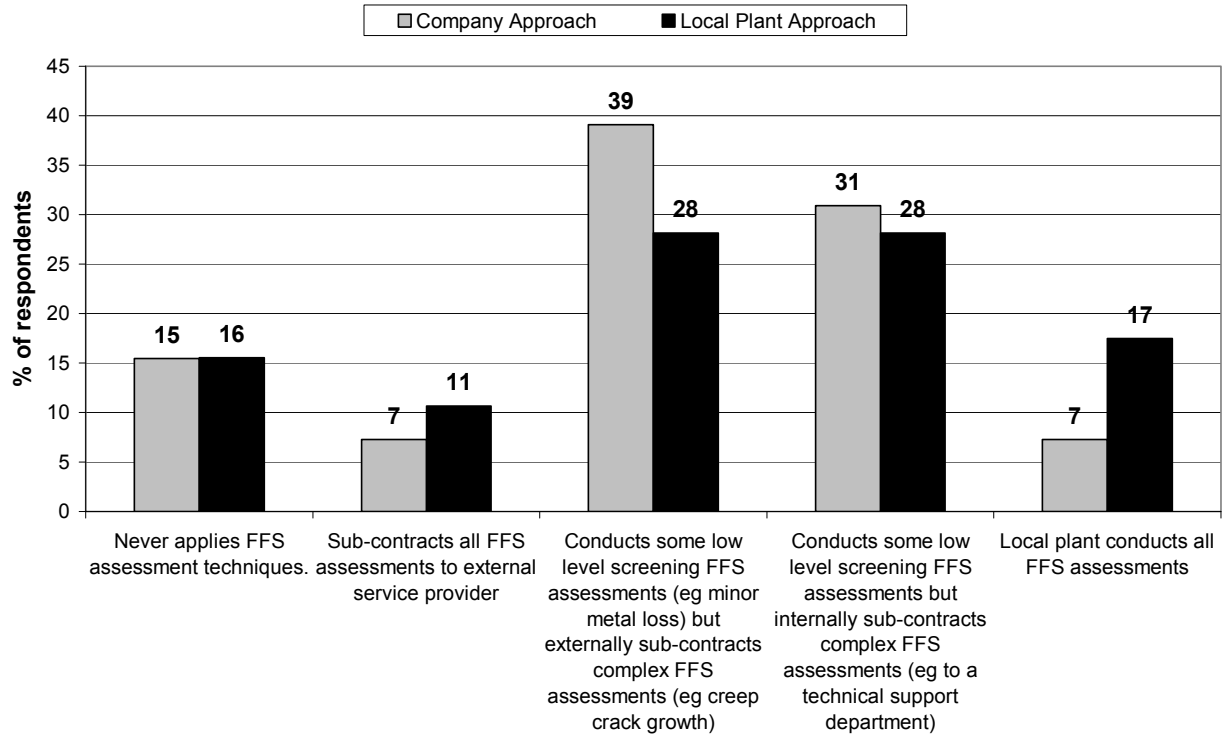

Figure 5 Company and local plant approach to Fitness-for-Service.

For example, a local plant (refinery, power station etc.) may have responsibility for low level screening FFS assessments but the overall operating company may have capabilities for complex cases. Multiple selections were not permitted so respondents had to select the most appropriate from the list provided. If a respondent did not know their companies or their local plant's approach they were requested to leave that section blank. Again, the results have been normalised by the number of responses to give the percentages shown in Figure 5. In addition to the results shown in Figure 5, 50 respondents considered themselves to work for specialist FFS sub-contract companies, SRAs or Engineering Insurers.

Respondents were then asked to describe what FFS was currently being used for, and were provided with the following list of statements describing typical FFS applications.

- Assess the acceptability of defects during fabrication and/or commissioning.
- Determine whether equipment is safe to operate until next planned shutdown.
- Determine whether equipment is safe to operate beyond the next planned shutdown (i.e. to extend period between shutdowns).
- Re-rate equipment prior to a change in use/operation.
- Determine the remaining life of equipment beyond design life.
- Assess in-service repairs.

They were asked to rank them in order of importance to their companies and/or their local plant's operations, the lowest number indicating the most important and highest number indicating the least important. If a particular FFS application was not relevant to or used by a respondents company they were requested not to rank that application by leaving it blank.

Figure 6 shows the percentage of respondents who ranked each FFS application as being the most important to their companies operations, filtered by industry sector.

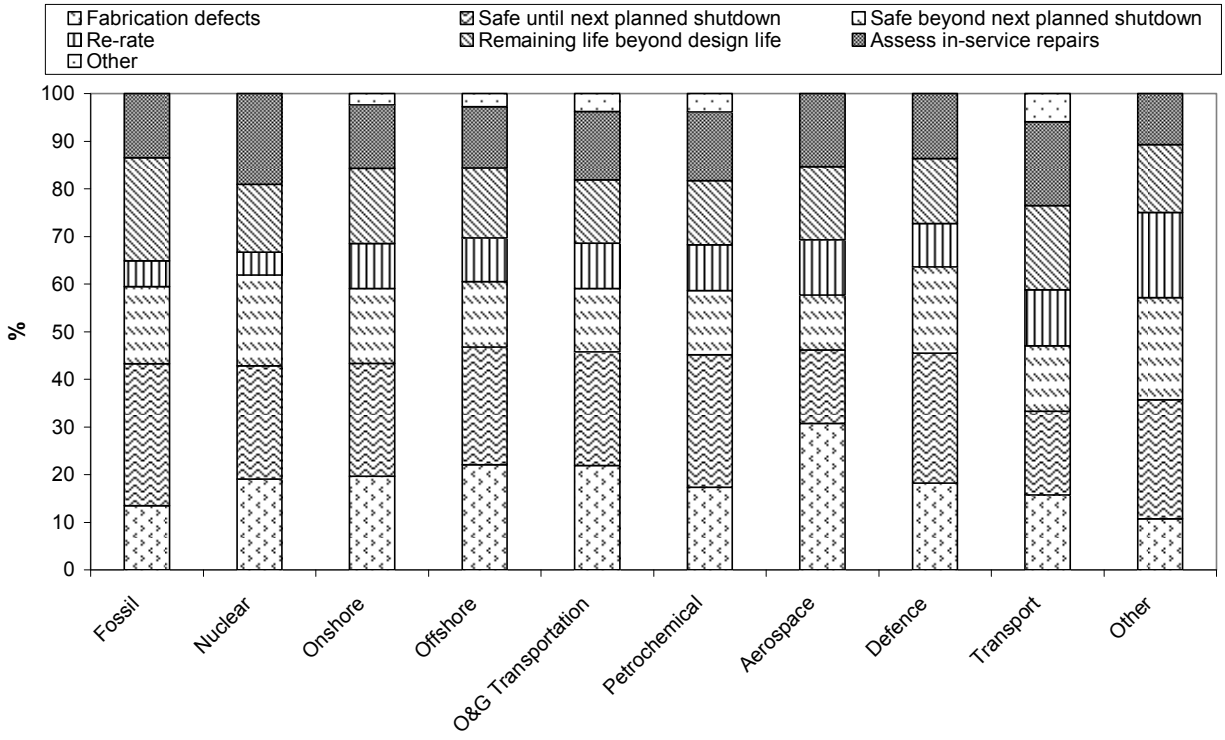

Figure 6 Importance of Fitness-for-Service applications to respondents' companies operations.

The most important FFS application to a companies operations is determining whether equipment is safe to operate until the next planned shutdown, in all industry sectors except aerospace and transport. The aerospace sector viewed assessing the acceptability of defects during fabrication and/or commissioning as the most important, which was also of considerable importance to the oil and gas and nuclear power generation sectors. The transport sector was also concerned about assessing in-service repairs and extending life beyond design. All categories received substantial support in the oil and gas and petrochemical sectors showing the broad application of FFS assessment techniques. The trends above were very similar in relation to the local plant approach although, as one might expect, the importance of in-service repairs increased and the importance of assessing the acceptability of defects during fabrication and/or commissioning decreased.

In TWI's 2002 survey [1], for those respondents who had previously undertaken FFS assessments, the two most important reasons for doing so were determining the remaining life of damaged plant, and assessment to ensure safe operation beyond design life. The least significant reason for undertaking FFS assessments was reducing the duration of an inspection/maintenance outage/shutdown, across all respondents. The results of the current survey reveal that determining whether equipment is safe to operate beyond the next planned shutdown (i.e. to extend the period between shutdowns) is now viewed as being equally important to determining the remaining life of equipment beyond design life and assessing in-service repairs. This may also indicate increased usage of risk based inspection over the past five years, particularly across the oil and gas and power generation industry sectors.

The survey also aimed to establish which type of FFS procedures were being used most frequently by asking respondents to rank the following list of damage mechanisms, in order of frequency of use by their companies.

- Metal loss due to corrosion/erosion.

- Crack-like flaws (fracture assessment) below the creep range.
- Creep rupture.
- Crack-like flaws (fracture assessment) in the creep range.
- Fatigue.
- Environment Assisted Cracking (e.g. Stress Corrosion Cracking, Corrosion Fatigue).
- Dents and gouges.
- Weld misalignment and equipment distortion.
- Equipment overload (e.g. plastic collapse of unflawed components.

Figure 7 shows the percentage of respondents who ranked each FFS procedure as being the most frequently used by their companies.

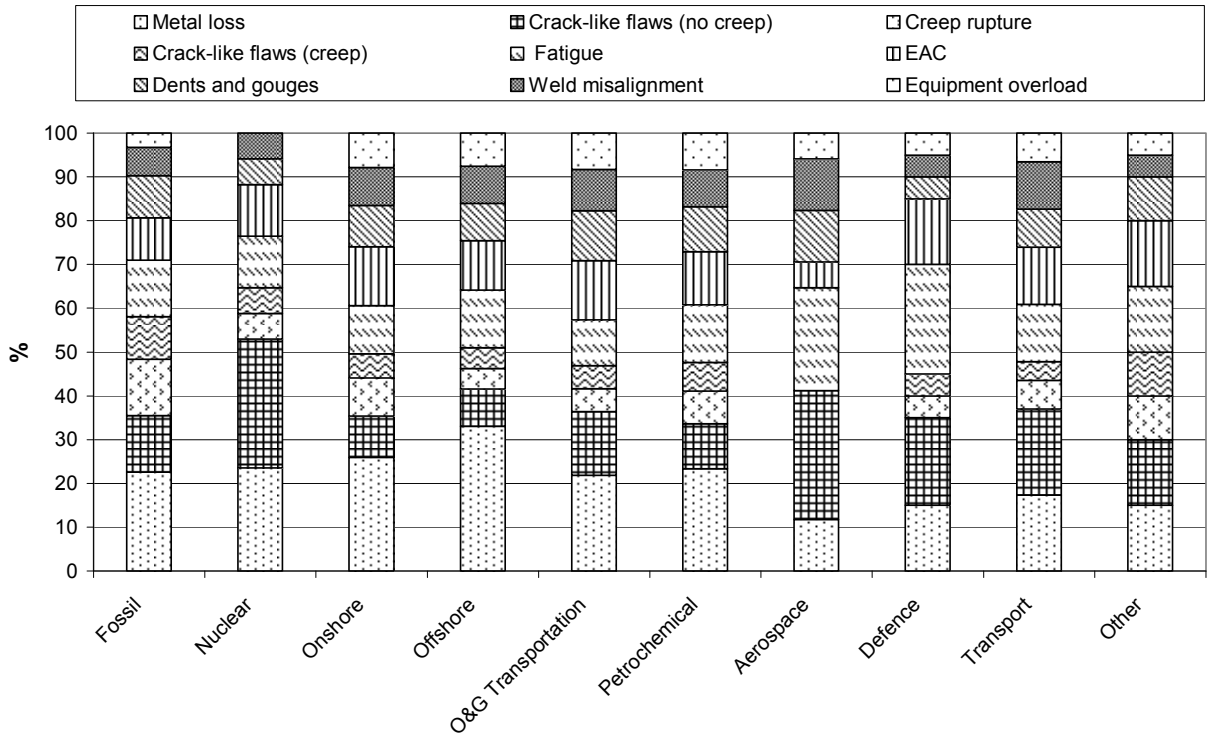

Figure 7 Frequency of use of Fitness-for-Service procedures by respondents' companies.

Metal loss procedures to assess corrosion and erosion were listed as being by far the most frequently used in all the oil and gas related industries with fatigue, environment assisted cracking (EAC) and fracture assessments below the creep range also frequently used. Corrosion is known to be a major problem in both the power generation and oil and gas industries. For example, direct corrosion costs in petroleum refining in 2002 were estimated to be $3.7 billion/year [9].

Metal loss procedures were also most frequently used in the fossil fuel power generation sector. Interestingly crack-like flaw assessments in the creep range were only ranked as being fifth most frequently used in the fossil fuel power generation industry, possibly indicating an increasing reluctance to leave cracks in-service if repair is an option. In the nuclear industry fracture assessments below the creep range came out on top. This was also most frequently used in the aerospace sector, where fatigue assessment procedures are also regularly used. Again, the trends in relation to the local plant were almost identical. The FITNET survey [2] asked respondents which damage assessment was most relevant in the overall FFS

assessments they perform and reported static fracture and fatigue assessments as being more relevant than corrosion. Perhaps this latest result suggests a growing trend towards removing cracks whenever possible and carrying out a metal loss assessment and repairing instead.

In the downstream oil and gas sector EAC procedures were listed as being the second most frequently used. Environmental damage is an increasing problem on ageing plant and although industry's knowledge and experience of EAC has improved markedly over recent years, and certainly since the design of much of the pressure equipment that is still operating in service, it is still not well covered in the main published standards. Most procedures simply point out that EAC is complicated, highlight the importance of only using data relevant to the actual environment and loading conditions and suggest that expert assistance be sought. FITNET [8] is the only document to include a specific section on EAC but API 579-1/ASME FFS-1 [4] now covers the assessment of hydrogen blisters and hydrogen damage associated with HIC and SOHIC in Part 7. These new assessment procedures essentially treat hydrogen induced cracking (HIC) as a reduced strength material (via a HIC damage parameter) and a crack-like flaw. Estimating how material properties may have degraded over time, especially in a corrosive environment, is a considerable challenge in FFS assessments.

A natural addendum to the above question regarding FFS procedures was to ask respondents which published procedures their companies apply, and to rank them in order of frequency of use. Respondents were asked to choose from the following list.

- API 579-1/ASME FFS-1 (previously API RP 579).
- BS 7910.
- British Energy R5/R6 procedure.
- SINTAP/FITNET.
- ASME B31.G.
- In-house procedures.
- Other (Please Specify).

Figure 8 shows the percentage of respondents that ranked each standard as being most frequently used in their companies, filtered by industry sector.

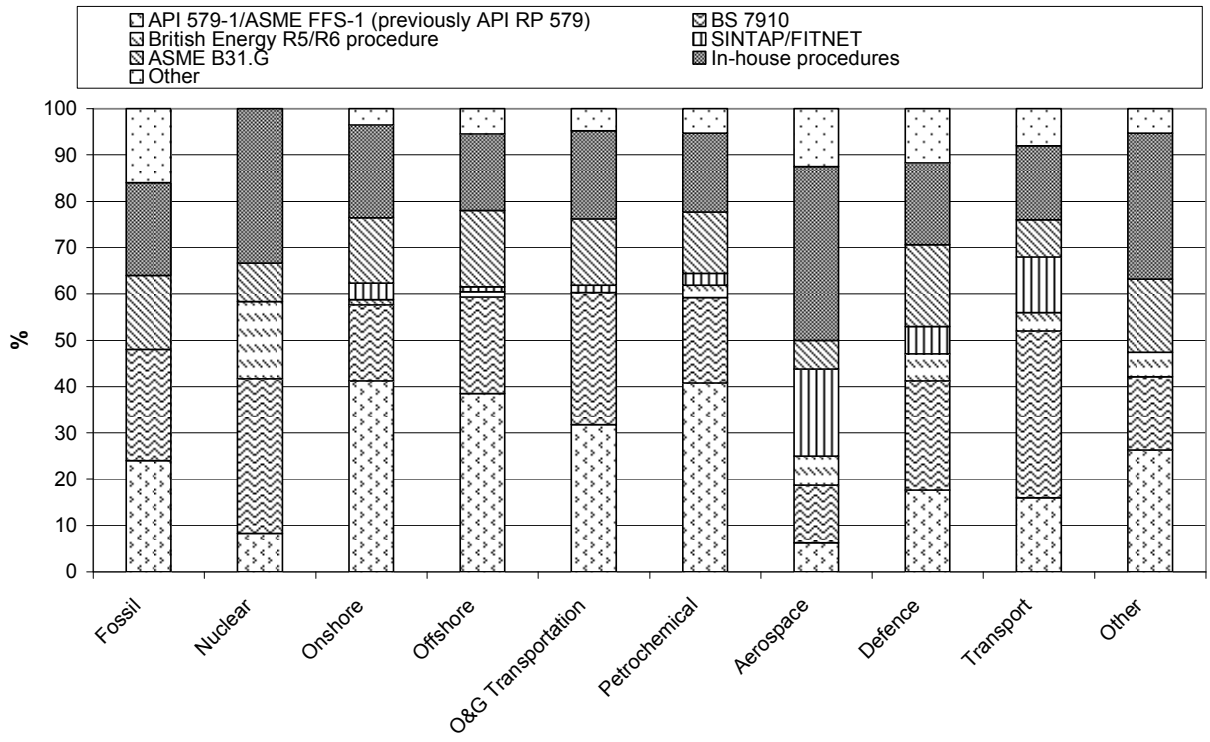

Figure 8 Frequency of use of published Fitness-for-Service procedures by respondents' companies.

API 579-1/ASME FFS-1 (no distinction was made between the new and old versions) came out as being most frequently used across all sectors and the results confirm that it is the most widely used within the oil and gas and petrochemical industry sectors. Based on corrosion assessment procedures being by far the most frequently used one might have expected B31.G [10] to be the most widely used but a key reason for the success of API 579-1/ASME FFS-1 is the fact it covers the broadest range of damage mechanisms. For example, if a company intends to purchase and apply the procedures of a single FFS document it would be very easy to justify the purchase of API 579-1/ASME FFS-1 on this basis alone. API 579-1/ASME FFS-1 also has the advantage of including Level 1 screening assessments which are often chart-based. This has made basic FFS assessment tools more accessible to on site personnel. However, it should be noted that API 579-1/ASME FFS-1 refers to many of the procedures contained in other published documents.

BS 7910 also features widely throughout all industry sectors and came out as being the most frequently used in the nuclear industry. The nuclear industry had listed fracture assessments below the creep range as being the most frequently used so this result confirms the quality of BS 7910 for assessing crack-like flaws. For example, a Level 3 API 579-1/ASME FFS-1 crack-like flaw assessment is essentially a (Level 2) BS 7910 fracture assessment. BS 7910 is also used almost as frequently as API 579-1/ASME FFS-1 in the oil and gas transportation sector. Again, this is indicative of the amount of fabrication flaws which are assessed in this sector as opposed to service-induced damage. BS 7910 also came out on top in the aerospace, defence and transport sectors indicating one of its key advantages, that it is applicable to all industry sectors.

Interestingly, no respondent from the fossil fuel power generation sector listed the British Energy R5/R6 documents as being the most frequently used, and likewise in the nuclear industry they appear to be less frequently used than both BS 7910 and in-house procedures. The release of a joint API/ASME FFS standard is presumably aimed at increasing its use in

the fossil fuel power generation industry, particularly with the inclusion of the new Part 10 for assessing components operating in the creep range. It already appears to be equally as widely used as BS 7910 and it will be interesting to see whether more power generation companies adopt API 579-1/ASME FFS-1 in the future. The micro-structural method for assessing creep is widely used in the fossil fuel power generation sector. However, this is barely mentioned in the new API/ASME document, which will potentially exclude large sections of the power sector.

In-house procedures also featured widely across all industry sectors, which is perhaps indicative of the gaps in the current array of published procedures. For example, if EAC is indeed one of the most widely encountered problems in the downstream oil and gas sector then one cannot simply rely on published procedures alone. Another reason for developing in-house procedures is that published procedures that are too prescriptive in their approach can potentially have a detrimental affect on plant management. Often, particularly in complex cases, a degree of pragmatism is required. The API 579-1/ASME FFS-1 approach seems reasonable whereby a Level 3 assessment does not always signify a greater degree of complexity than Level 2. It could simply mean that one has stepped outside the published procedures in some way in order to best address the situation that has been encountered.

When analysing the responses to this question it is interesting to not only filter by industry sector but also region of the world, to assess whether the dominance of API 579-1/ASME FFS-1 is regional at all. For example, in Western Europe BS 7910 is used equally as or more frequently than API 579-1/ASME FFS-1 in all industry sectors except downstream oil and gas and petrochemical. The results have also been filtered by those respondents who listed fracture (below the creep range) and fatigue assessments as being most frequently used by their companies. The results then show BS 7910 to be far more widely used than API 579-1/ASME FFS-1, which doesn't appear to be used any more frequently than in-house procedures.

'Other' published documents listed included DNV RP F101 [11] for the assessment of locally thinned areas, and storage tank assessment procedures such as EEMUA publication No. 159 [12] and API standard 653 [13]. Some respondents also mentioned local/national standards, for example in India, Australia and China.

4.3 ACCEPTANCE OF FFS ASSESSMENTS

It is clear that without support from regulatory bodies the benefits of FFS assessment tools are limited. The survey asked the question as to whether or not FFS assessments are accepted by SRAs. 80% of the respondents who answered this question said that FFS assessments were accepted by their SRAs as a basis for assessing the condition of plant for continued service. Only 3% of respondents stated that FFS assessments were not accepted by their SRA, a further 3% believed this situation to be under review, while the remaining 15% did not know. In fact, of all those who responded from the fossil fuel and nuclear power generation, aerospace, defence and transport sectors no-one reported that their SRA didn't accept FFS. This is interesting since the survey carried out by TWI in 2002 [1] reported that over half of all respondents indicated that their SRA did not accept FFS assessments as a basis for assessing the condition of plant for continued service. In 2002 it was concluded that certain countries in the Asia-Pacific, Middle East, North America, South America-Caribbean and Western Europe regions did not accept FFS as a basis for assessing the condition of plant for further service. This latest result therefore appears to indicate quite a significant change in how FFS assessments are viewed by certain SRAs around the world, particularly recalling the

number of respondents from companies operating in the Middle East and Asia Pacific regions. It is also indicative of how much more widespread and better understood the quality and potential benefits of FFS techniques are. It is perhaps also significant that FFS techniques for assessing standard/common damage forms have not changed significantly in the past five years.

Of the four SRAs that responded to the survey three said that they accepted FFS assessments. Of the five respondents who indicated that their SRA did not accept FFS assessments three came from the downstream oil and gas industry sector and two from the upstream oil and gas industry sector with regions listed as being either Asia-Pacific or the Middle East.

As an extension to the above question, those respondents who indicated that their SRA did accept FFS assessments as the basis of plant management decisions were asked which standards/procedures were accepted, and whether or not their SRA and/or their company specified a preference (Figure 9).

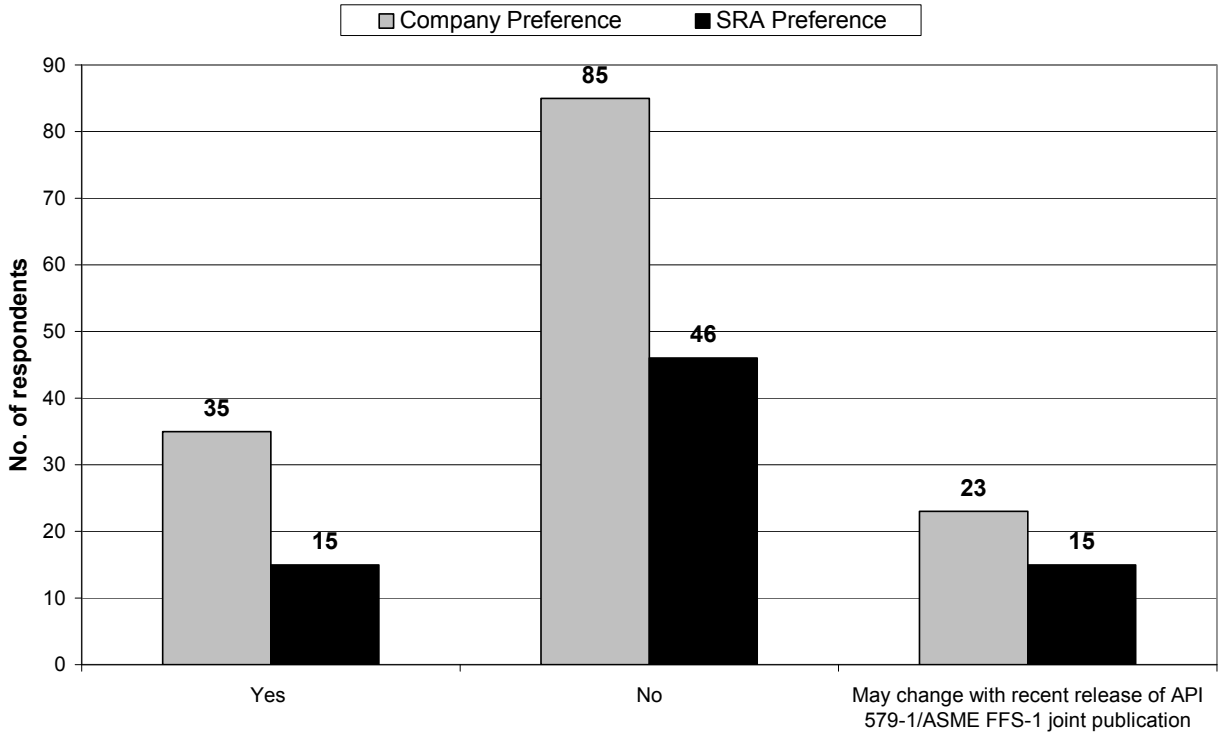

Figure 9 Number of companies/Safety Regulating Authorities that specify a preference for Fitness-for-Service standards/procedures.

Although the majority of respondents who answered these questions indicated that neither their company nor their SRA specified a preference, 35 companies and 15 SRAs do appear to specify a preference. Perhaps the most interesting aspect of the results in Figure 9 is the number of respondents who believe their company and/or their SRAs preference for a particular FFS standard will change with the release of API 579-1/ASME FFS-1.

Those respondents who answered 'yes' to their company and/or their SRA specifying a preference were asked to specify which assessment procedures were preferred (Figure 10). None of the respondents from Western Europe specified API 579-1/ASME FFS-1 as being preferred by either their company or their SRA. It is interesting to note that as well as

specifying a preference for a particular published FFS procedure, one respondent reported that their SRA had approved their in-house procedures.

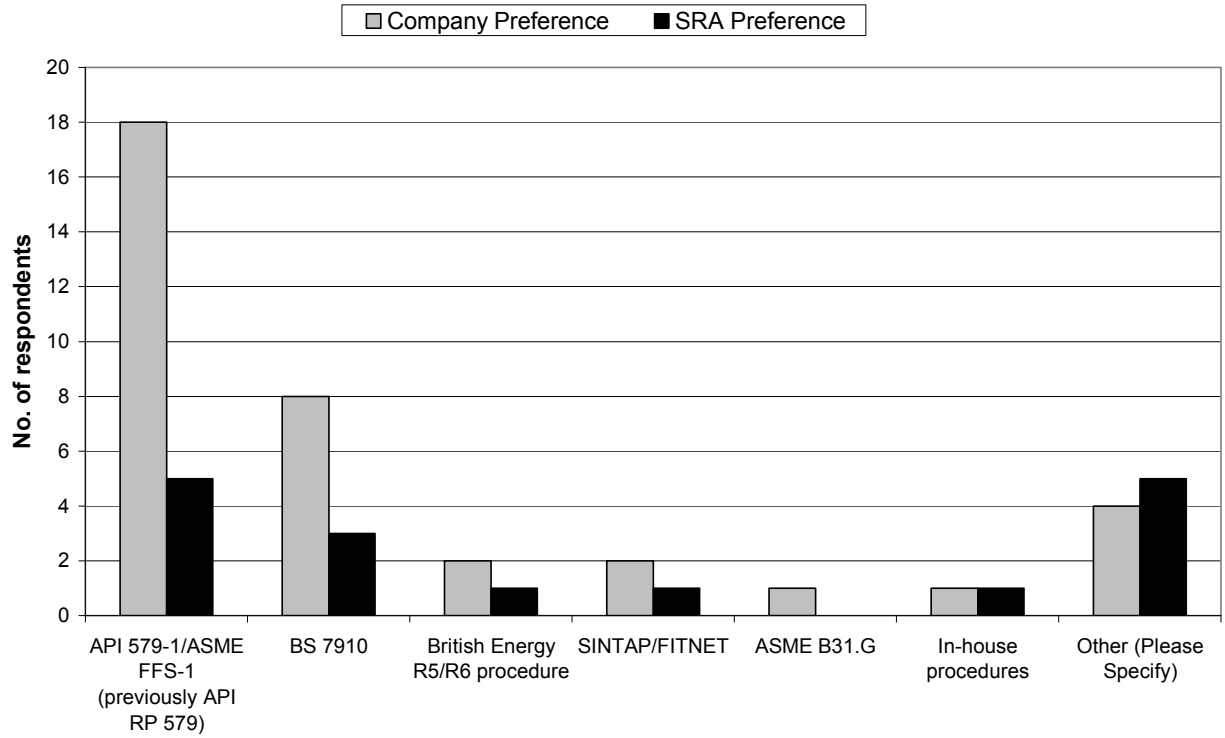

Figure 10 Company and Safety Regulating Authority preference for assessment procedures.

There is often confusion over which FFS standard/published procedure should be used and whether or not this varies depending on your industry sector and/or the type of damage or flaw encountered. Most of the leading FFS standards reference each other at some point, suggesting that certain standards are better for certain things. API RP 579:2000 [14] was aimed primarily at petrochemical refinery equipment built to ASME and API design codes. While it did not exclude other design codes and other industries, care is needed when using it outside its target field to prevent overly conservative results being obtained, often stemming from the fact that ASME code pressure vessels tend to be thicker than those built to say British Standards. API 579-1/ASME FFS-1 now supersedes the Recommended Practice and broadens the scope of the document beyond the downstream sector to include post-construction integrity issues for equipment operated in a wide range of process, manufacturing and power generation industries. It is this collaboration between API and ASME that suggests that regulatory bodies may start to formally adopt the procedures in this standard in certain regions of the world. BS 7910 is well regarded for the assessment of weld defects and crack-like flaws. As highlighted earlier, a distinct advantage of BS 7910 is that it is not affiliated to any design standards and can be used across industries. The survey asked respondents to comment on what influenced their personal choice of standard by ranking the list below.

- Acceptance by SRA.
- Specified by company or client.
- Accuracy.
- Most familiar to you.
- Ease of use.

- Wide recognition.
- Scope of guidance.
- Availability of appropriate software.

Figure 11 shows the percentage of respondents who ranked each influence as being the most important to their choice of FFS standard.

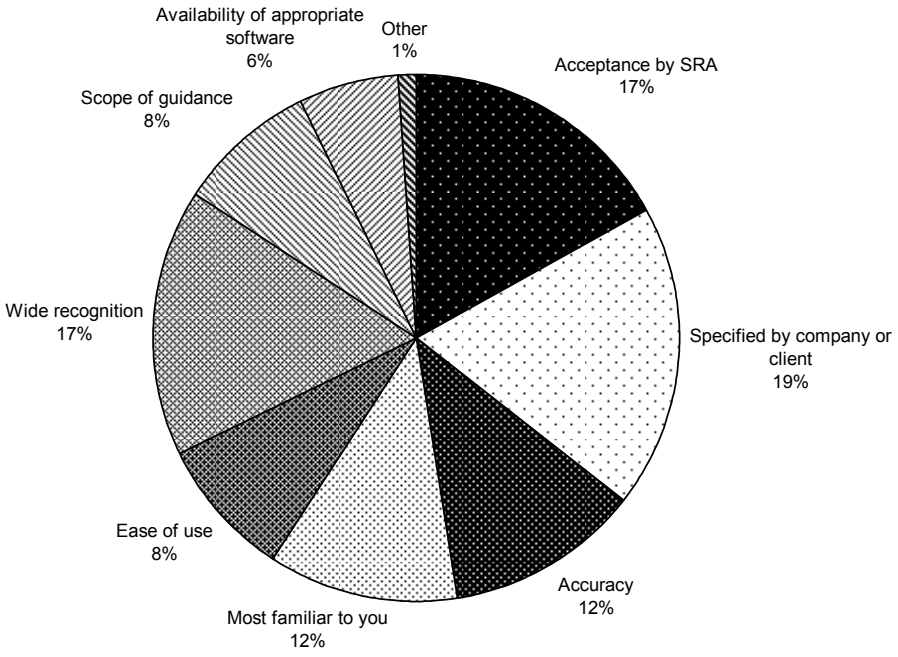

Figure 11 Influence on choice of Fitness-for-Service standard.

Overall the strongest influence on the choice of FFS standard was reported as that specified by company or client, closely followed by acceptance by SRA and wide recognition of the standard. Clearly from the point of view of a specialist FFS sub-contract company the client will often stipulate which FFS procedure should be used. Two interesting results are that the accuracy of the standard did not come in the top three influences in any industry sector. A similar result was reported in the FITNET survey [2]. This is perhaps indicative of a lack of clarity regarding the accuracy, or perhaps it is believed that all standards are sufficiently accurate. In many industry sectors accuracy seems to have a similar level of influence as ease of use, which perhaps provides more evidence that FFS activities are being driven more and more by economic factors as well as ensuring safety of assets. As Wintle [5] points out in his paper examining API RP 579:2000 and BS 7910 procedures, 'industry always likes quick, simplified procedures that can be used on site without detailed information, analysis and specialist knowledge'. This is not always possible however.

Also of interest is the low level of influence given to the availability of appropriate software for a particular standard. The availability of appropriate software did not come in the top five reasons for using a particular standard in any industry sector in any part of the world. This was even the case when the results were filtered by those respondents who listed fracture

(below the creep range) and fatigue assessments as being most frequently used by their companies. This result was somewhat unexpected as software tools are often required to carry out fracture assessments.

Respondents were asked whether their companies and/or their SRAs required independent/third party reviews of FFS assessments prior to using the results to make a plant management decision. The question did not stipulate whether the review was internal or external. The results have been normalised by the number of responses to this question to give the percentages in Figure 12. Only the results in relation to the respondents companies are shown; a similar trend was seen from the results pertaining to SRAs.

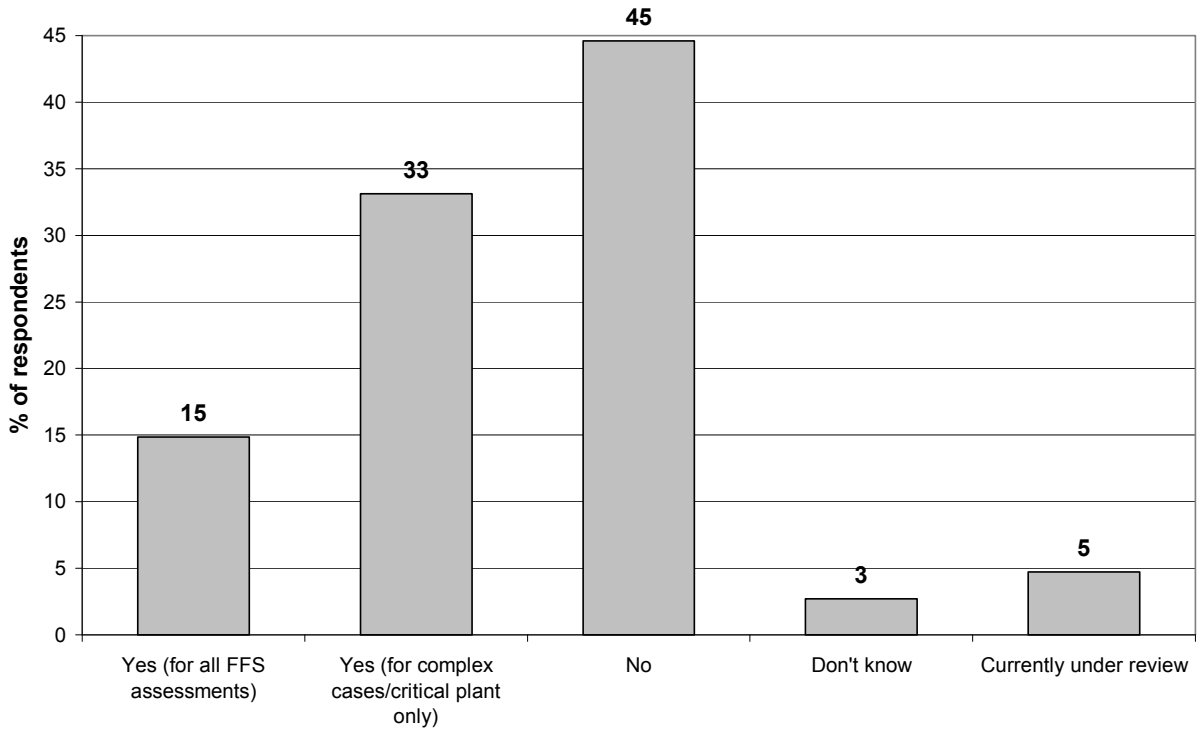

Figure 12 Company third party reviews.

Only 15% of companies (and 8% of SRAs) require an independent/third party review, whether internal or external, of all FFS assessments. This might suggest that companies and SRAs have confidence in the personnel who are undertaking FFS assessments, or the FFS procedures they are using, or perhaps both? This percentage more than doubles to approximately one third (one quarter for SRAs) for complex cases and critical plant perhaps indicating that companies do not see a need to check simple assessments.

4.4 FFS COMPETENCIES

A grey area in most FFS procedures and standards is the qualifications required for someone to perform such assessments. Training courses are available on all the main standards. For example API University offers two training courses on API 579-1/ASME FFS-1, one for engineers (covering all assessment levels) and one for inspectors (covering screening assessments only). While the API courses do provide continuing education units (required in the US to maintain a professional engineer's license) there is currently no certifying body or indeed examination that can be taken to demonstrate that someone is capable of correctly applying API 579-1/ASME FFS-1, or indeed any of the published standards.

API 579-1/ASME FFS-1 [4] refers to a 'competent' person carrying out Level 2 and Level 3 assessments but it is open to interpretation what is meant by a 'competent' person. Similarly, BS 7910 refers to qualified and experienced people trained in inspection, materials behaviour and fracture mechanics [15]. Over 70% of respondents (excluding those who worked for training providers) said their companies had undertaken or were planning to undertake formal FFS training. This suggests not only a training need throughout industry but also a desire to develop skills in the field of FFS. Companies seem to be prepared to invest time and money in training their staff in the field of FFS, presumably because they can identify direct benefits to the companies operations.

When asked about FFS training and whether it should aim to provide an overview of the underlying principles or aim to provide detailed worked examples, approximately two thirds of respondents said that it was important to provide both. Clearly this will depend on the audience to a certain degree. API 579-1/ASME FFS-1 is now over 1100 pages long so providing in depth training on all 13 parts would require a significant investment in time and money both from the training provider and the course delegates. The FITNET survey [2] also addressed the issue of FFS training. Here the majority of respondents supported the need for FFS training with the basic theory and concepts, and practical applications of FFS being given higher priority than advanced training.

The issue of FFS qualifications was specifically addressed in the survey. Over three quarters of respondents indicated that they thought FFS qualifications/exams should be introduced to set a minimum competency level as to who can apply codified FFS procedures. If FFS qualifications were introduced respondents were then asked whether they should be a legal requirement or purely a means to indicate professional competency/quality. Overall there was almost equal support for FFS qualifications being introduced as a legal requirement and simply being an indication of professional competence. Of particular interest was the fact that the fossil fuel power generation industry was the only sector that supported such qualifications being an indication of professional quality as opposed to a legal requirement. While the numbers were close in the other sectors the majority of respondents opted for them being a legal requirement. An interesting point was raised by one respondent, stating that codified FFS approaches should not need any additional qualifications to apply, beyond those of a competent, professional engineer. The real question is therefore whether or not FFS procedures are truly codified at present?

A similar question regarding FFS qualifications was asked in the FITNET survey [2] with less than two thirds of respondents supporting the establishment of a professional qualification for competence in the application of FFS technology, suggesting that support has increased over the past five years. It seems likely that the introduction of FFS qualifications aimed at those who perform (and use the results of) FFS assessments will be investigated by the various standards bodies over the coming years, perhaps similar to PCN and ASNT qualifications that inspection personnel require. However, the challenges involved in this should not be underestimated since the importance of a multi-disciplinary approach to FFS cannot be emphasised enough. One might argue that qualifications should only aim to cover Level 1 and basic/common/standard Level 2 assessments since a degree of flexibility is certainly required for more complex cases. Unfortunately this potentially creates the situation where a qualification is required to perform simple assessments but not complicated assessments!

In the final question of the survey, respondents were asked whether their companies currently use, or intend to use automated FFS assessment tools (Figure 13).

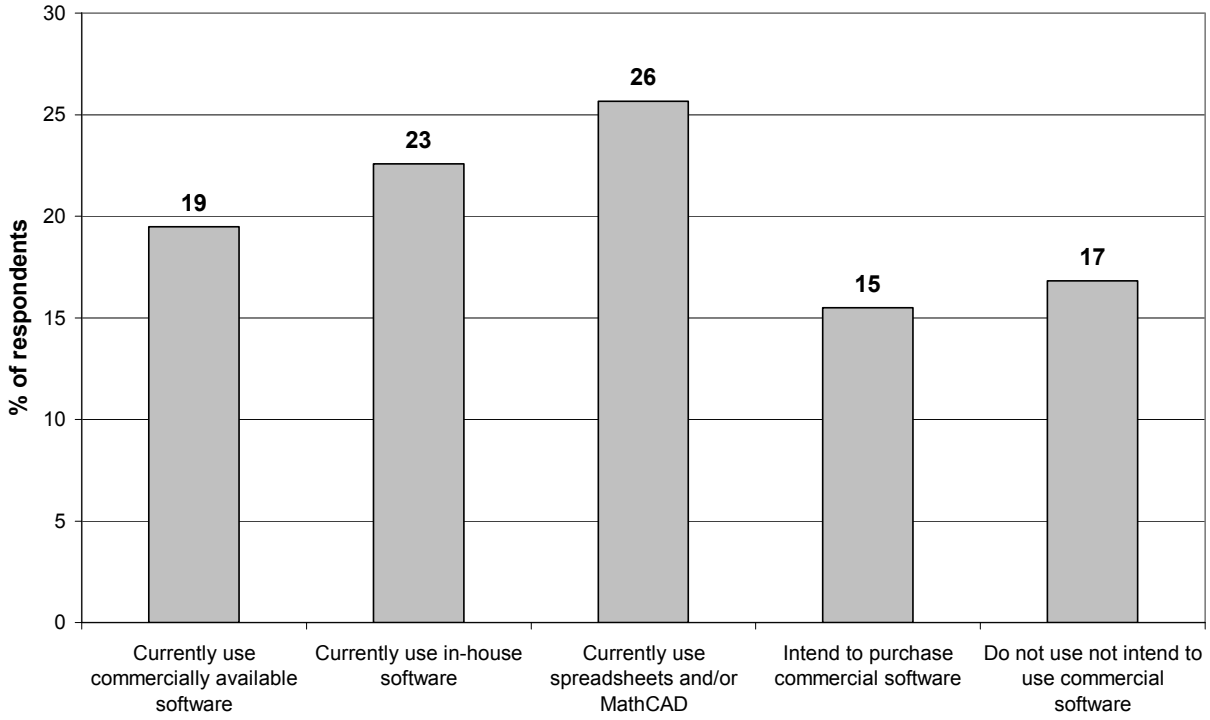

Figure 13 Use of Fitness-for-Service software.

While many companies rely on commercially available software more companies appear to prefer either writing their own software tools or producing their own spreadsheets than currently use or intend to buy commercially available software. One respondent did comment however that commercial software tends to be viewed as being more accurate than spreadsheets and/or hand calculations, regardless of the experience of the assessor. While the authors are unable to comment on the accuracy of this statement one should always carry out simple checks to verify FFS assessment results in exactly the same way as FEA results are often checked via quick/rough hand calculations.

Figure 14 shows which commercially available software packages were listed as being used by more than one respondent, across all industry sectors. Commercially available software did not refer to finite element packages. In a similar fashion to the earlier question regarding the use of published FFS procedures the results displayed below were filtered by those respondents who listed fracture (below the creep range) and fatigue assessments as being most frequently used by their companies. The aim of this was to investigate whether companies were more likely to buy software to assess crack-like flaws than other often more simple assessments (e.g. metal loss) but the proportions were very similar.

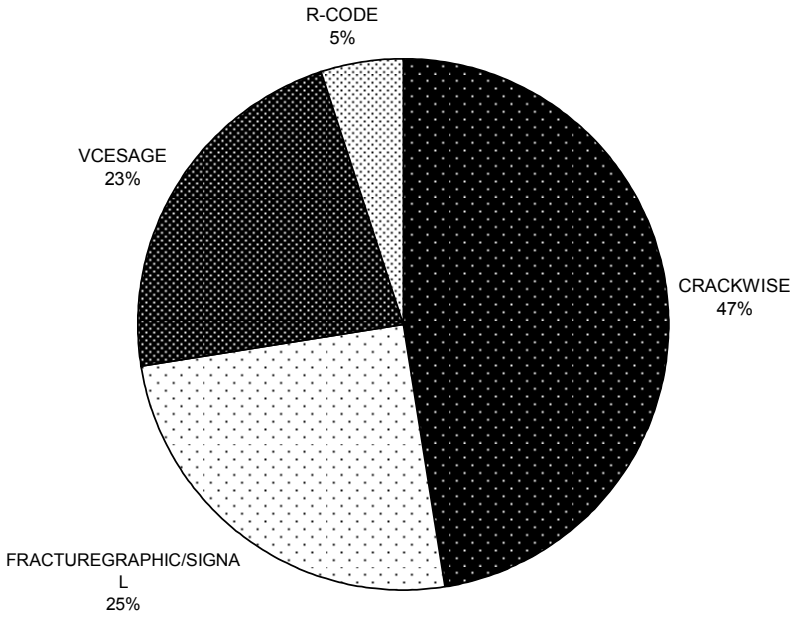

Figure 14 Use of commercial Fitness-for-Service software packages.

5 DISCUSSION

At the end of the survey respondents were given the opportunity to provide any additional information or comments that they felt were relevant to this survey. For example whether they thought there were aspects of procedures that needed updating or expanding, or whether there were certain aspects of FFS assessments they found particularly challenging. Some of these are discussed below along with some of the authors own experiences.

Some respondents were of the opinion that FFS procedures did not emphasise the importance of input data enough. In some cases, actually performing the FFS assessment is more straightforward and less time consuming than actually collating all of the information required. A FFS assessment is a 'one moment in time' assessment of the condition of an item of equipment based on certain assumptions and a set of input parameters. If the input data are inaccurate/approximate, the result will be equally as inaccurate. A pressure vessel being classed as fit for further service today does not necessarily mean it will last a further 20 years. FFS assessments are meant to be reviewed and updated regularly, and certainly whenever there is a change in operating conditions or a process excursion for example.

FFS assessment results can be likened to a company's accounts. If you ask ten different accountants to calculate the accounts of the same company you will invariably get ten different versions. It's possible that all of them are correct, within the assumptions that each individual has made. Which is the most accurate depends on what you are trying to achieve? Are you trying to bolster your profits for your shareholders or are you more interested in turnover and providing good customer service. In plant management terms are you solely interested in demonstrating the safety of your assets or is your motivation to extend run time between shutdowns, for example, both of which are realistic outputs from FFS assessments?

Regardless of who files a company's accounts the accounts themselves do not change, but our perception of them does. The same can be said for FFS assessments; different engineers (or multi-disciplinary teams of engineers) will potentially draw different conclusions depending on the goal they have in mind and the time/money/data they have available; but the condition of the equipment does not change. For example some practitioners might demand materials testing or additional more advanced inspection prior to undertaking an assessment, others may make assumptions based on previous experience. Differences in assessment results may simply come via knowledge of the inherent conservatisms within published FFS procedures. From a plant management perspective there is a huge difference between an item of equipment being reported as having a remaining life of 10 years to a remaining life of 5 years. What factor of safety was used? Were sensitivity analyses performed on the input parameters? It is important to question the accuracy of the procedures used, investigate the conservatisms and often to question the person who has actually carried out the assessment. Has he assessed the identified damage correctly? Have crack-like flaws been ruled out? Is the flaw active? Has it developed in-service?

It is important to balance the economic benefits of FFS with its true role: to assess the condition of industrial plant for continued safe operation. A lot of industrial plant is now operating well beyond its nominal design life demonstrating, for example, inherent conservatisms in the original design codes, conservatism in a particular design or perhaps operation loads lower than design. The HSE document on Plant ageing and the Management of equipment containing hazardous fluids or pressure [3] refers to ageing not being about how old your equipment is but about your knowledge of its condition and how that's changing over time. A component has reached 'end of life' when it is no longer fit for further service. Not being fit for further service means that the risk of a component failing can no longer be tolerated, not that it will fail immediately. Options are then to repair, re-rate or replace the component.

FFS competencies and training requirements are clearly a subject for debate. To be a FFS practitioner, first and foremost a good knowledge of the standard being used is required. FFS standards are often difficult documents to pick up and use immediately; most often one gets a feel for the procedures over time. Knowledge of stress analysis techniques, fracture mechanics, metallurgy and corrosion science (to name but a few) is required and quick, automated solutions are not always possible. Plant management decisions should rarely be made solely by NDT technicians based solely on NDT results, unless reliable acceptance curves are available. Even then it is important to ensure that all possible damage mechanisms have been considered. The effectiveness of the NDT technique should also be reported as part of the FFS assessment.

Integrity managers and inspection personnel often see identified flaws as a costly, time consuming inconvenience during a shutdown but this should not be the case; at least they were looking in the right place and using an appropriate inspection technique so as to be able to detect it. While flaws are seldom good news it is better to detect and manage them during a scheduled outage than have to endure an unplanned shutdown. Is a successful shutdown one in which no defects are detected or one in which numerous defects are detected?

6 FINAL THOUGHTS

FFS assessment techniques are now widely used throughout industry and their acceptance by regulatory bodies is increasing. While the financial benefits of FFS activities are clear, it is important to balance these with ensuring the safe and continued operation of industrial assets.

Published FFS procedures continue to be developed, although the majority still focus on static plant (e.g. pressure vessels and pipelines) as opposed to rotating machinery. There are still many areas of FFS procedures that require further development, for example the assessment of EAC, improvement of NDT, online monitoring techniques (i.e. early warning systems) and additional screening procedures. Users of FFS assessment results require an appreciation of their accuracy.

In the future it would be extremely interesting to contact again those companies who indicated that they thought their company's and/or their SRA's preference for a particular FFS standard may change with the release of API 579-1/ASME FFS-1. It would also be interesting to monitor the usage of API 579-1/ASME FFS-1 in the power generation sectors.

7 REFERENCES

[1] Iravani H and Speck J, 2002: 'Industry Survey of Risk Based Life Management Practices and their Relationship to Fitness-for-Service Assessment', TWI Report No. 13032/5/02.

[2] Filiou C, Taylor N, Lejuste P and Houghton R, 2003: 'Survey of Current Application and Future Requirements for European Fitness-for-Service Technology, Technical Report No. FITNET/TR2/03, FITNET consortium.

[3] Health and Safety Executive, 2006: 'Plant ageing: management of equipment containing hazardous fluids or pressure', RR509.

[4] API 579-1/ASME FFS-1, 2007: 'Fitness-For-Service', The American Petroleum Institute and The American Society of Mechanical Engineers, Washington, 1st Edition.

[5] Wintle, J. 2003: Which procedures for FFS assessment: API 579 or BS 7910?, International Conference on Pressure Vessel Technology Proceedings, Vienna.

[6] Wiesner, C. S., Maddox, S. J., Xu, W., Webster, G.A., Burdekin, F.M., Andrews, R.M., Harrison, J.D., 2000, Engineering critical analyses to BS 7910 – the UK guide on methods for assessing the acceptability of flaws in metallic structures, International Journal of Pressure Vessels and Piping, vol. 77, no.14-15, pp883-893.

[7] R6 Revision 4, 2001: 'Assessment of the integrity of structures containing defects', Amendment 7 (April 2009), British Energy Generation Ltd.

[8] FITNET, 2008: 'Fitness-for-Service', Revision MK8, ISBN 978-3-940923-00-4, prepared by the European Fitness-for-Service Thematic Network (FITNET).

[9] Koch, G., 2002. 'Corrosion Costs: Most Recent Study Shows Just How Much', Available from: http://www.corrosioncost.com/news/2002/corrosioncosts.htm.

[10] ASME B31G, 1991 (R2004): 'Manual for Determining the Remaining Strength of Corroded Pipelines: A Supplement to ASME B31 Code for Pressure Piping', The American Society of Mechanical Engineers, New York.

[11] DNV RP F101, 2006 'Corroded Pipelines' WITH AMENDMENT, DNV, Hovik, Norway.

[12] EEMUA 159, 2003: 'Users' guide to the inspection, maintenance and repair of aboveground vertical cylindrical storage tanks', Volume 1, Engineering Equipment and Materials Users Association, London, 3rd Edition.

[13] API 653, 2009: 'Tank inspection, repair, alteration, and reconstruction: downstream segment', American Petroleum Institute, Washington, 4th Edition.

[14] API Recommended Practice No. 579, 2000: 'Fitness For Service', American Petroleum Institute, Washington, 1st Edition.

[15] BS 7910. 'Guide to methods for assessing the acceptability of flaws in metallic structures', Amendment 1, British Standards Institution, London, 2005.

APPENDIX B

Holtam C M, Baxter D P, Ashcroft I A and Thomson R C, 2009: 'The behaviour of shallow cracks in a pipeline steel operating in a sour environment', Journal of Offshore Mechanics and Arctic Engineering (OMAE), August 2009, Vol. 131, 3, 031302, ASME.

The Behavior of Shallow Cracks in a Pipeline Steel Operating in a Sour Environment

C. M. Holtam
D. P. Baxter
Structural Integrity Technology Group
TWI Ltd
Cambridge
CB21 6AL
UK

I. A. Ashcroft
Wolfson School of Mechanical and Manufacturing Engineering
Loughborough University
Leicestershire
LE11 3TU
UK

R. C. Thomson
Department of Materials
Loughborough University
Leicestershire
LE11 3TU
UK

ABSTRACT

Setting conditions for the avoidance of in-service crack growth in aggressive corroding environments has long been a major challenge due to the number of variables that have a significant effect on material behaviour. One area where both experimental data and a validated assessment methodology are lacking is the behavior of shallow cracks. This paper describes the early results of an ongoing research program aimed at addressing the shortfall in experimental data to characterize material behavior in the shallow-crack regime, with the long-term aim of improving the understanding and assessment of the early stages of environment assisted cracking. There is an industry need for a better understanding of material behavior under these conditions and for the development of a more robust assessment methodology. API 5L X65 pipeline steel parent material was tested in a sour environment with initial flaw sizes in the range 1-2 mm. Fatigue crack growth rate tests have been performed to investigate the influence of crack depth on crack growth rate (da/dN). Initial results suggest that crack growth rates for deep flaws can increase by a factor of 5-100 compared with air depending on the applied stress intensity factor range (ΔK). Shallow cracks have been shown to grow up to 130 times faster in a sour environment than in air and up to an order of magnitude faster than deep cracks in a sour environment at the same value of ΔK. Constant load tests have also been performed to investigate the influence of crack depth on the threshold stress intensity factor for stress corrosion cracking (K_{ISCC}). Preliminary results suggest that in this case there is no crack depth dependence in the range of flaw sizes tested. While further experimental work is required, the results obtained to date highlight the potential nonconservatism associated with extrapolating deep crack data. Guidance is therefore provided on how to generate appropriate experimental data to ensure that subsequent fitness for service assessments are conservative.

1 INTRODUCTION

Offshore pipelines and risers constructed from carbon manganese steel have reduced levels of performance when operating in a sour (H_2S containing) environment. Fatigue crack growth rates (FCGRs) can be significantly higher than in air and material "toughness" may be significantly lower. While the use of corrosion resistant alloys can avoid these effects, it is not always economically viable to do so.

Characterizing material behavior in aggressive corroding environments requires experimental data, but generating appropriate data is challenging due to the number of variables that can influence behavior. Several researchers have investigated the corrosion fatigue behavior of pipeline steels [1-7] and a recent review of published data highlighted the extent to which numerous mechanical and environmental variables can affect performance [8].

It has been found that FCGRs in a sour environment at normal ambient temperature are 10-100 times higher than in air, and the environmental effects tend to be higher at high or intermediate ΔK [2-5]. Other parameters such as cyclic loading frequency and partial pressure of H_2S have also been shown to have a significant effect [3,4,6]. Experimental crack growth rate data are typically determined in simulated operating environments, and upper bound curves can be used in fracture mechanics calculations.

Under static loading conditions, pipeline steels in a sour environment can fail via sulphide stress corrosion cracking (SSCC). Weld material, most notably the heat affected zone (HAZ), is known to be particularly susceptible to SSCC owing to the hardened material in this region. There is a clear correlation between material hardness and cracking sensitivity, as expressed in terms of critical stress or stress intensity. The precise relationship depends on both microstructure and the severity of the environment, i.e., its propensity to induce hydrogen pickup [9].

1.1 REVIEW OF ASSESSMENT PROCEDURES

Current assessment procedures are based on the avoidance of EAC by limiting the stress ($\sigma < \sigma_{th}$) for crack-free components or limiting the stress intensity factor ($K_I < K_{ISCC}$) where a flaw already exists. Fracture mechanics based procedures, such as those described in BS 7910, describe a flaw acceptance criteria as follows [10]:

$$K_I < \frac{K_{ISCC}}{f_{SCC}} \qquad (1)$$

where K_I is the applied stress intensity and f_{SCC} is a factor of safety (to be agreed between the parties involved). This results in a modified two-parameter failure assessment diagram (FAD), similar to that illustrated in Fig. 1, which plots K_r (the ratio of the applied linear elastic stress intensity factor to the materials fracture toughness) against L_r (the ratio of the total applied load giving rise to the primary stresses to the plastic limit load of the flawed structure). For $K_I < K_{ISCC}/f_{SCC}$ the flaw is tolerable, and no crack growth is expected.

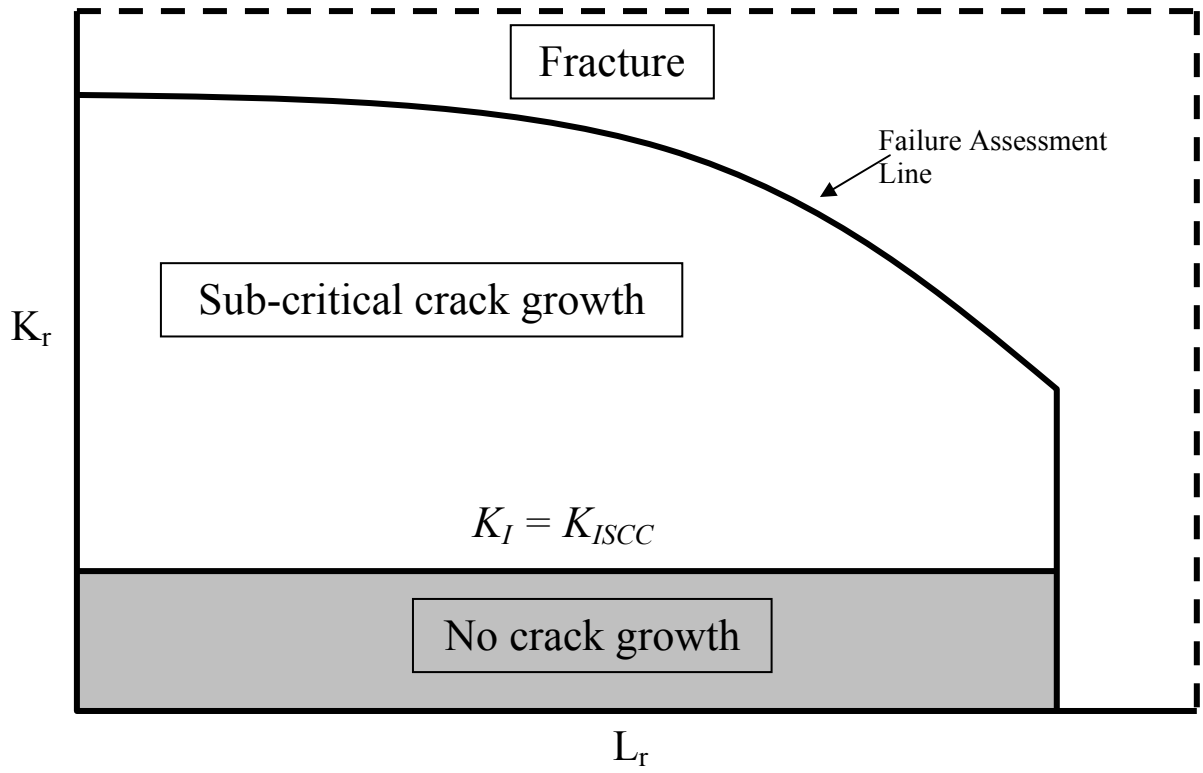

Fig. 1 FAD incorporating cutoff for EAC (after Ref. [11])

However, when $K_I \geq K_{ISCC}/f_{SCC}$ the possibility for stress corrosion crack growth should be recognized. Under these circumstances, it is often the case that some remedial action will be taken to prevent further crack extension (i.e., modification of the environment, elimination of the flaw via component replacement, weld repair, or stress relief). As an alternative, it may be possible to assess whether the flaw is likely to grow to an unacceptable size within the design life of the structure or within the appropriate inspection interval. This assessment is based on stress corrosion crack velocity data, da/dt, as a function of K. It is important to note, however, that these data are highly specific to the particular material-environment system concerned, and considerable care is required to ensure that the environment chosen for laboratory tests is either representative of that encountered in service or conservatively defined to be more aggressive. In many cases, crack velocity data for the precise application of interest are not available, and in these cases no subcritical crack growth can be tolerated.

Part 9 of the recently re-released joint publication API 579-1/ASME FFS-1 adopts a similar approach to the assessment of crack-like flaws and states that material properties used in an assessment should take account of any change over time as a result of, for example, aging, service environment, or past operation [12]. Fracture toughness can of course be a key parameter and Annex F in API 579-1/ASME FFS-1 provides guidance on how to derive a lower bound estimate of fracture toughness. In particular, it focuses on ferritic steels that may be hydrogen charged as a result of prolonged exposure to the service environment. As material specific data are often not available, a lower bound toughness is defined based on crack arrest data. It is argued that fracture initiation is enhanced by the presence of hydrogen, but that once rapid unstable crack propagation starts, hydrogen can no longer keep pace with the growing crack. The resistance to rapid crack propagation increases with increasing propagation rate, which decreases until an equilibrium subcritical crack growth rate is reached between crack growth and hydrogen delivery rate. It is proposed that crack arrest data can therefore be taken as a conservative estimate of the toughness of a steel containing

dissolved hydrogen. However, this approach does not provide a threshold against subcritical crack growth.

The British Energy R6 (Rev. 4) assessment procedures also use a two-parameter FAD approach [13]. Crack growth due to EAC processes is again described in terms of fracture mechanics parameters such as K_{ISCC} and avoidance of cracking is ensured by adopting a criterion similar to that in Eq. (1). The R6 document also mentions the need for care when considering fatigue crack growth in an aggressive service environment. It stresses the importance of considering the influence of crack depth on the crack tip environment and makes the recommendation that test data should be derived from specimens containing cracks of a size comparable to those being assessed.

The European Fitness-for-Service Thematic Network (FITNET) [11] document is structured along similar lines to the other published procedures described above, but also provides a review of assessment methods for EAC. It highlights a number of weaknesses in current materials testing and integrity assessment procedures, in particular, highlighting the importance of only using data relevant to the actual environmental and loading conditions.

1.2 BEHAVIOR IN THE SHALLOW CRACK REGIME

As well as the effect of the corrosive environment itself, several researchers have reported increased crack growth rates for EAC in the shallow crack regime. EAC generally progresses from initiation to propagation in a number of phases. Jones and Simonen [14] described the following sequence of events:

1. initiation;
2. short (i.e., shallow) crack growth;
3. Stage I growth;
4. Stage II growth;
5. crack coalescence;
6. failure.

Crack initiation usually refers to the formation of a 1-10 μm sized flaw from a defect free surface, and the transition to shallow-crack growth is hard to define. The “shallow-crack growth” period usually refers to defects that are small in relation to the scale of the microstructure or plastic zone size, but can also refer to instances where the defect size has an influence on crack tip chemistry, in which case cracks may be described as “environmentally” or “chemically” small [14].

For Stage I and Stage II growths, cracks are usually large enough to be uniquely characterized in terms of the applied stress intensity (K). Most experimental data are associated with Stage II growth, where a plateau in the crack growth rate is often encountered. Stage I growth precedes this period and describes a regime where the crack growth rate increases rapidly (as the applied K increases). Experimentally, Stage I and Stage II data are usually determined from specimens containing cracks that are very much deeper than those typically seen in service. Data in the shallow crack regime are very scarce.

As highlighted above, assessment procedures focus on quantifying the behavior of relatively deep cracks, and are based on determining a critical value of stress intensity factor for EAC (K_{ISCC}). Flaws are acceptable if the applied K is less than K_{ISCC}. A slightly more advanced analysis is possible if K is greater than K_{ISCC}, where the rate of crack growth (da/dt) may be

determined as a function of K, and an assessment carried out to determine whether a flaw would grow to an unacceptable size within the design life or appropriate inspection interval However, the analysis implicitly assumes that K is an appropriate characterizing parameter (i.e., that variations in crack depth can simply be modelled in terms of the resulting change in K), which will not necessarily be the case in the shallow-crack regime where values of K_{ISCC} may become dependent on crack depth.

Conventional test techniques to determine K_{ISCC} (or da/dt) use fracture mechanics specimens containing relatively deep fatigue precracks. For crack sizes greater than some minimum value, the data generated may indeed be independent of crack depth. However, it has long been recognized that small cracks may behave differently to deep cracks.

The first work to highlight the "shallow crack problem" was based on fatigue test data, which showed that size independence broke down when the crack was small compared with the extent of crack tip plasticity or microstructure. The Kitagawa-Takahashi diagram, first introduced in 1976 [15], describes the relationship between crack size and the observed threshold stress range ($\Delta\sigma_{th}$). For deep cracks, data lie on a straight line (on a log scale) and this represents a condition of constant stress intensity factor range (ΔK_{th}). However, for shallow cracks, crack growth was observed at applied ΔK values lower than the deep-crack threshold (ΔK_{th}) and tended toward the smooth specimen threshold stress range ($\Delta\sigma_{th}$). Models for the transitional behavior were based on determining an "effective" stress intensity factor range (ΔK_{eff}) that took into account the extent of crack closure, which was significantly less in the shallow-crack regime.

In an aggressive environment, FCGRs have similarly been shown to be sensitive to crack depth. For example, Gangloff [16] tested 4130 steel in 3%NaCl solution and observed that shallow cracks (0.1-1.0 mm) grew at a much higher rate than deep cracks (30-44 mm). Corresponding tests in air exhibited no crack size dependence so the effect was above and beyond what might be termed a "mechanical crack depth effect." It is therefore possible that an "environmental crack depth effect" may occur, even under conditions where crack tip stress distributions can be reliably modeled in terms of an applied stress intensity factor (K). Gangloff attributed the difference in crack growth rate to a difference in the crack tip environment, in particular, the pH, which led to enhanced hydrogen production and uptake in the case of shallow cracks.

Akid [17] also provided evidence that shallow cracks behave differently in a corrosive environment compared with air, concluding that the effect of the corrosive environment becomes more significant at low stress levels. In another study, Murtaza and Akid [18] made the point that only a brief introduction of an aggressive environment can lead to crack propagation and subsequent air fatigue failure. This comment may also be relevant to the use and effectiveness of corrosion inhibitors, which are often used to control the effects of aggressive environments. For example, a short inhibitor outage may be all that is required for the onset of EAC. Much of Akid's work refers to submillimeter size flaws that are smaller than those investigated in this work.

The work referenced above clearly shows that shallow fatigue cracks can grow faster than deep fatigue cracks, at the same ΔK and, therefore, highlights the potential nonconservatism in assessing shallow flaws based purely on deep crack data. Similarly, there is some evidence to suggest that shallow stress corrosion cracks may grow faster than deep cracks under static

loading conditions, although in some cases it is found that crack growth rates may, in fact, be slower [14].

The FITNET document highlights the need for caution when assessing shallow cracks using conventional fracture mechanics calculations, and introduces the concept of a two-parameter approach to the assessment of EAC, similar to that shown in Fig. 2. This diagram describes a transition between K-controlled and stress-controlled behaviors as the crack size is reduced, and emphasizes the need for care in the shallow-crack regime as the critical stress may be lower than that obtained by extrapolating the deep-crack data.

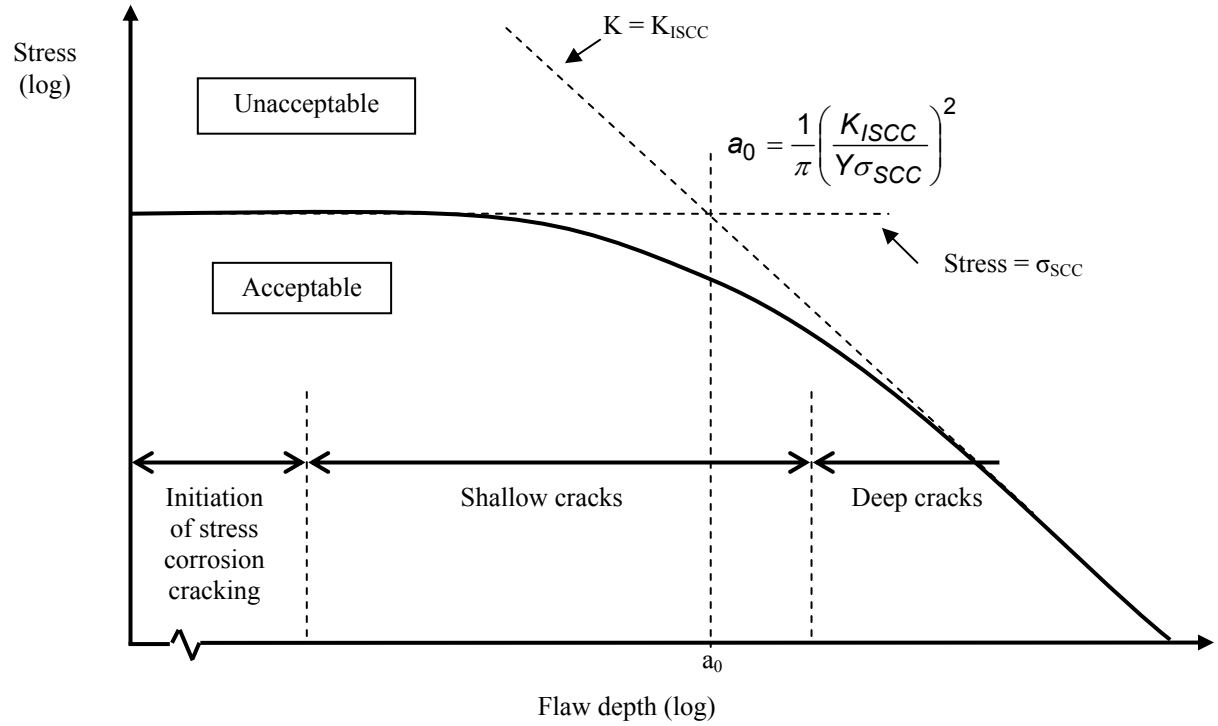

Fig. 2 Two-parameter approach to stress corrosion cracking (after Ref. [11])

The Kitagawa-type plot shown in Fig. 2 does not of course say anything about the rate of crack growth; it simply suggests that in the shallow-crack regime the "threshold stress" is expected to be lower than anticipated by extrapolating the deep-crack data. As crack size decreases, departure from the K-controlled regime is of course inevitable and is not necessarily linked with environmental effects associated with differences in crack tip chemistry.

A rather different approach to modeling the early stages of EAC has been reported by Turnbull et al. [19]. This work focused on predicting the transition between pitting and cracking in a steam turbine disk steel. The transition between the pit and crack was modeled in terms of a process competition between the rate of pit growth and the rate of crack growth, the latter being described by a power law for shallow cracks, and a constant for cracks deeper than a critical value. This was a similar approach to earlier work carried out to model the transition between pitting and fatigue cracking [20,21]. By using a Weibull distribution to create an initial set of corrosion pit depths, it was possible to predict the evolution of pits into cracks in a way that was consistent with available experimental data.
There are therefore clearly a number of ways that the early stages of EAC may be modeled. The diagram in Fig. 2 describes one aspect of the shallow-crack problem, in that the

appropriate characterizing parameter changes from K to stress as the crack size decreases. In the transitional regime, models developed to explain the nature of this transition will rely on the availability of suitable shallow crack test data, and this program of work has begun to address the lack of data in this regime, for the particular case of pipeline steels in a sour environment.

From examination of Fig. 2, it can be seen that the shallow-crack regime is essentially defined by the relative magnitude of K_{ISCC} and σ_{SCC}. The crack size over which the transition from stress-controlled behavior to K-controlled behavior occurs for pipeline steels in a sour environment is calculated to be of the order of 3-6 mm [22]. Other published works researching the behavior of short cracks tend to refer to cracks of less than 1 mm. However, for the specific case of pipeline steels in a sour environment, flaws of this size cannot be reliably detected using modern NDT techniques, so this paper focuses on the behavior of flaws of depth greater than 1 mm. Also of interest is the potential effect on K_{ISCC} or da/dt (or da/dN) caused by differences in crack tip chemistry.

The aim of this paper is to describe and compare the results of two test programs: one investigating the corrosion fatigue behavior of a pipeline steel in a sour environment and the other investigating the influence of crack depth on the threshold stress intensity factor for stress corrosion cracking (K_{ISCC}) (i.e., static loading) in the same steel exposed to a similar environment.

2 EXPERIMENTAL DETAILS

2.1 MATERIAL

API 5L X65 seamless line-pipe material was used in both the fatigue and static test programs. The chemical composition of the steel, determined using the optical emission spectrometry (OES) method, is summarized in Table 1. Hardness and tensile property data for the material used are provided in Table 2.

Table 1 Chemical composition of API-5L X65 (wt.%).

C	Si	Mn	P	S	Cr	Mo	Ni
0.11	0.28	1.12	0.010	0.003	0.082	0.11	0.099
Al	As	B	Co	Cu	Nb	Pb	Sn
0.025	0.008	0.0003	0.008	0.14	0.018	<0.005	0.010
Ti	V	W	Zr	Ca	Ce	Sb	
0.002	0.058	<0.01	<0.005	0.0017	<0.002	<0.002	

Table 2 Hardness and tensile property data for the X65 material used.

Hardness (HV)	196
UTS (MPa)	576
0.2% Proof Stress (MPa)	478

2.2 SPECIMEN GEOMETRY

Square section (B x B) single edge notched bend (SENB) specimens were extracted from the pipe material. Specimen geometry was B=W=16 mm and these were tested in three point bending. A standard span of 64 mm (i.e., 4W) was used in the fatigue crack growth tests while a span of 200 mm was used for the constant load tests.

Specimens were notched using electrical discharge machining (EDM) to introduce a starter notch, approximately 0.5 mm deep in the case of the fatigue tests and of differing depths for the static load tests depending on the initial flaw size desired. The notch was oriented circumferentially to allow crack growth in the through thickness direction, from the internal surface of the pipe.

This starter notch was then subjected to fatigue loading (R=0.1, cyclic loading frequency up to 100 Hz) to provide a total fatigue precrack length of approximately 1.6 mm, in the case of the fatigue tests. Several different flaw sizes were tested under static loading conditions, ranging from approximately 1.6 mm (a/W ~ 0.1) to 8.0 mm (a/W ~ 0.5). Initial estimates of flaw size were based on surface measurements each side of the specimen but this was confirmed after the test by breaking the specimen open and measuring directly from the fracture surface.

The final load at the end of precracking the shallow flaws (a ~ 1.6 mm) was 12.5 kN, which corresponds to a K_{max} of approximately 600–750 $Nmm^{-3/2}$ depending on the actual final crack length that was achieved. The final load at the end of precracking the deep flaws (a ~ 8.0 mm) was approximately 3.5 kN, which corresponds to a K_{max} of approximately 550–600 $Nmm^{-3/2}$ depending on the actual final crack length that was achieved. The reason for this lower final value of K_{max} is because for deeper flaws there is more time to shed the load once the crack has initiated but before it reaches its target length.

2.3 ENVIRONMENTAL CONTROL

All tests, whether in air or a sour environment, were carried out at ambient temperature. For FCGR tests in a sour environment the specimen was immersed in an aqueous solution of 5% sodium chloride and 0.4% sodium acetate, acidified to a pH of approximately 3.5. This solution was purged with nitrogen to remove oxygen (<20 ppb) and a test gas of 7% H_2S in N_2 was then introduced.

Following an initial fast purge (typically overnight but in all cases at least 7 hours) the gas flow was reduced, but was continuously passed through the test solution to maintain saturation. Solution pH and H_2S content were monitored at intervals during the test.

'Stopping off' lacquer to protect the bulk of the specimen and instrumentation from the corrosive environment, and to minimise the extent of solution contamination, was applied to all specimens tested in a sour environment. A 10 mm window was left un-coated on each side of the notch on all sides of the specimen to allow interaction between the environment and the crack tip.

For the static tests in a sour environment a standard NACE Test Solution A was used [23]. The specimen was immersed in an aqueous solution of 5% sodium chloride and 0.5 wt% glacial acetic acid acidified to a pH of approximately 2.5-3.0. This solution was purged with nitrogen to remove oxygen (<20 ppb) and a test gas of 100% H_2S was then introduced. Solution pH and H_2S content were monitored at intervals during the test.

Upon completion of the tests in a sour environment, the test solution was purged with nitrogen and the specimen removed from the environmental chamber. Each specimen was then broken open after immersion in liquid nitrogen, and the fracture surface examined to determine the initial (and final for the crack growth tests) flaw sizes.

2.4 FATIGUE TESTING

FCGR tests were carried out under conditions of increasing, decreasing, or constant ΔK conditions using a standard servo-hydraulic testing machine with computer control and data logging. The direct current potential drop (DCPD) method was used to monitor crack depth with a typical resolution of 50 μm. The stress ratio was kept constant for all tests at 0.5. Test frequency was 5–10 Hz for tests in air and 0.1 Hz for tests in a sour environment. Crack growth rates were determined from the DCPD data and the post test crack length measurements using an incremental secant method and a measurement interval of 0.2 mm.

One increasing ΔK test was carried out in air and one in a sour environment with ΔK ranging from approximately 310-925 $Nmm^{-3/2}$ and 245-654 $Nmm^{-3/2}$ respectively. Under decreasing ΔK conditions, the applied load range was continuously shed while maintaining a constant stress ratio to impose a decreasing ΔK gradient of -0.1 mm^{-1}. Two tests were carried out in a sour environment with ΔK varying between 795 $Nmm^{-3/2}$ (at the start of the test) and 315 $Nmm^{-3/2}$ at the end of the test). Finally, two constant ΔK tests were carried out in a sour environment and one in air, in all cases maintaining a ΔK value of 300 $Nmm^{-3/2}$ to within 15%.

2.5 STATIC TESTING

Specimens were tested under conditions of constant load. By testing multiple specimens at different loads, a threshold stress intensity factor for stress corrosion cracking (K_{ISCC}) can be determined. A test duration of 720 hours was employed to ensure sufficient time for the environment to interact with the material.

A summary of the crack depths tested can be found in Table 3. This table shows the specimen identification number, the initial crack length, the load applied during the test, a calculated K-value and an indication of whether the specimen failed or not.

Prior to the testing in a sour environment, two calibration tests were carried out in air: one deep crack (specimen precracked to a/W ~ 0.5) and one shallow crack (specimen precracked to a/W ~ 0.1). Tests were carried out in a standard servo-hydraulic test machine with computer control and data logging, and were instrumented with a clip gauge to provide a load-displacement plot and allow determination of J or CTOD.

The first two tests in a sour environment were step load tests: one at a flaw size of approximately a/W=0.5 (a ~ 8 mm) and one at a flaw size of approximately a/W=0.1 (a ~ 1.6 mm) The load was increased each week (based on an initial conservative estimate of K) until the specimen failed. A series of constant load tests (720 h duration) was then targeted close to the threshold at both a/W=0.5 (deep flaw) and a/W=0.1 (shallow flaw) to back up the results of the step load tests.

At the end of the test program, two additional step load tests were carried out at intermediate crack lengths (a ~ 3 mm and a ~ 5 mm). An unnotched specimen was also step loaded to failure (Table 4).

Table 3 Static load test results (pre-cracked specimens).

Specimen ID	Actual Flaw Size, a (mm)	Test Parameters		Result
		Load (kN)	K ($Nmm^{-3/2}$)	
M02-07	8.24	1.51 1.90	813 1023	Step load test (1-week at each applied load until specimen failed)
M02-08	8.33	1.51	828	Constant load test Specimen still intact after 720 hrs
M02-09	7.92	1.70	859	Constant load test Specimen still intact after 720 hrs but crack extension visible
M02-10	8.47	1.80	1016	Constant load test Specimen failed after ~180hrs
M02-21	8.36	1.60	883	Constant load test Specimen failed after ~40hrs
M02-13	2.10	4.90 6.10	906 1128	Step load test (1-week at each applied load until specimen failed)
M02-16	2.18	4.90	922	Constant load test Specimen still intact after 720 hrs
M02-17	1.60	5.60	918	Constant load test Specimen failed after ~200 hrs
M02-26	1.55	5.30	857	Constant load test. Specimen failed after ~365 hrs
M02-19	3.69	3.60 4.60	887 1133	Step load test (1-week at each applied load until specimen failed)
M02-20	5.34	2.60 3.30 4.00	834 1058 1283	Step load test (1-week at each applied load until specimen failed)

Table 4 Static load test results (un-notched specimen).

Specimen ID	Actual Flaw Size, a (mm)	Test Parameters		Result
		Load (kN)	Stress (MPa)	
M02-23	Un-notched	6.0 7.0 8.0 9.0 10.0 11.0	439 513 586 659 732 806	Step load test. (1-week at each applied load until specimen failed) Failed when test was increased to 11.0 kN.

3 RESULTS

3.1 FATIGUE CRACK GROWTH RATE DATA

Figure 3 shows the results of the increasing and decreasing ΔK test results plotted alongside the mean curve for ferritic steels in air (R>0.5) from BS 7910 [10].

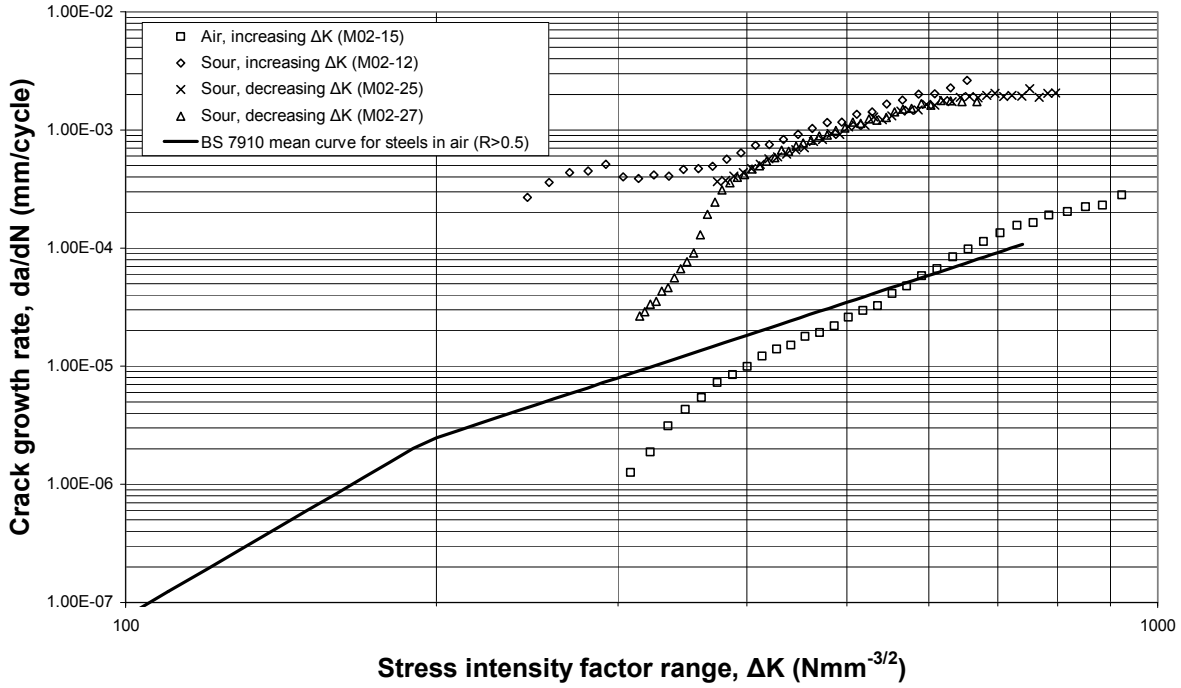

Fig. 3 Increasing and decreasing ΔK test results.

The observed crack growth rate for the increasing ΔK test in air was close to the mean curve from BS 7910, although at low ΔK (the beginning of the test) the crack growth rates were slightly lower. The increasing ΔK tests in a sour environment showed an increase in crack growth rate of 30-100 times compared with in air. Under decreasing ΔK conditions in a sour environment, there is a good agreement with the increasing ΔK results at high ΔK, but at low ΔK the crack growth rate under decreasing ΔK conditions drops off significantly and even starts to approach the mean curve for steels in air from BS 7910.

Constant ΔK test results are plotted in Fig. 4. A constant crack growth rate is observed in the test carried out in air, showing reasonably good correlation with the beginning of the increasing ΔK test and the mean curve for steels in air from BS 7910. In a sour environment, the crack growth rates are initially seen to be between 30 and 130 times higher than in air but fell to 5-12 times faster by the end of the test. While there are differences between the results of the two tests in a sour environment there appears to be a region of approximately constant crack growth rate at the start of the test. The crack growth rate then decreases as the crack depth increases until a constant deep-crack growth rate is reached for cracks deeper than approximately 6 mm. Crack growth rates at the end of the constant ΔK test are comparable to those at the end of the decreasing ΔK test when the values of ΔK are similar.

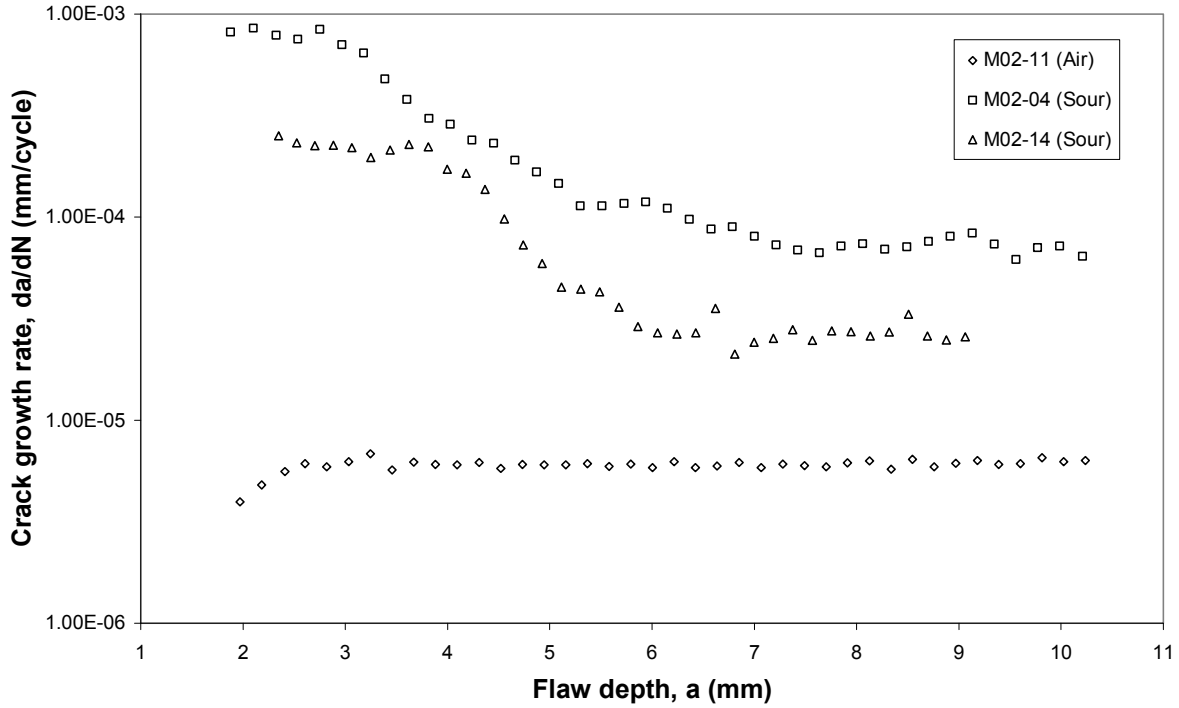

Fig.4 Constant ΔK test results (ΔK ~ 300 $Nmm^{-3/2}$).

3.2 STATIC TESTING

The results of the calibration tests in air showed that material behavior remains predominantly elastic up to an applied load of approximately 6.6 kN for a flaw size of a/W ~ 0.1 and 2.3 kN for a flaw size of a/W ~ 0.5. In all cases, the loads applied in the sour tests were below this limit so all subsequent analyses considered only the elastic component. The results of the static test program are illustrated in Fig. 5 with stress intensity factor (K) plotted against flaw size (a). Step loaded tests are indicated by dashed arrows.

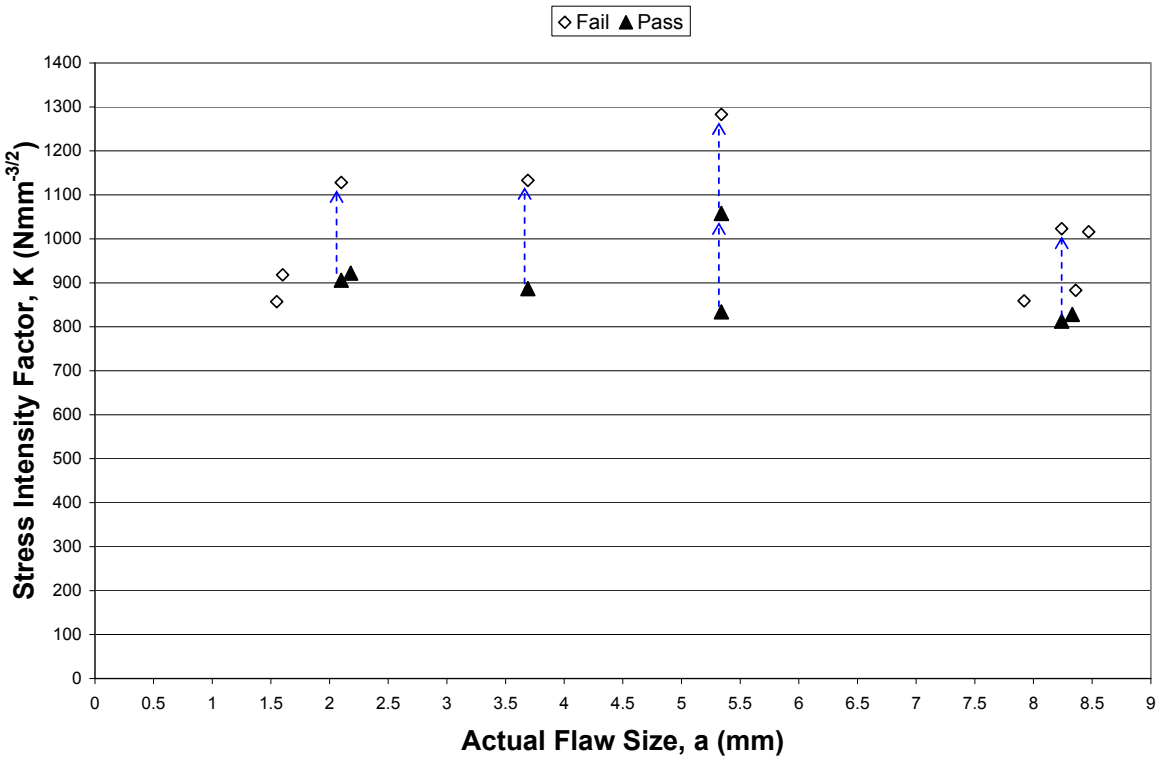

Fig. 5 Static test results in a sour environment; the arrow indicates a step load test.

The initial deep-crack step load test failed at a K-value of approximately 1023 $Nmm^{-3/2}$ (an applied load of 1.9 kN) after surviving 1 week at a K-value of approximately 813 $Nmm^{-3/2}$ (an applied load of 1.51 kN). Subsequent constant load tests were therefore targeted in the region of 800-1000 $Nmm^{-3/2}$, starting at approximately 813 $Nmm^{-3/2}$ since this was the lowest value that did not cause the step loaded specimen to fail.

Specimen M02-08 survived for 720 h at a K-value of 828 $Nmm^{-3/2}$ and this was the highest value of K that did not result in failure, which represents a lower bound estimate for K_{ISCC}. Specimen M02-09 was still intact after 720 h at a K-value of 859 $Nmm^{-3/2}$ but was deemed to have failed when post-test examination of the fracture face revealed a small region of crack extension (Fig. 6). This was therefore the lowest value of K that resulted in failure, which represents an upper bound estimate for K_{ISCC}.

The initial shallow-crack step load test failed at a K-value of approximately 1128 $Nmm^{-3/2}$ (an applied load of 6.1 kN) after surviving 1 week at a K-value of approximately 906 $Nmm^{-3/2}$ (an applied load of 4.9 kN). Subsequent constant load tests were therefore targeted in the region of 800-1100 $Nmm^{-3/2}$. Specimen M02-26 failed after approximately 365 h at a K-value of 857 $Nmm^{-3/2}$. This was the lowest value of K that resulted in failure and represents an upper bound estimate of K_{ISCC}.

The two additional step load tests carried out at intermediate flaw sizes produced broadly similar results to the deep- and shallow-crack results detailed above. The unnotched specimen failed when the load was increased from 10 kN to 11 kN. Outer surface stresses were calculated using standard beam theory and indicated that failure occurred when this reached between 732 MPa and 806 MPa, which is significantly higher than the material yield stress.

4 DISCUSSION

4.1 FATIGUE TESTING

The results of the crack growth tests carried out in a sour environment showed broad agreement with other published data, with crack growth rates typically 5-100 times faster than corresponding tests in air. For crack depths above 6 mm, there is a good correlation between those tests carried out in increasing, decreasing, and constant ΔK conditions.

At shallower flaw depths, there is a marked increase in crack growth rate and at low ΔK, as seen in the constant ΔK tests (Fig. 4) and the difference between increasing ΔK and decreasing ΔK tests (M02-12 and M02-27) at low ΔK. However at high ΔK this does not appear to be the case (i.e., M02-12 and M02-27 exhibit the same growth rate at ΔK ~ 700 $Nmm^{-3/2}$).

A possible explanation for this is an environmental crack depth effect caused by a difference in crack tip chemistry leading to enhanced production and absorption of hydrogen for a shallow crack. Other possible reasons include reduced crack closure in the shallow-crack regime or an influence of bulk hydrogen charging on material behavior close to the specimen surface.

A stress ratio of 0.5 was used in all tests in an effort to minimize crack closure effects but these cannot be ruled out. If crack closure is influencing the test results, then one would expect to see a diminished effect at higher ΔK, as was the case. If bulk hydrogen charging is influencing material behavior, then one would expect a higher crack growth rate for a shallow flaw (at the start of the test) compared with a deeper flaw where crack growth will be occurring through material containing less absorbed hydrogen, due to an increased average distance from the nearest external surface. One would also expect a higher crack growth rate at the edge of the specimen than along the specimen centerline, which was evident from the fracture faces of all tests, and particularly noticeable in the decreasing ΔK and constant ΔK tests. Under conditions where bulk charging is dominant, it is important to include an adequate “pre-soak” to maximize the environmental effect.

The decreasing ΔK tests in a sour environment (in particular, M02-27) illustrate the potential nonconservatism associated with using deep-crack data to model the behavior of much shallower flaws, and there is clearly a need to further examine this phenomenon.

4.2 STATIC TESTING

Figure 5 shows K_{ISCC} to be approximately 800-850 $Nmm^{-3/2}$ with no apparent influence of crack depth (in contrast with the fatigue crack growth rate data). Figure 5 also illustrates the problems with relying solely on step load tests as these tend to overestimate K_{ISCC}, hence the need to back up these tests with constant load tests.

A specimen still being intact after 720 h does not automatically indicate that the specimen has passed the static test at that applied load. For each test, it is also necessary to examine the fracture face for signs of crack extension, as was the case with specimen M02-09 (Fig. 6). In this case, specimen M02-09 has to be deemed a failure as crack extension has occurred and the specimen may have failed if left on for longer.

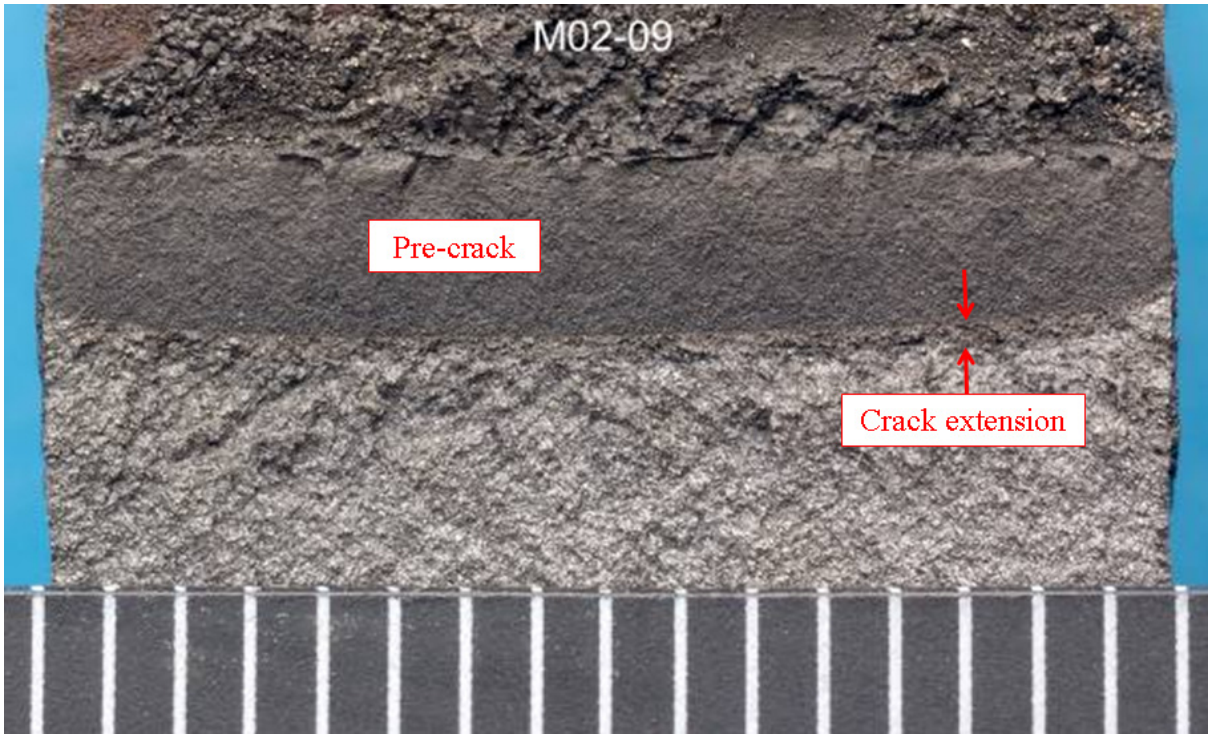

Fig. 6 Region of crack extension on fracture face of specimen M02-09 (constant load, a=7.92 mm).

A literature review for static test results in a sour environment has confirmed that the value of K_{ISCC} reported here is broadly comparable to that observed elsewhere, for steels of a comparable hardness [24-26]. Of particular interest is the work of Sponseller [26] who examined the sulphide stress cracking resistance of various materials, including C-90 low alloy steel using the double cantilever beam (DCB) method [23] and reported that K_{ISCC} varied with displacement/crack length. The DCB test method utilizes a specimen loaded to a fixed displacement, and as the crack grows the applied stress intensity decreases until the crack arrests. An estimate for K_{ISCC} can be determined by measuring the final crack depth. In an interlaboratory comparison, values of K_{ISCC} were 24-48 $MPam^{1/2}$, and most of this variation was attributed to differences in the initial applied displacement. Use of a larger initial displacement resulted in higher values of K_{ISCC}. For a larger initial displacement, the crack depth associated with a given applied K is higher, and it was argued that for deeper cracks there was reduced access of the environment to the crack tip and reduced hydrogen charging of the plastic zone, and this led to a higher value of K_{ISCC}.

The data in Fig. 5 can be replotted as a Kitagawa-type diagram (Fig. 7) by determining the outer surface stress associated with the applied load. Figure 7 shows a log-log plot of stress versus flaw size. The points plotted on the left of the diagram are the results of the step loaded unnotched specimen (i.e., flaw size is zero). A horizontal line has been added to the diagram to represent stress-controlled behavior at a stress value of 732 MPa, the stress which the unnotched specimen survived for 1 week before failing.

On the right hand side of the diagram are the results of the static tests in a sour environment, again plotted in terms of stress. An approximate line of best fit has been added to the diagram for the passed tests. The two lines intersect at a flaw size of approximately 1 mm suggesting that there may be a transition from K-controlled to stress-controlled behavior in this regime. This is comparable to that predicted in earlier work based on a review of published data [22].

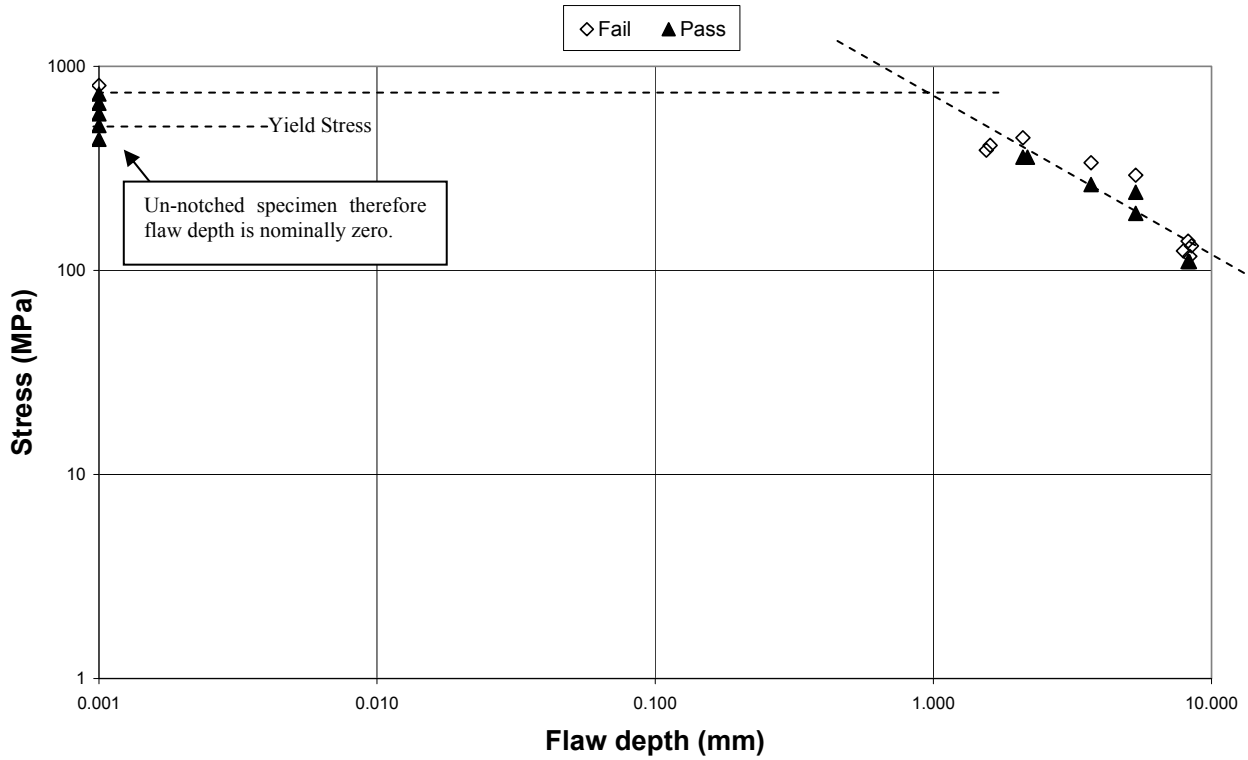

Fig. 7 Log-log plot of stress versus flaw size (Kitagawa-type diagram).

An alternative way of presenting these data is to construct a FAD based on sour-service material properties, i.e., using K_{ISCC} as a measure of the material's "toughness." This plots a fracture toughness ratio (the ratio of stress intensity factor to material fracture toughness) against either stress ratio (the ratio of reference stress to flow stress) or load ratio (the ratio of reference stress to yield stress). A generalized Level 2A FAD has been plotted in Fig. 8 using the equations in BS 7910 (although these also feature in Part 9 of API 579- 1/ASME FFS-1).

At Level 2, the less conservative load ratio is used on the horizontal axis. The vertical line represents the cutoff for this material, termed the maximum load ratio calculated using the tensile properties of the material. The unnotched specimen test results are also plotted to show that the assessment line falls roughly where the unnotched specimen failed. A material fracture toughness of 828 $Nmm^{-3/2}$ was chosen when constructing the Level 2A FAD. This estimate is based on the deep-crack test data only and is a conservative estimate because it is the value of the lowest definite pass after a 720 h duration lest. As mentioned previously, specimen M02-09 was also still intact after 720 h at a K-value of 859 $Nmm^{-3/2}$ but post-test examination of the fracture face revealed a small amount of crack extension and hence this specimen was judged to have failed (Fig 6).

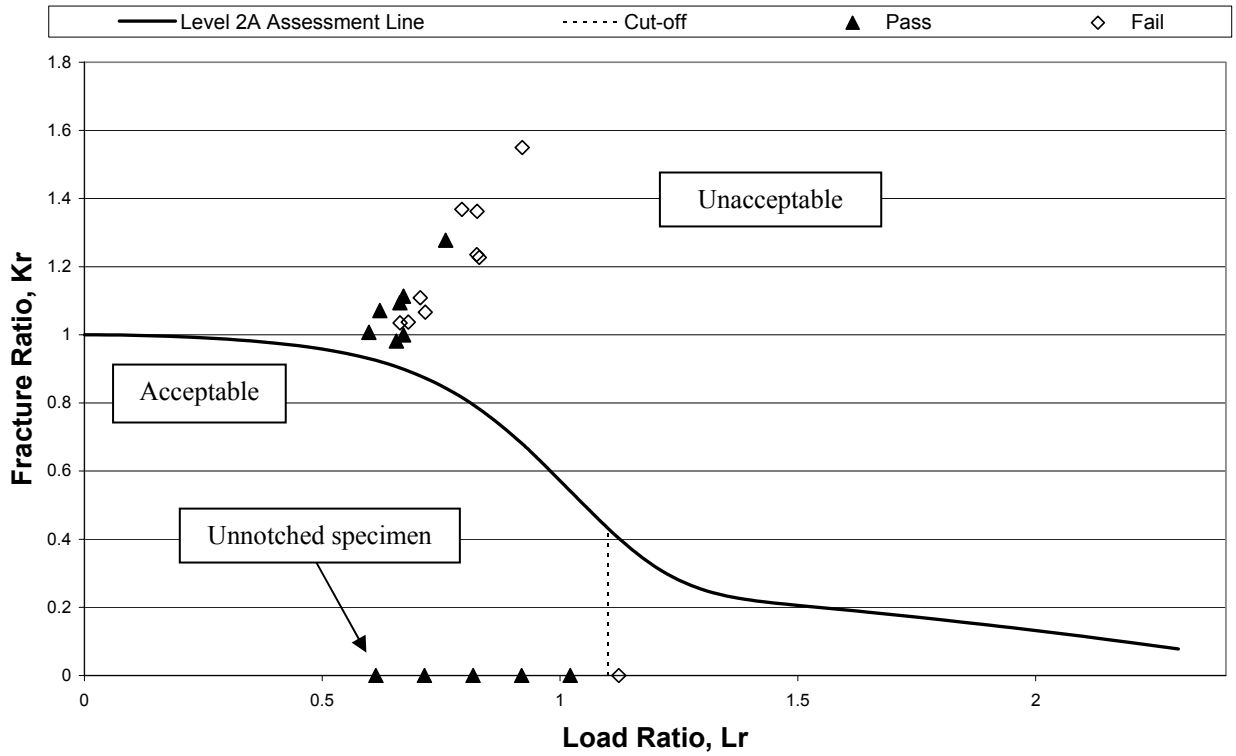

Fig. 8 FAD using K_{ISCC} as a measure of material's toughness.

The FAD indicates that for the range of flaw depths tested all assessment points lie in a similar region of the FAD, i.e., toward the K-controlled region. It would therefore be necessary to investigate shallower flaws (say, 0.1-1.0 mm) before a significant reduction in fracture ratio would be expected. Certain novel techniques are available for generating shallower flaws, for example, initiating a fatigue crack from a focused ion beam (FIB) notch, which has a far sharper root radius than an EDM notch.

5 CONCLUSIONS

Under cyclic loading conditions, shallow cracks have been shown to grow by fatigue up to 130 times faster in a sour environment than in air and up to an order of magnitude higher than deeper flaws in a sour environment. Possible explanations for this effect include the following.

- Differences in crack tip chemistry that lead to enhanced hydrogen uptake at shallower flaws.
- A reduced contribution from crack closure for shallower flaws; this would explain why an effect is seen at low ΔK but not at higher ΔK.
- An influence of bulk hydrogen charging on material behavior close to the specimen surface.

Under static loading conditions in a sour environment K_{ISCC} does not appear to be crack depth dependent between a ~ 1.6 mm and a ~ 8 mm. Potential differences in crack tip chemistry or bulk hydrogen charging do not appear to be affecting material behavior in this instance. It is therefore possible that these effects only become apparent under the conditions of dynamic equilibrium associated with fatigue loading and progressive crack extension. However, it is also worth reiterating that the static load tests were carried out in a much more

severely hydrogen charging environment than the FCGR tests, which may mask any crack tip chemistry effects.

Prolonged exposure of a stationary crack to a static load may exhibit reduced sensitivity to a transient environmental effect. A possible influence of cyclic loading frequency may be anticipated in this instance. Crack closure will, of course, not be a contributing factor in the static K_{ISCC} tests, so this may also explain the difference in behavior observed in the static and cyclic tests. Another possible explanation for the difference in crack growth rates under fatigue and static loading conditions is the pulsing effect of the fatigue cycling. This effect can force the sour environment into the crack tip.

6 RECOMMENDATIONS

When conducting tests in simulated sour operating environments, to determine crack growth laws or K_{ISCC} values for use in fracture mechanics design calculations, the potential influence of crack depth on material behavior should be considered. In the absence of reliable mechanistic models, the most appropriate advice is to ensure that the flaw size used is comparable to that being assessed, and in this respect, particular care should be taken when carrying out decreasing ΔK tests to generate crack growth rate data at low ΔK.

7 REFERENCES

[1] Bristoll, P., and Roeleveld, J., 1978, “Fatigue of Offshore Structures: Effect of Seawater on Crack Propagation in Structural Steel,” Proceedings of the European Offshore Steels Research, ECSC, Paper 18, The Welding Institute, Cambridge , UK.

[2] Webster, Se. E., Austen, I.M., and Rudd, W., 1985, “Fatigue, Corrosion Fatigue and Stress Corrosion of Steels for Offshore Structures,” ECSC Report No. EUR 9460.

[3] Vosikovsky, O., and Rivard, A., 1982, “The Effect of Hydrogen Sulphide in Crude Oil on Fatigue Crack Growth in a Pipeline Steel,” Corrosion (Houston), 38(1), pp. 19-22.

[4] Vosikovsky, O., Macecek, M., and Ross, D.J., 1983, “Allowable Defect sizes in a Sour Crude Oil Pipeline for Corrosion Fatigue Conditions,” Int. J Pressure Vessels Piping, 13, pp. 197-226.

[5] Watanabe, E., Yajima, H., Ebara, R., Matsumoto, S., Nakano, Y., and Sugie, E., 1994, “Corrosion Fatigue Strength of Ship Structural Steel Plates and Their Welded Joints in Sour Crude Oil,” Offshore Mechanics and Arctic Engineering Conference (OMAE 1974), ASME, New York, Vol. III, pp. 151-158.

[6] Eadie, R, C., and Szklarz, K.E., 1999, “Fatigue Crack propagation and fracture in Sour Dilute Brine,” Proceedings of Corrosion, NACE International, Houston, TX, Paper No. 611.

[7] Eadie, R. C., and Szklarz, K. E., 1999, “Fatigue Initiation and Crack Closure of Low Alloy Steels in Sour Brine Environments,” Proceedings of Corrosion, NACE International, Houston, TX, Paper No. 610.

[8] Baxter, D P., Maddox, S. J., and Pargeter, R. J., 2007, “Corrosion Fatigue Behaviour of Welded Risers and Pipelines,” Proceedings of OMAE2007 25th International Conference on Offshore Mechanics and Arctic Engineering, San Diego, CA., Paper No. OMAE2007-29630.

[9] Gooch, T. G., 1982, "Hardness and Stress Corrosion Cracking of Ferritic Steel," The Welding Institute Research Bulletin, 23(8), pp. 241-246.

[10] 2005, "BS 7910: Guide to Methods for Assessing the Acceptability of Flaws in Metallic Structures," British Standards Institution, London.

[11] FITNET, 2009, "Fitness-for-Service," Revision MK8, ISBN 978-3-940923-00-4, prepared by the European Fitness-for-Service Thematic Network, FITNET.

[12] 2007, "Fitness-For-Service," 1st ed., The American Petroleum Institute and The American Society of Mechanical Engineers, Washington, API 579-1/ASME FFS-1.

[13] 2006, "Assessment of the Integrity of Structures Containing Defects," R6 Revision 4, British Energy.

[14] Jones, R. H., and Simonen, E. P., 1994, "Early Stages in the Development of Stress Corrosion Cracks," Mater. Sci. Eng., A, 176, pp. 21-218.

[15] Kitagawa, H., and Takahashi, S., 1979, "Applicability of Fracture Mechanics to Very Small Cracks of the Cracks in the early State," Proceedings of the Second International Conference on Mechanical Behaviour of Materials, pp. 627-631.

[16] Ganglofff, R P., 1985, "Crack Size Effects on the Chemical Driving Force for Aqueous Corrosion Fatigue," Metall. Trans. A., 16A, pp. 953-969.

[17] Akid, R., 1994, "Modelling Environment-Assisted Short Fatigue Crack Growth," Advances in Fracture Resistance and Structural Integrity, Permagon, New York, pp. 261-269.

[18] Murtaza, G., and Akid, R., 1995, "Modelling Short Fatigue Crack Growth in a Heat-Treated Low-Alloy Steel," Int. J Fatigue, 17(3), pp. 207-214.

[19] Turnbull, A., McCartney, L. N., and Zhou, S., 2006, "Modelling of the Evolution of Stress Corrosion Cracks From Pits," Scr. Mater., 54, pp. 575-578.

[20] Kondo, Y., 1989, "Prediction of Fatigue Crack Initiation Life Based on Pit Growth," Corr., 45(1), pp. 7-11.

[21] Chen, G. S., Wan, K.-C., Gao, M., Wei, R. P., and Flournoy, T. H., 1996, "Transition From Pitting to Fatigue Crack Growth–Modelling of Corrosion Fatigue Crack Nucleation in a 2023-T3 Aluminium Alloy," Mater, Sci, Eng., A, 219, pp. 126-132.

[22] Holtam, C. M., and Baxter, D. P., 2007, "Environment Assisted Crack Assessment Methods: The Behaviour of Shallow Cracks," Proceedings of the UK Forum for Engineering Structural Integrity's Ninth International Conference on Engineering Structural Integrity Assessment (ESIA9), EMAS, pp. 862-866.

[23] NACE, 2005, "MR 0177-2005: Laboratory Testing of Metals for Resistance to Sulfide Stress Cracking and Stress Corrosion Cracking in H_2S Environments," Houston.

[24] Pargeter, R. J., Gooch, T. G., and Bailey, N., 1990, "The Effect of Environment on Threshold Hardness for Hydrogen Induced Stress Corrosion Cracking of C-Mn Steel Welds," Conference Proceedings on Advanced Technology in Welding, Materials, Processing and Evaluation, Apr., Japan Welding Society, Tokyo.

[25] Albarran, J. L., Martinez, L., and Lopez, H. F., 1999, "Effect of Heat Treatment on the Stress Corrosion Resistance of a Micralloyed Pipeline Steel", Corros. Sci., 41, pp. 1037-1049.

[26] Sponseller, D. L., 1992, "Interlaboratory Testing of Seven Alloys for SCC Resistance by the Double Cantilever Beam Method," Corrosion (Houston), 48(2), pp. 159-171.

APPENDIX C

Holtam C M, Baxter D P, Ashcroft I A and Thomson R C, 2010: 'Effect of crack depth on fatigue crack growth rates for a C-Mn pipeline steel in a sour environment', International Journal of Fatigue 32 (2010) pp288-296, Elsevier.

Effect of Crack Depth on Fatigue Crack Growth Rates for a C-Mn Pipeline Steel in a Sour Environment

C. M. Holtam
D. P. Baxter
Structural Integrity Technology Group
TWI Ltd
Cambridge
CB21 6AL
UK

I. A. Ashcroft
Wolfson School of Mechanical and Manufacturing Engineering
Loughborough University
Leicestershire
LE11 3TU
UK

R. C. Thomson
Department of Materials
Loughborough University
Leicestershire
LE11 3TU
UK

ABSTRACT

Setting conditions for the avoidance of in-service crack growth in aggressive corroding environments has long been a major challenge owing to the number of variables that have a significant effect on material behaviour. The fatigue behaviour of API 5L X65 pipeline steel parent material tested in a sour environment has been investigated. Fatigue crack growth rate (FCGR) tests have been performed to evaluate the influence of crack depth on crack growth rate (da/dN), over the range 2-10mm. The results obtained showed crack growth rates for deep flaws to be a factor of 5-30 higher in the sour environment than in air, dependent on the applied stress intensity factor range (ΔK). Shallow flaws have been shown to grow up to an order of magnitude faster than deep flaws in a sour environment at the same value of ΔK. The results highlight a potential non-conservatism associated with using deep-crack data to predict the behaviour of shallow flaws. The observed behaviour is attributed to the uptake of hydrogen at specimen surfaces exposed to the sour environment.

1 INTRODUCTION

Carbon manganese steel is generally the most economic material for the construction of offshore pipelines or risers. Steel catenary risers (SCR) are widely used in deepwater oil and gas developments for transporting production fluids from the seabed. They can be subjected to fatigue damage from numerous sources, for example wave motion or vortex induced vibration (VIV). When production fluids are sour (i.e. contain water and H_2S), the fatigue resistance is significantly degraded in comparison with the performance in air as a result of sulphide stress cracking (SSC); the endurance limit is lower [1-4] and the fatigue crack growth rate (FCGR) is higher [5-10]. Sour production fluids are common in oil and gas applications and therefore successful design of pipelines or risers is critically dependent on the availability of appropriate experimental data to quantify the extent to which fatigue lives are reduced, and rates of fatigue crack growth are increased by exposure to sour environments.

Both environmental variables (e.g. pH, temperature, H_2S concentration) and mechanical variables (e.g. applied stress intensity factor range, stress ratio, cyclic loading frequency) can influence fatigue performance in sour environments. A recent review of published sour data has highlighted the extent to which each of these variables can affect performance [5]. Bristoll and Roeleveld [6] tested non-welded plain C-Mn steel in seawater saturated with H_2S (3000 ppm) at 20°C with a stress ratio (R) of at least 0.6 and a loading frequency of 0.2 Hz. They found that crack growth rates were up to 50 times higher than those observed in air. This contrasts with corresponding tests in seawater (with no H_2S) in which crack growth rates increased by only 2-3 times. The increase in crack growth rate was also seen to be dependent on the applied stress intensity factor range (ΔK), with a less noticeable increase observed at low values of ΔK. This trend was also reported by Webster et al. [7] who tested BS 4360 Grade 50D steel in seawater saturated with H_2S at 25°C with stress ratios of 0.05 and 0.07 and a frequency of 0.17 Hz. At intermediate values of ΔK, crack growth rates were approximately 20 times faster than in air whereas at high ΔK the difference was as much as 100 times. The effect of ΔK has also been reported by numerous other researchers carrying out tests in a variety of sour service environments [8-10].

In a more recent study, Eadie and Szklarz [11] investigated the influence of several mechanical and environmental parameters on fatigue crack growth. A medium strength low alloy steel was tested in a sour dilute brine (at 30°C), and the partial pressure of H_2S was found to have an effect on crack growth rate. This agreed with earlier work by Vosikovsky but it was noted that the influence of partial pressure was less noticeable at low ΔK and low test frequency (0.1 Hz compared to 1 Hz) [8,9]. Stress ratio did not noticeably influence crack growth rates at medium to high values of ΔK, although a higher stress ratio did lower the apparent ΔK threshold [12].

A number of researchers have reported a diminished influence of a sour environment at low values of applied ΔK. In many cases it is behaviour in this low ΔK regime that dominates the prediction of total fatigue life. Experimental crack growth rate data (da/dN-ΔK) are typically determined in simulated operating environments, and upper bound curves can be used in fracture mechanics calculations to calculate critical flaw sizes. Experimental data at low values of applied ΔK are often determined using a decreasing ΔK type test where the crack is relatively deep by the end of the test. However, in some instances predicting the behaviour of relatively shallow flaws, using test data derived from specimens containing much deeper flaws has been shown to be non-conservative.

Several researchers have reported increased crack growth rates in the shallow crack regime and this is often attributed to differences in crack tip chemistry. For example, Gangloff [13] tested 4130 steel in 3% NaCl solution and observed that shallow cracks (0.1-1.0 mm) grew 6-7 times faster than deep cracks (30-44 mm). Corresponding tests in air gave similar crack growth rates for the two crack sizes, so the effect was above and beyond what might be termed a 'mechanical crack depth effect' associated with differences in crack closure. It is therefore possible that an 'environmental crack depth effect' may occur, even under conditions where the 'mechanical driving force' is constant. Gangloff attributed the difference in crack growth rate to a difference in the crack tip environment, in particular the pH, which led to enhanced hydrogen production and uptake in the case of shallow cracks. It should be noted at this stage that the terms 'shallow' and 'deep' will be used throughout this paper to describe the through thickness crack size. In other work the terms short and long may be used, but there is scope for confusion as these may also refer to the lateral extent of a defect.

Nakai et al. [14] examined the behaviour of HY13O steel in 3.5% NaCl under constant ΔK conditions using specimens containing fatigue pre-cracks as shallow as 0.4 mm. Four regimes of behaviour were reported. Regime I was considered to represent the initial growth from the starting crack where the crack growth rate was fairly low. The crack growth rate then increased up to Regime II where a steady-state short crack growth rate was reached. Regime III was a transition between the short crack regime and the long crack regime IV and beyond this the crack growth rate again reaches a plateau, lower than in Regime II.

In other work examining fatigue behaviour in inert environments, it has been suggested that near threshold crack growth rate data can depend on the type of test used, owing to differences in crack closure. Pippan et al. [15] reviewed three methods for determining the threshold value of ΔK: decreasing ΔK maintaining a constant stress ratio, increasing ΔK (on specimens pre-cracked in compression) and decreasing ΔK maintaining constant maximum stress intensity factor (K_{max}). All three methods predicted very similar thresholds at high stress ratio. At low stress ratio, however, the observed threshold depended on the test method: decreasing ΔK at constant K_{max} gave the lowest threshold value (which would therefore lead to the most conservative assessment) followed by increasing ΔK, with decreasing ΔK at constant stress ratio giving the highest threshold values. The authors attributed these differences to crack closure effects.

The aim of this paper is to investigate the corrosion fatigue behaviour of shallow cracks, for the specific case of a pipeline steel exposed to a sour environment. It can be shown that for this material-environment system 'shallow' refers to flaw depths of the order of a few millimetres [16]. It should be noted that there are numerous other investigations into short crack behaviour that focus on sub-millimetre sized flaws (e.g. Murtaza and Akid [17]). However, in this specific application modern non-destructive testing (NDT) techniques cannot reliably detect sub-millimetre sized flaws, so in the current work we restrict ourselves to flaws that are greater than 1 mm deep. Tests have been carried out under conditions of increasing, decreasing or constant ΔK to explore material behaviour over the range 2-10 mm to establish whether crack depth has an effect on the observed FCGR over this range.

2 EXPERIMENTAL DETAILS

2.1 MATERIAL

The material used in this test programme was seamless line pipe parent material to API 5L grade X65. The supplied pipe had an outer diameter of 355.6 mm and a wall thickness of 20.6 mm. Tests were carried out to confirm the properties of the material. The chemical composition of the steel, determined using optical emission spectrometry (OES), is summarised in Table 1. Hardness and tensile property data are shown in Table 2.

Table 1 Chemical Composition of API 5L X65 C-Mn steel (wt.%).

C	Si	Mn	P	S	Cr	Mo
0.11	0.28	1.12	0.010	0.003	0.082	0.11

Ni	B	Cu	Nb	Ti	V
0.099	0.0003	0.14	0.018	0.002	0.058

Table 2 Hardness and tensile property data for the API 5L X65 C-Mn steel.

Hardness (HV10)	196
UTS (MPa)	576
0.2% Proof Stress (MPa)	478

2.2 SPECIMEN GEOMETRY

Square section single edge notched bend (SENB) specimens were extracted from the pipe material. Specimen geometry was B = W = 16 mm, as shown in Fig. 1, and these were tested in three point bending using a standard span of 4W (i.e. 64 mm). Specimens were notched using electrical discharge machining (EDM) to introduce a starter notch approximately 0.5 mm deep. This notch was oriented circumferentially (Fig. 2) to simulate crack growth in the through thickness direction, from the internal surface of the pipe. This starter notch was then subjected to fatigue loading (R = 0.1, cyclic loading frequency up to 100 Hz) to provide a total fatigue pre-crack length of approximately 1.6 mm (based on surface measurements each side of the specimen). The final load at the end of pre-cracking was 12.5 kN which corresponds to a K_{max} of approximately 19-24 $MPam^{0.5}$, depending on the actual final crack length that was achieved.

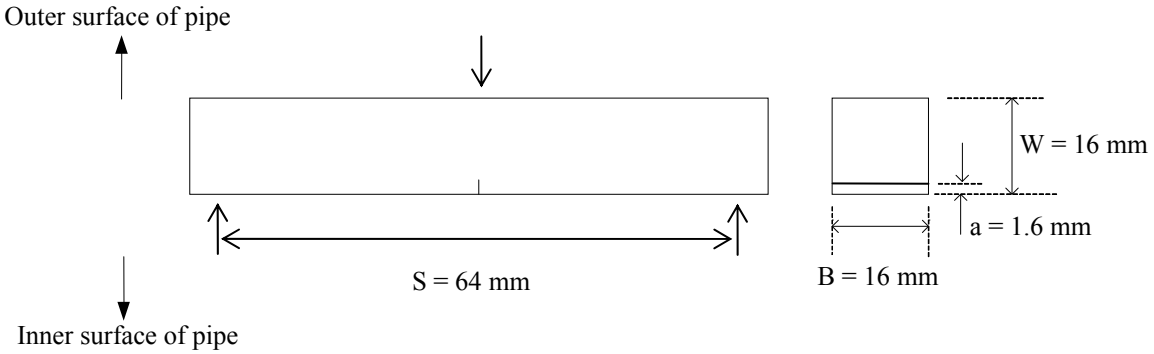

Fig. 1. Specimen geometry.

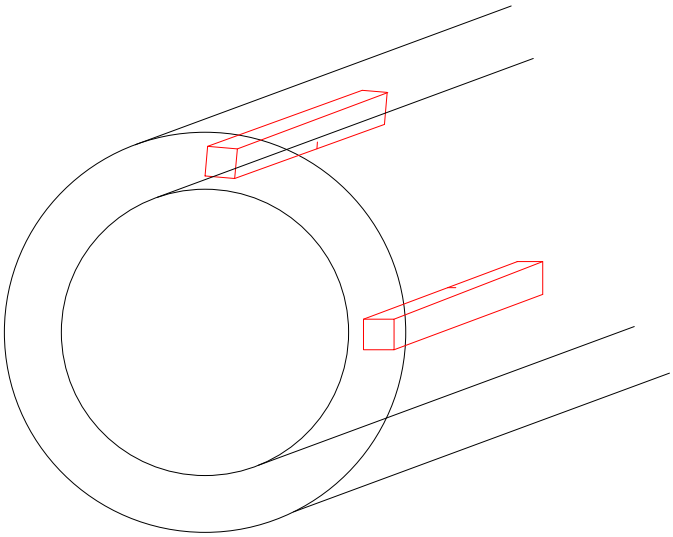

Fig. 2. Orientation of specimen notch relative to pipe.

2.3 FATIGUE TESTING

FCGR tests were carried out using a universal servo-hydraulic testing machine with computer control and data logging. Crack length was monitored using the direct current potential drop (DCPD) technique in which resolution is typically 10-20 μm for this material with the equipment used.

All tests were carried out using a stress ratio of 0.5. For those tests carried out in air the loading frequency was 5-10 Hz as one would not expect the result to be sensitive to frequency. For those tests carried out in a sour environment the loading frequency was reduced to 0.1 Hz to allow time for the environment to interact with the specimen. During each test, the applied load range was continuously monitored and adjusted to generate test data under the loading conditions described below. Because the objective of the reported work was to assess the influence of crack depth on FCGR for a pipeline steel exposed to a sour environment many of the tests have been carried out under conditions of constant ΔK, to ensure that the influence of crack depth can be directly observed. While the applied ΔK will have an effect on the FCGR, it is not the aim of this paper to develop a full crack growth rate law for all possible conditions. However, conventionally tests are carried out under conditions of either increasing or decreasing ΔK to generate ΔK data over the ΔK range of interest. In particular, low ΔK data are often generated under conditions of decreasing ΔK (for experimental convenience). For those tests carried out under conditions of increasing or decreasing ΔK, the range of ΔK that can be derived for a single test is predominantly a function of specimen size, and for the pipe material of interest (wall thickness 20.6 mm), and the specimen geometry used (SENB), the ΔK increases by approximately a factor of two. The range examined (9-19 $MPam^{0.5}$) is typical of that experienced by hypothetical flaws under consideration within an assessment of wave or VIV loading of an SCR.

2.3.1 INCREASING ΔK

The applied load range was kept constant so that the applied ΔK increased as the crack extended. One test was carried out in air (M02-01), where the initial value of ΔK was approximately 10 $MPam^{0.5}$, and at the end of the test the applied ΔK had increased to approximately 29 $MPam^{0.5}$. One test was also carried out in a sour environment (M02-02),

where the initial value of ΔK was approximately 8 $MPam^{0.5}$, and at the end of the test the applied ΔK had increased to approximately 21 $MPam^{0.5}$.

2.3.2 DECREASING ΔK

Two tests were conducted in a sour environment, where the applied load range was continuously shed (maintaining constant stress ratio) to impose a decreasing ΔK gradient of -0.1 mm^{-1}. The use of load shedding to maintain a constant stress ratio is the standard decreasing ΔK test technique as described in ASTM E647 [18] and BS 12108 [19].
For the first of these tests (M02-03), the initial value of ΔK was approximately 25 $MPam^{0.5}$, and at the end of this test (a ~ 9.8 mm) the applied ΔK had decreased to approximately 12 $MPam^{0.5}$. For the second of these tests (M02-04), the initial value of ΔK was approximately 21 $MPam^{0.5}$, and at the end of this test (a ~ 11.1 mm) the applied ΔK had decreased to approximately 10 $MPam^{0.5}$.

2.3.3 CONSTANT ΔK

The applied load range was continuously shed (maintaining constant stress ratio) as the crack grew, to impose a constant value of ΔK. The initial value of ΔK in this instance was approximately 9 $MPam^{0.5}$. One of these tests was conducted in air (M02-05) and two in a sour environment (M02-06 and M02-07). These tests maintained a constant ΔK of 9 $MPam^{0.5}$ to within 15% in all cases.

2.4 ENVIRONMENTAL CONTROL

All tests, whether in air or a sour environment were carried out at 25 ^{o}C (±3 °C). For tests carried out in a sour environment the specimen was immersed in an aqueous solution of 5% sodium chloride and 0.4% sodium acetate, acidified to a pH of 3.5 (±0.1) using acetic acid. This solution was purged with nitrogen to remove oxygen (<20 ppb) and a test gas of 7% H_2S in N_2 was then introduced at 0.1 MPa. Following an initial fast purge (typically overnight but in all cases for at least 7 h) the gas flow was reduced, but was continuously passed through the test solution to maintain saturation, and cycling commenced. Solution pH and H_2S content were monitored at intervals during the test.

'Stopping off' lacquer was applied to all specimens tested in a sour environment, to protect the bulk of the specimen and instrumentation from the corrosive environment, and to minimise the extent of solution contamination. A 10 mm window was left uncoated on each side of the notch on all sides of the specimen to allow interaction between the environment, the local surface and the crack tip (Fig. 3).

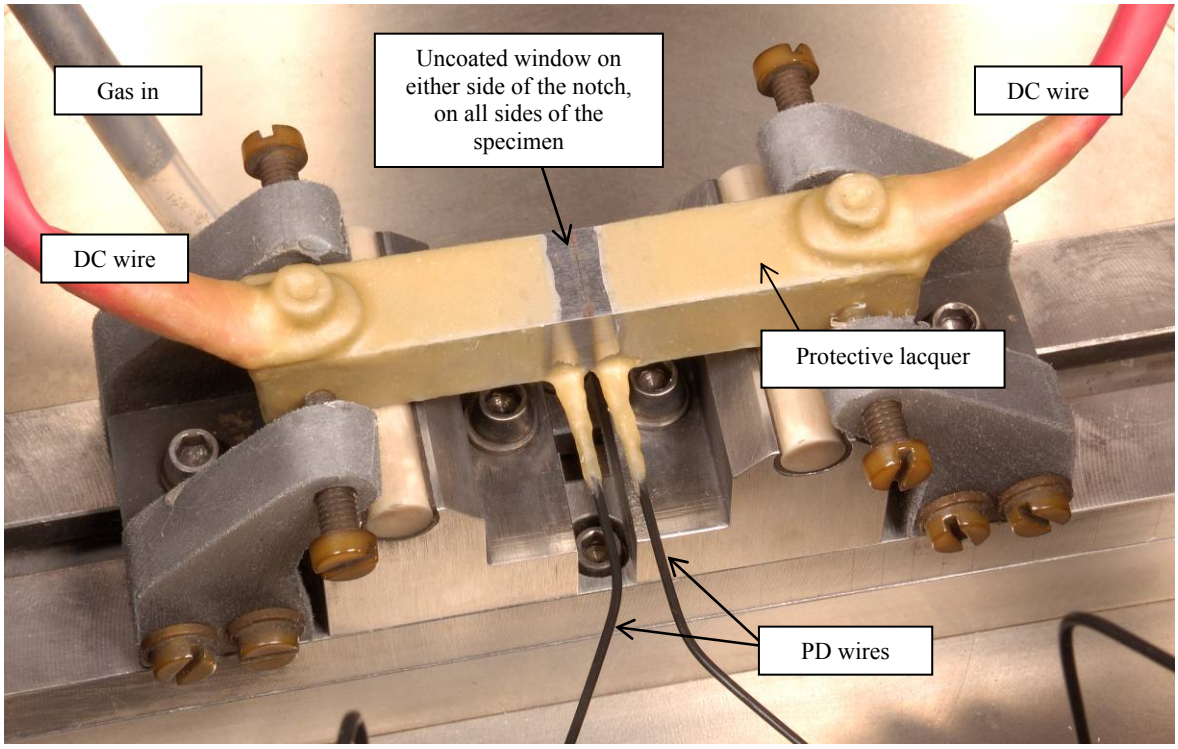

Fig. 3. Specimen mounted in crack growth rig, window left uncoated on each side of the notch on all sides of the specimen.

Upon completion of the tests in a sour environment, the test solution was purged with nitrogen and the specimen removed from the environmental chamber. Each specimen was then broken open after immersion in liquid nitrogen, and the fracture surface examined to determine the initial and final crack lengths based on a weighted nine point average, as described in BS 12108 [19]. Crack growth rates were then determined using an incremental secant method and a measurement interval of 0.2 mm.

3 RESULTS

3.1 CRACK GROWTH RATE DATA

Test data from the increasing ΔK and decreasing ΔK tests are illustrated in Fig. 4. For the increasing ΔK test carried out in air, the observed crack growth rates were similar to those in the mean curve for steels in air (R > 0.5) given in BS 7910 [20]. For the comparable test (increasing ΔK) carried out in a sour environment, crack growth rates were typically a factor of 30 higher than in air at high ΔK (>13 $MPam^{0.5}$), but this increased at lower ΔK (9-13 $MPam^{0.5}$).

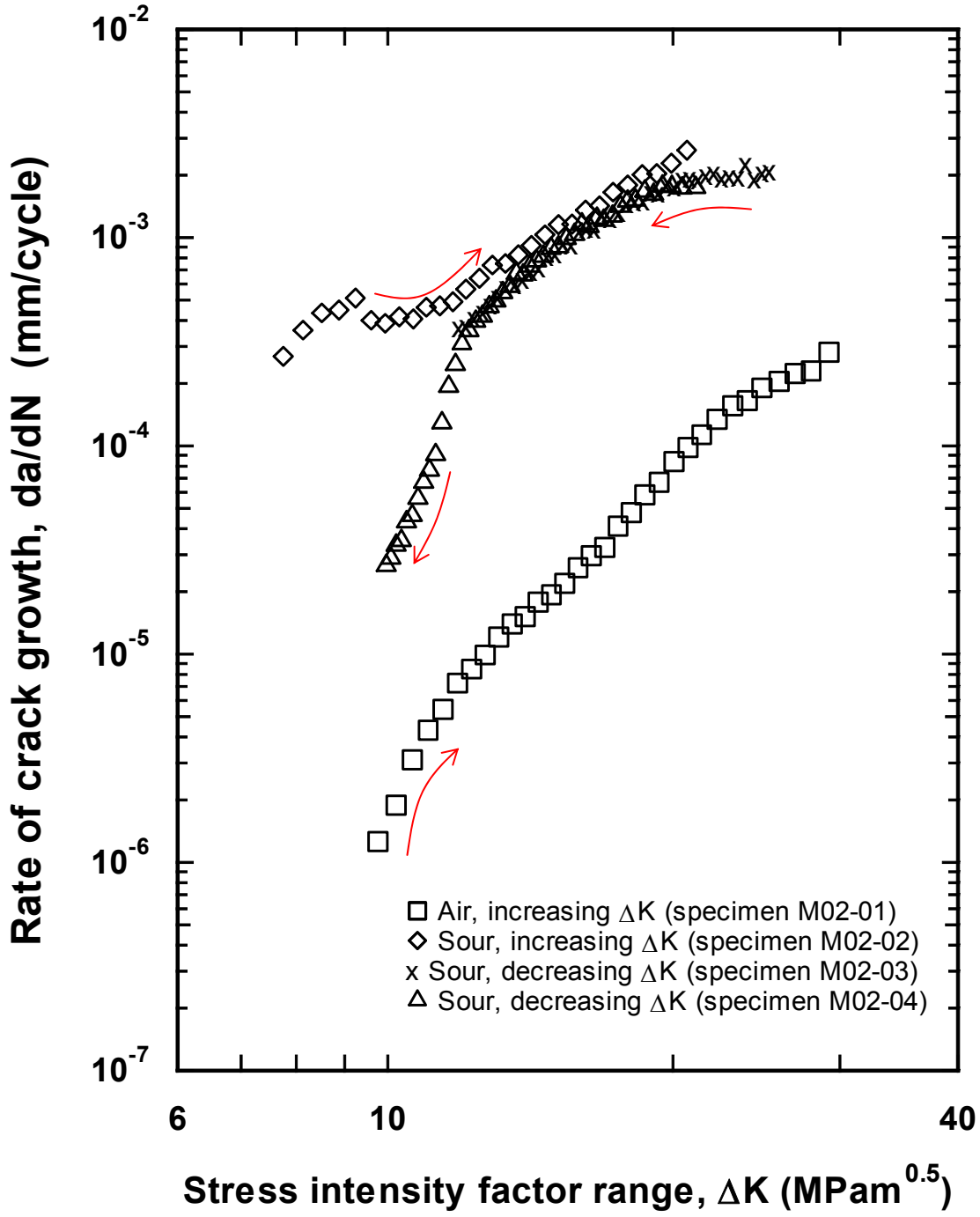

Fig. 4. Results of increasing and decreasing ΔK tests in a sour environment and in air. Arrows indicate increasing crack depth in each test.

For the decreasing ΔK tests (carried out in a sour environment), data from the two test specimens were very close where ΔK values overlapped. Crack growth rates at high ΔK (i.e. the beginning of the test) were similar to those seen in the increasing ΔK sour test (for a given ΔK). However, at lower ΔK (9-12 MPam$^{0.5}$) the crack growth rate seen in specimen M02-04, when the crack depth was between 8.4 mm and 11.1 mm, was significantly lower

than that seen under conditions of increasing ΔK (specimen M02-02) when the crack depth was between 2.7 mm and 4.1 mm. During this region of the test the crack growth rate decreased rapidly (more than an order of magnitude).

Test data from the constant ΔK tests are illustrated in Fig. 5. In the test carried out at constant ΔK in air, the observed crack growth rate remained approximately constant at 6 x 10^{-6} mmcycle^{-1}, (at least beyond ~2.5 mm). This is higher than that seen at the beginning of the increasing ΔK test (ΔK ~ 10 MPam$^{0.5}$) carried out in air, but very close to that expected from the mean curve for steels in air taken from BS 7910.

In the tests carried out at constant ΔK in a sour environment the crack growth rate was initially (a ~ 2-4 mm) a factor of between 30 and 130 times higher than in air, but fell to a factor of between 5 and 12 times higher than in air by the end (a ~ 6-10 mm) of the test. In these sour tests, there appeared to be three distinct regimes of behaviour as crack depth increased. For relatively shallow flaws (up to 3-4 mm) crack growth rates were approximately constant (although there was roughly a factor of three variation between the two tests). As crack depth increased to approximately 6 mm the crack growth rate decreased, by approximately an order of magnitude. For crack depths of greater than 6-7 mm, the crack growth rate remained constant for the rest of the test. It is also worth noting that the crack growth rates seen at the end of the test (2-8 x 10^{-5} mmcycle^{-1}) were comparable to those seen at the end of the decreasing ΔK sour test. The crack growth rates seen at the start of the test (2-8 x 10^{-4} mmcycle^{-1}) were also comparable to those seen at the beginning (a ~ 3 mm, ΔK ~ 10 MPam$^{0.5}$) of the increasing ΔK test.

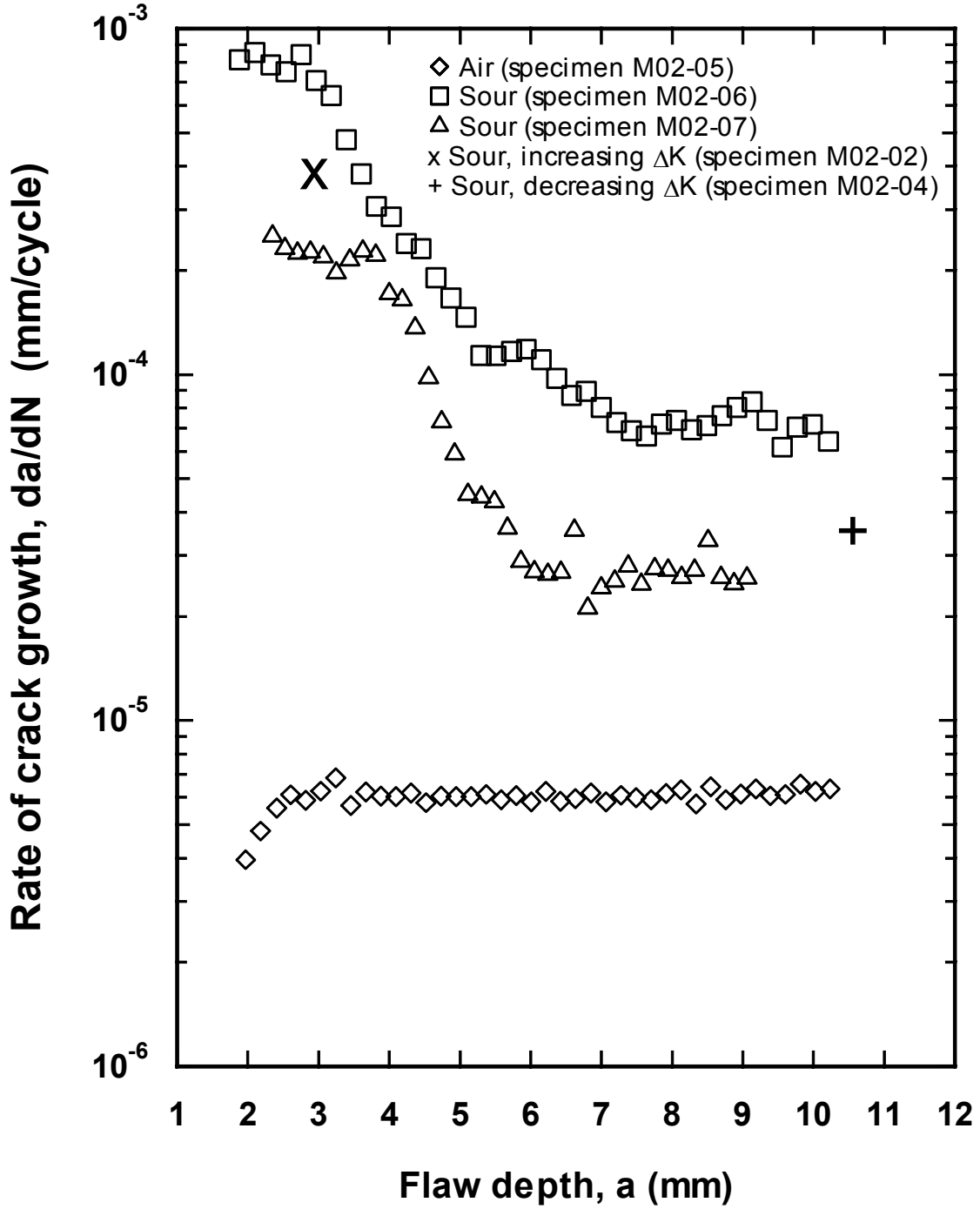

Fig. 5. Results of constant ΔK tests (~9 $MPam^{0.5}$) in a sour environment and in air. Also plotted for comparison are the crack growth rates from the beginning and end of an increasing ΔK and a decreasing ΔK test, respectively.

3.2 SPECIMEN FRACTOGRAPHY AND SECTIONING

Figs. 6-9 show one side of the fracture faces from specimens M02-01 (increasing ΔK in a sour environment), M02-03 and M02-04 (both decreasing ΔK in a sour environment), and M02-06 (constant ΔK in a sour environment). Specimens have been ultrasonically cleaned in

pyrene and the contrast on the images modified to emphasise the shape of the crack front. The crack fronts of all four specimens indicate to differing degrees that the final crack length at the end of the crack growth test was greater at the specimen edges than in the specimen centre. This is particularly pronounced in Fig. 8 (decreasing ΔK) and Fig. 9 (constant ΔK) due to the greater length of time spent in the test environment at low ΔK. For example, the test on specimen M02-03 (Fig. 7, decreasing ΔK), which exhibits a relatively straight crack front, was started at a ΔK of ~25 $MPam^{0.5}$. By the time this test had reached its specified upper crack depth limit the value of ΔK was approximately 12 $MPam^{0.5}$ and the test duration was less than 2 days. Specimen M02-04 (Fig. 8, decreasing ΔK) was therefore started at a lower value of ΔK (~20 $MPam^{0.5}$) in order to allow lower ΔK data to be generated. Specimen M02-04 was on test for more than 11 days, with 80% of this period being spent at low ΔK (<12 $MPam^{0.5}$) growing the final 2 mm of the specified target crack depth. Similarly, specimen M02-02 (Fig. 6, increasing ΔK) exhibits a relatively straight crack front having spent less than 3 days in the sour environment and very little time at low ΔK, while specimens M02-06 and M02-07 (Figs. 9 and 10, both constant ΔK) were on test for approximately 9 and 19 days, respectively, with the entire test at low ΔK and both fracture faces indicating higher crack growth rates at the specimen edges than in the specimen centre. In Fig. 8 the initial starter notch and fatigue pre-crack are most easily visible.

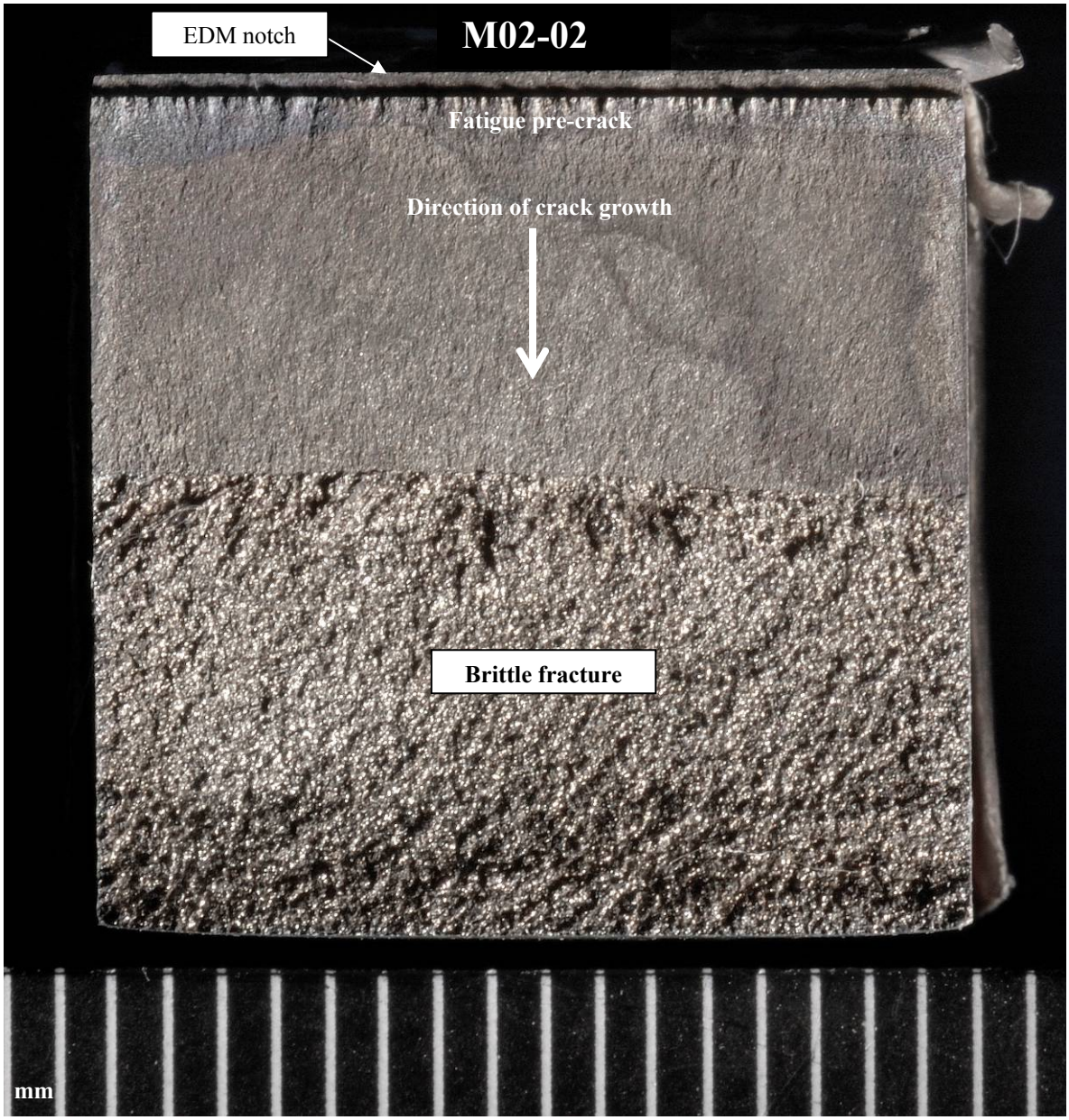

Fig. 6. Specimen M02-02 fracture face (increasing ΔK in a sour environment). Time spent in the sour environment: 67 h.

Fig. 7. Specimen M02-03 fracture face (decreasing ΔK in a sour environment). Time spent in the sour environment: 31 h.

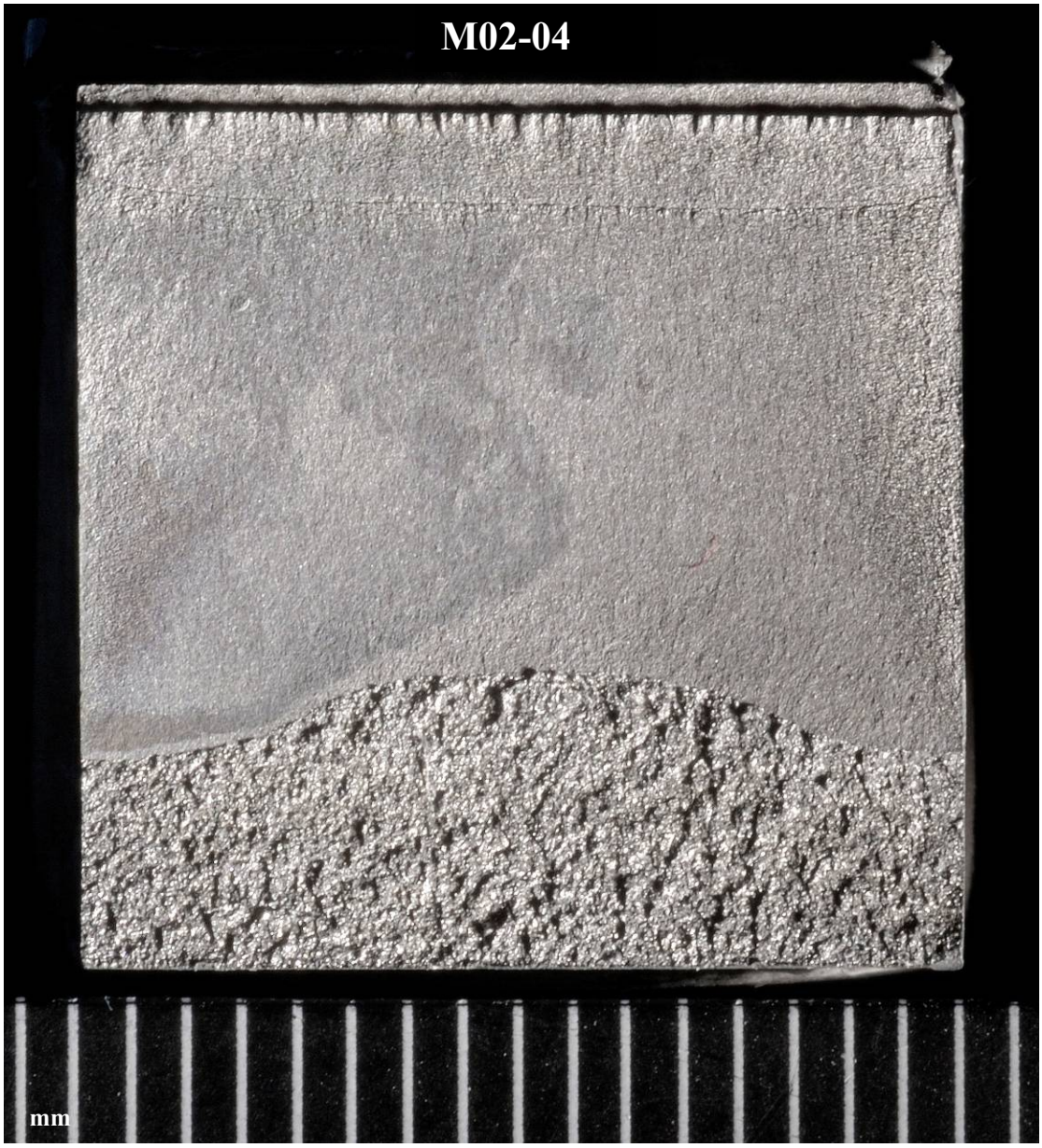

Fig. 8. Specimen M02-04 fracture face (decreasing ΔK in a sour environment). Time spent in the sour environment: 264 h.

Fig. 9. Specimen M02-06 fracture face (constant ΔK in a sour environment). Time spent in the sour environment: 216h.

Fig. 10 shows both sides of the fracture face of specimen M02-07 tested under constant ΔK conditions in a sour environment which was a repeat of the test on specimen M02-06. The right hand image illustrates how the specimen looked immediately after breaking open. The left hand image shows the specimen having been ultrasonically cleaned in pyrene ready for analysis under a scanning electron microscope (SEM). Also indicated in Fig. 10 are the locations for metallographic sectioning and the images shown in Figs. 11–13.

Closer examination of the fracture surfaces in a SEM revealed certain areas to be more pitted than others. For example, Fig. 11 shows the extent of pitting towards the beginning of the crack growth region, which had been exposed to the sour environment for a longer period than the end of the crack growth region. Only in the region close to the end of the crack growth region was it possible to observe what was likely to have been representative of the un-corroded fracture surface. In this region the fracture face morphology involved areas of

quasi-cleavage, as indicated in Fig. 12, which is consistent with hydrogen assisted crack growth in this type of material.

Metallographic sectioning, along the specimen centreline, also highlighted that the extent of pitting increased as the exposure time increased. At the beginning of the crack growth region (exposed to the corrosive environment for longest, after crack advance at the beginning of the test) pits were up to 50 µm deep and relatively broad whereas closer to the end of the crack growth region, pits were shallower and sharper, as illustrated in Fig. 13.

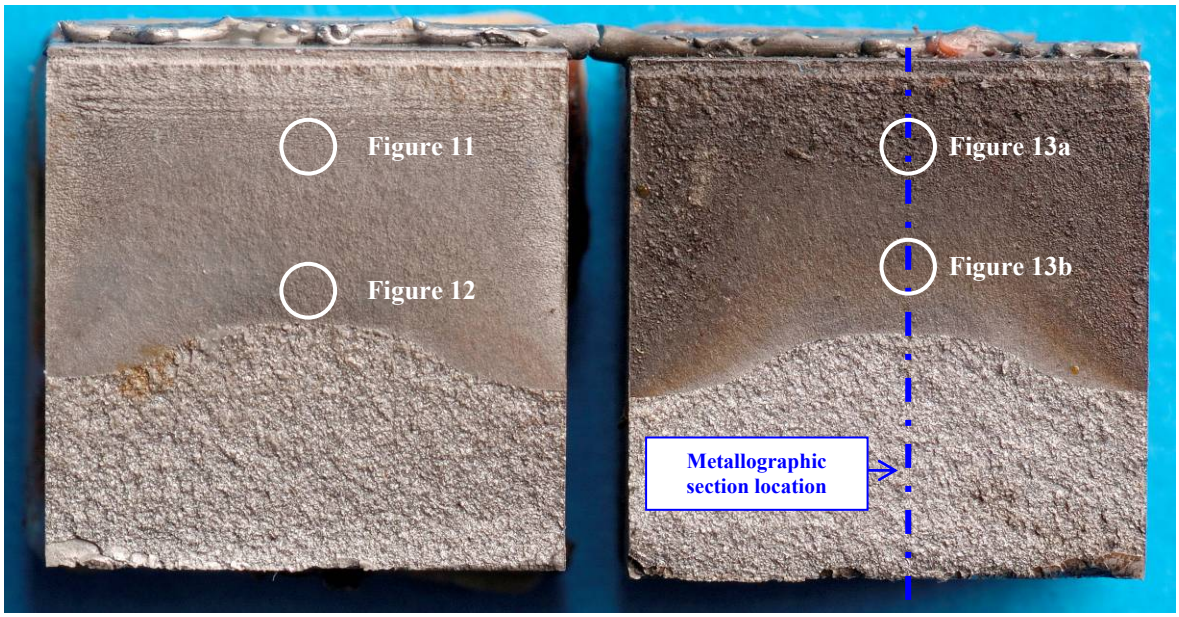

(a) (b)

Fig. 10. Both sides of the fracture face from specimens M02-07 (constant ΔK in a sour environment) having been ultrasonically cleaned in pyrene (a) and immediately after breaking open (b). Time spent in the sour environment: 462 h.

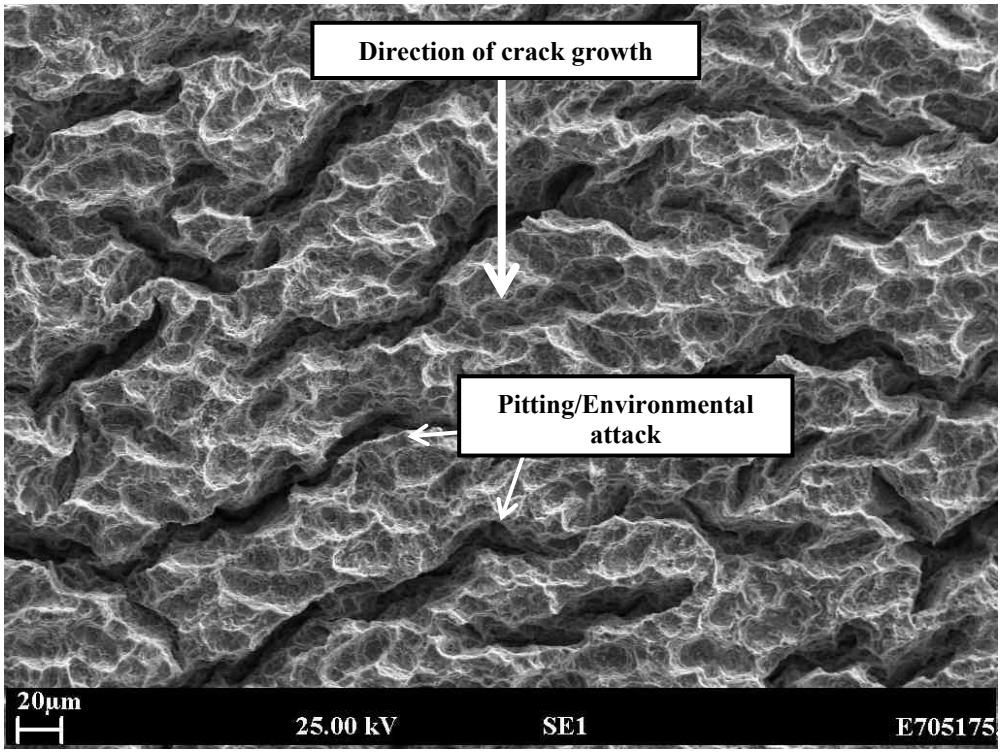

Fig. 11. Electron micrograph of environmental attach towards the beginning of the crack growth region of specimen M02-07, as indicated in Fig. 10.

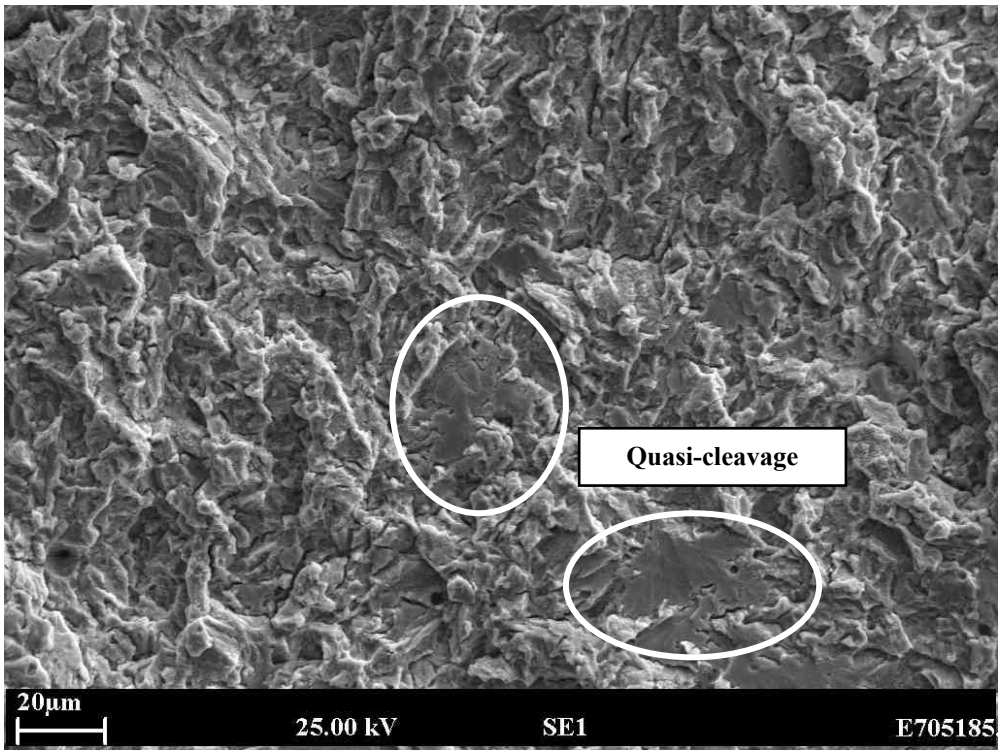

Fig. 12. Electron micrograph taken towards the end of the crack growth region of specimen. M02-07, as indicated in Fig. 10, showing areas of quasi-cleavage.

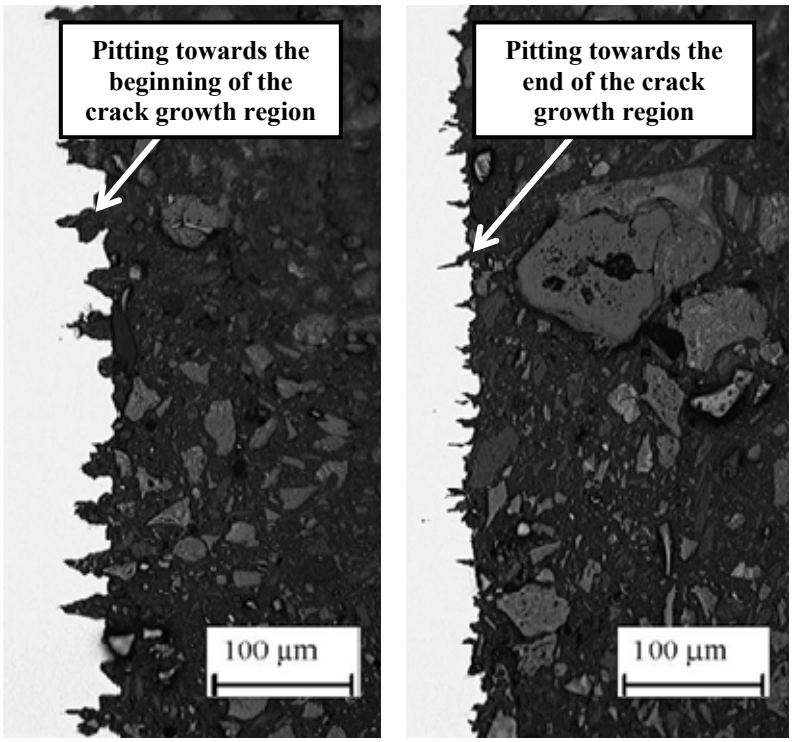

(a) (b)

Fig.13. Indicative cross-section images of environmental attach taken from the centre of specimen M02-07 fracture face, as indicated in Fig. 10. Broader, deeper pits are evident towards the beginning of the crack growth region (a) with sharper, shallower pits at the end of the crack growth region (b)

4 DISCUSSION

The aim of this work is to investigate the influence of crack depth on the observed crack growth rate in a sour environment. Test data from the decreasing ΔK tests are in broad agreement with other published data [6,7]. Crack growth rates at high ΔK are typically 30 times higher than in air. At lower ΔK (<13 $MPam^{0.5}$) the influence of the sour environment appeared to lessen and the crack growth rate approached that described by the mean curve for steels in air given in BS 7910 [20]. Under conditions of increasing ΔK the crack growth rate at high ΔK (>13 $MPam^{0.5}$) was similar to that seen under conditions of decreasing ΔK (for a given ΔK). However, at lower ΔK the crack growth rate data determined under conditions of increasing ΔK were noticeably higher than those determined under conditions of decreasing ΔK. At high ΔK there appears to be no influence of crack depth and crack growth rates are the same in each type of test. However, at low ΔK shallow cracks (increasing ΔK test) are seen to grow substantially faster than deeper flaws (decreasing ΔK test).

All constant ΔK tests were carried out at low ΔK and again a crack depth effect is observed. Crack growth rates at the start of the tests in a sour environment are 30-130 times higher than in air. This is similar to that observed in the corresponding part of the increasing ΔK test (a ~ 3 mm), as shown in Fig. 5. At the end of the tests crack growth rates are 5-12 times higher than in air, which is similar to that in the corresponding part of the decreasing ΔK test (a ~ 10 mm), also shown in Fig. 5. Therefore in the low ΔK regime there appears to be an influence of crack depth on the observed crack growth rate. This highlights the potential non-conservatism associated with using deep-crack data to predict the behaviour of shallow flaws. The results of the decreasing ΔK test in a sour environment also highlight the potential non-conservatism associated with generating design data from this type of test.

The constant ΔK data (Fig. 5) exhibit three distinct regions of behaviour as crack depth increases, similar to the trend reported by Nakai et al. [14]. The results presented in this paper appear to correspond to Regimes II-IV, most probably because the shallowest flaw tested was around 2 mm. Nakai et al. [14] tested specimens containing fatigue pre-cracks as shallow as 0.4 mm, therefore the results presented here possibly start towards the end of Regime II.

There are several possible mechanisms that might be influencing the observed material behaviour. The drop-off in crack growth rate at low ΔK in the decreasing ΔK tests may be because of an environmental crack depth effect as the deep crack (decreasing ΔK test) is growing much slower than the shallow crack at the start of the increasing ΔK test. A similar behaviour is observed in the tests carried out at constant ΔK. However, it is also possible that the observed influence of crack depth is the result of differences in the extent of crack closure. At low ΔK, crack closure may be more significant at the end of the decreasing ΔK test than at the beginning of the increasing ΔK test. This in itself may be attributable directly to the difference in crack depth, or to the progressive build-up of corrosion products during the test. In this respect, it is worth noting that the marked effect of crack depth seen at a ΔK value of 9 $MPam^{0.5}$ (as seen in the constant ΔK tests, and the appropriate portion of the increasing and decreasing ΔK tests) is not reproduced at higher ΔK (i.e. 19-22 $MPam^{0.5}$, within the same increasing and decreasing ΔK tests). Recalling the work by Pippan et al. [15] highlighted earlier, one would not expect closure effects to influence crack growth rates at a stress ratio of R = 0.5, regardless of the test method used, unless the environment causes a significant increase in crack opening force. All tests in the current programme were carried out at relatively high stress ratio (R = 0.5) to minimise any possible crack closure effect, and this is not believed to be the primary influence on material behaviour.

It is also worth noting that due to the relatively shallow flaws being examined, the value of K_{max} at the end of fatigue pre-cracking was relatively high in some instances, up to 19-24 $MPam^{0.5}$. For the increasing ΔK and constant ΔK tests, initial test conditions were slightly lower than this (16-19 $MPam^{0.5}$) so the initial crack growth data may have been influenced (retarded) by prior crack tip plasticity. This is evident in the air test data where crack growth rates were slightly lower than expected for the first 0.5-1.0 mm. However, for the majority of the data described in Figs. 4 and 5, differences in crack closure or prior fatigue pre-cracking are not believed to be the primary influence on material behaviour.

A more likely explanation for the observed increase in crack growth rates in the shallow crack regime is an environmental crack depth effect (i.e. a difference in crack tip chemistry leading to enhanced production and absorption of hydrogen for a shallow crack). Gangloff reported that shallow cracks grew faster than deeper flaws in 3% NaCl solution while corresponding tests in air gave similar crack growth rates [13]. The difference in crack growth rate was therefore attributed to a difference in the crack tip environment, in particular pH, leading to enhanced hydrogen production and uptake in the case of shallow cracks. The data described in Fig. 5 again illustrate that in air, crack growth rates are independent of crack depth, whereas in a sour environment crack growth rates increase by up to an order of magnitude in the shallow crack regime. However, it is also possible that bulk hydrogen charging (i.e. the uptake of hydrogen at specimen surfaces exposed to the sour environment) is influencing material behaviour. Under these circumstances, one would expect a higher crack growth rate for a shallow flaw (at the start of a test) compared to a deeper flaw where crack growth will be occurring through material containing less absorbed hydrogen, due to an increased average distance from the nearest exposed surface. One would also expect a higher

crack growth rate at the edge of the specimen than along the specimen centreline; this is clearly evident in Figs. 8-10.

The relative importance of crack tip charging and bulk charging has been investigated by Turnbull and Saenz de Santa Maria [21]. These authors examined the corrosion fatigue cracking of structural steel in cathodically protected seawater where the applied potential, loading frequency and bulk environment can all influence material behaviour and the relative importance of crack tip versus bulk charging. This work concluded that bulk charging was the main source of hydrogen for cathodically protected steel in a salt water environment (at a potential more negative than about 900 mV SCE and a loading frequency of 0.1 Hz). However, in a separate study Gangloff and Turnbull [22] reported no preferential crack growth near the external surfaces of the specimens when they tested 4130 steel in 3% NaCl, and in this case crack tip hydrogen production was believed to be the dominant source of hydrogen atoms.

Although both of these studies focussed predominantly on steel in marine environments, the relative importance of bulk versus crack tip hydrogen charging has also been examined for wet H_2S containing environments. Kobayashi and Takeshi [23] examined the influence of specimen thickness and test duration on the observed value of K_{ISCC} for a steel exposed to sour NACE solution, and concluded that hydrogen absorption inside the crack was negligible compared with that from external surfaces. The shape of the crack fronts shown in Figs. 8–10 also indicates that crack growth rates are higher near the edges (uncoated) of the specimen, and this may again be indicative of the influence of bulk hydrogen charging. If hydrogen absorption was dominated by crack tip charging one would expect to see the same crack growth rate at the centre of the specimen as at the specimen edges and therefore a straight crack front at the end of the test. Kobayashi and Takeshi [23] observed a similar crack front shape, and similar observations have been reported by Barsom [24], this time in relation to steel in a salt water environment. Under conditions where bulk hydrogen charging is dominant it is important to ensure that testing procedures include an adequate ‘pre-soak’ to maximise the environmental effect. For example Griffiths et al. [25] pre-charged a specimen for 147 days prior to testing and observed a significant increase in crack growth rate. In the case of a pipeline steel in a sour environment, however, a longer pre-soak period will not necessarily correspond to a higher concentration of hydrogen in the bulk material due to the build-up of an iron sulphide scale on the surface of the steel as a by-product of the corrosion process. The diffusion and transport of hydrogen in pipeline steel specimens tested in a sour environment is the subject of ongoing research at TWI.

In the current work (for a pipeline steel in a sour environment), hydrogen charging is likely to be dominated by absorption from external surfaces (rather than the crack tip). It therefore seems likely that the observed crack depth dependence is attributable to bulk charging. Shallower flaws, by their nature, are located within material that is more likely to have absorbed a high amount of hydrogen. The test data (and the observed crack front shape) suggest that the concentration of hydrogen at the centre of the specimen may be lower than at the edges, so deeper flaws have a tendency to grow at a lower rate.

Irrespective of the mechanism involved it is important to emphasise the potential non-conservatism associated with using test data derived under conditions of decreasing ΔK. In particular the use of low ΔK data determined in this way (by which time the crack is relatively deep), may be non-conservative if it is used to predict the behaviour of a much shallower flaw. Although it is easier to generate low ΔK test data under conditions of

decreasing ΔK, it has been shown here that it is possible to generate such data under conditions of increasing ΔK. In other work [15] specimens containing pre-cracks produced in compression have been used to facilitate the generation of data under increasing ΔK conditions. A number of authors have indicated that the influence of a sour environment is more noticeable at high ΔK than at low ΔK [6-12]. As precise test conditions are not always reported, it is not possible to say whether this is genuinely the case, or whether this is an artefact of testing under conditions of decreasing ΔK.

5 CONCLUSIONS

The influence of crack depth on crack growth rate in a sour environment has been investigated. Increasing, decreasing and constant ΔK tests in a sour environment have resulted in higher FCGRs than in air. The results of the three different types of crack growth test correspond reasonably well for deep flaws (greater than 6 mm) with crack growth rates increasing by a factor of 5-30 compared to in air. There is also reasonable correlation with available published data. At low ΔK crack growth rates determined under conditions of decreasing ΔK (sour) appear to be lower than those determined under conditions of increasing ΔK. Constant ΔK tests (carried out at low ΔK) suggest that this is due to an influence of crack depth. Shallow cracks have been shown to grow more than two orders of magnitude faster in a sour environment than in air at the same ΔK. Similarly shallow cracks in a sour environment have been shown to grow up to an order of magnitude faster than deep cracks in a sour environment at the same value of ΔK. One possible explanation for the increased crack growth rate is an environmental crack depth effect (i.e. a difference in crack tip pH and corresponding difference in the generation and absorption of hydrogen). However, it is likely that in this instance the observed behaviour is associated with bulk hydrogen charging (i.e. the uptake of hydrogen at specimen surfaces exposed to the sour environment). Under these circumstances, shallow flaws may grow more quickly than deeper flaws due to the lower concentration of hydrogen developed at the centre of the specimen. Further tests are required to confirm the mechanism responsible for the apparent crack depth dependence, and to establish appropriate testing procedures to ensure that experimental test data are appropriately conservative. It is clear that there is a potential non-conservatism associated with generating crack growth rate data under conditions of decreasing ΔK, where deep crack (low ΔK) data may be used to predict the early stages of crack growth for a much shallower flaw. It is therefore suggested that increasing ΔK tests (using shallow initial flaws) should ideally be used when generating crack growth rate data whenever possible.

6 REFERENCES

[1] Buitrago J, Weir MS. Experimental fatigue evaluation of deepwater risers in mild sour service. In: Deep offshore technology conference, New Orleans, USA; 2002.

[2] McMaster F. Thompson H. Zhang M. Walters O. Bowman J. Sour service corrosion fatigue testing of flowline welds. In: OMAE2007-29060. Proceedings of OMAE2007 26th international conference on offshore mechanics and Arctic engineering. San Diego, California. USA; 2007.

[3] Buitrago J. Baxter O. Hudak S. High-cycle and low-cycle fatigue resistance of girth welds in sour service. In: OMAE2008-57545. Proceedings of 27th international conference on offshore mechanics and Arctic engineering. Estoril. Portugal: 2008.

[4] McMaster F, Bowman J. Thompson 14. Zhang M, Kinyon S. Sour service corrosion fatigue testing of flowline and riser welds. In: OMAE 2008-57059.Proceedings of 27th international conference on offshore mechanics and Arctic engineering. Estoril. Portugal: 2008.

[5] Baxter OP. Maddox SJ. Pargeter RJ. corrosion fatigue behaviour of welded risers and pipelines. In: OMAE2007-29360 Proceedings of OMAE2007 26th international conference on offshore mechanics and Arctic engineering. San Diego. California, USA: 2007.

[6] Bristoll P. Roeleveld J. Fatigue of offshore structures: effect of seawater on crack propagation in structural steel. In: Proceedings of conference on European offshore steels research. ECSC: 1978.

[7] Webster SE, Austen IM. Rudd W. Fatigue, corrosion fatigue and stress corrosion of steels for offshore structures. ECSC report no. EUR 9460, Brussels: ECSC Steel Publications. European Commission: 1985.

[8] Vosikovsky O, Rivard A. The effect of hydrogen sulphide in crude oil on fatigue crack growth in a pipeline steel, corrosion 1982;38(1):19–22.

[9] Vosikovsky O. Macecek M. Ross DJ. Allowable defect sizes in a sour crude oil pipeline for corrosion fatigue conditions. Intl J Press vessels Piping1983:13;197–226.

[10] Watanabe E. Yajima H, Ebara R. Matsumoto 5, Nakano Y, Sugie E. Corrosion fatigue strength of ship structural steel plates and their welded joints in sour crude oil. In: Offshore mechanics and Arctic engineering conference (OMAE1994), ASME. vol. III. 1998. p. 151–8.

[11] Eadie RC. Szklarz KE. Fatigue crack propagation and fracture in sour dilute brine. In: Proceedings of corrosion 99, NACE international. Houston, TX: 1999 [paper no. 611].

[12] Eadie RC. Szklarz KE. Fatigue initiation and crack closure of low alloy steels in sour brine environments, In: Proceedings of corrosion 99. NACE international, Houston. TX: 1999 [paper no, 610].

[13] Gangloff RP. Crack size effects on the chemical driving force for aqueous corrosion fatigue. Metal Trans A 1985:1 6A:953–69.

[14] Nakai Y, Tanaka K. Wei RP. Short-crack growth in corrosion fatigue for a high strength steel. Eng Frau Mech 1986:24(3):433–44,

[15] Pippan R, Stuwe HP. Gobs K. A comparison of different methods to determine the threshold of fatigue crack propagation. Int J Fatigue 1994:16(8):579–82.

[16] Holtam CM. Baxter DP. Environment assisted cracking assessment methods: the behaviour of shallow cracks. In: Ninth international conference on engineering structural integrity: research, development and application. China Machine Press: 2007.

[17] Murtaza G,. Akid R. Modelling short fatigue crack growth in a heat-treated low alloy steel. Int J Fatigue 1995:17(3):207–14.

[18] ASTM E647 Standard test method for measurement of fatigue crack growth rates. West Conshohocken PA): American Society for Testing of Materials: 2005.

[19] BS ISO 12108. Metallic materials fatigue testing — fatigue crack growth method, London: British Standards Institution: 2002.

[20] BS 7910. Guide to methods for assessing the acceptability of flaws in metallic structures. London: British Standards Institution: 2005.

[21] Turnbull A, Saenz de Santa Maria M. The relative importance of crack-tip charging and bulk charging in hydrogen-assisted cracking in aqueous solutions. In: Scott P. editor. Environment assisted fatigue.ECF7, London: Mechanical Engineering Publications: 1990, p. 145–53.

[22] Gangloff RP, Turnbull A, Crack electrochemistry modelling and fracture mechanics measurement of the hydrogen embrittlement threshold in steel. Metall Soc AIME Circ 1986:55—SI.

[23] Kobayashi JI. Takeshi V. Evaluation of resistance of steel plate to sulphide stress cracking in sour wet service. In: Rungta R. editor. Proceedings of conference on predictive capabilities in environmentally assisted cracking. New York: ASME: 1985. p. 223—34.

[24] Barsom JM. Mechanisms of corrosion fatigue below K_{ISCC}. Int J Fract Mech 1971:7:163–82.

[25] Griffiths AJ. Hutchings RB. Turnbull A. Validation of the role of bulk charging of hydrogen in the corrosion fatigue cracking of a low alloy steel. Scripta Metall et Mater 1993:29:623–6.

APPENDIX D

Holtam C M, Baxter D P, Ashcroft I A and Thomson R C, 2010: 'An investigation into fatigue crack growth test methods in a sour environment', International Journal of Offshore and Polar Engineering (IJOPE). *Paper in press.*

An Investigation into Fatigue Crack Growth Test Methods in a Sour Environment

C. M. Holtam
D. P. Baxter
Structural Integrity Technology Group
TWI Ltd
Cambridge
CB21 6AL
UK

I. A. Ashcroft
Wolfson School of Mechanical and Manufacturing Engineering
Loughborough University
Leicestershire
LE11 3TU
UK

R. C. Thomson
Department of Materials
Loughborough University
Leicestershire
LE11 3TU
UK

ABSTRACT

Steel catenary risers (SCR) are used in deepwater oil and gas developments to transfer produced fluids from the seabed to surface facilities. SCRs can be subject to fatigue loading from a variety of sources including wave and tidal motion, vortex induced vibration and operating loads. When the produced fluids are sour (ie contain water and H_2S) higher fatigue crack growth rates (FCGR) are expected and therefore shorter overall life compared to performance in air, as a result of sulphide stress cracking (SSC).

Successful design is critically dependent on the availability of appropriate experimental data to quantify the extent to which fatigue lives are reduced, and rates of fatigue crack growth are increased in a sour environment. The aim of this paper is to provide guidance on the current best practice methods for generating experimental FCGR data in a sour environment. Recent sour test data generated as part of this research is presented and the influence of a number of key variables is investigated including loading conditions, crack depth, specimen geometry, pre-soak and coating configuration.

KEY WORDS

Fatigue, sour service, sour testing, pipeline, shallow, steel, corrosion.

1 INTRODUCTION

Previously published data from fatigue tests carried out at TWI on X65 pipeline steel have shown that crack growth rates in a sour environment can be 100 times higher than in air (Holtam et al., 2008). Tests have also illustrated a possible crack depth dependence whereby shallower flaws (up to 4 mm) appear to grow faster than deeper flaws subject to the same value of stress intensity factor range (ΔK) (Fig. 1). In the test carried out in air (at a constant applied ΔK of ~300 $Nmm^{-3/2}$ and a stress ratio, R = 0.5) the observed crack growth rate remained approximately constant at 6 x 10^{-6} $mmcycle^{-1}$. This is very close to that expected from the mean curve for steels in air (R ≥ 0.5) taken from BS 7910 (2005). In the tests carried out under similar conditions in a sour environment, the crack growth rate was initially (flaw depth, a ~ 2-4 mm) a factor of between 30 and 130 times higher than in air, but fell to a factor of between 5 and 12 times higher than in air by the end (a ~ 6-10 mm) of the test. It is also worth noting that the crack growth rates seen at the end of the test (2-8 x 10^{-5} $mmcycle^{-1}$) are comparable to those seen at the end of a decreasing ΔK test (ΔK = 670 $Nmm^{-3/2}$ down to 315 $Nmm^{-3/2}$), and the crack growth rates seen at the start of the test (2-8 x 10^{-4} $mmcycle^{-1}$) are also comparable to those seen at the beginning of an increasing ΔK test (ΔK = 240 $Nmm^{-3/2}$ up to 650 $Nmm^{-3/2}$).

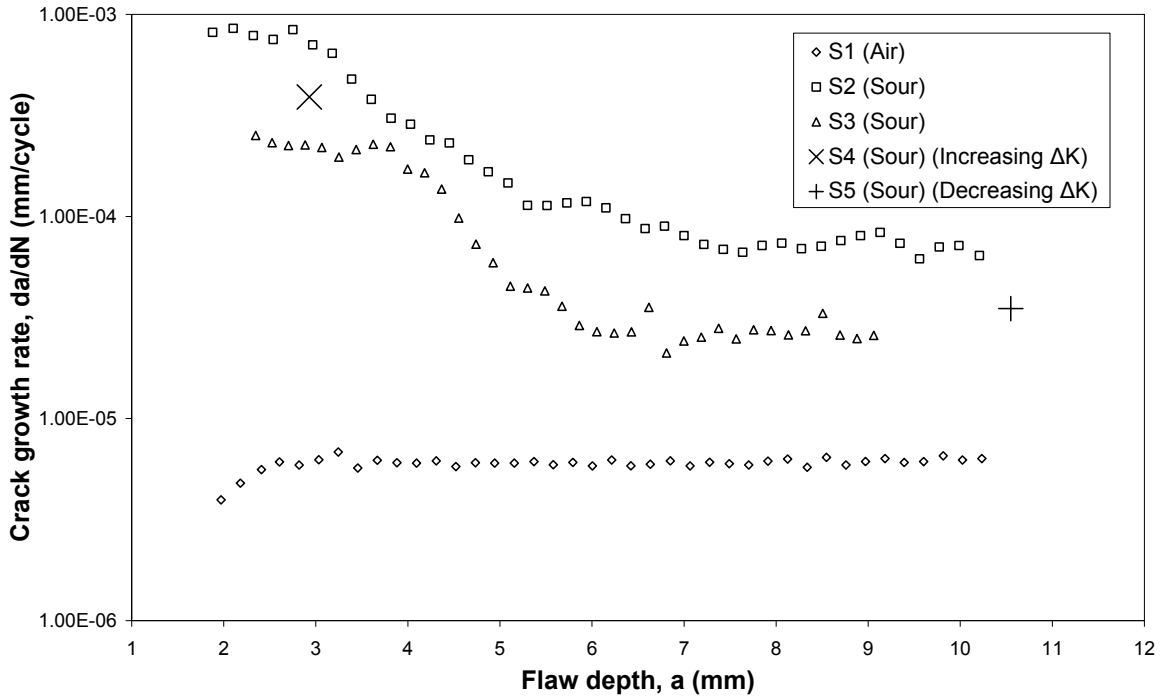

Fig. 1 Results of constant ΔK tests (~300 $Nmm^{-3/2}$) in a sour environment and in air. Also plotted for comparison are the crack growth rates from the beginning and end of an increasing ΔK and a decreasing ΔK test respectively (Holtam et al., 2008).

In these sour tests there appeared to be three distinct regimes of behaviour as crack depth increased. For relatively shallow flaws (up to 3-4 mm) crack growth rates were approximately constant (although there was roughly a factor of three variation between the two tests). As crack depth increased to approximately 6 mm the crack growth rate decreased, by approximately an order of magnitude. For crack depths of greater than 6 mm, the crack growth rate remained constant for the rest of the test. There are several possible explanations for this observed effect, for example a difference in crack tip chemistry, reduced crack

closure in the shallow crack regime, or an influence of bulk hydrogen charging on material behaviour close to the specimen surface.

Examination of the specimen fracture surfaces suggested higher fatigue crack growth rates (FCGR) at the specimen edges than at the specimen centre (Fig. 2). Together with the observation that crack growth rates were also higher when the entire crack front was close to the top face of the specimen, this may suggest that bulk hydrogen charging effects are dominating (ie hydrogen charging of the steel is dominated by absorption from the external surfaces of the specimen rather than at the crack tip, and a lower concentration of hydrogen exists in the centre of the specimen than at the specimen edges).

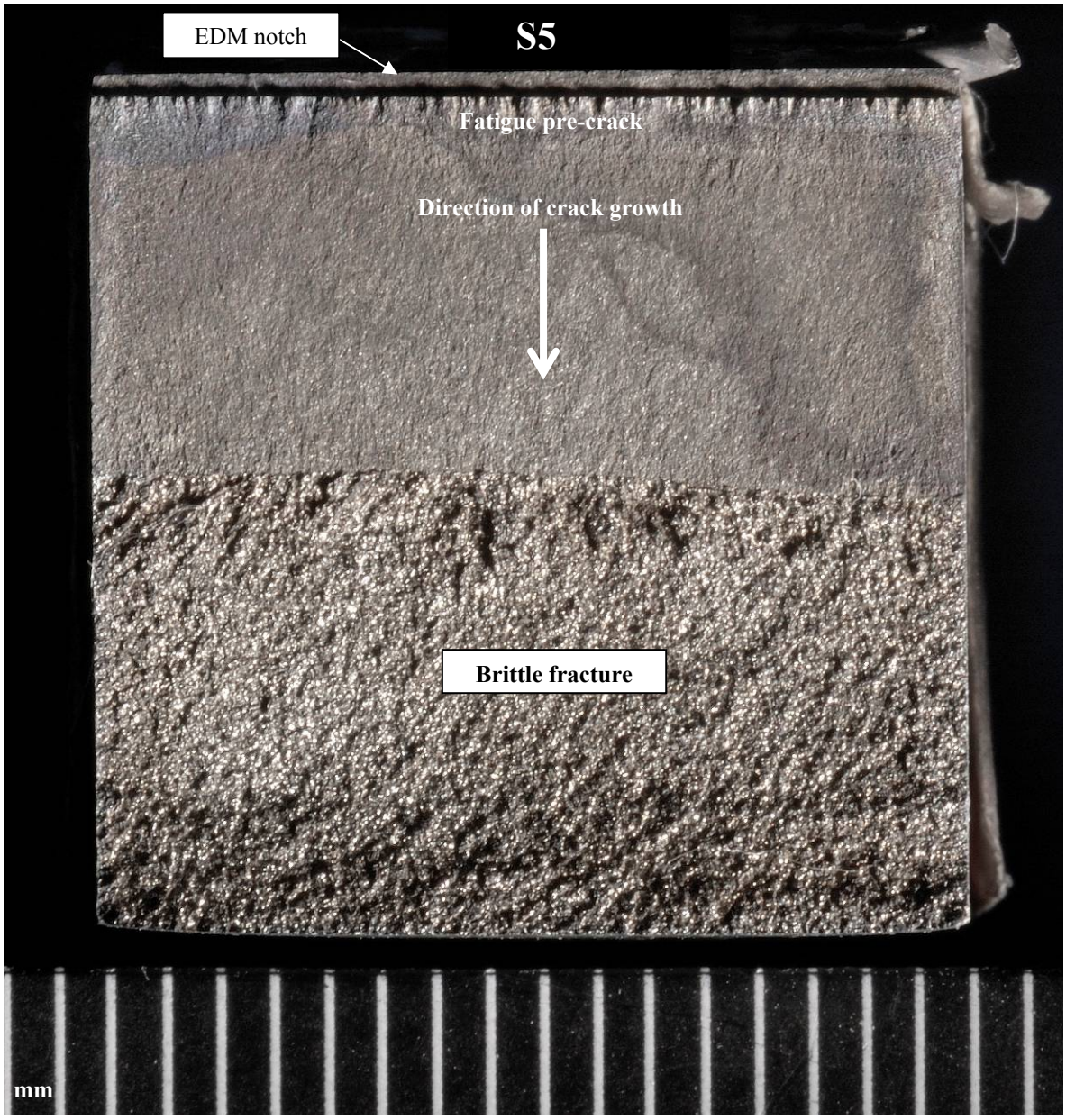

Fig. 2 Fracture face from a fatigue crack growth rate test carried out in a sour environment under conditions of decreasing ΔK.

However, neither crack closure effects nor differences in crack tip chemistry can be ruled out entirely. Crack closure effects could also result in an apparent dependence on crack depth,

due to a reduced level of closure for a shallow flaw, or due to the progressive build up of corrosion products within the crack during a test. Likewise differences in crack tip chemistry could also lead to a crack depth dependence due to enhanced production and absorption of hydrogen for a shallow crack due to a difference in crack tip pH.

The aim of this paper is to report the results of further FCGR tests carried out on X65 pipeline steel in a sour environment, investigating the influence of key variables such as loading conditions, crack depth, specimen geometry, pre-soak and coating configuration. The resulting test data provide a further insight into the mechanism responsible for the crack depth dependence, which is important to establish in order to ensure that test methods used are appropriately (but not overly) conservative.

The terms shallow and deep will be used throughout this paper to describe the through-thickness crack size. In other work, the terms short and long may be used, but there is scope for confusion as this may also refer to the lateral extent of a defect.

2 EXPERIMENTAL DETAILS

2.1 MATERIAL

The material used in the current work was a C-Mn X65 seamless API 5L parent material from a 14 inch (355.6 mm) diameter pipe of wall thickness 20.6 mm. The chemical composition of the steel, determined using optical emission spectrometry (OES), is summarised in Table 1. Hardness and tensile property data are shown in Table 2.

Table 1 Chemical composition of API 5L X65 C-Mn steel (wt.%) (TWI analysis reference no. S/05/255).

C	Si	Mn	P	S	Cr	Mo
0.11	0.28	1.12	0.010	0.003	0.082	0.11

Ni	B	Cu	Nb	Ti	V
0.099	0.0003	0.14	0.018	0.002	0.058

Table 2 Hardness and tensile property data for the X65 material used.

Hardness, HV10	196
UTS, MPa	576
0.2% proof stress, MPa	478

2.2 SPECIMEN GEOMETRY

Three different single edge notched bend (SENB) specimen geometries were used in the current test programme (Fig. 3), each tested in three point bending.

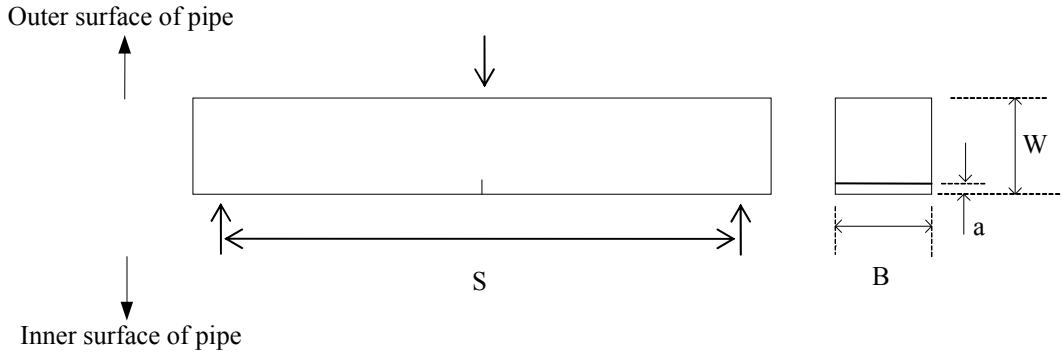

Fig. 3 Single edge notched bend specimen geometry.

The standard geometry was a square section with B = W = 16 mm, identical to that used in the previous tests reported in Fig. 1. However, to investigate the effects of bulk hydrogen charging two further geometries were used, one with B = 6 mm ('thin') and one with B = 32 mm ('wide'). In each case a standard span (S) of 64 mm (ie 4W) was used. Specimens were notched using electrical discharge machining (EDM) to introduce a starter notch approximately 0.5 mm deep. This notch was oriented circumferentially to simulate crack growth in the through thickness direction, from the internal surface of the pipe. This starter notch was then subjected to fatigue loading (R = 0.1, cyclic loading frequency up to 100 Hz) to provide a total fatigue pre-crack length of approximately 1.6 mm (based on surface measurements either side of the specimen).

2.3 FATIGUE TESTING

FCGR tests were carried out using a universal servo-hydraulic testing machine with computer control and data logging. Crack length was monitored using the direct current potential drop (DCPD) technique in which resolution is typically 10-20 μm for this material and the equipment used.

Tests were carried out using a stress ratio of 0.5, a loading frequency of 0.1 Hz and under conditions of constant ΔK. The applied load range was continuously shed as the crack grew, to impose a constant ΔK value of approximately 300 $Nmm^{-3/2}$. Post test analysis confirmed that the target value was successfully maintained to within 10% in all cases.

2.4 ENVIRONMENTAL CONTROL

All tests were carried out at 25°C (+/- 3°C). The sour environment was based on NACE TM0177 (2005) solution B. Specimens were immersed in an aqueous solution of 5% sodium chloride and 0.4% sodium acetate, acidified to a pH of approximately 3.5 using acetic acid. This solution was purged with nitrogen to remove oxygen (<20 ppb) and a test gas of 7% H_2S in N_2 was then introduced at 0.1 MPa. Following an initial fast purge (in all cases at least 7 hours) the gas flow was reduced, but was continuously passed through the test solution to maintain saturation. Solution pH and H_2S content were monitored at intervals during the test.

Upon completion of the tests, the test solution was purged with nitrogen and the specimen removed from the environmental chamber. Each specimen was broken open after immersion in liquid nitrogen, and the fracture surface examined to determine the initial and final crack lengths based on a weighted nine point average, as described in BS 12108 (2002). Crack growth rates were then determined using an incremental secant method and a measurement interval of 0.2 mm.

2.5 COATING CONFIGURATION

'Stopping off' lacquer was applied to all specimens tested in a sour environment, to protect the bulk of the specimen and instrumentation from the corrosive environment, and to minimise the extent of solution contamination. In the first three tests a 10 mm window was left uncoated on each side of the notch on all sides of the specimen (Fig. 4). This was the configuration used in the previous tests reported in Fig. 1. A further test was then carried out with the specimen completely coated on all sides, except for the notched surface (Fig. 5). A summary of all specimen geometries and test conditions is provided in Table 3.

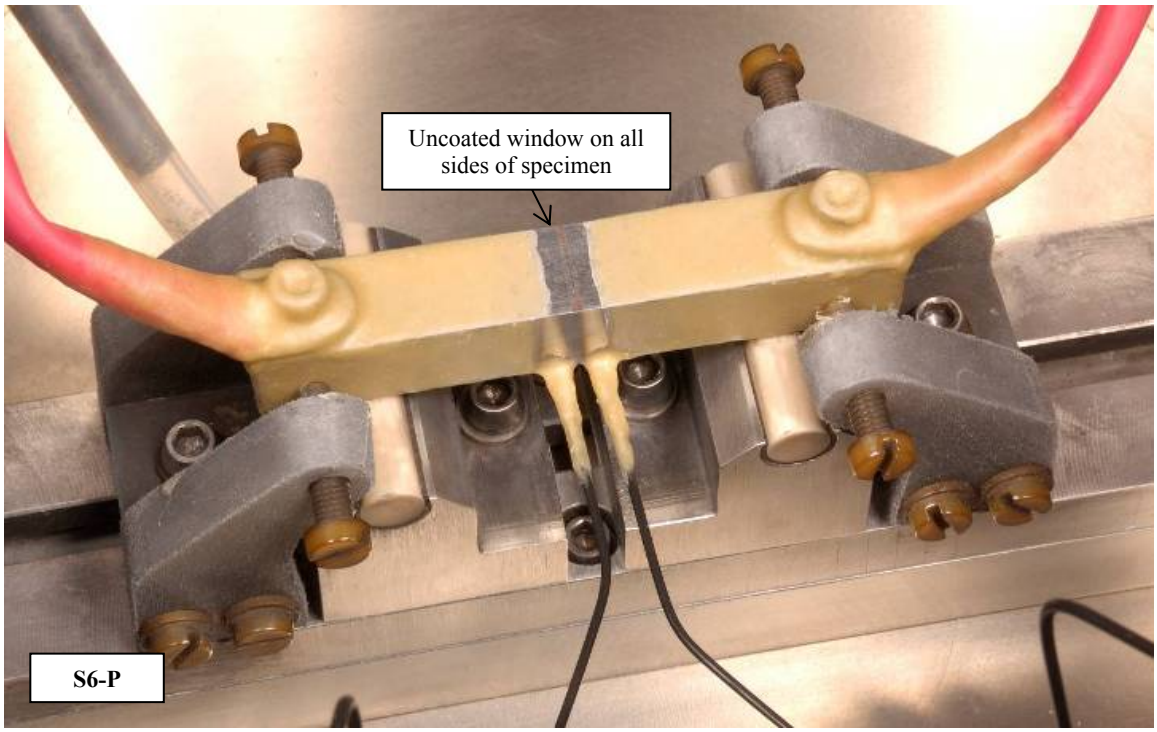

Fig. 4 Specimen (S6-P) mounted in crack growth rig, uncoated on each side of the notch on all sides of the specimen.

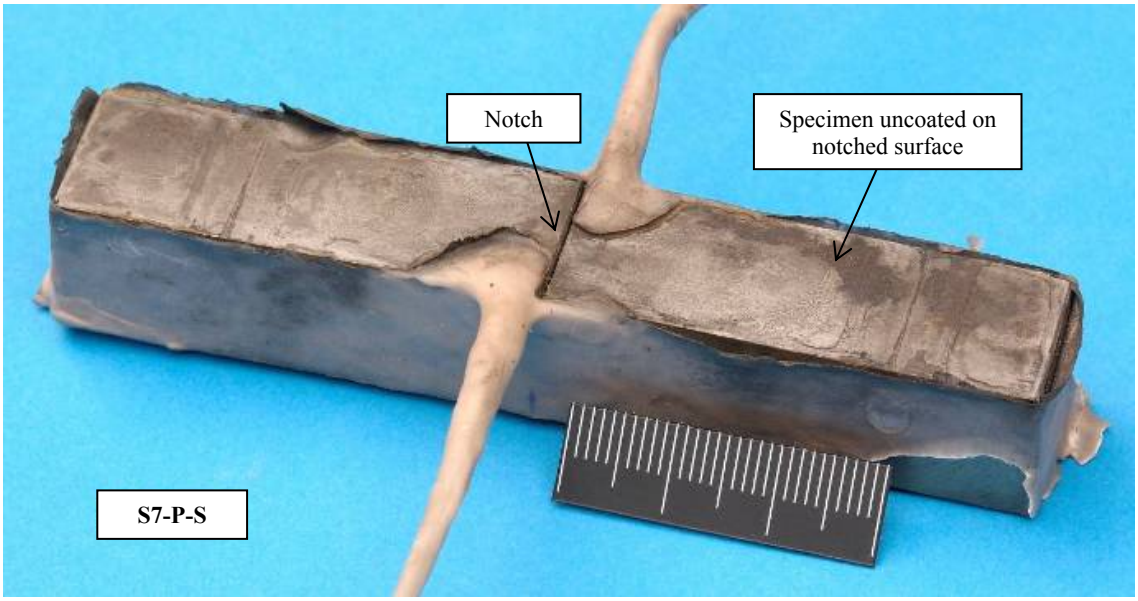

Fig. 5 Single-sided coating configuration (S7-P-S). (Photo taken upon completion of the test).

Table 3 Main testing parameters for sour fatigue crack growth rate tests.

Specimen ID	Specimen geometry	Coating configuration	One-week pre-soak? (Y/N)	ΔK, $Nmm^{-3/2}$	Stress ratio	Test frequency, Hz
T1	B = 6mm W = 16mm	Standard	N	300 (constant)	0.5	0.1
W1	B = 32mm W = 16mm	Standard	N	300 (constant)	0.5	0.1
S6-P	B = 16mm W = 16mm	Standard	Y	300 (constant)	0.5	0.1
S7-P-S	B = 16mm W = 16mm	Single-sided	Y	300 (constant)	0.5	0.1

3 RESULTS

3.1 FATIGUE TESTING

3.1.1 EFFECT OF SPECIMEN GEOMETRY

The results of the constant ΔK tests in a sour environment using the thin and wide specimen geometries are plotted in Fig. 6, alongside the comparable results from square section specimens reported in Fig. 1.

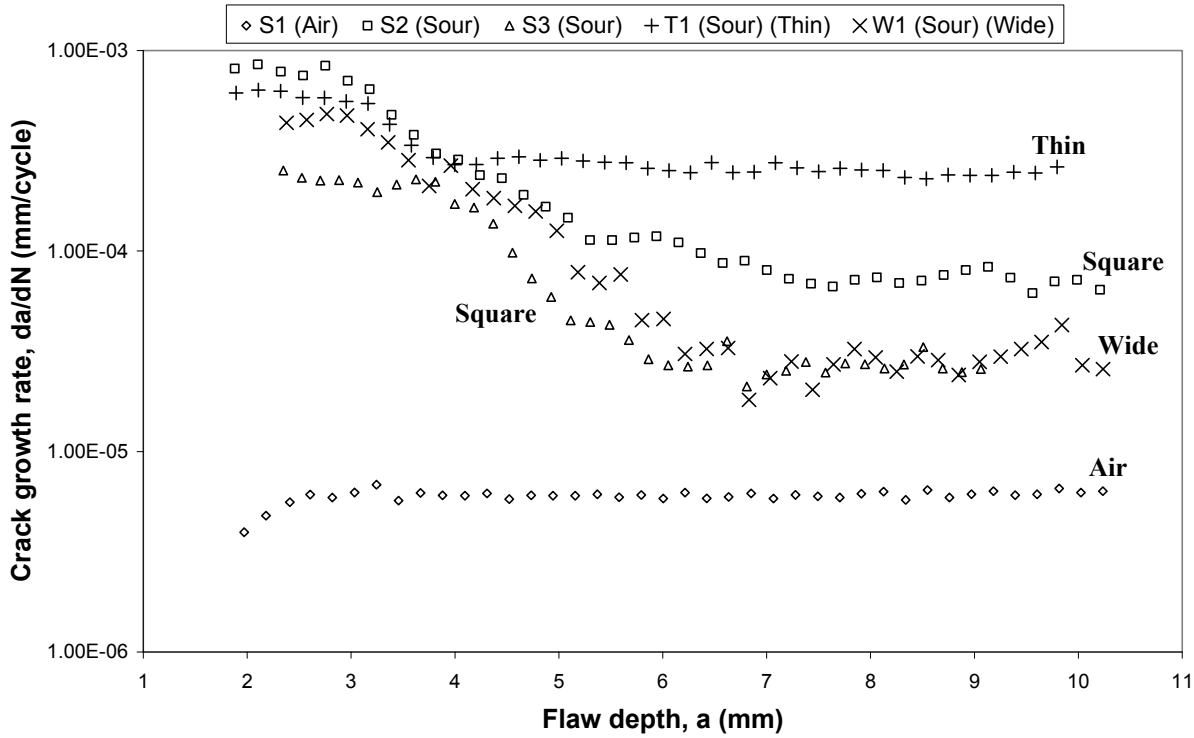

Fig. 6 Results of constant ΔK tests (~300 $Nmm^{-3/2}$) on thin and wide specimens in a sour environment, plotted alongside previous constant ΔK data in Fig. 1.

In the test carried out on the thin specimen the crack growth rate was initially a factor of 90 higher than in air, but fell to a factor of 40 times higher than in air by the end of the test. In the test carried out on the wide specimen the crack growth rate was initially a factor of 70 higher than in air, but fell to a factor of 5 higher than in air by the end of the test. In both

cases there still appeared to be three distinct regimes of behaviour as reported above (see Introduction). However, the thin specimen did not exhibit as marked a drop-off in crack growth rate for deeper flaws.

3.1.2 EFFECT OF PRE-SOAK AND SINGLE-SIDED EXPOSURE

The results of the constant ΔK tests in a sour environment on standard specimen geometries but with an additional pre-soak period, and single-sided exposure are plotted in Fig. 7. Also indicated in Fig. 7 is the shape of the crack front at the end of each test.

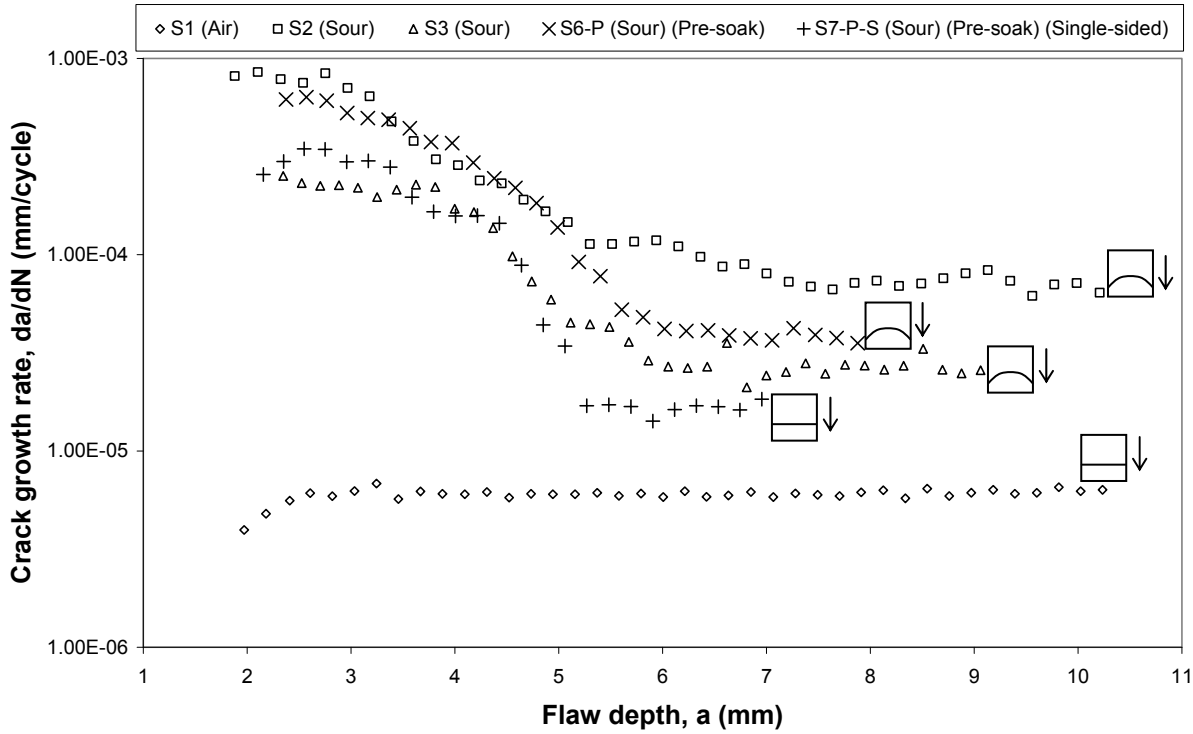

Fig. 7 Results of constant ΔK tests (~300 $Nmm^{-3/2}$) in a sour environment with additional pre-soak and different coating configurations plotted alongside previous constant ΔK data in Fig. 1.

Specimen S6-P, which was exposed on all sides but was subjected to a one week pre-soak prior to cycling commencing, initially had a crack growth rate that was a factor of 80 higher than in air, but this fell to a factor of 7 higher than in air by the end of the test.

Specimen S7-P-S which had single-sided exposure and was again subjected to a one week pre-soak prior to cycling commencing, was initially a factor of 40 higher than in air, but fell to a factor of 4 higher than in air by the end of the test. In both cases there still appeared to be three distinct regimes of behaviour as reported above (see Introduction), but for deep flaws (a > ~5-6 mm) specimen S7-P-S exhibited the lowest crack growth rates observed in any of the sour tests.

3.2 SPECIMEN FRACTOGRAPHY

Figs 8 to 11 show one side of the fracture face from specimens T1, W1, S6-P and S7-P-S respectively. Specimens have been ultrasonically cleaned in pyrene. The shape of the crack front on specimen T1 (Fig. 8) is essentially straight although the crack length at the specimen sides is slightly longer than at the centre of the specimen. Specimen W1 (Fig. 9) exhibits a similar shape crack front as that in Fig. 2, indicating that at the end of the test the crack length was greater at the specimen edges than in the specimen centre. This is also the case for pre-

soaked specimen S6-P (Fig. 10) that was exposed on all sides. However, the pre-soaked specimen S7-P-S, that had single-sided exposure, exhibited a straight crack front (Fig. 11); in fact the crack length was slightly shorter at the specimen edges, as was the case for the specimen tested in air.

Fig. 8 Fracture face from thin specimen T1 tested under constant ΔK conditions (~300 $Nmm^{-3/2}$).

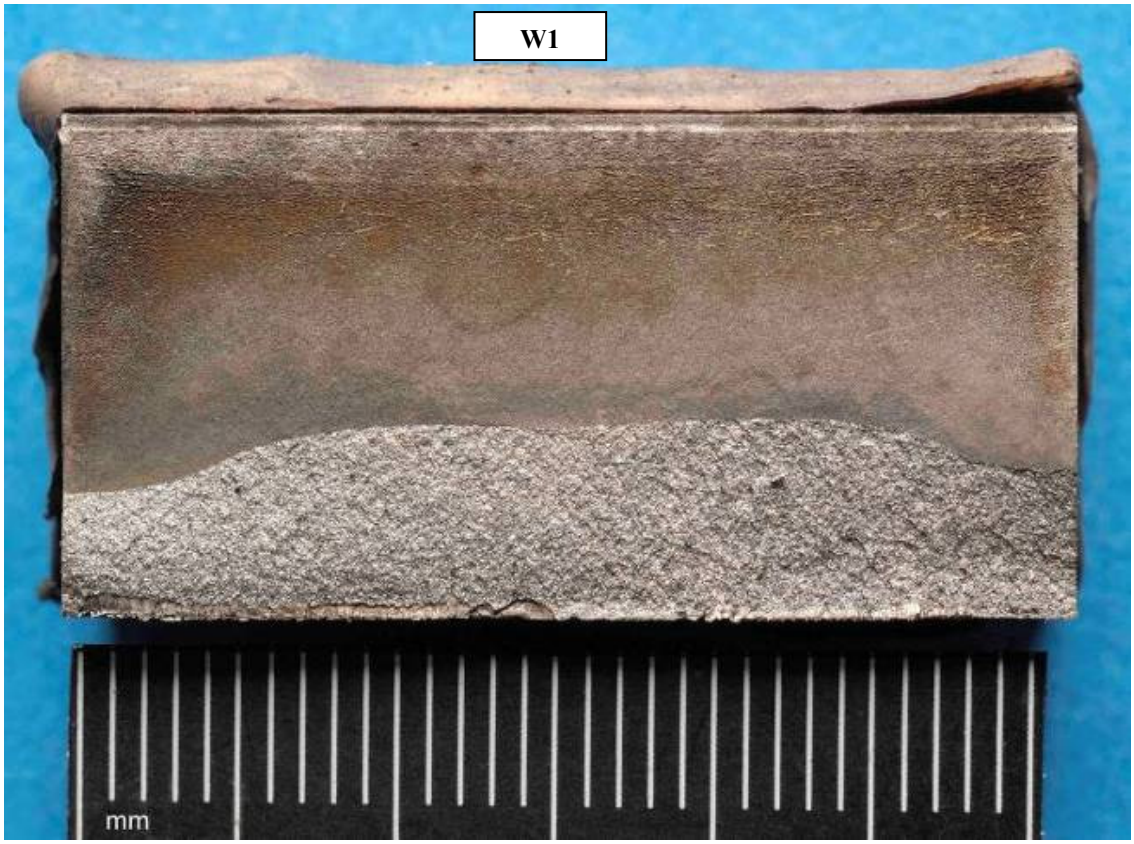

Fig. 9 Fracture face from wide specimen W1 tested under constant ΔK conditions (~300 $Nmm^{-3/2}$).

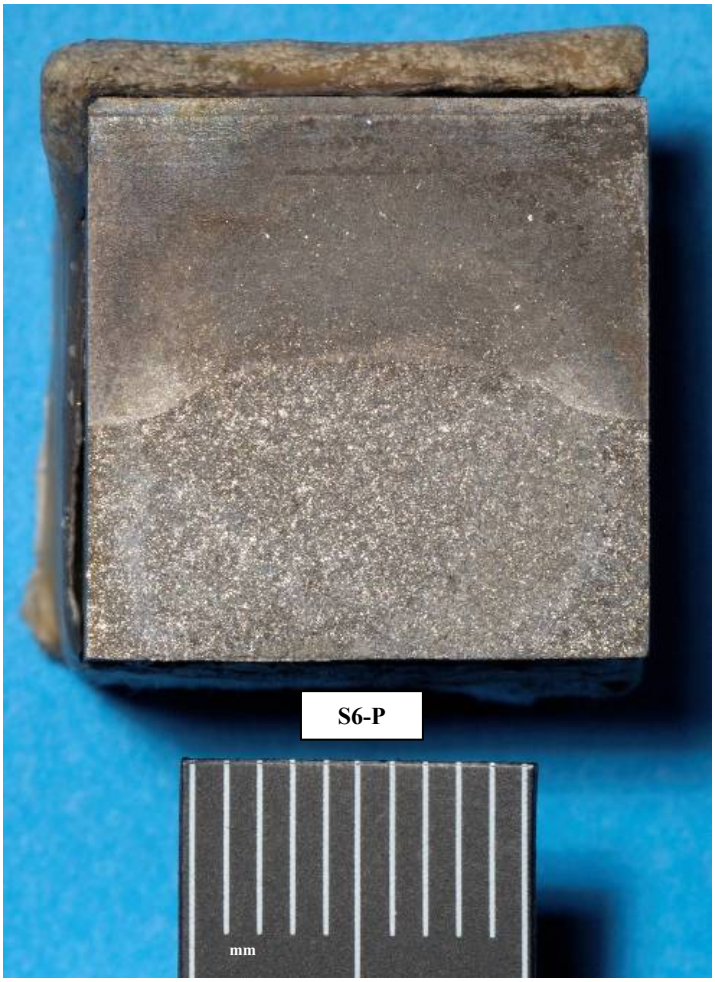

Fig. 10 Fracture face from specimen S6-P tested under constant ΔK conditions (~300 $Nmm^{-3/2}$), after a one week pre soak in the sour environment.

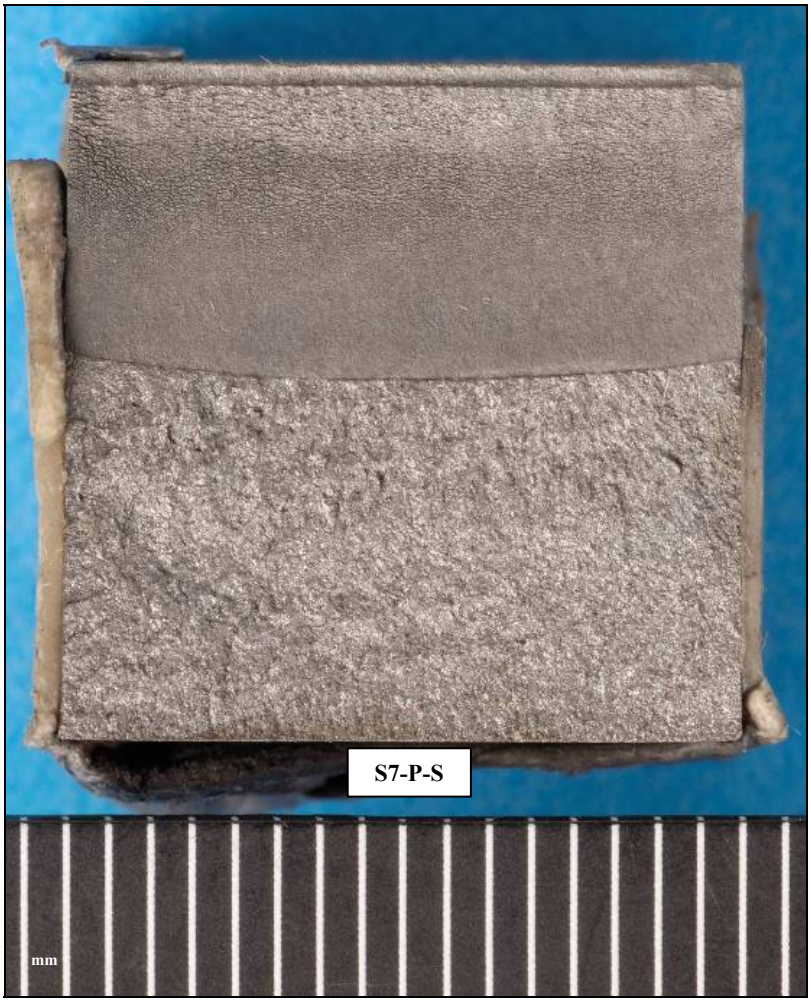

Fig. 11 Fracture face from specimen S7-P-S tested under constant ΔK conditions (~300 $Nmm^{-3/2}$) after a one week pre-soak in the sour environment and with single-sided exposure.

3.3 HYDROGEN ANALYSIS

Measurements of diffusible hydrogen content were carried out using two specimens immersed in a sour environment, but coated such that only one face was exposed (ie the same as specimen S7-P-S for example). Upon completion of each test the specimen was removed from the environmental test chamber and transferred into storage in liquid nitrogen.

The amount of diffusible hydrogen was determined using gas chromatography after heating at approximately 150^{o}C for six hours. One full thickness slice was taken from each specimen, and these were each cut into four sections, so that hydrogen content could be determined at different through thickness locations. Care was taken to ensure that specimen heating was minimised during the cutting procedure, by intermittent immersion in liquid nitrogen.

The results of the two separate hydrogen analyses are plotted in Fig. 12. A through-thickness variation in diffusible hydrogen content was observed in both specimens, with the highest concentration occurring closest to the exposed surface. Also stated in Fig. 12 is the test duration in each case, defined as the time from when the H_2S environment was introduced to when the test vessel was purged with nitrogen prior to the sample being removed.

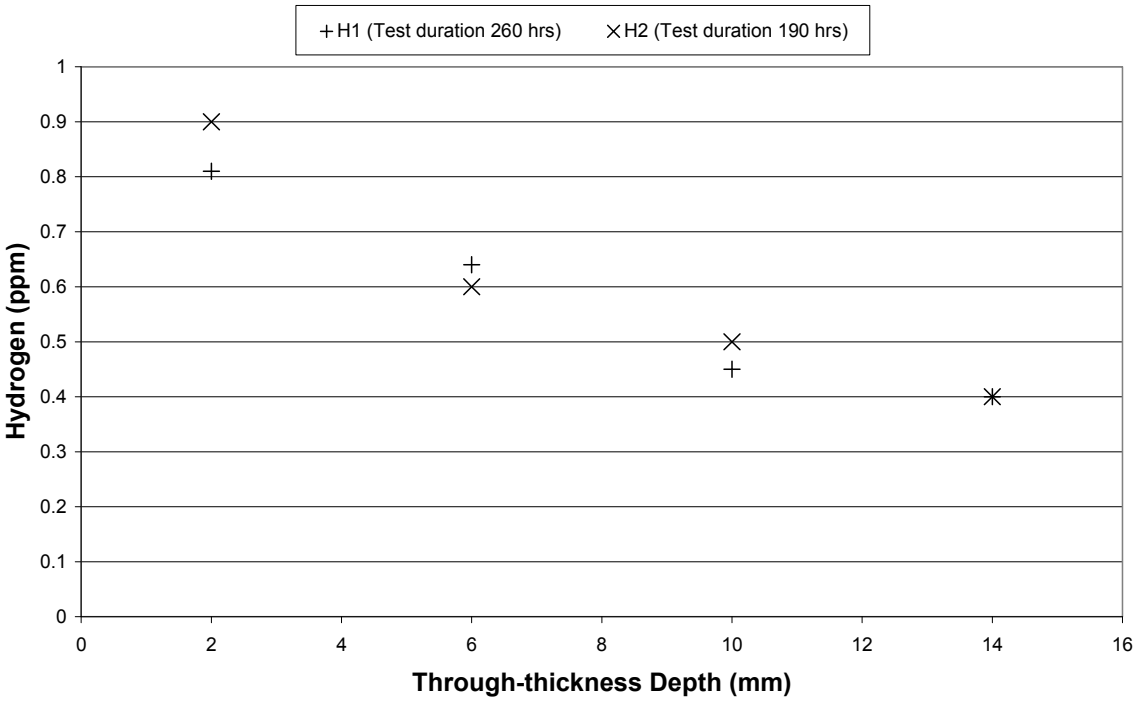

Fig. 12 Average hydrogen concentration versus through-thickness depth as measured on two fatigue crack growth rate specimens tested in a H_2S containing environment.

4 DISCUSSION

The test data in Fig. 1 illustrate that shallow flaws (up to 3-4 mm) can grow up to an order of magnitude faster than deeper flaws (>6 mm) subject to the same applied ΔK. As described above (see Introduction), the observed crack depth dependence could be attributable to bulk charging effects, differences in crack tip chemistry or crack closure. With respect to the latter, it has not been possible to obtain a direct measurement of the closure load due to the practical difficulties associated with instrumenting the test specimen while immersed in a sour environment. However, it is thought to be unlikely that crack closure is the dominant mechanism. All tests were carried out at relatively high stress ratio (R = 0.5) in an attempt to minimise possible closure effects (Pippan et al., 1994).

Considering the relative importance of bulk hydrogen charging and crack tip charging, it is clear that this will depend on the chemistry and pH developed at the crack tip. For marine environments it has been shown that crack tip hydrogen production can be dominant (Turnbull and Saenz de Santa Maria, 1990) (Gangloff and Turnbull, 1986). However, under sour service conditions, Kobayashi and Takeshi (1985) concluded that hydrogen absorption inside the crack was negligible compared to that from external surfaces. Kobayashi and Takeshi (1985) also observed similar crack front shapes to those in Fig. 2 for example (ie longer at the exposed edges). However, an accurate description of local crack tip reactions and transport phenomenon is acknowledged as being one of the key uncertainties when attempting to model environment assisted crack processes (Scully and Gangloff, 2002).

The test data in Fig. 6 indicate that in addition to shallow flaws growing quicker than deep flaws, crack growth rates in material close to an exposed surface are faster than in material far away from an exposed surface. The shape of the crack fronts illustrated in Figs 8-11 provides further support for the idea that bulk charging from exposed surfaces is influencing the observed behaviour. Under these circumstances it becomes necessary to consider the rate

at which hydrogen diffuses into the bulk material (with respect to both test specimens and real pipelines) to ensure that test conditions and associated data are appropriately conservative.

In the final two tests the specimen was subjected to a one week pre-soak in the sour environment prior to cycling commencing, to allow hydrogen to diffuse into the bulk material and therefore maximise the environmental effect. Hydrogen is expected to diffuse into the steel more rapidly to begin with and then slow down as iron sulphide scale builds up on the surface of the steel as a product of the sulphide corrosion process.

The diffusion of hydrogen out of metals can be described by a differential equation, similar to that used to describe heat flow in solids (Bailey et al., 2004). Russell (1936) provides solutions for the conduction of heat through different solid geometries, which have been applied by Bailey et al. (2004) to generate hydrogen evolution curves. For example, Fig. 13 shows a plot of hydrogen concentration remaining at the centre of an infinite plate (with thickness 2L) versus the dimensionless expression Dt/L^2, which accounts for time (t), diffusivity (D) for the material and temperature of interest and the critical dimension of the solid (L), which is half the thickness of the plate. The initial hydrogen level is not known but is defined as being 100%.

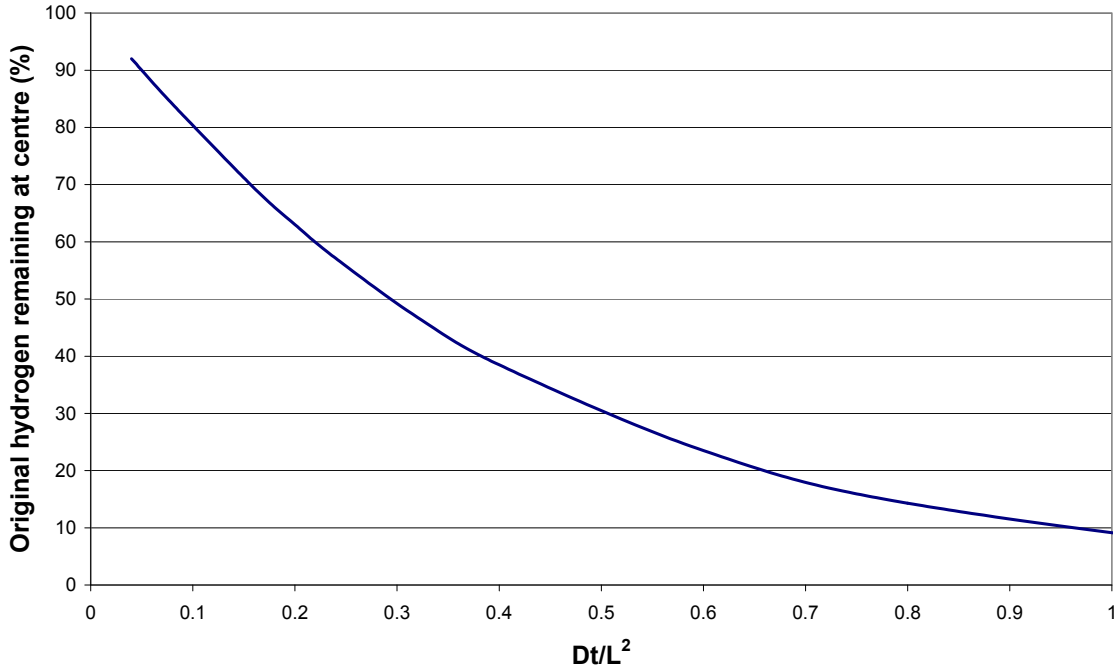

Fig. 13 Loss of hydrogen from infinite plate (thickness 2L) as a function of time, based on actual values of hydrogen remaining at various values of Dt/L^2 (Bailey et al., 2004).

The relationship in Fig. 13 can be used to estimate the time and temperature required to reduce the hydrogen concentration to a particular level. While the work of Bailey et al. (2004) refers to the diffusion of hydrogen out of a solid (after welding for example), the same logic can be applied to the diffusion of hydrogen into a solid. Again the initial hydrogen level at the surface of the steel is not known but is defined as being 100%. The model does not account for the build-up of scale on the surface of the steel, nor does it account for the fact that some of the hydrogen generated on the surface of the steel may not be absorbed into the steel but may evolve as molecular hydrogen.

An infinite plate (thickness 2L), as illustrated in Fig. 14 is an appropriate geometry to represent the case of a SENB specimen that is exposed to hydrogen on both sides. Assuming the standard square section specimen geometry used in the current work, L = 8 mm and one can generate a hydrogen removal curve, but use it to estimate the time taken for hydrogen to diffuse into the centre of the specimen (ie the removal curve shows the percentage difference between the surface of the steel and the centre of the specimen so when the percentage is zero the specimen is saturated with hydrogen). Upper and lower bound estimates of D for ferritic materials at ambient temperature are taken as approximately $D_{max} = 2 \times 10^{-6}$ cm^2s^{-1} and $D_{min} = 2 \times 10^{-9}$ cm^2s^{-1} (Bailey et al., Fig 5.17, 2004). It is clear therefore that there is significant scatter in the expected diffusion rate in ferritic steels at ambient temperature, approximately three orders of magnitude depending on the exact material composition for example. However one can say that the observed behaviour of the ferritic material and temperature of interest is unlikely to fall outside of this scatter band. Furthermore, with the levels of carbon (0.11 wt.%) and sulphur (0.003 wt.%) in the API 5L X65 material tested (Table 1) it is likely that the scatter band of D is closer to $D_{max} = 2 \times 10^{-6}$ cm^2s^{-1} and $D_{min} = 4 \times 10^{-8}$ cm^2s^{-1} (Bailey et al., Fig 5.18, 2004). The observed scatter in values of D for ferritic materials also reduces significantly at higher temperatures, above say 150°C.

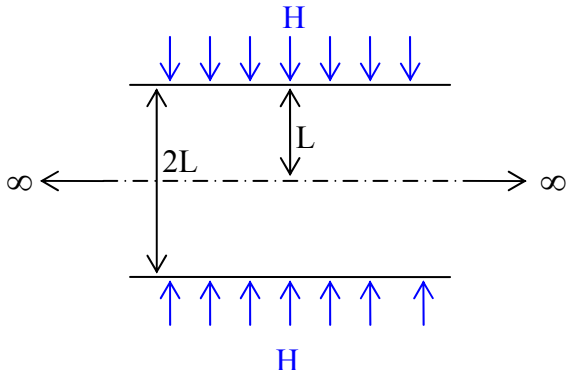

Fig. 14 Infinite plate (thickness 2L) exposed to hydrogen containing environment on both sides.

The generated removal curve for L = 8 mm is plotted in Fig. 15 for a temperature of 20°C and D adjusted to account for the actual carbon and sulphur content of the API 5L X65 material used. A lower bound estimate for the time it would take this specimen geometry to become saturated with hydrogen is around 2-3 hours. The corresponding upper bound estimate would be that it would take more than 100 hours for the specimen to become saturated. At a higher temperature these times would be reduced. A pre-soak period of one week (168 hours) was subsequently chosen in an attempt to maximise the environmental effect.

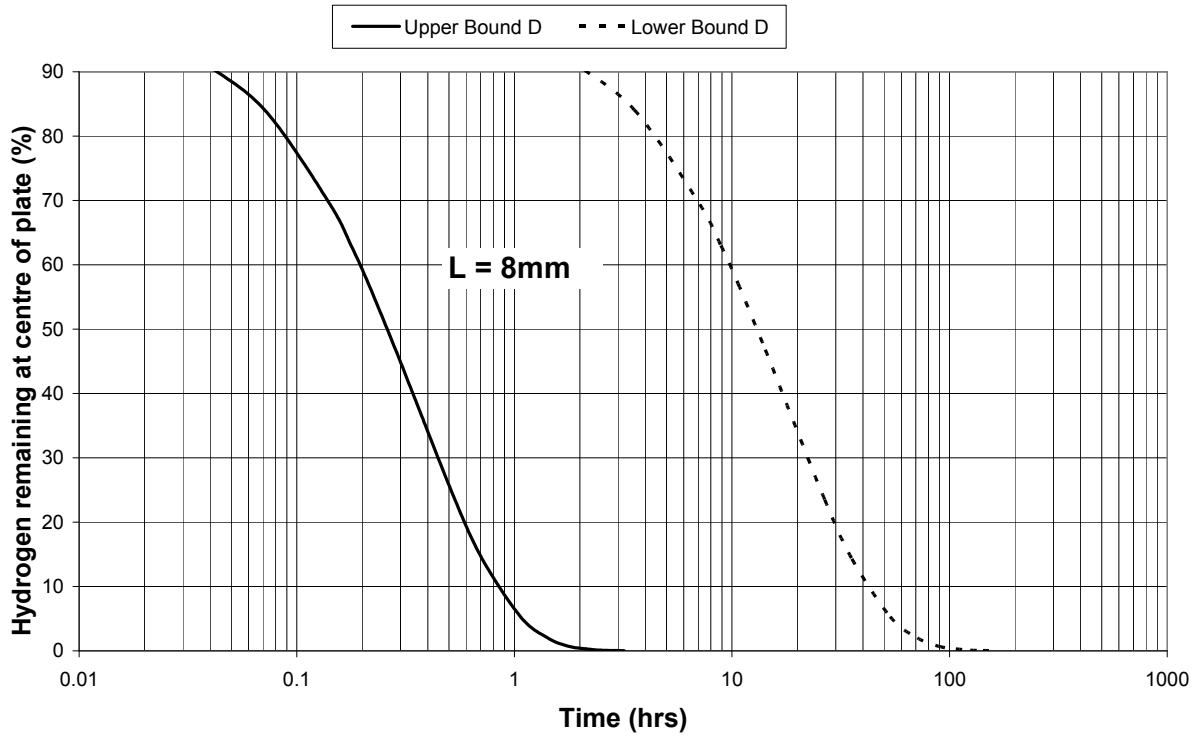

Fig. 15 Hydrogen removal curve for an infinite plate (thickness = 2L) with T = 20°C, L = 8 mm and D adjusted for the carbon and sulphur content of the API 5L X65 steel used.

It is evident from the data in Fig. 7 that a pre-soak period of one week has not had a significant effect on the observed crack growth rates. Crack growth rates for deeper flaws are still significantly lower than for shallower flaws, and Fig. 10 suggests that crack growth rates close to the exposed edges are still faster than the crack growth rate at the specimen centre. If local hydrogen concentration is the dominant factor controlling the observed crack growth rate, then this would suggest that a uniform distribution of hydrogen is not developed within the test period. If this is the case then perhaps the pre-soak period should be increased, however, according to the calculations above, hydrogen should have diffused into the centre of the specimen (ie 8 mm) during the test period even with a lower bound estimate of diffusivity. Hydrogen measurements have not been taken on a specimen exposed to the sour environment on all sides.

It is also worth noting that the simple diffusion calculations presented above relate to a case where the surface concentration remains constant. However, when corrosion rates may be initially high, but then fall due to the formation of surface scale, the surface concentration may itself decay with time. Mishael et al. (2004) presented the results of similar calculations where a decay constant (τ) was used to represent this behaviour, and hydrogen concentrations at the centre of a plate were then predicted to initially rise, but then reach a peak and fall with increasing time. This is a further factor which may have to be taken into account when considering the influence of crack depth on the observed crack growth rate; it may not be possible to reach an equilibrium condition where the hydrogen concentration is both uniform and constant throughout the test.

5 CONCLUSIONS AND RECOMMENDATIONS

FCGR tests have been carried out on a pipeline steel in a sour environment to investigate the influence of key variables such as loading conditions, crack depth, specimen geometry, pre-soak and coating configuration.

Regardless of any of the above variables there were increased crack growth rates for shallow flaws (at low ΔK) compared to deeper flaws in the same sour environment. It is possible therefore that using crack growth data generated using specimens containing deep flaws may be non-conservative in predicting the behaviour of shallow flaws.

Tests on specimens of differing thickness and coating configuration suggest that, in addition to shallow flaws growing faster than deeper flaws, crack growth rates in material closer to an exposed surface are faster than in material far away from an exposed surface. For samples exposed on one side only, measurements of diffusible hydrogen content have also confirmed that the concentration of hydrogen is also highest close to an exposed surface.

It may be argued that the use of specimens coated on all sides except for the notched surface is more representative of real service conditions, where a through wall variation in hydrogen concentration will develop. However, it is important to ensure that the hydrogen distribution in the test specimen conservatively reflects that in the real pipe. The use of a test specimen where the hydrogen concentration varies spatially also makes it difficult to generate da/dN - ΔK data in the conventional manner, as the inferred influence of ΔK may be confused with simultaneous variation in local hydrogen concentration. In particular, the use of decreasing ΔK tests may provide a non-conservative estimate of the crack growth rate at low ΔK, as low ΔK data will be generated when the flaw is relatively deep and the hydrogen concentration may be low. In reality a flaw is likely to grow under conditions of increasing ΔK, and at the beginning of life (when ΔK is low) the flaw will be shallow and the concentration of hydrogen may be high. Increasing ΔK tests are, therefore, recommended whenever possible, although it is acknowledged that the determination of very low ΔK data may then be difficult. The use of thin specimens, exposed on all sides, may provide an alternative method for determining conservative data in this regime.

6 REFERENCES

Bailey N, Coe F R, Gooch T G, Hart P H M, Jenkins N and Pargeter R J, 2004: 'Welding steels without hydrogen cracking', 2nd edition (revised), Woodhead Publishing, Cambridge.

BS ISO 12108, 2002: 'Metallic materials - Fatigue testing - Fatigue crack growth method', British Standards Institution, London.

BS 7910, 2005: 'Guide to methods for assessing the acceptability of flaws in metallic structures', British Standards Institution, London.

Gangloff R P and Turnbull, 1986: 'Crack electrochemistry modelling and fracture mechanics measurement of the hydrogen embrittlement threshold in steel', Metallurgical Soc AIME Circ, pp55 81.

Holtam C M, Baxter D P, Ashcroft I A and Thomson R C, 2008: 'The Behaviour of Shallow Cracks in a Pipeline Steel Operating in a Sour Environment', OMAE2008-57083, 27th

International Conference on Offshore Mechanics and Arctic Engineering, ISBN 0-7918-3827-8, ASME.

Kobayashi J I and Takeshi Y, 1985: 'Evaluation of resistance of steel plate to sulphide stress cracking in sour wet service', Proceedings of Conference on Predictive capabilities in environmentally assisted cracking (Edited by R. Rungta), ASME, New York, pp223-234.

Mishael S J, Dean F W H, and Fowler C, 2004: 'Practical applications of hydrogen permeation monitoring', Corrosion 2004, Paper No. 04476, NACE International.

NACE, 2005: 'MR 0177-2005: Laboratory testing of metals for resistance to sulfide stress cracking and stress corrosion cracking in H2S environments,' Houston.

Pippan R, Stuwe H P and Golos K, 1994: 'A comparison of different methods to determine the threshold of fatigue crack propagation', Fatigue, Vol. 16, Butterworth-Heinemann Ltd.

Russell T F, 1936: 'Some Mathematical Considerations on the Heating and Cooling of Steel', First Report of the Alloy Steels Research Committee by a Joint Committee of the iron and Steel Institute, pp149-187.

Scully J R, Gangloff R P, 2002: 'Environment-Assisted Cracking: Unresolved Issues', Corrosion Science: A Retrospective and Current Status, (Organiser) The Electrochemical Society Centennial Meeting, Philadelphia, PA.

Turnbull A and Saenz de Santa Maria M, 1990: 'The relative importance of crack-tip charging and bulk charging in hydrogen-assisted cracking in aqueous solutions', Environment Assisted Fatigue, EGF7 (edited by P. Scott), 1990, Mechanical Engineering Publications, London, pp. 145-153.

APPENDIX E

Holtam C M, Baxter D P, Ashcroft I A and Thomson R C, 2009: 'Influence of fatigue loading on the engineering critical assessment of steel catenary risers in sour deepwater oil and gas developments', Key Engineering Materials, Vols. 413-414, pp313-325, Trans Tech Publications, Switzerland.

Influence of Fatigue Loading on the Engineering Critical Assessment of Steel Catenary Risers in Sour Deepwater Oil and Gas Developments

C. M. Holtam
D. P. Baxter
Structural Integrity Technology Group
TWI Ltd
Cambridge
CB21 6AL
UK

I. A. Ashcroft
Wolfson School of Mechanical and Manufacturing Engineering
Loughborough University
Leicestershire
LE11 3TU
UK

R. C. Thomson
Department of Materials
Loughborough University
Leicestershire
LE11 3TU
UK

ABSTRACT

Steel catenary risers (SCR) are used in deepwater oil and gas developments to transfer produced fluids from the seabed to surface facilities. SCRs can be subject to fatigue loading from a variety of sources including wave and tidal motion, vortex induced vibration (VIV) and operating loads. When the produced fluids are sour (ie contain water and H_2S) higher fatigue crack growth rates (FCGR) are expected, and this can have a significant effect on defect tolerance.

The aim of this paper is to provide guidance on the current best practice methods for performing engineering critical assessments (ECA) on internal surface breaking defects in SCRs operating in a sour environment and subject to VIV fatigue loads. Example ECA calculations are presented for circumferential girth weld flaws, based on the failure assessment diagram (FAD) approach within the framework of BS 7910 [1]. The influence of certain key input variables is demonstrated, including the FCGR, determined from recent sour test data generated as part of this research.

KEY WORDS

Sour, fatigue, risers, defect assessment.

1 INTRODUCTION

An engineering critical assessment (ECA) is a fracture mechanics based approach, used to evaluate the significance of a flaw, based on a particular combination of material, stress and environmental conditions. An ECA approach can therefore provide maximum allowable flaw sizes at the manufacture and installation stage to ensure that, for example, girth weld flaws do not reach a critical size during the projected life of the component. This differs from conventional fatigue design philosophy which uses a stress-life (S-N) approach, whereby, an endurance curve is generated from a series of representative tests. S-N design curves can be found in BS 7608 [2] and DNV-RP-C203 [3], for example, and will typically be based on the statistical mean of the experimental data minus two standard deviations.

When using S-N design curves to evaluate offshore structures a safety factor is used (usually of the order of 1 to 20) to ensure a conservative estimate of fatigue life. This factor of safety depends on, for example, the consequence of failure and confidence in the assumed fatigue loading spectrum, ie a high consequence of failure and an unpredictable loading spectrum would warrant a higher factor of safety. In a corrosive environment (eg sour service) a further fatigue life reduction factor (or knock-down factor) needs to be applied to account for the detrimental effect that the environment may have on fatigue performance. There are relatively few published S-N data for steels in a sour environment [4,5,6,7] and as environmental factors such as pH, partial pressure of H_2S, and temperature can have a significant influence on the observed behaviour, it is often necessary to generate project-specific S-N or crack growth rate data to assist in design. The S-N approach can be used to assess the performance of a nominally defect free weld, although factors such as weld misalignment are included. However, for welds with known defects, an ECA approach is required to demonstrate adequate fatigue life. While it remains appropriate to incorporate a safety factor (with respect to fatigue life) within ECA calculations, it is a matter of debate as to whether the factor used should be the same as that used in S-N calculations. In some cases it is believed that doing so would be overly conservative [8]. Ensuring safe riser design is the primary objective, but it is recognised that estimates of fatigue life that are overly conservative would result in greater numbers of repair at the design and manufacture stage, lower operational lives and possibly more stringent inspection intervals. Each of these has the potential to make SCRs unviable from either a technical or an economic standpoint. While the safety factor with respect to fatigue loading can be a critical parameter when conducting an ECA, other inputs such as the assumed toughness, residual stress or fatigue crack growth law can similarly have a significant influence, particularly under sour service conditions.

The aim of this paper is, therefore, to provide guidance on the current best practice methods for performing ECAs on internal surface breaking defects in SCRs operating in a sour environment and subject to VIV fatigue loads. Example ECA calculations are presented for circumferential girth weld flaws in a typical SCR, based on the failure assessment diagram (FAD) approach within the framework of BS 7910 [1], using TWI's commercial software package CRACKWISE 4. The influence of certain key (mechanical) input variables is demonstrated, including the fatigue crack growth rate (FCGR), determined from recent sour test results generated as part of this research. It should be noted that BS 7910 [1] currently contains only limited guidance on the assessment of flaws in sour service conditions. Methods for the determination of the critical stress intensity factor for stress corrosion cracking (K_{ISCC}) and the assessment approach when using this type of laboratory data are still the subject of ongoing research.

2 APPROACH

2.1 FAILURE ASSESSMENT DIAGRAM

It is possible to represent material properties, defect geometry and loading conditions in a mathematical form, and generate what is known as a failure assessment diagram (FAD). In this regard, the FAD approach can be considered as independent of component geometry. A FAD represents a two-parameter approach, acknowledging that either brittle or ductile fracture might occur, or plastic collapse. For fracture to occur the stress intensity factor at the crack tip must be greater than the material fracture toughness (or critical stress intensity factor). However, plastic collapse can also occur if the stress is high relative to the material proof stress or ultimate tensile strength (UTS), hence the need for a two-parameter approach to combine these two possible failure mechanisms. A generalised Level 2A FAD is shown in Fig. 1, which is suitable for materials that do not exhibit a yield discontinuity (commonly referred to as Lüders plateau).

The vertical axis of the FAD represents the criteria for brittle or ductile fracture, often known as the fracture toughness ratio (K_r), which is the ratio of stress intensity factor (K_I) to material fracture toughness (K_{mat}). Both primary and secondary stresses (such as residual stresses) contribute to the applied stress intensity factor. The horizontal axis represents the likelihood of plastic collapse, often known as the load ratio (L_r), which is the ratio of the in-service (or reference) stress to yield strength (or 0.2% proof strength) or flow stress. Secondary stresses (such as residual stresses) do not contribute towards plastic collapse. The fracture toughness and load ratios are connected via a locus, and the proximity to this locus is an indication of how close a specific material, flaw and stress combination is to failure. As indicated in Fig. 1, on or below the locus represents an acceptable or stable flaw, whereas a point outside the locus represents an unacceptable flaw where the risk of failure cannot be tolerated. If the damage mechanism and service conditions are adequately understood then predictions can be made as to how a flaw might grow and what size flaw can ultimately be tolerated in-service, assuming no interaction with adjacent flaws.

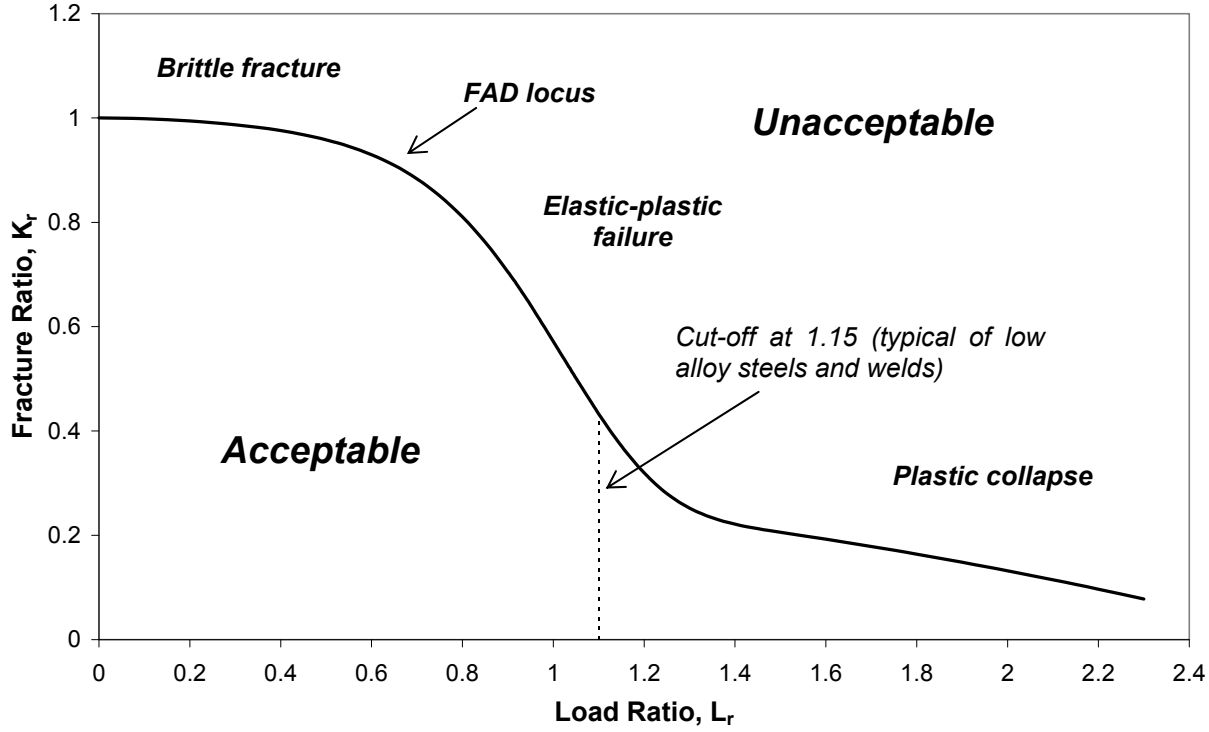

Fig. 1. Generalised Level 2A failure assessment diagram with typical cut-off for low alloy steels and welds [after 1].

For internal surface breaking flaws in a sour environment the dominant form of crack extension can be sulphide stress cracking (SSC), which can occur at applied stress intensities much lower than the material's fracture toughness. At applied stress intensities higher than a critical value (K_{ISCC}) flaws will grow, usually rapidly, until their size reaches a point where fracture or plastic collapse intervenes. It is therefore necessary to restrict the value of the applied stress intensity factor to a value less than K_{ISCC}. It is then possible to account for sour service conditions by using K_{ISCC}, generated from laboratory data, as an estimate of the material's 'fracture toughness' in a sour environment and therefore define the FAD envelope in terms of sour service properties. This differs slightly from the approach defined in documents such as BS 7910 [1], but is believed to be conservative.

2.2 FLAWS CONSIDERED

The case considered in this paper assumes a circumferential surface breaking flaw on the internal surface of a SCR, located at a girth weld (Fig. 2). The relevant stress intensity factor and reference stress solutions for this type of flaw are M.4.3.3.2 and P.4.3.2 respectively [1].

The case of an embedded or external flaw has not been considered in the current work. An external flaw would be exposed to a seawater environment, which is known to be less severe than a sour environment in terms of increased FCGR [eg 9]. The case of an embedded flaw is more complicated as the flaw could propagate through material that contains a significant amount of absorbed hydrogen, even though the environment does not have direct access to the crack tip region. Use of a crack growth law derived from tests conducted in a sour environment is probably conservative in this instance, but perhaps overly so. An experimental study to investigate this aspect of material behaviour is currently underway at TWI.

For assessment purposes, flaws are idealised as being elliptical (or-semi-elliptical in the case of surface breaking flaws). Standard practice is to calculate an applied stress intensity factor, K, at the base of the flaw (ie the deepest point) and at the surface of the flaw, and select the maximum (or worst case).

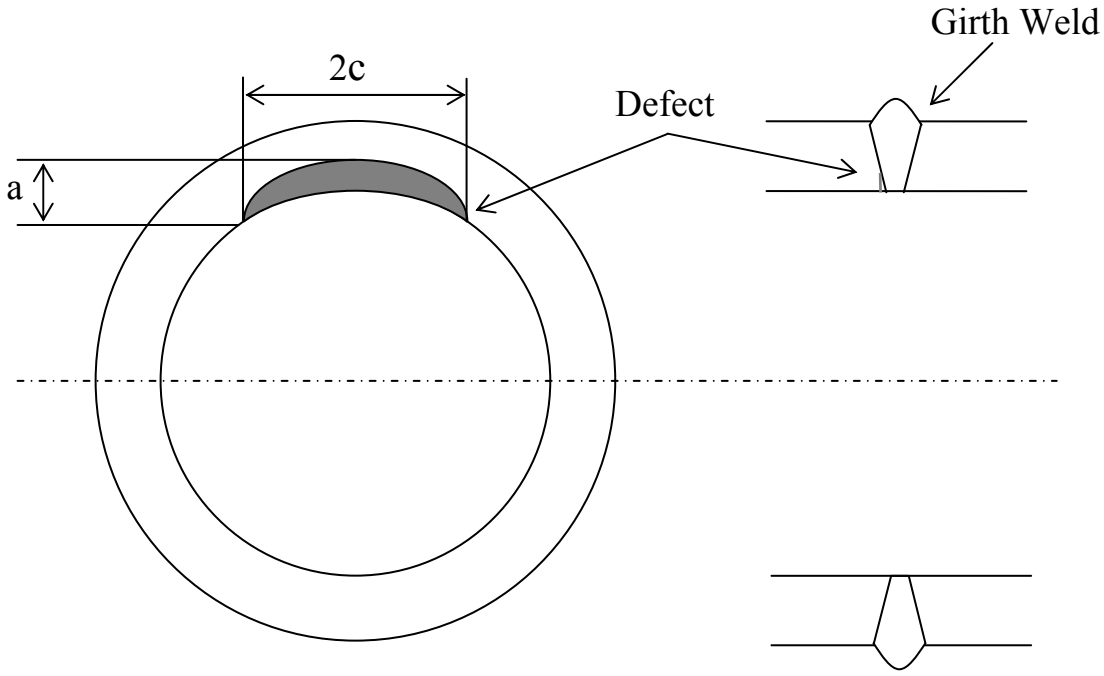

Fig. 2. Defect orientation relative to steel catenary riser; circumferential internal surface breaking flaw located at a girth weld.

3 INPUT PARAMETERS

3.1 SCR GEOMETRY AND INITIAL FLAW DIMENSIONS

The SCR is assumed to be constructed from C-Mn X65 seamless API-5L parent material, with dimensions as indicated in Table 1. An aspect ratio of 10 (flaw length to flaw height) was chosen for the initial flaw size.

Table 15 Assumed geometry of steel catenary riser.

Outside Diameter	355.6 mm (14 ”)
Wall thickness	20.6 mm
Mean radius	167.5 mm
Weld cap width	12 mm
Weld root width	4 mm
Weld Misalignment	1 mm

3.2 WELD GEOMETRY

The weld is assumed to be a full-penetration girth weld produced using mechanised processes. A typical example of such a weld is shown in Fig. 3. Weld material, particularly the heat affected zone (HAZ) can be susceptible to SSC due to the hardened material (untempered or partially tempered martensite) that may be present in this region. Welds designated for sour

service are restricted to a maximum hardness limit of 250 HV. The internal surface breaking flaw is therefore assumed to be located at a girth weld, close to the weld root toe.

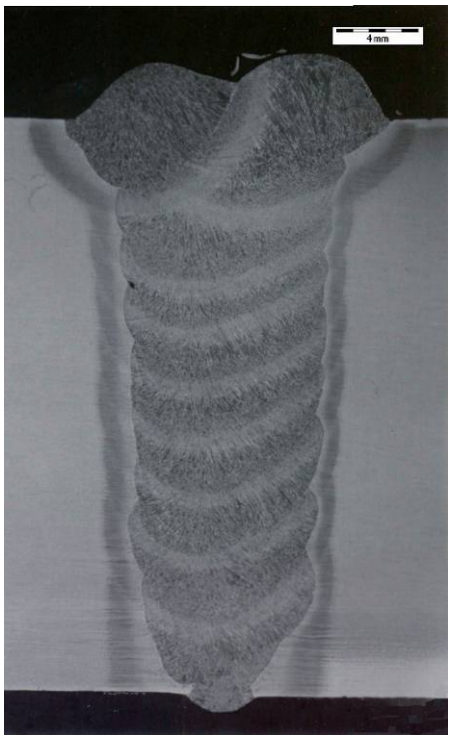

Fig. 3. Image of a typical steel catenary riser girth weld produced using mechanised welding processes.

3.3 STRESS CONCENTRATION FACTOR DUE TO PRESENCE OF WELD (M_K)

The local stress concentration at the weld toe is characterised using the parameter M_k. Standard solutions for surface breaking flaws are provided in Annex M of BS 7910 [1], derived from 2-D (and for certain geometries 3-D) finite element analyses. M_k is dependent on what is termed the attachment length, which in the case of an internal surface breaking flaw in a full penetration pipeline girth weld is the width of the weld root protrusion. For the purposes of this assessment a weld root width of 4 mm was adopted (Table 1). M_k is maximum near the surface of the pipeline and its influence decreases as flaw depth increases. M_k is calculated automatically within CRACKWISE 4 for an inputted attachment length and in this assessment the standard 2-D solutions for an internal surface breaking flaw were used (M.4.3.3.2) [1], assuming a full penetration weld.

3.3.1 AXIAL MISALIGNMENT

Axial misalignment can be defined as the offset between the centrelines of the pipe wall across the girth weld. Axial weld misalignment generates a bending stress at the location of the flaw. In the current work a maximum level of misalignment of 1 mm was assumed. The stress magnification factor, K_m, was calculated, based on this assumed misalignment, using equation 3.3.3 from DNV-RP-C203 [3], which is known to be slightly less conservative than the equivalent equation in BS 7910 [1].

$$K_m = 1 + \frac{6\partial}{t} \frac{1}{1 + \frac{T}{t}^{2.5}} e^{-\alpha} \quad (1)$$

where ∂ is the misalignment, T and t are the wall thicknesses either side of the weld, D is the outside diameter of the pipe, L is the attachment length (or width of the girth weld cap) and;

$$\alpha = \frac{1.82L}{\sqrt{Dt}} \frac{1}{1 + \left(\frac{T}{t}\right)^{2.5}} \quad (2)$$

A weld cap width of 12 mm was assumed (Table 1).

3.3.2 WELDING RESIDUAL STRESSES

Welding residual stresses are dependent on the welding process used and whether any stress relief was performed. SCR girth welds tend not to be heat treated and therefore a uniform welding residual stress of yield strength magnitude was assumed in the calculations, in line with the guidance provided in BS 7910 (7.2.4.1) [1]. This stress will relax under the influence of applied load, but if the applied loads are low then this will have little effect.

For an internal circumferential surface breaking flaw at a pipeline girth weld, the residual stress profile perpendicular to the flaw (and in this case the weld) will be limiting. While the assumption of uniform residual stresses of yield strength magnitude is a common approach, it is also recognised as being conservative, even if the residual stresses are allowed to relax under applied load. For relatively thick walled pipe it has also been shown that residual stresses tend to be lower on the inner surface of a pipeline girth weld but it is difficult to provide quantitative guidance. A combination of residual stress measurement and modelling (for a specific welding procedure) does however provide a possible method for determining an appropriate but less conservative assumption regarding the assumed residual stress state.

3.4 TENSILE PROPERTIES

The tensile properties used in this paper (Table 2) are based on tests carried out at TWI, using the same X65 parent material as that used to generate the FCGR data (see section 3.7 “Fatigue Crack Growth Rate Laws”).

Table 2 Room temperature material properties used in the assessment.

Hardness (parent)	196 HV
UTS	576 MPa
0.2% proof stress	478 MPa
Young’s modulus	207 GPa
Poisson’s ratio	0.3

3.5 STATIC STRESSES

A maximum axial static stress of 150 MPa has been assumed in the current work, representing a typical maximum operating stress for a SCR.

3.6 FATIGUE STRESSES

Fatigue stresses can result from numerous sources including the pressure cycles experienced by the riser during operation, wave and tidal motion and VIV. The extent of fatigue damage is dependent on the combination of stress range and the number of cycles. SCRs can experience very high numbers of low stress cycles due to VIV, a phenomena caused by the constant passage of marine currents past a riser, causing turbulence.

Experience from the offshore industry suggests that the majority of fatigue damage that occurs in SCRs is due to relatively low stress range cycles (ie due to the high number of cycles at these low stresses and the relatively few cycles at higher stresses). In this regard stresses due to VIV often tend to dominate for the specific case of SCRs. Shutdown-restart sequences, which can dominate the fatigue assessment of high pressure, high temperature flowlines subject to lateral buckling, tend not to be significant in the case of SCRs. In the current work, the life of the SCR is also not affected by the position of the flaw around the circumference of the pipe as is the case with the assessment of flaws in reeled pipelines for example. For stresses due to VIV, a safety factor of 20 is often applied to design life to provide a conservative prediction of fatigue life.

The first weld at the top of the SCR and the touchdown point (TDP), where the nominally vertical riser meets the pipeline or flowline on the seabed, are the most stressed locations and therefore critical in terms of fatigue loading [9, 10]. The critical location for VIV is often the top of the riser since this is subject to higher stress ranges than the TDP, if only for a small number of cycles.

The fatigue spectrum used in the current work is based on a design life of 30 years for the SCR. A typical VIV fatigue spectrum for the TDP and top weld of a SCR was scaled such that a simple S-N analysis (using a class E design curve and a knock-down factor of 30 for the sour environment) gave a design life of 600 years (ie 30 years with safety factor of 20). For stress ranges below the constant amplitude fatigue limit a reduced fatigue slope was used in this S-N analysis, as recommended in BS 7608 section 4.4 [2]. The final annual fatigue spectrum for both the TDP and the top weld is shown in Fig. 4. It can be seen that the TDP is subject to a greater number of low stress cycles whereas the top weld has a greater number of higher stress cycles but fewer low stress cycles.

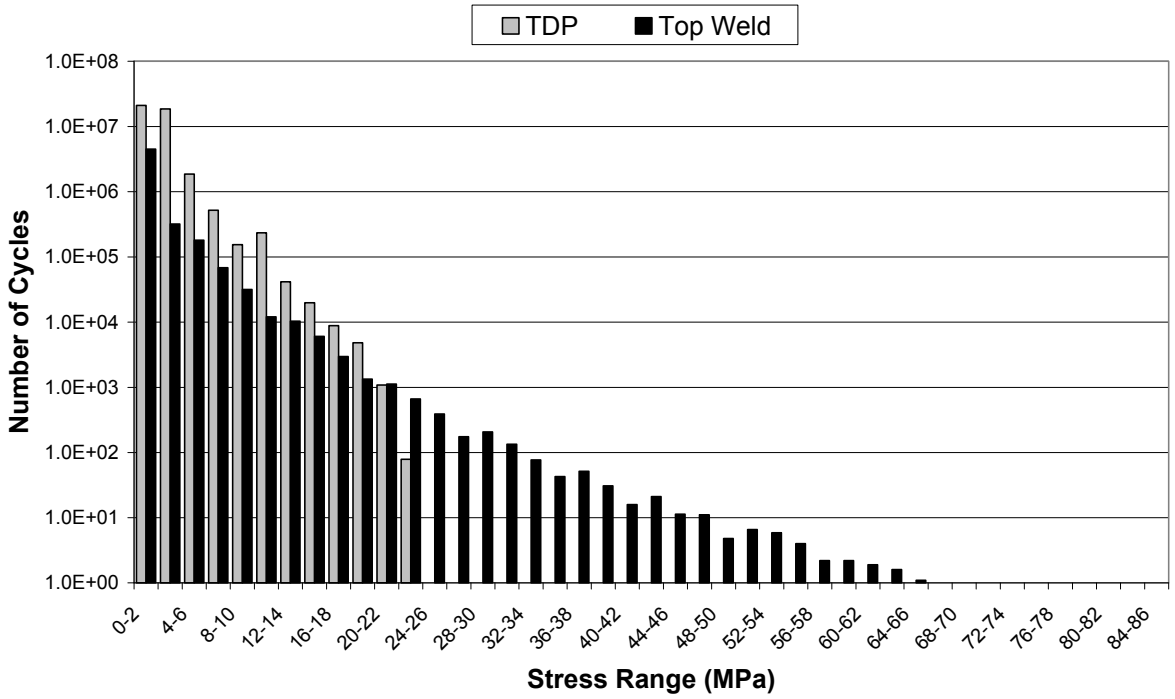

Fig. 4. Simplified representation of the assumed annual fatigue spectrum due to vortex induced vibration at the touchdown point and top weld.

3.6.1 ECA SAFETY FACTORS

As noted above a safety factor of 20 has been assumed in the S-N analysis, and this has been used to scale the fatigue loading spectrum accordingly. It is however standard practice to apply a smaller safety factor on fatigue life when performing ECA calculations. For example a safety factor of 10 would mean a target life of 300 years, a safety factor of 5 would mean a target life of 150 years and no safety factor at all would reduce the target life to 30 years.

3.7 FATIGUE CRACK GROWTH RATE LAWS

The assumed FCGR usually takes the form of a Paris law which relates the crack growth per cycle to the stress intensity factor range (ΔK), as shown in the equation below, where m and C are constants.

$$\frac{da}{dN} = C(\Delta K)^m \qquad (3)$$

However, below a certain value of ΔK (known as the threshold) no fatigue crack growth is expected. BS 7910 [1] contains standard crack growth laws for steels in air and in marine (ie seawater) environments. However, in a sour environment, FCGRs can be significantly higher and so an appropriate crack growth law needs to be determined from laboratory testing.

Representative data generated from a decreasing ΔK test carried out in an aqueous solution of 5% sodium chloride and 0.4% sodium acetate, acidified to a pH of approximately 3.5 and saturated with a mixture of 7% H_2S in N_2 is shown in Fig. 5. Also plotted is the mean curve for steels in air ($R \geq 0.5$) taken from BS 7910 [1], and the design curve for steels in air (ie mean plus two standard deviations).

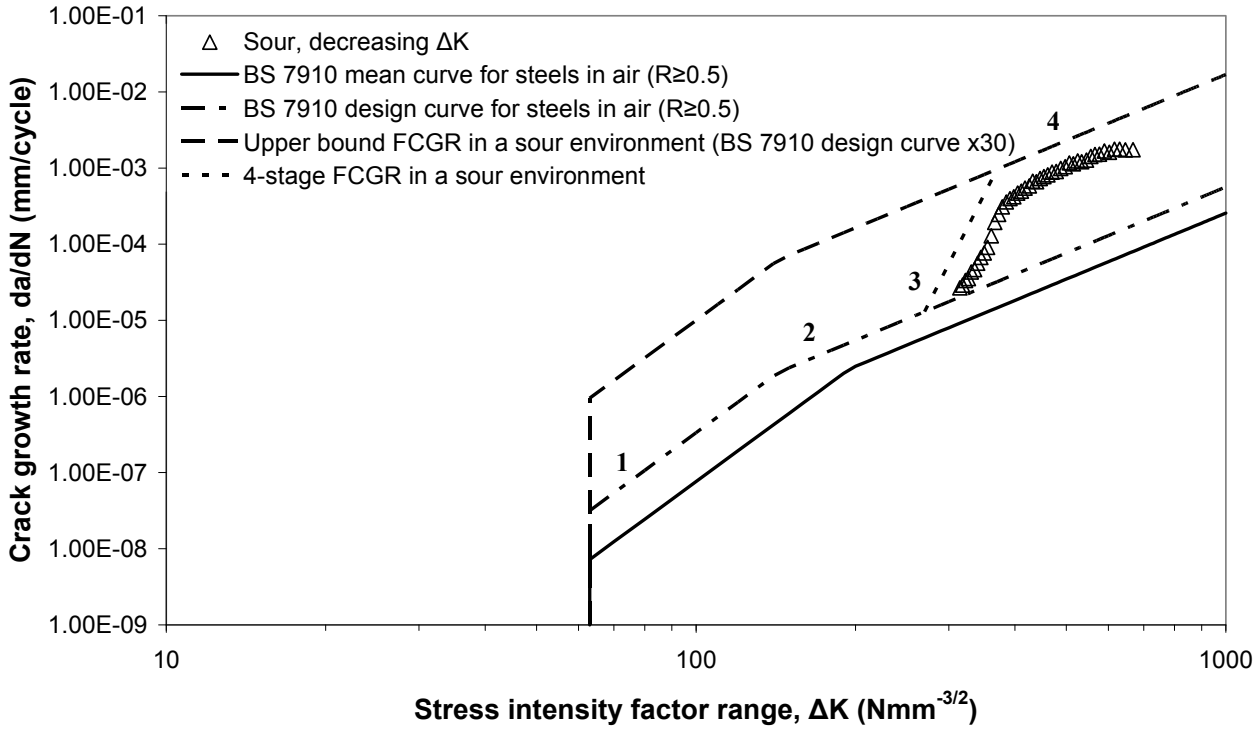

Fig. 5. Fatigue crack growth rate data used in the engineering critical assessment calculations.

At high ΔK the FCGR is approximately 30 times higher than the mean curve for steels in air. An appropriate crack growth law for a sour environment can therefore be determined by offsetting the design curve (mean plus two standard deviations) for steels in air by a similar amount. As illustrated in Fig. 5, this provides a relatively simple means of determining an appropriate upper bound to ensure a conservative assessment, but does not take advantage of the fact that the influence of the sour environment appears to be less significant at lower ΔK.

It can be seen that at lower ΔK (400-300 $Nmm^{-3/2}$), the FCGR decreased rapidly (more than an order of magnitude) and approached the design curve for steels in air. The reduced influence of environment at low ΔK has also been reported elsewhere [11, 12].

It is likely that adopting a crack growth law which provides a better fit to the experimental data at low ΔK will have a significant influence on associated ECA calculations. A four stage law (Fig. 5) has therefore also been used in the current work to assess the extent to which this affects the determined fatigue lives.

3.8 FRACTURE TOUGHNESS AND K_{ISCC}

Values of K_{ISCC} are known to depend on environmental parameters such as pH, partial pressure of H_2S and temperature. At ambient temperature, and low pH (around 3.5), K_{ISCC} may be in the range 800-1600 $Nmm^{-3/2}$ (25-50 $MPam^{0.5}$) [13, 14]. However, in less aggressive service environments (eg pH5 and elevated service temperature) values of K_{ISCC} may be substantially higher. A K_{ISCC} value of 3160 $Nmm^{-3/2}$ (100 $MPam^{0.5}$) was therefore assumed in the current work, based on TWI's project experience.

4 RESULTS

Calculations have been performed using TWI's software package CRACKWISE 4, which is fully compliant with the latest version BS 7910 [1].

4.1 STATIC ASSESSMENTS

The first assessment carried out was a static fracture assessment to demonstrate the effect of fracture toughness (or K_{ISCC}) on sour defect assessments under static loading conditions. A sensitivity analysis was performed whereby critical flaw height (maintaining a constant aspect ratio of 10) was determined as a function of fracture toughness, for yield strength magnitude residual stress. Fig. 6 shows the resulting plot of critical flaw height against fracture toughness. This shows that for an assumed value of K_{ISCC} of 3160 $Nmm^{-3/2}$ (100 $MPam^{0.5}$), and yield strength magnitude residual stress, a maximum tolerable flaw size of 4.5 mm x 45 mm might be tolerated, whereas if the assumed value of K_{ISCC} is 2500 $Nmm^{-3/2}$ (80 $MPam^{0.5}$) a flaw of the order of 3 mm x 30 mm could be tolerated. A 3 mm x 30 mm flaw is of the order of magnitude that could be reliably detected via automated ultrasonic (AUT) inspection while at the same time not triggering an unfeasibly large number of repairs.

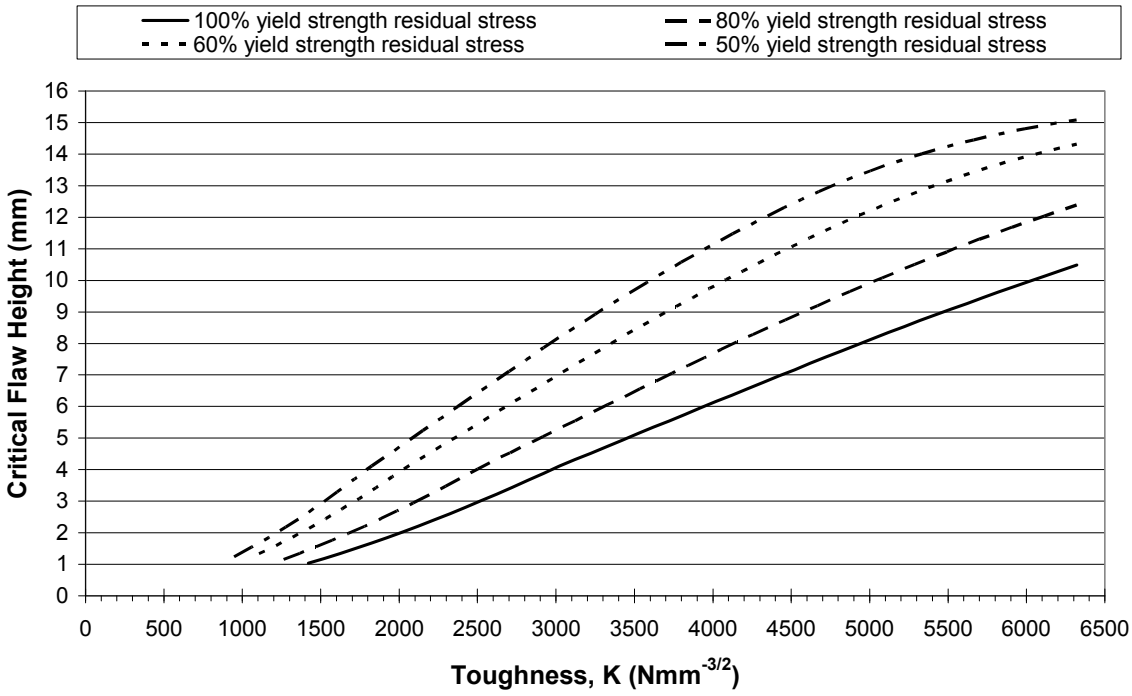

Fig. 6. Critical flaw height (constant aspect ratio of flaw length to flaw height of ten) as a function of fracture toughness, for different magnitudes of residual stress.

Fig. 6 also demonstrates the effect of welding residual stress. Based on an assumed value of K_{ISCC} of 3160 $Nmm^{-3/2}$ (100 $MPam^{0.5}$), if welding residual stress could be reliably shown to be of only half yield strength magnitude, then the critical flaw size would increase from approximately 4.5 mm x 45 mm to approximately 8.6 mm x 86 mm. Similarly, if this could be shown to be the case then the minimum value of K_{ISCC} for a 3 mm x 30 mm flaw to be tolerable would decrease to approximately 1600 $Nmm^{-3/2}$ (50 $MPam^{0.5}$).

4.2 FRACTURE AND FATIGUE ASSESSMENTS

Combined fracture and fatigue assessments were performed using an assumed initial flaw size (for example 3 mm x 30 mm), a K_{ISCC} value of 3160 $Nmm^{-3/2}$ (100 $MPam^{0.5}$) and yield strength magnitude welding residual stresses that were allowed to relax under applied load. Two different fatigue spectrums were used representing VIV loading at the TDP and top weld, as described in Fig. 4. At both the TDP and the top weld, three assessments were performed using an assumed fatigue crack growth law as follows:

1. In air conditions, based on the two stage design curve for steels in air from BS 7910 [1].
2. A two stage upper bound sour environment curve, a factor of 30 higher than the two stage design curve for steels in air from BS 7910 [1] but with the same threshold ΔK_{TH}.
3. A four stage sour environment curve; the first two stages correspond to the design curve for steels in air and the final stage the upper bound sour environment curve (Fig. 5).

The results of the above assessments are summarised in Table 3. For the TDP there is no difference between using the design curve for steels in air and the four stage law for a sour environment, with both achieving the desired fatigue life of 600 years. This is because the stresses are so low that they never result in a value of ΔK in either stage 3 or 4 of the four stage fatigue crack growth curve. The upper bound curve on the other hand results in a fatigue life of only 22 years. A similar result is obtained for the top weld although now there is an observed difference between the in air curve and the four stage sour curve. This is due to there being higher stress ranges at the top weld (Fig. 4).

For both the TDP and top weld, critical flaw sizes have also been calculated based on no safety factor on fatigue life in the ECA (target fatigue life 30 years), a safety factor of 5 (target fatigue life 150 years) and a safety factor of 10 (corresponding to a target fatigue life of 300 years) (Table 3). Despite the upper bound curve producing short estimates of life for an initial flaw of 3 mm x 30 mm, the TDP could tolerate an initial flaw of 2 mm x 20 mm with a safety factor of 5, which is still close to a typical AUT inspection limit. At the top weld however a safety factor of 5 on fatigue life results in a critical flaw size of approximately 1.3 mm x 13 mm.

5 DISCUSSION

Toughness has been shown to be a critical parameter in performing sour ECAs under static loading conditions. With a yield magnitude residual stress, the minimum K_{ISCC} value to tolerate a 3 mm x 30 mm flaw is approximately 2500 $Nmm^{-3/2}$ (80 $MPam^{0.5}$). If K_{ISCC} was lower than this, then this might be expected to lead to a significant repair rate during fabrication. It is also clear that an accurate estimate of K_{ISCC} is essential as conservative assumptions, in the absence of actual experimental data, could easily lead to failed assessments. Even when experimental data are available there can be considerable scatter between nominally identical tests. It should also be noted that K_{ISCC} may be strongly influenced by temperature so, for example, K_{ISCC} may be lower during shutdown (at ambient temperature) than during operation (at elevated temperature).

Although K_{ISCC} has been shown to be a critical input parameter under static loading conditions, it is interesting to see whether this remains the case within a fracture and fatigue assessment. Examining the upper bound case at the TDP for a fatigue life of 150 years, the critical flaw size is 2.0 mm x 20 mm (Table 3) for a value of K_{ISCC} of 3160 $Nmm^{-3/2}$ (100

$MPam^{0.5}$). If K_{ISCC} is increased to approximately 4700 $Nmm^{-3/2}$ (150 $MPam^{0.5}$) the critical flaw size remains at 2.0 mm x 20 mm to achieve a design life of 150 years. If the value of K_{ISCC} is reduced to approximately 2200 $Nmm^{-3/2}$ (70 $MPam^{0.5}$) the critical flaw size is 1.9 mm x 19 mm. In this regard the value of K_{ISCC} has little effect on the critical flaw size and the assessment is dominated by fatigue. Similarly for the top weld, increasing the value of K_{ISCC} to 4740 $Nmm^{-3/2}$ (150 $MPam^{0.5}$) the critical flaw size remains unchanged at 1.3 mm x 13 mm and reducing the value of K_{ISCC} to 1600 $Nmm^{-3/2}$ (50 $MPam^{0.5}$) reduces the critical flaw size to 0.8 mm x 8 mm.

Table 3 Results of fracture and fatigue engineering critical assessment calculations at the touchdown point and top weld positions for in air conditions, an upper bound sour environment curve and a four stage sour environment curve.

		Air	Sour - Four Stage	Sour - Upper Bound
TDP	Life (based on initial flaw size of 3 mm x 30 mm)	686 years	686 years	22.2 years
	Final Flaw Size (based on initial flaw size of 3 mm x 30 mm)	4.8 mm x 31.1 mm	4.8 mm x 31.1 mm	4.7 mm x 31.0 mm
	Critical Flaw Size for 30 Years Life (ie no safety factor on fatigue life in ECA)	4.2 mm x 42 mm	4.2 mm x 42 mm	2.4 mm x 24 mm
	Critical Flaw Size for 150 Years Life (ie safety factor of 5 on fatigue life in ECA)	3.8 mm x 38 mm	3.8 mm x 38 mm	2.0 mm x 20 mm
	Critical Flaw Size for 300 Years Life (ie safety factor of 10 on fatigue life in ECA)	3.4 mm x 34 mm	3.4 mm x 34 mm	1.8 mm x 18 mm
Top Weld	Life (based on initial flaw size of 3 mm x 30 mm)	537 years	435 years	17 years
	Final Flaw Size (based on initial flaw size 3 mm x 30 mm)	4.8 mm x 31.7 mm	4.8 mm x 31.5 mm	4.6 mm x 31.6 mm
	Critical Flaw Size for 30 Years Life (ie no safety factor on fatigue life in ECA)	4.2 mm x 42 mm	4.1 mm x 41 mm	2.5 mm x 25 mm
	Critical Flaw Size for 150 Years Life (ie safety factor of 5 on fatigue life in ECA)	3.8 mm x 38 mm	3.6 mm x 36 mm	1.3 mm x 13 mm
	Critical Flaw Size for 300 Years Life (ie safety factor of 10 on fatigue life in ECA)	3.4 mm x 34 mm	3.2 mm x 32 mm	0.9 mm x 9.0 mm

It is therefore apparent that for SCRs subject to VIV, the assumption made regarding fatigue crack growth law may be more significant than the assumption made regarding either K_{ISCC} or welding residual stress. Indeed the assumed fatigue crack growth law, particularly at low ΔK, is likely to be a factor which influences whether a C-Mn material can be used as opposed to a

corrosion resistant alloy (CRA) or a clad material, particularly at critical locations such as the TDP and top weld.

The test data illustrated in Fig. 7 suggest that the influence of environment at low ΔK is far less severe than at high ΔK, and this has similarly been reported in other work [11, 12]. At low ΔK the data approach the standard curve for steels in air. However, it should be noted that these data were derived from a test conducted under conditions of decreasing ΔK, so that low ΔK data were determined at the end of the test, when the flaw was relatively deep. This is in contrast to the real situation in which a flaw will grow under conditions of increasing ΔK, and will be subject to low ΔK cycling when the flaw may be relatively shallow. Published data for flaws growing under these conditions suggest that at low ΔK, shallow flaws may grow substantially faster than deeper flaws, and this casts doubt on whether FCGRs in a sour environment genuinely approach those seen in air at low ΔK. It is clear that additional data, at lower ΔK, is needed to provide a better indication of material behaviour under these conditions. The test data illustrated in Fig. 7 were also derived from tests in a low pH ambient temperature sour environment, and similar tests in a more realistic operating environment (perhaps high pH and elevated temperature) are also required.

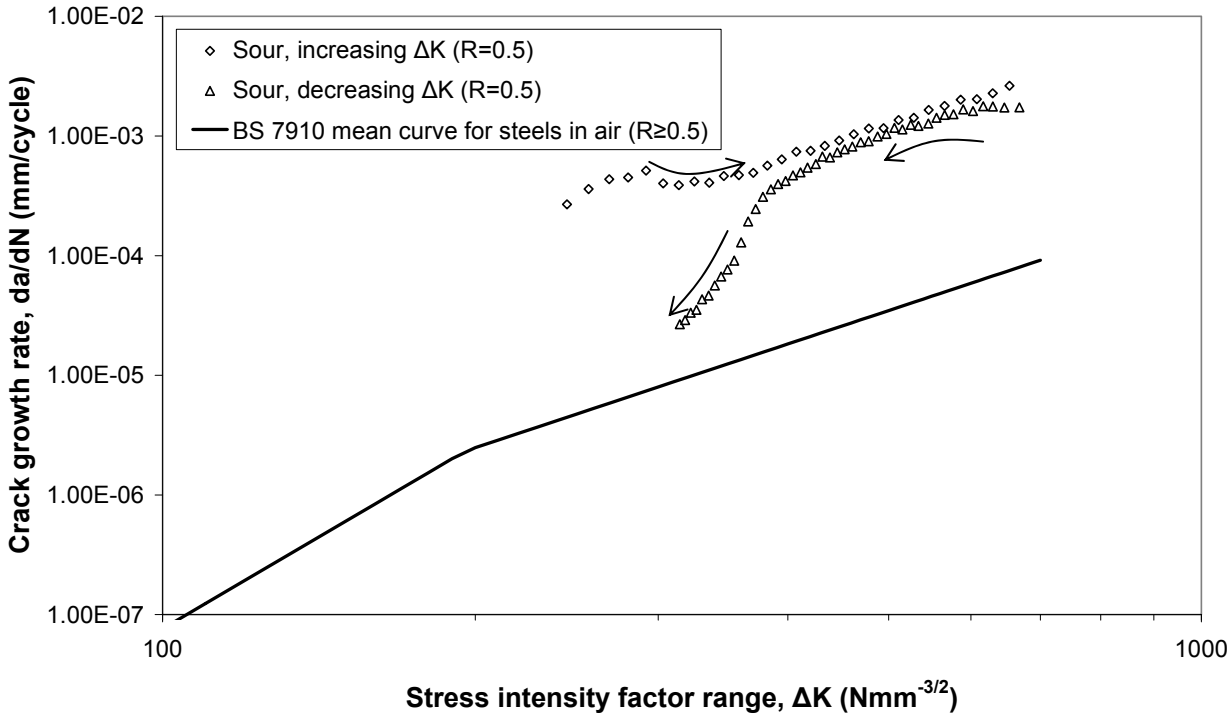

Fig. 7. Sour fatigue crack growth rate data generated under conditions of increasing and decreasing ΔK, illustrating a possible crack depth effect at lower ΔK (<400 $Nmm^{-3/2}$). (Arrows indicate increasing crack depth in each test).

6 CONCLUSIONS

This paper has demonstrated the effect of three critical parameters when performing sour ECA calculations; the value of K_{ISCC}, the welding residual stress and the assumed FCGR law. The current case considered these in relation to a typical SCR operating under VIV fatigue loading.

The value of K_{ISCC} has a significant effect on the maximum tolerable flaw size, particularly under static loading conditions. However, for the case of an SCR under VIV fatigue loading, the value of K_{ISCC} becomes less significant as the ECA becomes dominated by fatigue, and the assumption made regarding fatigue crack growth law becomes more significant.

The effect of welding residual stress is also particularly important for sour (ie low toughness) ECAs, where a high tensile residual stress can provide a significant part of the crack driving force. For thick walled pipe the assumption of yield strength magnitude residual stress may be overly conservative, but a combination of measurement and modelling is recommended to justify any less conservative assumption. However, where fatigue dominates, this is similarly expected to have less influence on defect tolerance.

The selection of the assumed fatigue crack growth law is therefore critical when conducting ECA calculations for SCRs subject to VIV. There are relatively few published FCGR data for pipeline steels in a sour environment, particularly at low ΔK. Possible differences in behaviour, in this regime, between shallow flaws (under conditions of increasing ΔK) and deeper flaws (under conditions of decreasing ΔK) should also be considered.

7 REFERENCES

[1] BS 7910: 'Guide to methods for assessing the acceptability of flaws in metallic structures', British Standards Institution, London (2005).

[2] BS 7608: 'Code of practice for Fatigue design and assessment of steel structures', British Standards Institution, London (1993).

[3] DNV-RP-C203: 'Fatigue design of offshore steel structures', Det Norske Veritas (2005).

[4] Buitrago J and Weir M S: 'Experimental fatigue evaluation of deepwater risers in mild sour service', Deep Offshore Technology Conference, New Orleans, USA (2002).

[5] McMaster F, Thompson H, Zhang M, Walters D and Bowman J: 'Sour service corrosion fatigue testing of flowline welds', OMAE2007-29060, Proceedings of OMAE2007 26th International Conference on Offshore Mechanics and Arctic Engineering, San Diego, California, USA (2007).

[6] Buitrago J, Baxter D and Hudak S: 'High-cycle and low-cycle fatigue resistance of girth welds in sour service', OMAE2008-57545, Proceedings of 27th International Conference on Offshore Mechanics and Arctic Engineering, Estoril, Portugal (2008).

[7] McMaster F, Bowman J, Thompson H, Zhang M and Kinyon S: 'Sour service corrosion fatigue testing of flowline and riser welds', OMAE 2008-57059, Proceedings of 27th International Conference on Offshore Mechanics and Arctic Engineering, Estoril, Portugal (2008).

[8] Smith A and Osman M: 'Comparison of safety factors used for the determination of remaining life of girth welded pipelines using fracture mechanics and conventional endurance assessment techniques', OMAE2008-58050, Proceedings of the 27th International Conference on Offshore Mechanics and Arctic Engineering, Estoril, Portugal (2008).

[9] Baxter D P, Maddox S J, Pargeter R J: 'Corrosion fatigue behaviour of welded risers and pipelines', OMAE2007-29360, Proceedings of OMAE2007 26th International Conference on Offshore Mechanics and Arctic Engineering, San Diego, California, USA (2007).

[10] Petruska D, Ku A, Masson C, Cook H, McDonald W and Spong R: 'Calculation of reliability-based safety factors for establishing defect acceptance criteria for deepwater riser welds', Deep Offshore Technology Conference (D.O.T.) (2006).

[11] Bristoll P and Roeleveld J: 'Fatigue of offshore structures: effect of seawater on crack propagation in structural steel', Proc. Conf. European Offshore Steels Research, ECSC (1978).

[12] Webster S E, Austen I M and Rudd W J: 'Fatigue, corrosion fatigue and stress corrosion of steels for offshore structures', ECSC Report No. EUR 9460, ECSC Steel Publications, European Commission, Brussels (1985).

[13] Pargeter R J, Gooch TG and Bailey N: 'The effect of environment on threshold hardness for hydrogen induced stress corrosion cracking of C-Mn steel welds', Conference Proceedings 'Advanced Technology in Welding, Materials, Processing and Evaluation', Japan Welding Soc, Tokyo, April (1990).

[14] Sponseller D L: Corrosion, Vol. 48 (1992) p.159.